OPTIMAL SIZING AND LOCATION OF PHOTOVOLTAIC GENERATORS ON THREE PHASE RADIAL DISTRIBUTION FEEDER

AMMAR M. MUNIR AL-SABOUNCHI

PhD

DE MONTFORT UNIVERSITY

2011

This Thesis is submitted in partial fulfillment of the requirements of De Montfort University for the award of Doctor of Philosophy

Supervised by

Dr. John Gow and Prof. Marwan Al-Akaidi

Faculty of Technology

De Montfort University

Leicester, UK

2011

ACKNOWLEDGMENTS

I would like to commence my acknowledgements with the saying of J.F. Kennedy "*As we express our gratitude, we must never forget that the highest appreciation is not to utter words, but to live by them*".

In this essence, I would like to thank my supervisors, Dr John Gow and Prof Marwan Al-Akaidi for their wise guidance and immense support since the first day I set about my PhD study.

My deepest thanks are to Dr John Gow for his valuable supervision throughout the tiring journey of my PhD study. Dr Gow spared no efforts in providing what is the best for my research. His support did not stop at the scientific supervision but extended to facilitate many administrative issues. I highly appreciate all what he has done for me.

I have been waiting for this moment to express my sincere gratitude to Prof Marwan Al-Akaidai for the immeasurable support he has given me ever since I enrolled at the DMU. I consider myself very lucky to be with Prof Al-Akaidi who has kept fostering me and raising my self-confidence until I achieved this work. Prof Al-Akaidi was there every time I needed him. I hope he knows how much I truthfully cherish his kind acts with me that I would never forget.

My genuine thanks are to Dr Hamda Al-Thani the director of the National Energy and Water Research Centre in Abu Dhabi. I appreciate very much her outstanding support in providing the research tools and facilities that I needed, which was a key factor in implementing this work.

Very sincere thanks are due to Prof. Munther Al-Tikriti who firstly made every effort to put me on the right track of my PhD study. His credible recommendation on my behalf was the main reason that I gained the opportunity of joining my PhD program.

On family side, I have not enough words to thank my ever first teachers in this life, my parents, who have been inspiring me and pushing me forward all the way. Their prayers and blessings were no doubt the true reason behind any success I have realized in my life.

I owe this work to my dear wife who used always to support me and stay by me in thick and thin. I thank her for the limitless patience she used always to show and for the times she backed me in the family being the mother and father at the same time.

My thanks and love to my beloved sons Ahmed, Hasan and Abdulla who were very thoughtful about me. I apologize to them for the times I felt short of being with them and for any moments I was absent-minded when they were telling me about their things. I want they know how much I feel proud of them.

LIST OF ABBREVIATIONS (main list)

Abbreviation	Description
ΔEL	Line energy loss reduction
ΔPPL	Line peak power loss reduction
ΔPL_{FOI}	Line power loss reduction at the FOI
A_{Poss}	Possibility of compensated power flow area
E^{j}_{j-1}	Energy flow in line section j-1 with the PVDG unit at node j
$ET^{j}_{(j+1)\rightarrow n}$	Total energy flow of sections j+1 up to feeder end with the PVDG at j
$ET^{X_2}_{X_1}$	Energy flow area along the feeder with 2 PVDG units at nodes X_1 & X_2
$ET^{j}_{1\rightarrow j}$	Total energy flow of sections 1 up to j with the PVDG unit at j
ET^{j}	Total energy flow along the feeder with the PVDG unit at j
$LD^{P}_{(Ts)}$	Real load demand at Ts interval
$LD^{Q}_{(Ts)}$	Reactive load demand at Ts interval
$LD^{P}_{cp(FOI)}$	Real load demand of the CP node at the FOI
$LD^{Q}_{cp(FOI)}$	Reactive load demand of the CP node at the FOI I
$LD_{F(FOI)}$	Load demand of the feeder at the FOI
$PL_{k(FOI)}$	Line power loss of line section k at the FOI
$V_{L1(Ts)}$	Live voltage of node 1 at Ts interval
AVR	Automatic voltage regulator
CO_2	Carbon dioxide
CP	Coupling point node
CPj	Coupling point node at which the j^{th} PVDG unit is located
D_{ab}	Distance between phase conductors a and b
DG	Distributed generation
Eff_{Inv}	Efficiency of the inverters interfacing the PV array with the grid
E_j	Energy flow of a line section j
EL	line energy loss
FOI	Feasible optimization interval
GMR_i	Geometric Mean Radius of conductor i
I_{abc}	Current of phases a, b & c in vector form
I_L	Line current
ini_CP	Initial feasible locations of the CP node on the normalized feeder
$L_{1(i)}$	Load curve value of line section 1 at interval i
$L_{1(i)pu}$	Load curve value of section 1 at interval i in per-unit of that at the FOI

$LD_{F(FOI)pu}$	Load demand of feeder in per unit of $LD_{F(pk)}$,
$VP_{k(FOI)}$	Phase voltage of node k at the FOI
$LD_{F(pk)}$	Load demand of feeder at the peak load interval
$LD_{j(FOI)}$	Load demand of node j at the FOI
$LD_{j(i)}$	Load demand of node j at interval i
$LD_{j(i)pu}$	Load demand of node j at interval i in per-unit of that at the FOI
$LD_{j(p)}$	Peak load demand of node j
LD_{jpu}	Load demand of node j in per-unit of $LD_{j(p)}$
Le_{k_act}	Actual length of line section k
Le_{k_norm}	Normalized length of line section k
Le_{m1}	Length from the substation to node m1
Le_{mid}	Length form the substation to midpoint node
Leq	Equivalent length of the uniform feeder
Leq_CPj	Equivalent uniform length corresps ini_CP node of the j^{th} PVDG unit
Leq_{span}	Length span between the PVDG units on the equivalent uniform feeder
L_{ii}	Self inductance of line section i
L_{ij}	Mutual inductance between line sections i and j
$L_{j(FOI)}$	Load curve value of line section j at the FOI
$L_{m^j(FOI)}$	Load curve value of the line section ends by node m^j at the FOI
L_{norm}	Length of the normalized feeder
$L_{X1(FOI)}$	Load curve value of the line section ends by node X_1 at the FOI
$mPV_{CP(FOI)}$	Modified size of the PVDG unit connected to CP node at the FOI
mid	Midpoint node
m^j	Node at which the reverse power flow, due to PVDG at j, clears away
m^j	Midpoint divide the distance from the substation to the CP node j
$nLD_{cp(FOI)}$	New load demand of the CP node after connecting the PVDG unit
PF	Power factor
PF_{FOI}	Power flow area/profile along the feeder at the FOI
P_i & Q_i	Real & reactive power flow in line section i
PL_j	Line power loss in line section j
PL_T	Total line power loss
PPL	Line peak power loss
PQ bus	Load bus in power flow calculations
pu	Per-unit value
PV_{com}	Commercial PV array capacity in dc power
$PV_{cp(FOI)}$	Ac power production at the FOI of the PVDG unit connected to node CP
PVDG	Photovoltaic distributed generation

$PVDG_{(i)pu}$	PVDG output at interval i in per-unit of its output at $SI_{(FOI)}$
$PVDG_{pu}$	PVDG output in per-unit of its output at $SI_{(FOI)}$
$PV_{j(FOI)}$	Amplitude of the PVDG production curve
RPF	Reverse power flow
r_k	Wire conductor resistance of the actual line section k (Ω/km)
r_{ref}	Reference wire conductor resistance (Ω/km)
s/s	Sub-station
$SI_{(FOI)}$	Solar irradiance at the FOI
$SI_{(FOI)sum}$	Solar irradiance at the FOI of a summer day
$SI_{(i)}$	Solar irradiance at interval i
SI_{pu}	Solar irradiance values in per-unit of $SI_{(FOI)}$
Ts : Te	Start time : End time of daylight hours
V_{abc}	Voltage of phases a, b & c in vector value
V_{ag}	Phase a voltage to ground
V_i	Line voltage of node i
V_{ss}	Voltage at substation
x_i	Wire conductor reactance of line section i per one km
Z_{abc}	Phase impedance matrix of the three phases in vector form
z_i	Impedance of line section i
z_{ii}	Self impedance of line section i
z_{ij}	Mutual impedance of line sections i and j
$\hat{z}_{ii}$	Primitive self mutual impedance of section i
$\hat{z}_{ij}$	Primitive mutual impedance of sections i and j
λ_i	Flux linkage of conductor i

LIST OF FIGURES

TABLE OF CONTENTS

ABSTRACT

The aim of this work is to research the issue of optimal sizing and location of photovoltaic distributed generation (PVDG) units on radial distribution feeders, and develop new procedures by which the optimal location may be determined. The procedures consider the concept that the PVDG production varies independently from changes in feeder load demand. Based on that, the developed procedures deal with two performance curves; the feeder daily load curve driven by the consumer load demand, and the PVDG daily production curve driven by the solar irradiance. Due to the mismatch in the profile of these two curves the PVDG unit might end up producing only part of its capacity at the time the feeder meets its peak load demand. An actual example of that is the summer peak load demand in Abu Dhabi city that occurs at 5:30 pm, which is 5 hours after the time the PV array yields its peak. Consequently, solving the optimization problem for maximum line power loss reduction (ΔPPL) is deemed inappropriate for the connection of PVDG units. Accordingly, the procedures have been designed to solve for maximum line energy loss reduction (ΔEL).

A suitable concept has been developed to rate the ΔEL at one time interval over the day, namely feasible optimization interval (FOI). The concept has been put into effect by rating the ΔEL in terms of line power loss reduction at the FOI (ΔPL_{FOI}). This application is deemed very helpful in running the calculations with no need to repeat the energy-based calculations on hourly basis intervals or even shorter. Mathematical derivations have been expressed establishing that the optimal solution resulting in maximum ΔPL_{FOI} also results in maximum ΔEL.

The procedures developed as part of this work have been applied on actual feeders at the 11kV level of Abu Dhabi distribution network. Two main scenarios have been considered relating to the avoidance and allowance of reverse power flow (RPF). In this course, several applications employing both single and multiple PVDG units have been solved and validated. The optimization procedures are solved iteratively. Hence, effective sub-procedures to help determine the appropriate number of feasible iterative steps have been developed and incorporated successfully.

Additionally, the optimization procedures have been designed to deal with a 3-phase feeder under an unbalanced load condition. The line impedances along the feeder are modeled in terms of a phase impedance matrix. At the same time, the modeling of feeder load curves along with the power flow calculations and the resulting losses in the lines are carried out by phase.
The resulting benefits from each application have been evaluated and compared in terms of line power loss reduction at the FOI (ΔPL_{F0l}) along with voltage and current flow profile.

Regarding the application avoiding RPF, the resulting ΔEL benefit, rated by the ΔPL_{FOI}, has exceeded 50% of the original line losses with no PVDG units. In this course, the highest benefit has been realized with the application of three PVDG units, followed by two then one unit respectively. Based on that, the conclusion is to distribute the total size on multiple units along the feeder rather than to put it in a single unit.

As far as the voltage profile is concerned, the applications showed considerable improvement. The applications have the same order of preference of three PVDG units, followed by two then one unit respectively. As a matter of fact, the reduction in voltage drop at the end of the feeder has exceeded 25% disparately in the three applications. The same order of preference has been also realized when evaluating the current flow profile, where the application of three PVDG units showed the lowest over the others. It is worth mentioning that the reduction in current flow has exceeded 35% in the line sections affected by the PVDG units for the three applications. Hence, in terms of voltage and current flow profile, the preference is once more for distributing the total size on multiple units rather than to put it in single unit.

Coming to the scenario where RPF is permitted, this work has dealt with the application of single PVDG and multiple (represented by two) units. The application with multiple PVDG units has shown higher ΔEL benefit, rated by the ΔPL_{FOI}, than with a single PVDG unit. The same preference appears when evaluating the improvement in voltage profile and reduction of current flow.

In order to compare the results of applications that both permit and avoid, the application of single PVDG unit for both has been considered. In terms of ΔEL, rated by the ΔPL_{FOI}, the level when the RPF is allowed was 9% higher than when RPF is avoided. The same preference has been realized when evaluating the improvement in voltage and current flow profiles. Based on that, the comparison has yielded a preference for the allowance of reverse power flow; subject to that the RPF does not reach the substation.

Another interesting observation has been realized regarding the optimal locations of the PVDG units. For a single PVDG unit, with avoidance of RPF, the optimal location is likely to be at a coupling point (CP) node around the mid-point of the feeder. In the same course, a sort of rule-of thumb has been determined for use with multiple PVDG units. The rule is that the optimal location of the j^{th} PVDG unit is most likely at a CP node within the j^{th} zone on the feeder. Another interesting observation is that the CP node gets closer to the zone end as much the zone is closer to the substation. For the scenario allowing RPF and considering a single PVDG unit, the optimal CP node is found to be at a node in the downstream half of the feeder. At the same time, the associated mid node at which the PVDG unit clears away is located in the upstream half. The same concept is applied with two PVDG units, where CP2, mid2, CP1 and mid1 are located in the relevant quarters starting for last downstream quarter upwards respectively.

The work has been completed showing promising proposals for further applications and/or avenues of research. Among the proposed applications is to utilize the developed procedures in solving for optimal size and location of conventional DG units for both of peak power loss and energy loss reduction at the same time. Further research has been proposed also related to the sizing of the PVDG unit, with the RPF allowance, considering load demands over the whole year. The incorporation of non-linear programming technique in the optimization procedure for more reduction in the iteration process was also among the proposed topic.

1 INTRODUCTION

Until the late 1980s, the mainstream applications of photovoltaic (PV) applications were in stand-alone systems that generate electricity at areas far away from the utility grid [1]. The relatively high cost of PV modules was mainly behind this limitation [2]. However, the cost of PV modules has reduced more than 25 times comparing to the costs in 1978 [3]. At the same time, conventional fossil-fuel sources are not sustainable and will run out some day. Additionally, the cost aspect is no longer the only motive for spreading out renewable technologies including photovoltaic. The threat of global warming and the negative impact of conventional energy generation on the environment have become an additional driving force for wider deployment of renewable technologies. As a matter of fact, reduction of carbon dioxide emission due to the deployment of renewable generators is worth a considerable amount of money these days. Considering conventional power plants operating on coal and natural gas combustion turbines, the generation of 1MWh may emit 1.04MT and 0.47MT of carbon dioxide (CO_2) respectively [4]. From the stand point of emission trading, groups that offset part of the CO_2 they emit can sell this part to others who need to exceed their credits. There is no fixed price for the credits and it could be in the range of $6.10 per ton of CO_2 [5].

One of the main methods to achieve greater deployment of renewable energy is by connecting renewable electric generators at the distribution level of the utility grid, in so called Distributed Generation (DG) systems. Several renewable DG technologies are being developed worldwide like photovoltaic, wind, and fuel cells. However, photovoltaic DG (PVDG) technology shows distinct growth over other techniques, mainly in the countries of high solar radiation rates. Regarding distribution networks, it is worth mentioning that most of them use radial feeders in distributing the electric power to consumers [6]. Hence, connection of PVDG units at optimal sizing and locations along radial distribution feeders has ended up as a matter of significant importance.

On the other hand, the traditional distribution networks are designed and constructed on the basis of unidirectional power flows from the substation to the end of distribution feeders [7]. However, connection of DG units at some coupling point(s) along the feeder may result in power flow in both directions. This may result in undesirable modes of operation in light that it

could disturb the traditional automatic voltage regulators and unidirectional relays. Beside it may increase undesirably the voltage and current at some parts of the distribution network.

1.1 Distribution System

The distribution substation is traditionally fed from one or more subtransmission line(s) via step down transformers. The substation transformer can be installed in one three-phase unit or three single-phase units connected together in a star or delta standards. Regarding distribution voltage levels, they could be in the range of 34.5kV down to 4.16kV [8]. The most common ones according to the IEC standard are 33kV and 11kV. The substation transformer feeds several primary feeders that are usually radial distribution feeders characterized by having one power path from the substation to consumers. Figure 1.1 illustrates simple line diagram of distribution substation serving four primary radial feeders (F1-F4) via two 33/11kV distribution transformers T1 and T2.

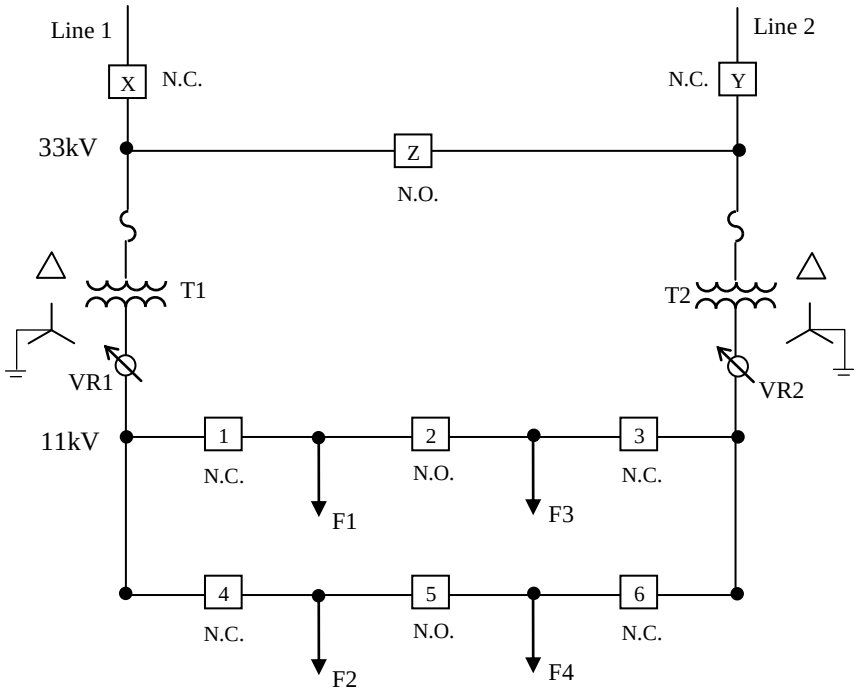

Figure 1.1 Distribution substation serving four radial distribution feeders

Based on the structure in Fig.1.1, the tie circuit breakers X, Y, 1, 3, 4 and 6 are normally closed while breakers Z, 2 and 5 are normally opened. This way Line 1 serves transformer T1, which in turn serves feeders F1 and F2. Similarly, transformer T2 is served by Line 2 and serves

feeders F3 and F4. If Line 1, for example, goes out of service then breaker X is opened and breaker Z is closed so that both of T1 and T2 are served by Line 2. Assume T1 is out of service then breakers 1 and 4 are opened and breakers 2 and 5 are closed so that the four feeders F1-F4 are served by T2. It is worth mentioning that the circuit breakers of Fig.1.1 are called sectionalizing breakers in some literature.

In order to maintain the voltage profile along the feeders within an acceptable range, the voltage regulators VR1 and VR2 are connected at the low voltage bus of T1 and T2. These regulators are interfaced with on-load tap changers that can change the taps of the low voltage windings of the transformer within around ±10% as long as load varies. The substation is protected with reliable protection schemes against short circuit and over/under voltage faults. This includes directional protection in the ring of T1 and T2 to discriminate at which of the two transformers is the short circuit fault to be isolated. Based on the same concept, directional protection may even be added at certain places in the ring of the four feeders. Suitable circuit breakers are added also to disconnect short circuit faults outside the substation.

Radial Distribution Feeder

The physical structure of typical radial distribution feeder consists of 3-phase primary 'main' feeder and lateral feeders branching from it. The laterals could be 3-phase, 2-phase (V phase) and 1-phase feeders. The power is served to customers through distribution transformers connected at suitable nodes along the primary feeder and its laterals. Voltage regulators and capacitor banks are added at the input of the feeder and/or the nodes of distribution transformers. The wire conductors of the feeder are constructed in underground or overhead lines, or combination of the both. The common characteristics of traditional radial distribution feeders can be summarized as follows [9]:

- The distribution voltage levels range from 4.16 kV to 34.5 kV based on the used electrical standard by the utility. The voltage level of radial distribution feeder considered in this work is 11kV.
- The lengths of primary radial distribution feeders are most likely in the range of 1.5-30 km.
- The capacity of distribution transformers along the feeder is in the range of 0.15-2MVA.
- Distribution feeders include control devices. The most common are shunt capacitors to meet improve the power factor and/or support voltage regulation. Voltage regulators are used to maintain adequate line voltage along the feeder up to the customer located furthest from the distribution substation.
- Multi-grounded, uni-grounded, ungrounded, and resistively or reactively grounded distribution systems are used in the industry.

- Protective devices are installed on distribution feeders to meet the safety standard requirements, protect the equipment of the system, and improve the service reliability. The protection units of distribution feeders consist of a circuit breaker at the substation and line reclosers, sectionalizing breakers, and fuses at intermediate locations along the primary feeders and laterals.
- The 3-phase primary radial distribution feeders are extended out in three or four wire systems with Δ and Y configurations.

The nature of radial distribution feeder drives the power flow showing decreasing trend in the downstream direction towards the end of feeder. Figure 1.2.a illustrates the concept presenting practical feeder with discrete distributed loads, while Fig.1.2.b shows a virtual feeder with uniformly distributed loads.

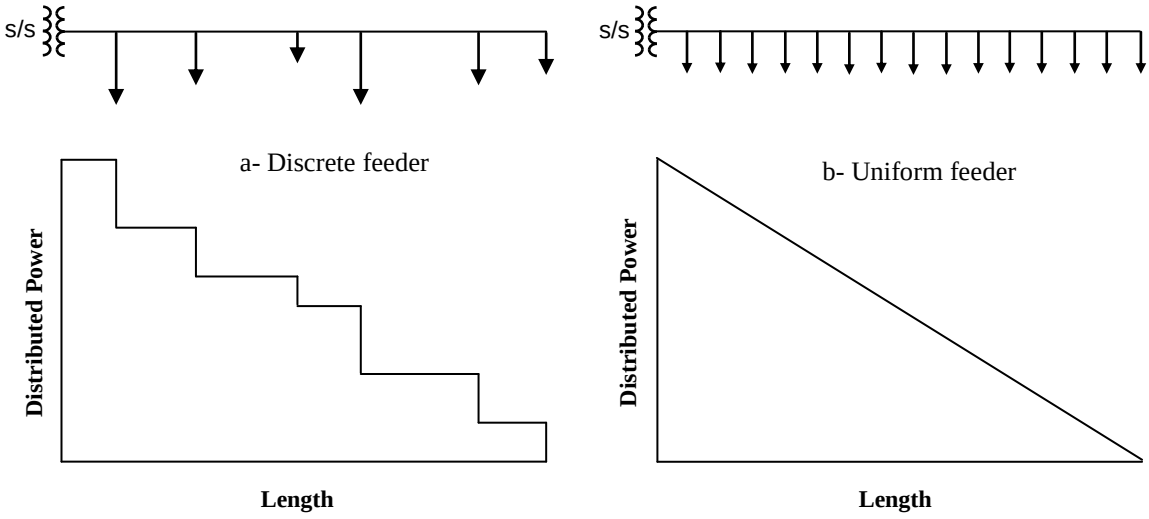

Figure 1.2 Concept of discrete and uniform feeders

1.2 Distributed Generation

The distribution system is traditionally designed and implemented based on the concept of unidirectional power flow from higher to lower voltage levels. The concept of Distributed Generation (DG) is fundamentally different from this tradition, where dispersed generators of small capacities not more than 20MW are connected at the distribution level [10]. The interest in DG units is evolved in the last two decades driven by the technological development of DG technologies and liberalization of the electricity market along with economical and regulatory factors related to the distribution network [11]. The delaying of distribution system upgrade

associated with the growing demand for reliable electricity is among the main motives behind the evolvement of DG technologies. The investment in DG units generating and selling electricity back to grid could be also one of the motives.

In the same connection, the global warming concerns and the current trend of adopting clean energy resources have shed light on renewable DG technologies. At the present time, the most common types of DG technologies worldwide are listed as follows [12]:

- Reciprocating Engines,
- Gas Turbines,
- Micro-turbines
- Photovoltaic,
- Fuel cells,
- Wind Turbines,

Considering the capacity range of DG units, it's deemed suitable connecting them to distribution feeders at voltage levels not more than 33kV or equivalent. Figure 1.3 shows an example on connecting single DG unit to the radial distribution feeder F4. In this example, the coupling point (CP) is selected on the 11kV side of one of the 11/0.4kV transformers along the feeder.

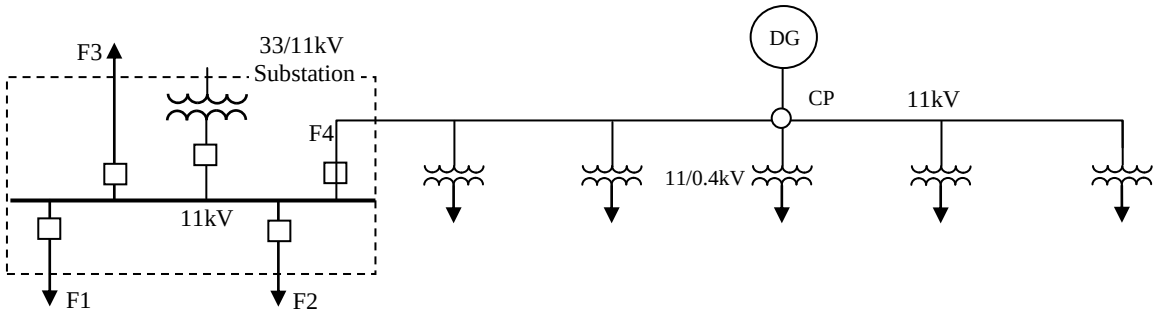

Figure 1.3 DG unit connected to the high voltage side of radial distribution feeder

Connection of DG units to radial distribution feeders can result in many benefits to the feeders and the network as a whole. These include reduction of line power losses, improvement of voltage profile, peak power shaving, the ability to postpone network upgrade to increase capacity, improvement of system reliability, and reduction of carbon output [13].

The rate of the benefits above is highly dependent on the optimal sizing and location of the DG units. Reduction of line power losses in the conductors of distribution feeder is among the main objectives for this optimization. It is known that the line power loss reduction increases as much as the power flow through the lines decreases. Hence, serving part of the loads along the feeder locally via DG unit(s) can compensate part of the original power flows from the substation.

Consequently, this will reduce the power losses through the line conductors between the substation and the CP. In this work, the line power loss reduction is classified either as peak power loss reduction (ΔPPL) or as accumulated line power loss reduction over the day, called line energy loss reduction (ΔEL). On one hand, the ΔPPL is usually considered for peak shaving benefits as it reduces the peak load demand and postpones network upgrade. On the other hand, consideration of ΔEL is a better approach for improved efficiency over the day, including reduction of CO_2 emission.

1.3 Concerns of Distributed Generation

Apart from the benefits of connecting DG units, there are several economical and technical concerns of this connection. The main economical ones could be the high capital cost of renewable DG units and the generation efficiency of conventional DG units comparing to centralized power plants. In case of PVDG units, the site area required to install the PV array is also a considerable economical constraint. The building integrated photovoltaic (BIPV) application could be an exception as the PV modules are integrated in the walls of the building.

On technical side, the power quality along with protection and safety are the most serious issues. Regarding power quality; disturbance of voltage level, power factor control, and total harmonic distortion (THD) are among the main concerns. While islanding operation, disturbance of unidirectional relays, contributing to short circuit current faults are among the major protection and safety concerns. As a matter of fact, the generation of electric power at downstream points of distribution feeders could be the main reason behind several technical concerns. To this end the impact of reverse power flow (RPF) toward the substation due to possible generation of surplus DG power is given consideration in this work.

Reverse Power Flow (RPF)

The connection of a DG unit at some CP along a radial distribution feeder will inject a certain amount of power. At any interval if this power exceeds the demand, the surplus amount will flow in the reverse direction towards the substation. Reverse power can disturb the inherent integrity of existing protection and regulation systems of the radial system that are designed to work with power flow in one direction. This may include the automatic voltage regulators [14 & 15] and the unidirectional protection devices [16]. Also, it may increase undesirably the voltage level and current at some parts of the feeder. Additionally, it can result in increased line power losses in the upstream direction [17]. Additionally, RPF complicates the islanding protection of

inverter-based DG units [18]. Upgrading the control system of the substation with intelligent bidirectional protection and control devices could deal with the above issues. However, the systems were originally designed and set to operate with unidirectional power flow. Therefore, allowing RPF may lead to unstable operation. The idea is that if the intelligent devices are adjusted to be effective during DG operation, they should be also effective when the DG unit is not working [19].

Impact on unidirectional protection

Figure 1.4 shows an example on the impact of reverse power on the traditional unidirectional relays R1 and R2. At no DG unit and no fault condition the circuit breakers CB1 and CB2 are closed and the feeder(s) are served from transformers Ta and Tb. If a short circuit fault occurs at F1 it would be cleared by the protection system of Tb. However, CB2 is still desired to open in order to remove the fault that could continue to generate an arc. This is achieved by connecting the directional relay R2 associated with CB2. Normally, this relay is sensitive enough to detect the magnetizing current taken by transformer Tb, even if its protection has cleared F1 [16]. R2 is also active in clearing short circuit faults at F2. However, the fault current will be high enough in this case so the sensitivity feature is not that much important.

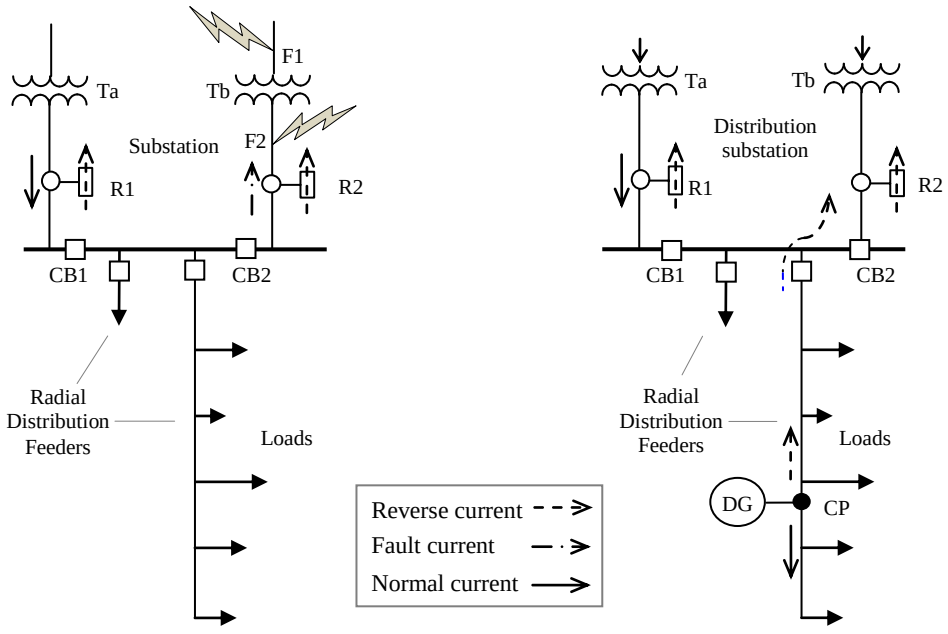

(a) At fault and with no DG connection (b) At no fault but with DG reverse power flow

Figure 1.4 Example of the impact of RPF on a unidirectional relay

Part ‘a’ illustrates the system with no DG unit, but with faults at F1 and F2. On the other hand, part ‘b’ illustrates the same system with a DG unit connected at one of the radial distribution

feeders served by the substation. In the event the DG production is higher than the demand at the coupling point (CP) node the surplus power will flow in the reverse direction toward the substation. This power could disturb the operation of R2 even with no faults at F1 or F2. There are several possibilities of such disturbances based on the connection schemes of the unidirectional devices in the system.

Impact on voltage regulation

The RPF may also disturb the operation of automatic voltage regulators (AVR) at the substation. The function of many traditional AVR devices relies on that the power flows in one direction from the substation to the end of distribution feeder. Hence, they are set on the basis that the voltage profile decreases in the downstream direction away from the substation. With RPF this concept no longer applies [14]. In such a case the voltage of feeder sections witnessing reverse power will decrease in the upstream direction the matter that may interfere with the operation of AVR control [19]. The RPF could even disturb the operation of bidirectional line voltage regulators [18&20]. As a matter of fact, many voltage regulators have specific issues with RPF [18]. Figure 1.5 illustrates the configuration of bidirectional line voltage regulation on a distribution feeder based on the literature in [20&21].

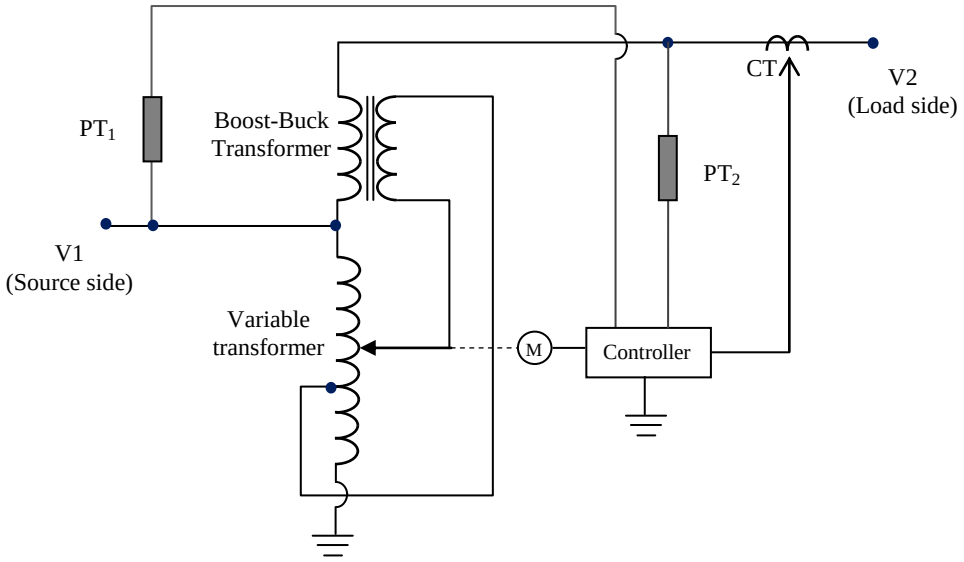

Figure 1.5 Configuration of bidirectional line voltage regulators

The bidirectional voltage regulator measures the voltage at the source and load sides by the means of potential transformers (PT). Also it can determine the direction of power flow by checking the phase shift between the voltage and the line current measured by the current transformer (CT) [20]. In the event that the substation is on the source side, the device will

regulate V_2 on the load side based on the measurements of PT_2. In case that V_2 is lower than the set point, the controller changes the tap trying to raise V_2 by increasing the voltage across the boost-buck transformer. The opposite happens if V_2 was higher than the set point limit.
In the same course, assume that the feeder is sectionalized with an adjacent feeder in a way that it is served from the load side. Such being the case, the controller will switch the device to regulate V_1 on the source side based on the measurements of the PT_1. To this end if V_1 is lower than the set point, the controller will change the tap to decrease the voltage across the boost-buck transformer. This way V_1 will be increased by voltage divider rule.

Figure 1.6 illustrates a part of radial distribution feeder with a line voltage regulator and DG unit connected on the load side of the regulator. With such configuration there is a possibility that the operation scenario above is totally confused.

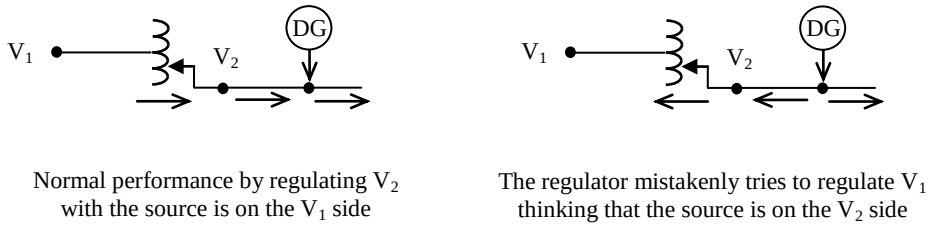

Normal performance by regulating V_2 with the source is on the V_1 side

The regulator mistakenly tries to regulate V_1 thinking that the source is on the V_2 side

Figure 1.6 Line voltage regulator and DG unit on radial distribution feeder

If at any time the power produced by the DG unit exceeds the demand at the CP node there will be a certain amount of RPF towards the substation. In such a case, the voltage regulator will determine that the substation has been switched to the load side so it will attempt to regulate V_1. Consequently, if V_1 is measured by the PT_1 to be higher than the set point, the regulator will attempt to decrease it by raising the voltage across the boost-buck transformer. Nothing will happen with V_1 because the voltage is held constant on the source side by the utility. However, V_2 on the load side will be increased further. The regulator will continue tapping the variable transformer attempting to decrease V_1, but will raise V_2 instead further and further. The process stops when the tap reaches the limit ending with V_2 increased to an undesirable level. The same confusion happens in the opposite way if V_1 was lower than the set point.

It is worth mentioning that the line voltage regulator can perform normally if the capacity of DG unit was lower than the level that starts to create RPF.

Impact on feeder ampacity and line power losses

In the same connection, the RPF may result in ampacity problems. Actually, if the surplus power of the DG unit is high enough, the rate of reverse current could exceed the ampacity limit of the upstream line sections next to the CP node.

In addition to the unidirectional relay and voltage and current concerns, the relation between the line power losses and RPF is also an issue. In principle, the line power losses in any line section along radial distribution feeder are proportional to the power flow through that section. Hence, local power generation via a DG unit at a certain CP along the feeder shall reduce the power sent from the substation. Consequently, this reduces the line power losses in the wire conductors between the substation and the CP. Figure 1.7 explains the reduction in current flow with DG connection.

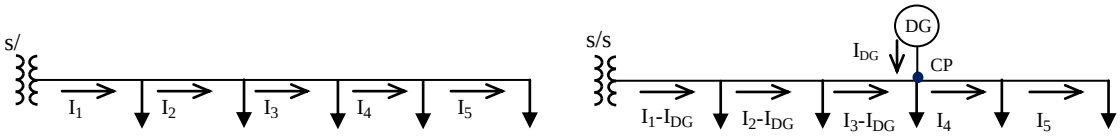

Figure 1.7 Current flows with and without DG unit connection

However, if the DG power production exceeds the demand at the CP, the surplus power will flow back in the reverse direction causing the line power losses to increase again in the reverse direction. Higher reverse power leads to higher reverse losses that may eventually result in no line power loss reduction. The losses could even end with higher than original values if the net currents of the first three sections in the figure exceed the original currents.

Impact on passive islanding protection

Among the critical concerns with the application of DG units is so-called *islanding*. Islanding is a condition where the DG unit is able to continue supplying part of the feeder even when the utility service is interrupted. This can result in a safety hazard, and it can also disturb the protection and voltage regulation devices [18].

The most common means to protect against islanding is by applying passive protection techniques using voltage and frequency relays. Consider the case where a DG unit is connected at some arbitrary coupling point on a radial distribution feeder. Upon the formation of an island the DG unit generation and the demand at the CP node are normally not matched the same way as before the interruption. If the generation exceeds the demand at coupling point (CP) then the DG unit will speed up raising the voltage and frequency beyond the limit at which the voltage and frequency relays will disconnect the DG unit [18]. The opposite will occur if the generation

is less than the demand, where the relays can disconnect the DG due to reduction in voltage and frequency. It is worth mentioning that if the production of the DG unit exceeds the demand, the surplus power will flow in the reverse direction from the CP to the substation. Hence, the passive islanding protection is effective with the conventional DG units on radial distribution feeders even in the case of RPF.

However, the above technique could be confused with the application of a PVDG unit where the production of the PVDG exceeds the load demand. In such a case, where RPF is implicit, the voltage and frequency of the grid-tied inverters may not drift easily because there are no moving parts with inertia. As a matter of fact, the excess in power will flow in the reverse direction supplying upstream loads until it clears up at some point. To this end, the voltage and frequency of inverters are controlled by fast response microprocessor that can keep these parameters consistent. Therefore, the passive islanding technique may not feel the interruption and continue to allow the PVDG unit to island part of the feeder. On the other hand, there is not such a problem when the demand exceeds the production where there will be no RPF. In such a case, the inverter fails to supply the load the matter that drifts down its output voltage below the setting of the voltage relay. This is apart from the activation of the over-current protection at the output of inverter. The conclusion of the above is illustrated in Fig.1.8 below.

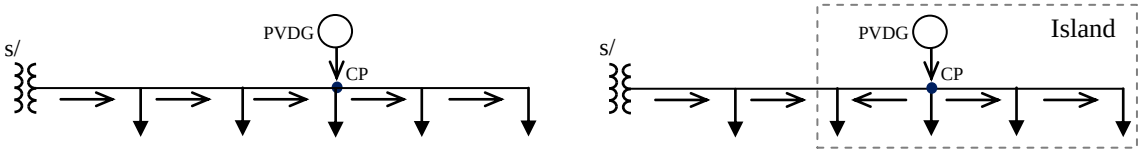

Demand exceeds production, associated with avoidance of reverse power flow. The drifting voltage relay and the over-current protection can feel the interruption and protect effectively against islanding.

Production exceeds demand, associated with allowance of reverse power flow. The voltage and frequency are controlled instantly so the drifting voltage & frequency relays may feel nothing and allow islanding.

Figure 1.8 Impact of RPF on passive islanding protection

1.4 Photovoltaic Distributed Generation

The photovoltaic technology has been developed rapidly over the last two decades supported by market forces. It is now one of the main sources of renewable DG units worldwide, and perfectly matches the conditions of countries with high solar radiation levels. The photovoltaic modules convert sunlight into dc power. Hence, the photovoltaic DG units (PVDG) are

interfaced with the grid via grid-tied inverters as shown in Fig.1.9. The grid-tied inverters convert the dc power produced by the PV array into ac power synchronized with the utility grid.

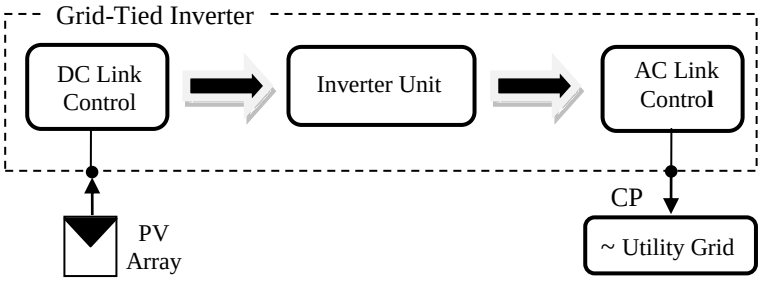

Figure 1.9 Typical configuration of the PVDG unit

It is important to mention that the power output of the PVDG system normally will not be equal to the capacity of the PV array. Commercially speaking, the capacity of PV array is rated to its dc output power at standard solar irradiance equals to $1000w/m^2$. On the other hand the PVDG power production is the actual ac power converted by the inverter and injected in the utility grid at the CP. Hence, the conversion efficiency and actual rates of solar irradiance should be considered in estimating the PV capacity required to produce the targeted PVDG power production.

Unlike traditional DG units, that can yield controllable amounts of power, the PVDG unit produces variable power driven by the variations of solar irradiance. Figure 1.10 depicts the characteristic of power flow in section 1 of the feeder in Fig.1.7, considering both traditional and PVDG units. The traditional DG unit is assumed to produce constant power with time. Part 'a' is related to traditional DG unit while part 'b' is related to PVDG unit.

Looking at 'a', the production of constant power over time by the traditional DG unit drags each point on the original load curve down by the same amount of P_{DG}. Hence, the load curve will keep the same shape but at a lower level. On the other hand, 'b' indicates that each point on the original load curve is dragged down by different value at each time (t) according to the amount of P_{PVDG} at that time. Also 'b' shows that the variation in load curve occurs only during daylight hours from T1 to T2.

The conclusion of Fig.1.10 states that the connection of PVDG unit originates the need to dealing with two time-variant curves at the same time; the load curve of the feeder and the production curve of the PVDG unit.

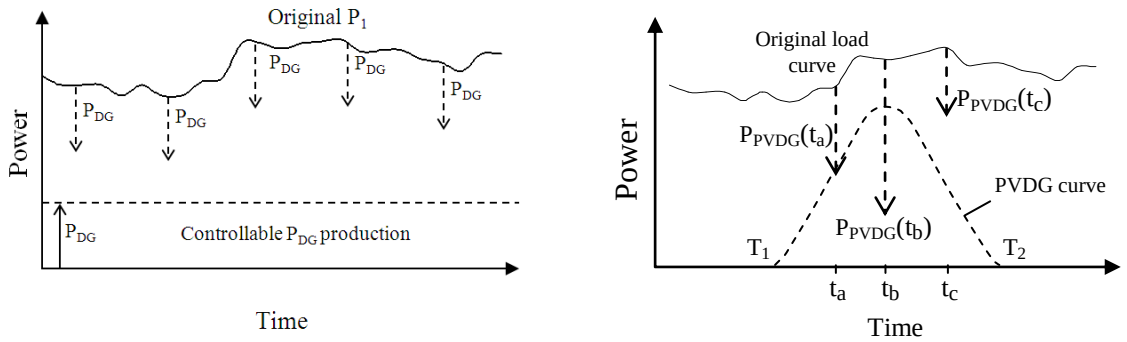

(a) With traditional DG unit

(b) With PVDG unit

Figure 1.10 Relation between feeder load curve and DG production curves

1.5 Objectives of Current Work

The main objective of this work is to develop new procedures for optimal sizing and location of PVDG units on radial distribution feeder. The optimization objective is set to minimize the accumulated line power losses along the feeder over the day, namely energy line losses (ΔEL). However, dealing with energy-based quantities requires lengthy calculations on hourly or even shorter intervals. Hence, this work aims at deriving a new method to rate the ΔEL considering one specific interval in the day.

In the same course, the line peak power loss reduction (ΔPPL) is considered as subordinate benefit in this work. This is due to the different shapes of load and PVDG production curves that result in mismatch between the peaks of the two curves. With this mismatch, the PVDG unit can produce only part of its capacity at the time the feeder meets its peak load demand. Many feeders even meet their peak load demand after nightfall that turns in no ΔPPL.

Regarding constraints, part of the work has considered the avoidance of RPF towards the substation. However, avoiding RPF over the year is not a straightforward matter. The reason is that the load curve and PVDG production curve differ over the changing seasons [22]. Based on that, a careful correlation between them is required.

On the other hand, some power distribution companies upgrade their networks with smart protection and control systems equipped with microprocessor units. These systems could be able to deal reasonably with RPF conditions. To this end, this work has extended to develop an optimization procedures dealing with single and multiple PVDG units allowing RPF.

Emphasis is placed to develop the procedures dealing with optimal sizing and location of one, two and multi PVDG units on the same feeder

Chapter 2 is dedicated to review the previous background studies related to this work. While Chapter 3 covers the modeling and simulation of 3-phase balanced and unbalanced radial distribution feeders along with the associated backward/forward power flow calculation. The results are applied on actual 11kV feeders existing in the Abu Dhabi distribution network. In Chapter 4 the new approach of rating the ΔEL at one time interval over the day is presented. Chapter 5 is the core of the work dealing with the development of the new optimization procedures. The procedures deal with one and multiple PVDG units subject to the avoidance and allowance of RPF. Last but not least, Chapter 6 is dedicated for the discussion, conclusion and presentations of future work.

References

[1] R. Hacker, J. Thornycroft, D. Munro, and E. Rudkin, "Coordinated Experimental Research into PV Power Interaction with the Supply Network," *Technical report ETSU S/P2/00233 by Halcrow Gilbert Associates for the Department of Trade and Industry*, UK, 1999. http://webarchive.nationalarchives.gov.uk/+/http://www.berr.gov.uk/files/file16531.pdf

[2] M. Campdell, "The Drivers of the Levelized Cost of Electricity for Utility-Scale Photovoltaic," *Technical report by SunPower Corporation*, USA, Aug.2008. http://us.sunpowercorp.com/downloads/SunPower_levelized_cost_of_electricity.pdf

[3] R. A. Messenger & J.Ventre, "Photovoltaic Systems Engineering," 2nd edition, *CRC Press LLC*, USA, 2004, p.16.

[4] S. Segrest, "Carbon Dioxide Reduction and Carbon Sequestration by Co-Firing Tree Energy Crops in Florida's Coal-fired Power Plants," *Technical report by The Common Purpose Institute*, USA. http://www.treepower.org/papers/co2.pdf

[5] M. Lewis, Jr., "Keyoto-by-Inches is Just a Foolish," *Technical report issued by the Competitive Enterprise Institute*, USA, Jun 2005. http://cei.org/sites/default/files/Marlo%20Lewis,%20Jr-%20Kyoto-by-Inches%20Is%20Just%20as%20Foolish.pdf

[6] A. T. Moore, "Distributed Generation (DG) Protection Overview," *Technical report by the University of Western Ontario*, Canada, May 2008.

[7] S. Naka, T. Genji, and Y. Fukuyama, "Practical Equipment Models for Fast Distribution Power Flow Considering Interconnection of Distributed Generators," *in Proc. July 2001 IEEE Power Engineering Society Summer Meeting, Canada*

[8] W. H. Kersting, "Distribution System Modeling and Analysis," *Electric Power Engineering Series, CRC Press LLC*, USA, 2002, ch.1.

[9] M. Behnke, W. Erdman, S. Horgan, D. Dawson, W. Feero, F. Soudi, D. Smith, C. Whitaker, and B. Kroposki, "Secondary Network Distribution Systems Background and Issues Related to the Interconnection of Distributed Resources," *Technical Report: NREL/TP-560-38079 by National Renewable Energy Laboratory*, USA, July 2005. http://www.nrel.gov/docs/fy05osti/38079.pdf

[10] Sauli Jäntti (Editor), "Connection of Distributed Energy Generation Units in the Distribution Network and Grid," *CODGUNet final report, Issued by Merinova Ab on behalf of four Nordic countries*, Finland, Sep. 2003.

[11] J. Driesen, R. Belmans, " Distributed generation: Challenges and possible solutions," *in Proc. Jun. 2006 IEEE Power Engineering Society General Meeting*, Montreal, Canada.

[12] B. Kroposki, R. DeBlasio, "Technologies for the New Millennium: Photovoltaics as a Distributed Resource," *in Proc.2000 IEEE Power Engineering Society Summer Meeting*, vo.3, USA, pp.1798-1801.

[13] M. F. AlHajri, A. R. AlRashidi, and M. E. El-Hawary, "Hybrid Particle Swarm Optimization Approach for Optimal Distribution Generation Sizing and Allocation in Distribution Systems," *in Proc. Apr. 2007 IEEE Canadian Conference on electrical and computer engineering*, Canada, pp.1290 – 1293.

[14] S. Conti, A. Greco, N. Messina, and S. Raiti, "Local voltage regulation in LV distribution networks with PV distributed generation," *in Proc. May 2006 SPEED AM (IEEE) International Symposium on Power Electronics, Electrical Drives, Automation and Motion*, Greek, pp.23 – 28.

[15] Turan Gonen, "Electric Power Distribution System Engineering," *McGraw-Hill Series in Electrical Engineering*, USA, 1986, ch.1.

[16] Kenneth Winick, "A Guide to the Application of Power Relays for the Detection of Overpower or Reverse Power Conditions on a Power System," *A technical guide GER 2309A by General Electric Company on the applications of some power relays*, USA. http://store.gedigitalenergy.com/FAQ/Documents/GGP/GER-2309A.pdf

[17] P. N. Vovos, A. E. Kiprakis, A. R. Wallace, and G. P. Harrison, "Centralized and Distributed Voltage Control: Impact on Distributed Generation Penetration," *IEEE Trans. Power Systems*, vol.22, no.1, pp.476-483, Feb.2007.

[18] T.A. Short, "Electric Power Distribution Handbook," *Electric Power Engineering Series, CRC Press LLC*, USA, 2004, ch.14.

[19] G. P. Harrison, A. E. Kiprakis, and A. R. Wallace, "A new era for mini hydro?", *Article in the International Water Power and Dam Construction magazine (IWP&DC)*, 4 Nov. 2002. http://www.waterpowermagazine.com/story.asp?storyCode=2017803

[20] F. Katiraei, C. Abbey, and R. Bahry, " Analysis of Voltage Regulation Problem for a 25-kV Distribution Network with Distributed Generation," *in Proc.2006 IEEE-PSE general meeting*, Canada, pp.1-8

[21] ISE Incorporation, "Voltage Regulators and Power Conditioners," *Technical sheet on buck-boost voltage regulators*, Cleveland, USA. http://instrumentation-central.com/Staco/AVR/AVRCat.pdf

[22] A. Al-Sabounchi, E. Al-Hammadi, S. Yalyali, and H. Al-Thani, "Photovoltaic-Grid Connection in the UAE: Technical Perspectives", *in Proc. Sep. 2010 World Renewable Energy Congress-XI, Abu Dhabi*, pp.1207-1213.

2 BACKGROUND STUDIES

The connection of autonomous power sources at optimum sizing and locations along radial distribution feeders is previously carried out with shunt power capacitors. Many approaches have been developed and applied using different modeling and optimization techniques. The potential optimization objectives specifically targeted are minimization of peak power and energy losses [1, 2 & 3], increasing of installed capacity [4], control of power factor [5], and improvement of voltage profile [6]. The optimization objectives are usually placed subject to the cost of installed units, statutory levels of voltage profile and ampacity of wire conductors.

During the last two decades, global warming concerns and endeavors to secure clean energy sources have been on the increase. As a result, the concept of optimal sizing and location of shunt capacitors has been elaborated to deal with renewable distributed generation (DG) units. It is worth mentioning, however, that shunt capacitors continue to be used as fixed or controllable switched units being switched on and off based on the objectives they were installed for. This performance is incompatible with renewable DG units such as photovoltaic plant, owing to their non-dispatchable nature and time-variant behavior. The rational trend of putting the renewable systems in service as long as they can produce power may be at odds with the manner in which shunt capacitors operate. Nevertheless, the modeling and derivation of optimal sizing and location of both shunt capacitors and DG units are deemed to be similar in fundamental nature. For this reason, the part of shunt capacitors has been also included in the literature review of this work.

This chapter reviews a set of previous work dealing with the theories and studies of optimal sizing and location of shunt capacitors and DG units on radial distribution feeders.

2.1 Optimal Sizing and Location of Shunt Capacitors

During the fifties and early sixties the optimal connection of shunt capacitors on radial distribution feeders considered the model of the uniformly distributed feeder. Hence, the load distribution along the feeder is assumed constant per unit length. The line losses are divided into real and reactive components assuming only the reactive component is potentially affected by

the installed capacitors. The reduction in line peak power losses is calculated as the difference in losses before and after capacitors installation. This concept is represented in Fig.2.1, with the original line peak power losses (PPL) due to reactive current flow are expressed as follows:

$$PPL = \int_0^1 i^2\, R.\, dx = \int_0^1 [I(1-x)]^2\, R.\, dx = I^2R \int_0^1 [(1-x)]^2\, .\, dx$$

$$PPL = I^2R\, [x - x^2 + \frac{X^3}{3}]_0^1 = \frac{1}{3}\, I^2R \qquad (2.1)$$

Where, I - Total reactive current of the feeder
R & x - Total feeder resistance & length respectively

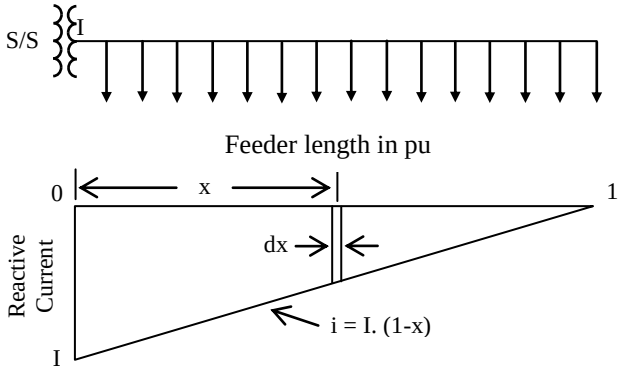

Figure 2.1 Uniformly radial distribution feeder without capacitor

In the same course, Fig.2.2 represents the case when a shunt capacitor is connected at some location (CL) along the feeder, which breaks the continuity of the load profile.

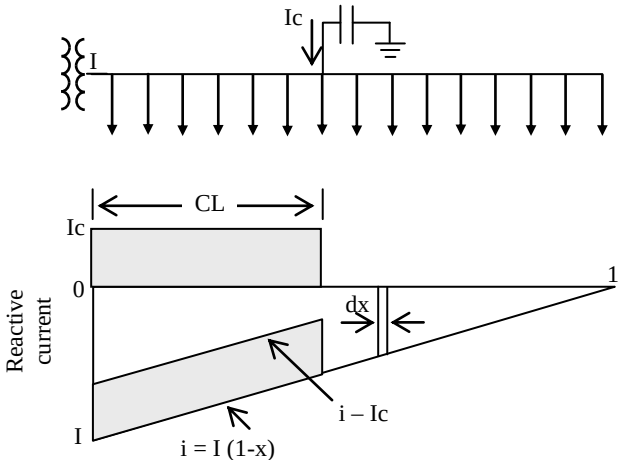

Figure 2.2 Radial uniformly distributed feeder with capacitor at location CL

The formulation of line peak power losses with the reactive current Ic injected in the feeder is formulated as follows:

$$PPLc = \left(\int_0^{CL}[I(1-x) - Ic]^2 + \int_{CL}^{1}[I(1-x)]^2\right) R \cdot dx$$

$$PPL = \int_0^1 [I(1-x)]^2 \, R.\, dx \qquad (2.2)$$

$$\Delta PPL = PPL - PPLc$$

Where, PPLc - Line peak power losses with capacitor
PPL - Original line peak power losses
ΔPPL - Line peak power loss reduction

The literature shows considerable work in the field based on the concept of Eq.2.2. The work by Neagle and Samson [7] is one of these. They built their procedure by setting the first derivative of Eq.2.2 with respect to 'CL' and equating to zero; then solving for maximum peak power loss reduction. The procedure was applied in identifying the optimal locations of single and multiple fixed capacitors with specified ratings of the same value.

Cook has upgraded the procedure, in [8], by considering the effect of single and multiple fixed capacitors on the total line energy losses of the feeder. The distribution of current along the feeder over time is modeled in Fig.2.3.

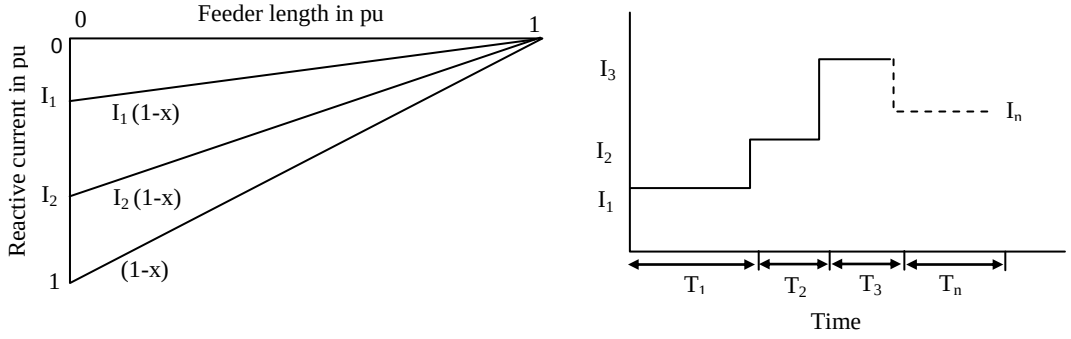

Figure 2.3 Line current vs. resistance of radial feeder at different durations

According to Fig.2.3, the total line energy losses (EL) due to the connection of fixed capacitor with per-unit rated current Ic and location CL is expressed as follows:

$$EL = \left(\int_0^{CL}[(I_1(1-x) - Ic)^2 T_1 + (I_2(1-x) - Ic)^2 T_2 + \cdots + (I_n(1-x) - Ic)^2 T_n] + \right.$$

$$\left.\int_{CL}^{1}[I_1(1-x)^2 T_1 + I_2(1-x)^2 T_2 + \cdots + I_n(1-x)^2 T_n]\right) R \cdot dx \qquad (2.3)$$

Where I_i is the total reactive current of the feeder in duration T_i, and x is the per-unit (pu) resistance up to certain point along the feeder. Suitable formula for optimal CL of fixed capacitor resulting in minimum line energy losses EL is found by solving Eq.2.3 then having its first derivative with respect to CL equals to zero.

Similar analysis is done for N fixed capacitors with equal Ic by extending Eq.2.3 as follows:

$$EL = \left(\int_0^{CL_1}[(I_1(1-x) - N \cdot Ic)^2\, T_1 + \cdots] + \int_{CL_1}^{CL_2}[(I_1(1-x) - (N-1)Ic)^2\, T_1 + \cdots] + \cdots + \int_{CL_n}^{1}[(I_1(1-x))^2\, T_1 + \cdots]\right) R \cdot dx \quad (2.4)$$

Solving Eq.2.4 then having its first derivative with respect to each CL equals to zero results in the formula below for optimal locations of each of the N capacitors. Where j is the index of installed capacitor and LF is the reactive load factor of the feeder.

$$CL_j = 1 - \frac{[(2N - (2j-1)] \cdot Ic}{2LF} \quad (2.5)$$

On the same basis, Cook identified the optimal Ic values for N fixed capacitors with equal Ic installed at optimal CL locations. The formula is derived by repeating the analysis of Eq.2.5 but with respect to Ic equals to zero this time. The derivation ended up with the following formula for the total rating (Ic_T) of the N fixed capacitors:

$$Ic_T = \frac{2N.\,LF}{2N+1} \quad (2.6)$$

In [9] Cook developed a method to analyze the application of fixed and/or switched capacitors, considering the effect of line peak power and energy losses as well as reduction in KVA demands. The resulting formula for optimal locations of fixed capacitors is stated below. K_1 and K_2 are constants converting energy and peak power loss reduction, respectively, into money.

$$CL_j = 1 - \frac{[(2N - (2j-1)]\, Ic \cdot (K_1 + K_2)}{2[K_1 LF + K_2]} \quad (2.7)$$

According to Cook's derivations, if multiple fixed capacitors are to be used on a feeder, then all capacitors have the same rating.

In the consideration of the effects of fixed and switched capacitors, Cook divided the load factor of the feeder into two periods. From zero time up to T_f only the fixed capacitor is connected, while the switched capacitor is connected from T_f until 1-pu time. The modeling is represented in Fig.2.4.

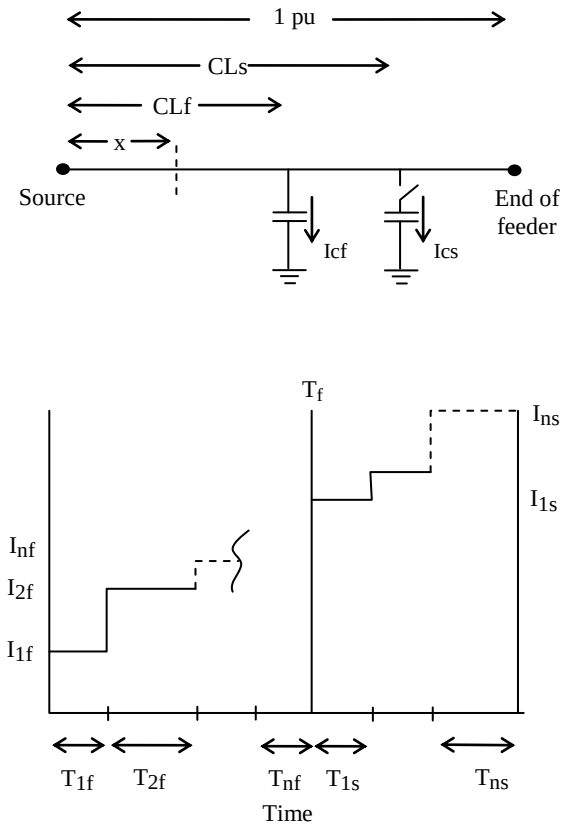

Figure 2.4 Fixed and switched capacitors on radial distribution feeder

The total line energy losses (EL) according to Fig.2.4 are derived below, where CLf & CLs alongside Icf & Ics are the locations and ratings of the fixed and switched capacitors respectively:

$$EL = \left(\int_0^{CLf} [\sum_{i=1f}^{nf} (I_i(1-x) - Icf)^2 \, T_i] \; + \int_{CLf}^{1} [\sum_{i=1f}^{nf} (I_i(1-x)^2 \, T_i] \; + \right.$$
$$\int_0^{CLf} \{\sum_{i=1s}^{ns} [(I_i(1-x) - (Icf + Ics)]^2 \, T_i\} \; + \int_{CLf}^{CLs} [\sum_{i=1s}^{ns} (I_i(1-x) - Ics)^2 \, T_i] \; +$$
$$\left. \int_{CLs}^{1} [\sum_{i=1s}^{ns} I_i(1-x)^2 \, T_i] \right) R \cdot dx \qquad (2.8)$$

The optimum CLs and CLf are found by solving Eq.2.8 and setting its first derivative with respect to the location of each capacitor equals to zero. The resulting formulas are stated below, where LFs is the reactive load factor during the time that the switched capacitor is connected:

$$CLf = 1 - \frac{Icf(K_1 + K_2) + 2Ics[K_1(1 - Tf) + K_2]}{2[K_1 LF + K_2]} \quad (2.9)$$

$$CLs = 1 - \frac{Ics[\, K_1(1 - Tf) + K_2]}{2[K_1 LFs(1 - Tf) + K_2]} \quad (2.10)$$

Going through the aforementioned works, a set of shortcomings can be found. First of these is the impractical modeling of uniformly distributed loads and the consideration of flat voltage profile along the feeder. Also the assumption of a 3-phase balanced load feeder is likely to be not practical. Additionally, they dealt with the sizing and location variables assuming one of them is known so the other can be found.

Based on above, work had been done in considering radial distribution feeder with discrete loads giving more practical modeling. The work by Duran [10] and Shmill [11] were among those. Taking Duran's work as example, it solved for the optimal sizing and location of fixed capacitors considering cost. The optimization based on dynamic programming techniques aiming at maximizing the line losses saving due to connecting of fixed capacitors considering the cost. Duran assumed one fixed capacitor at each node as shown in Fig.2.5.

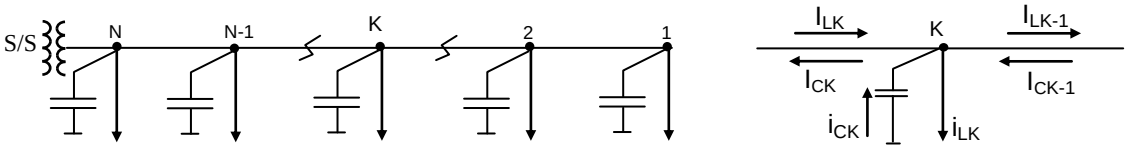

Figure 2.5 Fixed capacitors to radial distribution feeder with discrete loads

The realized saving of losses in branch K (SL_K) of line resistance R_K is calculated by Eq.2.11. Where A and B are functions of Load Factor (LF) and duration of load cycle (T) along with factors turn energy and peak power losses into money.

$$SL_K = 3R_K\,(2A\,I_{CK}\,I_{LK} - B\,I_{CK}^2) \quad (2.11)$$

Nevertheless, the main shortcoming of Duran's method is the assumption of 3-phase balanced load feeder with flat voltage profile. Also it overlooked the influence of reverse current flow and assumed a capacitor is connected to each node along the feeder.

In [12], Chang presented a developed procedure considering the control of voltage profile along the feeder as a main function. The procedure is applied by installing fixed and switched capacitors that provide line peak power and energy losses as additional function. A computer

program consisting of two parts had been developed for the analysis. Part 1 calculates the voltage profiles of the feeder at light-load and peak-load conditions. If a voltage problem does exist, part 2 then determines the optimum rating and location of fixed and switched capacitors that fix the voltage with best possible line loss saving. Additional constraint was considered in the process, which is to set the power factor at light-load condition close to unity.
The shortcomings of the assumption of a 3-phase balanced load and the overlooking of RPF are still there. Besides, the main objective of the shunt capacitors is placement to control the voltage profile rather than to minimize the line losses.

Grainger and Lee, in [13], developed a procedure considering line peak power and energy losses. It is applied on actual radial feeder having line sections with different wire sizes. To simplify the analysis, the total physical length of the feeder in Fig.2.6 is turned to unity with its line sections generalized to equivalent per-unit lengths of similar wire size. This is done by setting the wire size of one of the line sections as a reference (r_{ref}). Then, the lengths of whole line sections are generalized to equivalent lengths with the same wire size of the reference. Hence, the equivalent length of line section i ($L_{i\text{-}eq}$) of wire size 'r_i' is expressed as follows:

$$L_{i-eq} = \frac{L_i r_i}{r_{ref}} \quad i = 1,2,\dots,n \tag{2.12}$$

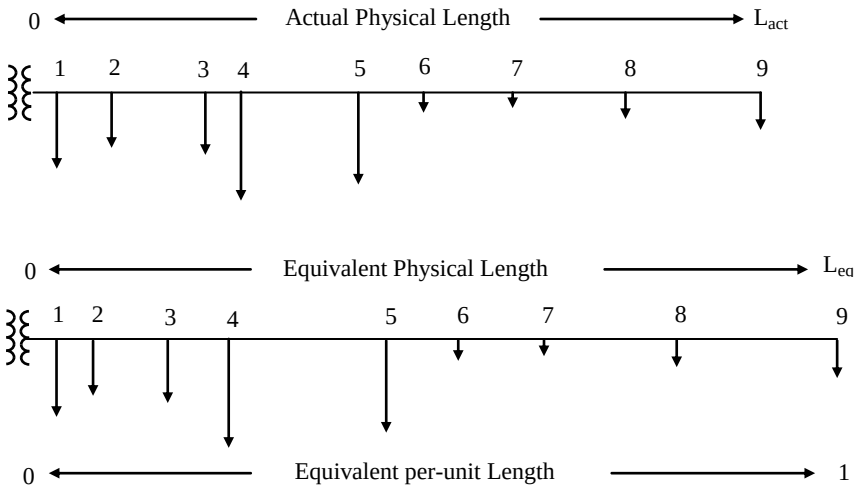

Figure 2.6 Feeders with generalized line sections of equivalent lengths

Figure 2.7 shows equivalent radial distribution feeder with three fixed capacitors (n=3). The variables hi and Ici denote the location and size of each of the three capacitors respectively.

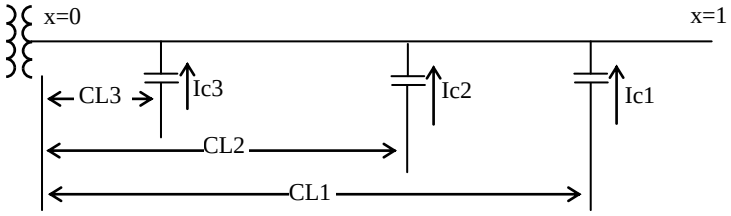

Figure 2.7 Radial distribution feeder with three fixed capacitors

The line peak power loss reduction (ΔPPL) and energy loss reduction (ΔEL) are calculated by taking the difference in losses before and after capacitors connection. The net saving resulting from ΔPPL and ΔEL is given by Eq.2.13. Where K_P, K_E, & K_C are constants converting losses and capacitor rating into money:

$$S = K_P\,\Delta PPL + K_E\,\Delta EL - K_C \sum_{i=1}^{n} I_{Ci} \qquad (2.13)$$

The optimal locations for capacitors of specified ratings, and vice versa, are determined by setting the first derivative of Eq.2.13, with respect to hi and Ici separately, equal to zero.

Grainger and Lee developed their work further determining the optimal hi and Ici both together. They developed a certain procedure called Equal Area Criterion (EAC) managing the interaction between the two variables. The procedure requires that the power flow distribution along the feeder is smoothed and curved into the shape of Fig.2.8. Starting with an arbitrary location for CL1, an initial capacitor rating Ic1 is determined. The contour I is drawn through g1 determining CL2 that gives equal areas A1 and B1. The same procedure is applied consecutively until contour III is drawn. At that stage, if A3≠B3 the process is iterated with a revised value of CL1, and so on until meeting a tolerance value of equal areas.

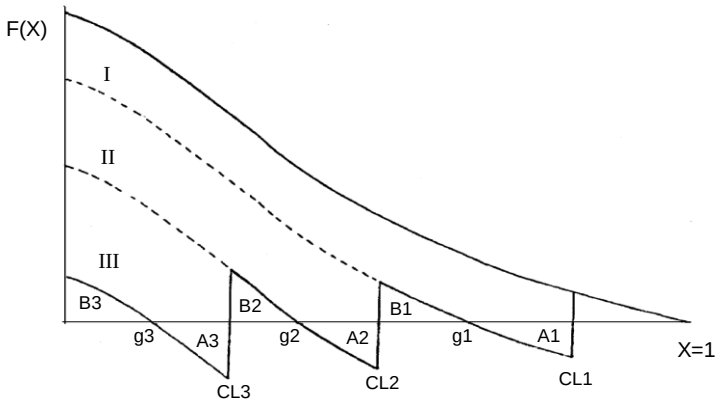

Figure 2.8 Procedure of determining the optimal hi and I_{ci} for n=3

In [4], Grainger and Lee presented a voltage-dependent methodology optimizing the size and location of fixed capacitors while accounting for voltage variation along the feeder. Thus, for the feeder of Fig.2.9, the voltage at node i is denoted by |Vi|δi with all phase-angles measured with respect to the voltage at the substation. Consequently, an ac power flow technique is included in the iterative procedure of determining the optimal values of Ici and hi.

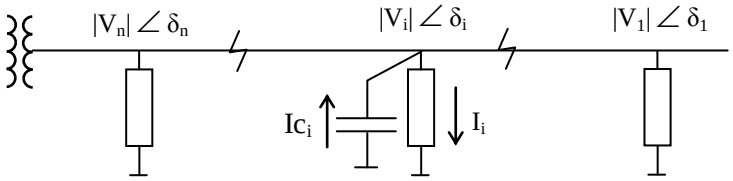

Figure 2.9 Radial distribution feeder with voltage notation

It is worth a mention that further research was conducted considering switched capacitors [14, 15] and continuous capacitive compensation [16 & 17].

Despite the developments been achieved by Grainger and Lee, their works had also ended up with several shortcomings. The major ones are the 3-phase balanced load modeling of the feeder and overlooking the influence of RPF.

Baran and Wu [18] have contributed the efforts of engaging the non-linear-programming methods in the optimization procedures. They developed a methodology for optimal sizing of specified capacitors placed on the feeder of Fig.2.10. Voltage profile and cost of capacitors were included in the analysis.

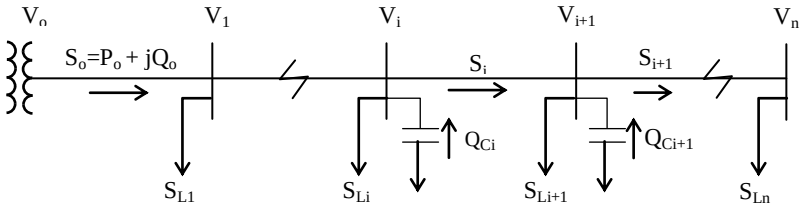

Figure 2.10 One line diagram of the main radial feeder

As the voltage profile was considered, they incorporated an ac power flow technique in the optimization process. In this course, a new formulation of power flow equations for radial distribution feeders, called Dist-Flow, is presented. According to the figure, the substation voltage (V_o) is assumed constant. The line sections along the feeder are modeled by a series impedance $Z_i = R_i + jX_i$ while loads are modeled as $S_i = PL_i + jQL_i$. The shunt capacitors at the nodes of the system are modeled by reactive power sources. With this representation, the feeder becomes like a ladder circuit with nonlinear shunt loads.

If the total power supplied from the substation, $S_O = P_O + jQ_O$, is known then the following formulas are derived for each line section based on Fig.2.10.

$$P_{i+1} = P_i - \frac{R_{i+1}(P_i^2 + Q_i^2)}{V_i^2} - P_{Li+1} \quad (2.14.a)$$

$$Q_{i+1} = Q_i - \frac{X_{i+1}(P_i^2 + Q_i^2)}{V_i^2} - Q_{Li+1} + Q_{Ci+1} \quad (2.14.b)$$

$$V_{i+1}^2 = V_i^2 - 2(R_{i+1}P_i + X_{i+1}Q_i) + \frac{(R_{i+1}^2 + X_{i+1}^2)(P_i^2 + Q_i^2)}{V_i^2} \quad (2.14.c)$$

Where,

Pi & Qi	- Real & reactive power flow into the sending end of section i+1
Vi	- Node voltage magnitude at node i
QCi	- Reactive power injection by the capacitor at node i

To solve for the optimal sizing of 'N' fixed capacitors, the objective function below is placed comprising two terms. The first term is for the line real power losses along the feeder while the second is for the cost of capacitors.

$$F = K_P\, P(x) + \sum_{i=1}^{N} K_{Ci}\; Q_{Ci} \quad (2.15)$$

Where, P(x) is the real power losses along the feeder. K_P is the cost factor for the real power losses, while K_{Ci} and Q_{Ci} are the cost and rating of installed capacitor at node i respectively.
The authors solved the nonlinear programming problem for optimal Q_{Ci} that minimizes the objective function F, subject to specified constraints, as follows:

Minimize F, (2.16)

Subject to,

- complying with the power flow of Eqs.2.14
- $\min V_i^2 \le V_i^2 \le \max V_i^2$
- $0 \le Q_{Ci} \le \max Q_{Ci}$

The formulation of Eq.2.16 is solved using first order optimization method called Phase I-Phase II Feasible Direction Method, obtaining the solution in two phases. In Phase I, a feasible point is obtained if the initial point was infeasible. While in Phase II, the solution is improved iteratively until the solution converges to the optimal point.

In [19], the same authors developed their optimization procedure, this time to identify both the optimal location and sizing of the capacitors. The solution is based on the decomposition of the problem into hierarchical levels. The problem at the top level, called the master problem, is an integer programming problem and is used to place the capacitors. A search algorithm was developed for this purpose. The problem at the bottom level is solved to identify the type (fixed or switched) and the size of already located capacitors. The work assumed 3-phase balanced load modeling and overlooked the influence of RPF.

2.2 Optimal Sizing and Location of DG Units

During the last two decades, connection of Distribution Generation (DG) units on distribution feeders has significantly evolved. Unlike shunt capacitors, DG units are not limited to reactive power generation as they can deal with real and reactive power at the same time. To this end, connection of DG units on distribution feeders has a wide impact on the performance of distribution network. With proper installation of DG systems, significant benefits could be acquired in terms of reducing power and energy losses, releasing KVA capacity, improving voltage profile, real and reactive power flow control, improving network reliability amongst others.

Many works dealing with optimal sizing and location of DG units on radial distribution feeders are reviewed in this chapter. The work of Willis [20] who used the uniformly distributed load model in discussing the relation between RPF and the sizing and location of DG units provides a suitable starting point. He presented a concept called ‘Zero Point Analysis’ and applied it on the feeder. The concept focuses on a point on the feeder (if it exists) where power flow is zero due to the DG unit output. Accordingly, he put the impact of DG units into two categories:

1. The output of the DG unit is less than the total load demand of the downstream nodes from the point of common coupling (PCC) to the end of the feeder. In this case the power flow in the line sections between the substation and the PCC is reduced. A model of uniformly distributed feeder with 2miles length and 4MW total demand is taken as example. A DG unit of 1MW is connected 1mile from the substation, as illustrated in Fig.2.11. The dotted line shows the reduction in power flow profile along the feeder.

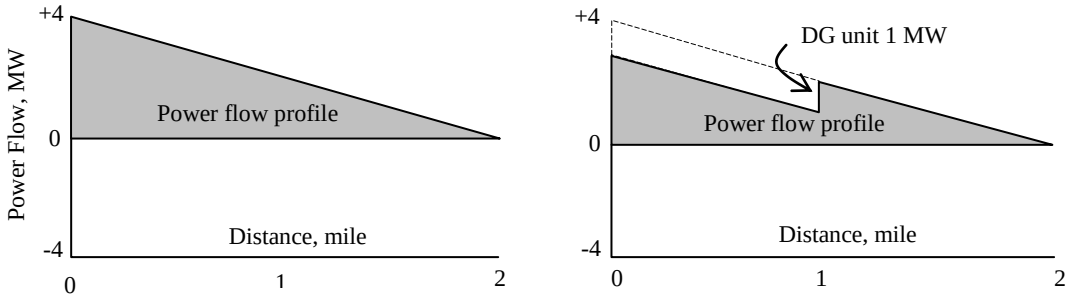

Figure 2.11 DG unit output lower than the total demand of downstream nodes

2. The output of the DG unit exceeds the load demand of the downstream nodes from the PCC to the end of the feeder. In such a case the DG unit reverses the surplus power it generates in the upstream direction towards the substation. To represent this category, the DG unit size is raised to 3MW that turns the power flow profile into the shape of Fig.2.12. The figure shows zero point is created between the substation and the PCC.

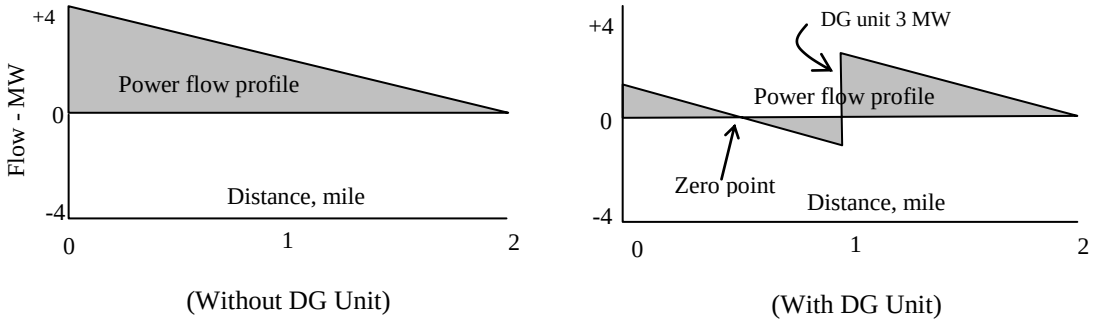

Figure 2.12 DG unit output exceeds the total demand of downstream nodes

Willis [20] analyzed the impact of the DG unit on the line losses in a similar way to the old 2/3 rule-of-thumb used with capacitors placement on uniformly distributed feeders. He suggested the same rule for the DG unit by sizing it to 2/3 of the total feeder load, at 2/3 the distance from the substation. The method combines almost all of the shortcomings been stated so far in the previous works.

Hoff and Shunger [21] developed a method to simulate the line peak power and energy loss savings based on the daily load and the PVDG unit output along with few distribution system characteristics. To calculate the line power losses on 3-phase radial distribution feeder, the basic equation '$3.I_F^2.R$' is applied. I_F and R are the 1-phase instantaneous current and the resistance of the line respectively. Hence, the instantaneous line power loss saving (SL) in a line section

affected by PVDG unit is equal to the difference between losses before and after connecting PVDG unit(s). This relation is derived as Eq.2.17 below:

$$SL = 3.I_F^2.R - 3(I_F - I_{PV})^2.R = 6.R.I_F.I_{PV} - 3.R.I_{PV}^2 \quad (2.17)$$

The formula of LS is expressed for any n-sections radial feeder shown in Fig.2.13 as follows:

$$SL = \left(6.I_F.I_{PV}\sum_{i=1}^{n} a_i\ b_i\ R_i\right) - \left(3.I_{PV}^2\sum_{i=1}^{n} b_i^2\ R_i\right) \quad (2.18)$$

Where, a_i is the fraction of current flows in section i in terms of I_F while b_i is the fraction of I_{PV} summation on the remainder sections after i in terms of total I_{PV} on the whole feeder.

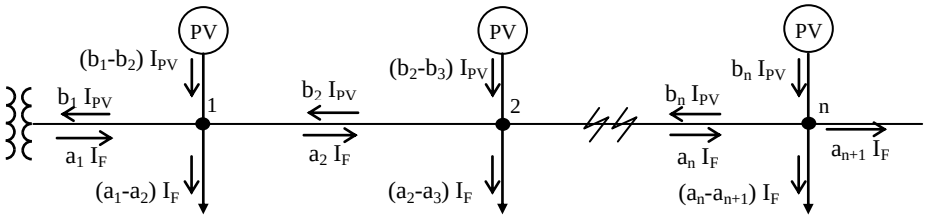

Figure 2.13 Current flow on a distribution feeder with multi DG units

The authors [21] rewrote Eq.2.18 in terms of the instantaneous power of the PVDG unit in MW (PV), size of the PVDG unit in MW (S), and the 3-phase load of the feeder in MVA (L_F). Note that I_F is substituted by L_F divided by $\sqrt{3}$ times line-to-line voltage (V). At the end, the derivation resulted in the formula of Eq.2.19 below:

$$SL = A\ (L_F\,PV)\ S - B\ (PV^2)\ S^2 \quad (2.19)$$

Where,

$$A = \frac{\sum_{i=1}^{n}(a_i\ b_i\ R_i)}{500V^2} \quad \text{and} \quad B = \frac{\sum_{i=1}^{n}(b_i^2\ R_i)}{1000V^2}$$

Equation 2.19 is extended to calculate line energy loss savings (SEL) by taking the summation of line power loss savings on hourly basis over a time period of m hours. The extension resulted in Eq.2.20, where j is the index of hours over time of m hours:

$$SEL = A\left(\sum_{j=1}^{m} L_{Fj}\ PV_j\right)S - B\left(\sum_{j=1}^{m} PV_j^2\right)S^2 \quad (2.20)$$

For already known locations, the optimal size of the PVDG units (S) is determined by taking the first derivative of Eq.2.20 with respect to S, setting the result equals to zero. Then, a certain formula is placed by the authors to calculate bi on each node so that S is distributed properly along the feeder.

As it can be seen, the work in [21] is based on solving the optimization problem considering either line peak power or energy losses. The work assumed that the locations of the PVDG units are already known. Also 3-phase balanced load model with flat voltage profile was considered. Moreover, the energy loss calculations are repeated on hourly basis over the day, while the impact of RPF is overlooked.

In [3], Griffin et al. presented an algorithm determining the optimal locations of DG units that have specified sizing. The analyses are performed considering line peak power losses and capacity release savings. The authors presented two distribution feeder models for uniformly distributed loads and uniformly increasing distributed loads, as shown in Fig.2.14.

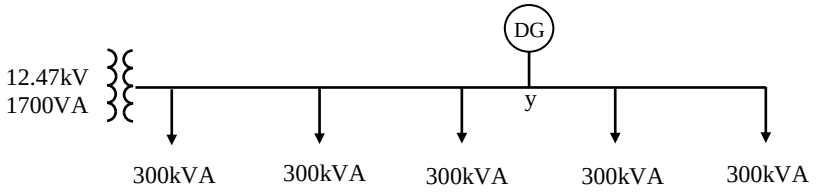

(a) Uniformly distributed loads)

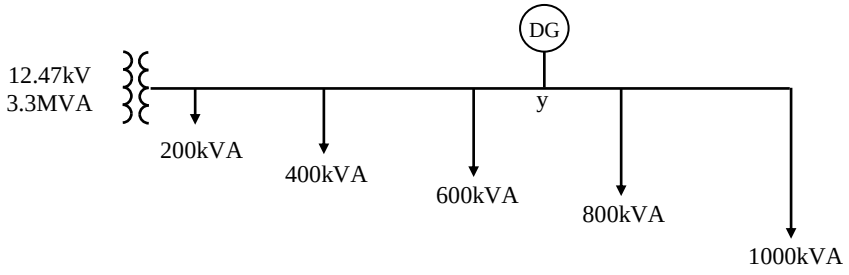

(b) Uniformly increasing distributed loads)

Figure 2.14 Feeder with uniformly distribution loads

The original line peak power losses considering uniformly distributed loads (PL_U), is given by Eq.2.21. Where I(x) is the current at location 'x' from the end of the feeder and 'L' is the feeder length. While 'I_o' and 'R' are the total per-unit current and resistance of the feeder respectively:

$$PL_U = \int_0^L I^2(x)\, R\, d(x) = I_o^2\, R \int_0^L x^2\, dx = \frac{1}{3} I_o^2\, R\, L^3 \qquad (2.21)$$

Assuming one DG unit of output current 'I' is connected at location 'y', the derivation of line peak power losses yields:

$$PL_U = R\left(I_o^2 \int_0^L x^2\, d(x) - 2I\, I_o \int_y^L x\, dx + I^2 \int_y^L dx \right) \quad (2.22)$$

$$= \frac{1}{3} I_o^2\, R\, L^3 - 2I\, I_o\, R(L^2 - y^2) + I^2 R(L - y) \quad (2.23)$$

Differentiating Eq.2.23 with respect to 'y' and setting the result equals to zero, results in the following equation for the optimal location of the DG unit:

$$y = \frac{I}{2I_o} \quad (2.24)$$

Applying the same derivation to the uniformly increasing distributed loads feeder, the line peak power losses (PL_{UI}) with DG unit at point y is ended up with:

$$PL_{UI} = I_o^2\, R\left(\frac{L^3}{5} - L^2\, y - 2L\, y^2 + \frac{2}{3}\, y^3\right) \quad (2.25)$$

Similarly, differentiating Eq.2.25 with respect to 'y' and setting the result to zero can give the optimal location of the DG unit.

As it can be seen, the work of Griffin et al is modeled on the basis of a uniformly distributed load feeder, which is usually not the case in actual conditions. Also it determined the optimal location of the DG unit assuming the size is already known. Additionally, it assumed a 3-phase balanced load feeder and it solved the problem considering line peak power losses only.

Later on, some works tried to apply heuristic techniques in solving the optimization problem. Of these are the works in [22, 23, 24 & 25]. They tried to solve for optimal DG sizing and location using Genetic Algorithm (GA) method. The GA method is suitable for multi-objective problems, like DG sizing and location. However, these methods are also computationally demanding and slow in convergence [26].

In this course, Haesen et al. [24] tried to apply the GA technique in finding the optimal sizing and location of a set of PVDG and CHP units. The optimization problem is solved considering minimization of line energy losses. It defines strings G1 and G2 such that each one of them consists of five binary bits; G1 related to the PVDG units and G2 to the CHP units. The first bit of each string shows the state of the unit (1 for 'On' and 0 for 'Off'). The remaining 4 digits are dedicated to show the size of the DG unit; for example 0000 for zero size, 1000 for 1/16 of full capacity and 1111 for full capacity. Thus, the string G1= [11111] means a PVDG unit works at full capacity, and so on. Now for any node a new string T= G1G2 is defined to show the status

of the PVDG and CHP units at this node. For example, T= [1111100000] means only PVDG unit is connected and it works at full capacity. In this study, only one DG unit was allowed per node.

For a feeder with 20 nodes, a string S is defined consisting of 20 T that ended up with 200 bits representing the status of the whole feeder. Thus, any string S represents a set of solution for the feeder and therefore it corresponds to the chromosome in the GA analyses.

At this stage, the authors proposed to implement the optimization by initiating 40 strings 'S' then compute the fitness of each one of them based on the line energy loss reduction it yields. The strings are ranked in this iteration according to their fitness. At the end of the iteration another 40 strings based on the previous set are produced by a certain genetic operator. The process is iterated over a number of cycles (300 in the example) until getting the 'S' of best fitness. The authors applied this procedure on a 20 nodes feeder and ended up with the optimal solution that around 50% of the nodes should be connected to DG units.

Nevertheless, the authors assumed 3-phase balanced load feeder and no problem with RPF. Additionally, the checking on the fitness required energy-based calculation over the whole daily duration. Moreover, their case study has ended up with optimal solution that about 50% of feeder nodes should be connected to DG units. This rate looks like impractical for one distribution feeder especially with PVDG units. It is worth mentioning that Ho Kim et al., in [23], considered the number of DG units as constraint but didn't solve the other shortcomings.

In other works, like [25 & 27], the authors applied GA method using line peak power losses in their fitness formula, but disregarding line energy losses this time. The work of Borges and Falcao [25] is one of these. Additionally, they incorporated the capital cost of the DG unit in the formula. Also they considered the feeder reliability as a constraint in addition to the normal voltage constraint.

Apart from missing the consideration of line energy losses in the fitness formula, the authors assumed always available DG energy to ensure acceptable reliability. This assumption could be adequate for traditional DG units like gas generators, but it's not for time-variant energy sources like PVDG units. Also, they kept the assumptions of a 3-phase balanced load feeder and overlooked the RPF impact.

In [2], AlHajri et al. incorporated Non-Linear-Programming (NLP) methods in the optimization problem. This approach has the impact of using NLP methods in updating the calculated possible solution in the feasible hyperspace at the end of iteration before going into the next iteration. On the other hand, the main body of the optimization problem is kept the same so that

it solves for minimization/maximization of objective function subject to sets of equality and/or inequality constraints. In this work, the authors have solved for minimization of line peak power losses (P_{Loss}) subject to satisfying the voltage constraints, as follows:

$$P_{Loss} = \sum_{i=1}^{n} I_i^2 . R_i \tag{2.26}$$

Where; I_i is the current in branch i, n is the total number of line sections in the system, and R_i is the section resistance. Hence, the objective function to be minimized is:

$$\text{Minimize} \qquad P_{Loss} \tag{2.27}$$

The equality constrains are set to be the non-linear power flow equations of the radial distribution system. While the inequality constraints are the voltage limits at each bus j along with the limits of output power produced by the DG unit, as follows:

$$V_j^{min} \leq V_j \leq V_j^{max} \tag{2.28}$$

$$P_{DG}^{min} \leq P_{DG} \leq P_{DG}^{max} \tag{2.29}$$

The authors treated the DG unit as a PQ bus of negative load delivering power with a lagging power factor of 0.85. The optimization problem is solved by incorporating the Particle Swarm optimization (PSO) considering possible solutions as a number of particles fly as a swarm or group in the problem feasible hyperspace. Each particle i is associated with two vectors namely position 'x_i' and velocity 'v_i'. The particles update their vectors, over each iteration k, using the following equation:

$$V_i^{k+1} = wv_i^k + c_1 r_1 \left(pbest_i - x_i^k\right) + c_2 r_2 (gbest_i - x_i^k) \tag{2.30.a}$$

$$x_i^{k+1} = x_i^k + v_i^{k+1} \tag{2.30.b}$$

Where
- c_1 & c_2 are two positive acceleration constants,
- r_1 & r_2 are two randomly generated numbers with a range of (0, 1),
- w is the inertia weight,
- pbest is the best solution achieved by individual particle, and
- gbest is the best solution achieved among the entire swarm.

The problem is solved for a single DG unit and applied on a 69-bus distribution system, consisting of a main radial distribution feeder with seven laterals. The solution yielded optimal values that showed successful results in minimizing the line peak power losses and improving the voltage profile.

Equation 2.30 was improved by Prommee and Ongsakul [28] with a formula updating the inertia weight (w) throughout the iteration process. The formula based on the fact that w is used

to regulate the trade-off between the local and global exploration abilities of the swarm. A large w facilitates global exploration, minds that PSO tends to have more global search ability at the beginning of the run while having more local search ability at the end. Consequently, w is updated through Eq.2.31, where K is the pre-defined maximum number of iterations; while w_{max} and w_{min} are demonstrated to be 0.9 & 0.4 respectively.

$$w^{k+1} = w^{k} + \frac{(w_{min} - w_{max})}{K} \tag{2.31}$$

In [6 & 29], AlHajri and El-Hawary tried to incorporate Sequential Quadratic Programming in their optimization process. The work in [5] investigated the effect of optimal sizing and location of single and multiple DG units on the voltage profile of the feeder. At the beginning, they solved for optimal location of single DG unit that minimizes the line peak power losses of 33-bus feeder. Nevertheless, they found that such a location failed to keep the voltage profile along the feeder from going below the limits at many nodes. Accordingly, the problem is solved for two DG units that resulted in slightly higher power losses, but with a healthy voltage profile along the whole feeder.

The same authors extended their work in [30] to investigate the modeling impact of each of the DG unit and static load on the losses, voltage profile and DG sizing. They tried different modeling of DG units and static loads. Thus, they modeled the DG units as PQ-bus and PV-bus; and the static loads as constant power, constant current and constant impedance models. Each DG model is tested and optimally sized against the three different static load representations. The problem is solved by incorporating Sequential Quadratic method. The PQ-bus model of the DG source is represented by a negative load delivering real power at specified power factor. While the PV-bus model is represented by a real and reactive power source that secures the terminal voltage at a specific value. Regarding static load representation, the voltage dependency of static load characteristics is considered. Thus, it is represented as follows, mind that α and β determine the type of the static load:

$$P = P_o(\frac{V}{V_o})^{\alpha} \qquad \text{and} \qquad Q = Q_o(\frac{V}{V_o})^{\beta} \tag{2.32}$$

Where, V_o is the nominal voltage, V is the operating voltage; while P_o and Q_o are the real and reactive power consumed by the load at the V_o. For equality constraints, the nonlinear power flow equations should be satisfied throughout the iteration process. As for inequality constraints, they are manifested by lower and upper limits imposed on the real and reactive power flows, as well as the feeder ampacity and the substation capacity limits.

Regarding the aforementioned works incorporating NLP methods, it can be seen that the shortcomings been identified earlier are almost still available. As a matter of fact, they solved for line peak power loss benefits but disregarded the energy losses benefits. Also they disregarded the influence of RPF. Moreover, they assumed traditional DG units with controllable power production, which is not aligned with time-variant DG units like PV. Besides, they modeled the feeder in 3-phase balanced load status.

The work reviewed so far in this chapter has shown a sort of 'luck' in dealing with the optimal sizing and location of PVDG units. Also those that have dealt with this issue have most likely considered part of the relevant parameters but overlooked others. Moreover, most of them missed dealing efficiently with the correlation between the load curve of the feeder and the production curve of the PVDG unit.

Regarding the correlation between the load and PVDG production curves, the work of F. Viawan et al. [31] may worth a mention. It used a probabilistic approach to assess the optimal PVDG sizing based on annual statistical model for the solar irradiance and load demand. The statistical model is placed by developing a probabilistic curve for each of the irradiance and load variation. Each curve is generated based on thousands of daily measurements for the both. However, the work correlated between the two curves in terms of comparing average values. Actually this may miss the efficient correlation between the corresponding values on the two curves as a function of time.

J.K. Kaldellis et al. [32], dealt with the load and PVDG production curves by splitting the daily duration into two separate periods, one during sunlight and the other during the rest of the day. On the other hand, they did their analysis assuming storage system to store any possible surplus energy from the PVDG unit. Thus, the correlation between the two curves is seemed to be no longer real.

In [33], Richard Perez et al. mentioned the inconvenience of the non-dispatchable nature of the power produced by PVDG units. They raised the idea of an anticipated relation between the PVDG system output and the summer peak load demand in hot summer regions. They built their idea on the opinion that peak demands are likely driven by the cooling load that reaches its maximum at the time the PVDG unit gives its best.

However, the peaks of load curve and PVDG production curve are not necessarily matching in time, even in hot summer regions. This has been manifested by A. AlSabounchi et al. [34], based on six case studies for existing 11kV distribution feeders in Abu Dhabi city, known by its hot summer season. The summer peak load demands (PLD) of the feeder along with their associated peak load times (PLI) are illustrated in Fig.2.15. The figure shows that the PLT of

four of the six feeders occur at late daylight hours, while the other two showed PLT even after nightfall. According to the figure, the average PLT of the six feeders is at 5:30pm which is far from noon time during which the PVDG unit gives its peak.

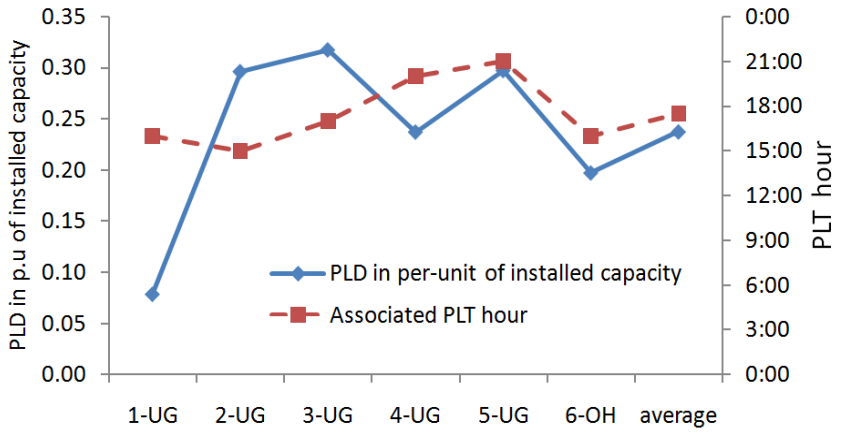

Figure 2.15 Summer PLD and PLT of six case study feeders in Abu Dhabi

In light of the mismatch in the peaks of the load and PVDG production curves, the work in [34] concluded that consideration of line peak power losses could make no sense in hot summer regions like Abu Dhabi. The reason is that the PVDG unit can produce only part of its capacity at the PLI when the feeder is loaded to its peak. Alternatively, the work recommended solving the optimization problem considering the accumulated line power losses over the day, namely line energy losses. At the same time the reduction in line peak power losses is still considered as sub-benefit, provided that the PLT occurs during daytime hours.

2.3 Summary on Reviewed Literature

A significant number of credible previous works have been reviewed over the period from fifties up to 2010. The review is deemed providing reliable background about the potential approaches of optimal sizing and location of autonomous power sources on radial distribution feeders. The works have been compiled into two categories, starting with the former concept of connecting shunt capacitors for reactive power control purposes. The second category is dedicated to cover the development of the concept towards the connection of DG units aiming at a set of significant benefits. Both categories reviewed works presenting various methods for solving the optimization problems. Some works went for analytical methods, others used genetic algorithm, and another incorporated nonlinear programming techniques, like particle

swarm analysis or sequential quadratic, in the process. The objective function is most likely placed in terms of line peak power loss reduction (ΔPPL) and/or line energy loss reduction (ΔEL). The objective function is placed usually subject to several equality and inequality constraints related to system voltage profile and feeder ampacity along with capacity and cost of DG units.

On the other hand it has been concluded that the majority of reviewed works modeled the distribution feeder in 3-phase balanced load status, which is not the case in actual conditions. In addition to that, many works used to apply their approaches on dispatchable DG units of controllable power generation rates. This does not go along with the case of stochastic power sources with time-variant behavior like PVDG systems. In the event of a PVDG unit the optimization process deals with the feeder load curve and the PVDG production curve that are different in shape but affecting the same feeder. In such a case, an efficient correlation between the two curves becomes significant in considering the impact of the both in the optimization process. It is worth mentioning that dealing with load and PVDG production curves over time requires consideration of energy-based quantities. The trend of previous works in considering such quantities is to repeat the calculation on hourly basis (or even shorter intervals) over the targeted duration then take the overall summation, which is deemed a time consuming process.

Apart from above, the RPF towards the substation was not clearly considered in the previous works. As been stated in Section 1.3, reverse power could disturb the performance of voltage regulator [35] alongside the unidirectional protection devices [36]. Also, it may increase undesirably the voltage level and current at some parts of the feeder. Additionally, it set out the line power losses to go up again in the upstream direction [37]. Over and above, RPF complicates the islanding protection of inverter-based DG units [38]. Upgrading the control system of the substation with intelligent bidirectional protection and control devices could deal with the above inconveniences. However, the system were originally designed and set to operate with unidirectional performance. Therefore, this may lead to a sort of unstable operation. The idea is that in case the intelligent devices are adjusted to be effective during DG operation, it should be also effective when the DG unit is not working [39].

This work aims at contributing the valuable efforts in the field been reviewed in this chapter. It considers several related issues that are deemed deserve more attention and further development.

References

[1] A.O. Zue & A. Chandra, "Grid Connected Photovoltaic Interface with VAR Compensation and Active Filtering Functions," *in Proc. Dec. 2006 IEEE International Conference on Power Electronics, Drives and Energy Systems (PEDES '06)*, pp. 1 – 6.

[2] M. F. AlHajri, A. R. AlRashidi, and M. E. El-Hawary, "Hybrid Particle Swarm Optimization Approach for Optimal Distribution Generation Sizing and Allocation in Distribution Systems," *in Proc. Apr. 2007 IEEE Canadian Conference on electrical and computer engineering*, Canada, pp.1290 – 1293.

[3] T. Griffin, K. Tomsovic, D. Secrest, and A. Law, "Placement of dispersed generation systems for reduced losses," *in Proc. Jan.2000 IEEE 33rd Annual Hawaii International Conference on System Sciences*, vol.4, pp. 4043.

[4] J.J. Grainger and S.H. Lee, "Capacity Release by Shunt Capacitor Placement on Distribution Feeders: A New Voltage-Dependent Model," *IEEE Transactions on Power Apparatus and Systems*, vol. PAS-101, Issue 5, pp.1236 – 1244, May 1982

[5] S. Huang and F. Pai, "Design and operation of grid-connected photovoltaic system with power-factor control and active islanding detection," IEE Proc. Generation, Transmission and Distribution, vol.148, Issue 3, pp.243 – 250, May 2001.

[6] M. F. AlHajri and M. E. El-Hawary, "Improving the voltage profiles of Distribution Networks using multiple Distribution Generation Sources," *in Proc. Oct. 2007 IEEE Conference on Power Engineering, 2007 Large Engineering Systems*, pp.295 – 299.

[7] N. M. Neagle and D. R. Samson, "Loss Reduction from Capacitors Installed on Primary Feeders," *AIEE Trans.* part III, vol. 75. pp. 950-959, Oct 1956.

[8] R. F. Cook, "Analysis of Capacitor Application as Affected by Load Cycle," *AIEE Trans*. part III, vol. 78, pp. 950-956, April 1959.

[9] R. F. Cook, "Optimizing the Application of Shunt Capacitors for Reactive-Volt-Ampere Control and Loss Reduction," *AIEE Transaction*, part III, vol. 80, pp. 430-444, Aug.1961.

[10] H. Duran, "Optimum Number, Location, and Size of Shunt Capacitors in Radial Distribution Feeders," *IEEE Trans. on on Power Apparatus*, vol. Pas-87, no.9, pp. 1769-1775, Sep 1968.

[11] J. V. Schmill, "Optimum size and location of shunt capacitors on distribution feeders," *IEEE Trans. Power Apparatus and Systems*, vol. 84, pp. 825-832, Sep.1965.

[12] N. E. Chang, "Locating shunt capacitors on primary feeder for voltage control and loss reduction," *IEEE Trans. Power Apparatus and Systems*, vol. 88, pp. 1574-1577, Oct.1969.

[13] J. J. Grainger and S. H. Lee, "Optimum Size and Location of Shunt Capacitors for Reduction of Losses on Distribution Feeders," *IEEE Trans. on Power Apparatus and Systems*, vol. PAS-100, no.3, pp.1105-1118, Mar.1981.

[14] S. H. Lee and J. J. Grainger, "Optimum Placement of Fixed and Switched Capacitors on Primary Distribution Feeders", *IEEE Trans. on Power Apparatus and Systems*, vol. 100, pp. 345-352, Jan.1981.

[15] M. Ponnavaikko and K. S. hakasa Rao, "Optimal Choice of Fixed and Switched Shunt Capacitors on Radial Distribution Feeders by the Method of Local Variations", *IEEE Trans. on Power Apparatus and systems,* vol. 102, pp.1607-1614, June 1983.

[16] J. J. Grainger, S. H. Lee, and A. A. El-Kib. "Design of a Real-Time Switching Control Scheme for Capacitive Compensation of Distribution Feeders", *IEEE Trans. on Power Apparatus and Systems.* vol. 101. pp. 2420-2428. Aug.1982.

[17] J. J. Grainger. S. Civanlar, and S. H. Lee, "Optimal Design and Control Scheme for Continuous Capacitive Compensation of Distribution Feeders", *IEEE Trans. on Power Apparatus and Systems*, vol. 102, pp. 3271-3278, Oct.1983.

[18] M.E. Baran and F.F. Wu, "Optimal Sizing of Capacitors Placed on a Radial Distribution System," *IEEE Trans. on Power Delivery*, vol.4, no.1, pp.735-743, Jan.1989.

[19] M.E. Baran and F.F. Wu, "Optimal Capacitor Placement On Radial Distribution Systems," IEEE Transactions on Power Delivery, vol. 4, no. 1, pages 725 – 734, Jan.1989.

[20] H.L. Willis, "Analytical methods and rules of thumb for modeling DG-distribution interaction," *in Proc. Jul.2000 IEEE Power Engineering Society Summer Meeting,* vol.3, pp.1643 - 1644.

[21] T. Hoff, and D.S. Shugar, "The value of grid support photovoltaic in reducing distribution system losses", *IEEE Trans. Energy Conversion*, vol. 10, no. 3, pp. 569-576, Sep. 1995.

[22] G. Celli and F. Pilo, "Optimal distributed generation allocation in MV distribution networks", *in Proc. May 2001 IEEE Power Industry Computer Applications Conf.*, pp. 81-86.

[23] K.H. Kim, Y.J. Lee, S.B. Rhee, S.K. Lee, S.K. You, "Dispersed Generator Placement using Fuzzy-GA in Distribution Systems," *in Proc. Jul.2002 IEEE Power Engineering Society Summer Meeting,* vol.3, pp.1148 – 1153.

[24] E. Haesen, M. Espinoza, B. Pluymers, I. Goethals, V. Thong, J. Driesen, R. Belmans, and B. DeMoor "Optimal Placement and sizing of distributed generator units using genetic optimization algorithms", Electrical Power Quality and Utilization Journal, vol. XI, no.1, pp. 97-104, 2005.

[25] L.T. Borges and M. Falcao, "Optimal distributed generation allocation for reliability, losses, and voltage improvement", *Electrical Power and Energy Systems Journal*, vol. 28, pp. 413–420, 2006.

[26] N. Acharya, P. Mahat, and N. Mithulananthan, "An analytical approach for DG allocation in primary distribution network," Electrical Power and Energy Systems Journal, vol. 28, pp.669–678, 2006.

[27] R. Singh and S. Goswami, "Optimum Sitting and Sizing of Distributed Generations in Radial and Networked Systems", *Electric Power Components & Systems Journal*, vol. 37, pp. 127-145, Feb. 2009.

[28] W. Prommee and W. Ongsakul, "Optimal Multi-Distributed Generation Placement by Adaptive Weight Particle Swarm Optimization", *in Proc. Oct. 2008 IEEE Control, Automation & Systems Conf*., pp.1663-1668.

[29] M. AlHajri and M. El-Hawary, "Optimal Distribution Generation Sizing via Fast Sequential Quadratic Programming", *in Proc. Oct. 2007 IEEE Power Engineering Conf.*, pp. 63–66.

[30] M. F. AlHajri and M.E. El-Hawary, "The effect of Distributed Generation modeling and static load representation on the optimal integrated sizing and network losses," *in Proc. May 2008 IEEE Canadian Conference on Electrical and Computer Engineering (CCECE 2008)*, pp.1543–1548.

[31] F.A. Viawan, F. Vuinovich, and A. Sannino, "Probabilistic Approach to the Design of Photovoltaic Distributed Generation in Low Voltage Feeder," *in Proc. Jun.2006 International Conference on Probabilistic Methods Applied to Power Systems*, pp.1–7.

[32] J.K. Kaldellis, D. Zafirakis, and E. Kondili, "Optimum sizing of photovoltaic-energy systems for autonomous small islands," Elsevier, Electrical Power and Energy Systems Journal (2009), pp.1-13.

[33] R. Perez, M. Taylor, T. Hoff, and J.P. Ross, "Reaching Consensus in the Definition of Photovoltaics Capacity Credit in the USA: A Practical Application of Satellite-Derived Solar Resource Data," *IEEE Journal of Selected Topics in Applied Earth Observations and Remote Sensing*, vol.1, Issue 1, pp.28 -33, Mar.2008.

[34] A. Al-Sabounchi, E. Al-Hammadi, S. Yalyali, and H. Al-Thani, "Photovoltaic-Grid Connection in the UAE: Technical Perspectives", *in Proc. Sep. 2010 World Renewable Energy Congress-XI, Abu Dhabi*, pp.1207-1213.

[35] S. Conti, A. Greco, N. Messina, and S. Raiti, "Local voltage regulation in LV distribution networks with PV distributed generation", *in Proc. May 2006 IEEE Power Electronics, Electrical Drives, Automation and Motion Symposium*, pp. 519–524.

[36] Kenneth Winick, "A Guide to the Application of Power Relays for the Detection of Overpower or Reverse Power Conditions on a Power System," *A technical guide GER 2309A by General Electric Company on the applications of some power relays*, USA. http://store.gedigitalenergy.com/FAQ/Documents/GGP/GER-2309A.pdf

[37] P.N. Vovos, A.E. Kiprakis, A.R. Wallace, and G.P Harrison, "Centralized and Distributed Voltage Control: Impact of Distributed Generation Penetration", *IEEE Trans. Power Systems*, vol.22, no.1, pp. 476 - 483, Feb. 2007.

[38] T.A. Short, "Electric Power Distribution Handbook," *Electric Power Engineering Series, CRC Press LLC*, USA, 2004, ch.14

[39] G. P. Harrison, A. E. Kiprakis, and A. R. Wallace, "A new era for mini hydro?", *Article in the International Water Power and Dam Construction magazine (IWP&DC)*, 4 Nov. 2002. http://www.waterpowermagazine.com/story.asp?storyCode=2017803

3 MODELING OF RADIAL DISTRIBUTION FEEDER

The distribution substations serve their local customers by the means of primary distribution feeders that are often radial. Such feeders are extended in overhead wires or underground cables, or combination of the both. The primary distribution feeders most likely form part of a 3-phase system. Nevertheless, lateral feeders of 1-phase, 2-phase, and 3-phase systems may branch out from them. As a matter of fact, this is one of the main reasons that distribution feeders are most likely operated in unbalanced load condition. The different natures and demands of the loads served by the phases of these feeders are another reason for this unbalance. Hence, more accurate results will be realized if the line impedance modeling and the distribution power flow calculations are applied considering unbalanced load conditions. Additionally, the load demands along the feeder and the production of interfaced PVDG units should be modeled correctly in the process.

3.1 Series Impedance for Radial Distribution Feeder

The modeling of series impedance along radial distribution feeders is a matter of significant importance in running accurate power flow calculations. Several references can be found dealing with this topic. For this work, the relevant modeling is developed mainly based on reference [1]:

3.1.1 Balanced Load Feeder

The series impedance of overhead and underground distribution lines consists of the resistance of conductors and the self and mutual inductive reactance resulting from the magnetic fields surrounding the conductors. The resistance component is typically determined from the product specification sheets. On the other hand, the self and mutual reactance are determined based on several parameters characterize the type and configuration of the line.

Looking at Fig.3.1, the inductance of conductor ‘i’, in the magnetic field on ‘n’ adjacent conductors, is determined by finding its flux linkage with each of the other conductors.
Hence, the following equation of total flux linkage is applied:

$$\lambda_i = 2.10^{-7}\left(I_1 \times \ln\frac{1}{D_{i1}} + I_2 \times \ln\frac{1}{D_{i2}} + \cdots + I_i \times \ln\frac{1}{GMR_i} + \cdots + I_n \times \ln\frac{1}{D_{in}}\right) \quad (3.1)$$

Where,

λ_i - Flux linkage of conductor 'i' with 'n' adjacent conductors (Wb-t/m)
D_{in} - Distance between conductor i and conductor n (ft)
GMR_i - Geometric Mean Radius of conductor i (ft)

If the currents in the lines are balanced then, $I_1 + I_2 + \ldots + I_i + \ldots + I_n = 0$.

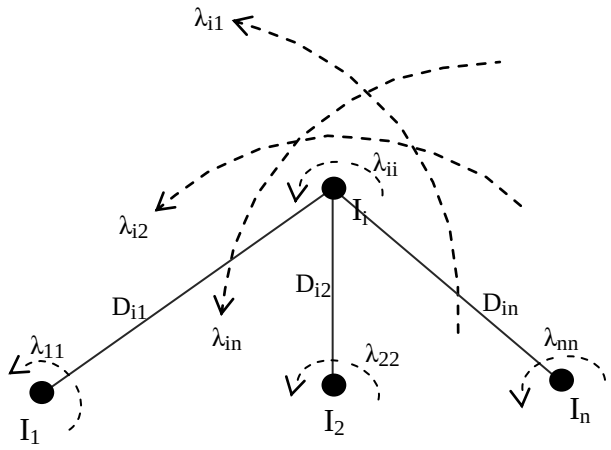

Figure 3.1 Flux linkage of conductor i with n adjacent conductors

The inductance of conductor 'i' consists of the self inductance (L_{ii}) and the mutual inductance (L_{ij}) between the conductor and all of the adjacent conductors. By definition:

$$L_{ii} = \frac{\lambda_{ii}}{I_i} = 2.10^{-7} \ln\frac{1}{GMR_i} \quad H/m \quad (3.2.a)$$

$$L_{ij} = \frac{\lambda_{ij}}{I_j} = 2.10^{-7} \ln\frac{1}{D_{ij}} \quad H/m \quad (3.2.b)$$

In the event that the 3-phase conductors of the feeder are equally loaded, the self and mutual inductances can be combined in one equation for each phase as follows [1]:

$$L_i = 2.10^{-7} \ln\frac{D_{eq}}{GMR_i} \quad H/m \quad (3.3)$$

$$D_{eq} = \sqrt[3]{D_{ab}\, D_{bc}\, D_{ca}} \quad ft \quad (3.4)$$

Where,

L_i - Phase inductance of any of the 3-phase conductors 'a, b, c'
D_{ab} - Distance between phase conductors 'a' and 'b' (ft)

For 50Hz system frequency, the reactance of any of the three phases (x_i) per one km length is expressed by multiplying Eq.3.3 in 2πf×1000. Thus, for f=50Hz,

$$x_i = 0.06285 \ln \frac{D_{eq}}{GMR_i} \quad \Omega/km \tag{3.5}$$

Hence, the series phase impedance of any of the three phases (z_i) in 3-phase balanced load feeder is given below, where r_i is the ac series resistance of the conductor.

$$z_i = r_i + j\, 0.06285 \ln \frac{D_{eq}}{GMR_i} \quad \Omega/km \tag{3.6}$$

3.1.2 Unbalanced load feeder

It was mentioned earlier that distribution feeders could be installed in 1-phase, 2-phase, and 3-phase lines serving unbalanced loads. This will most likely turned into unbalanced loading in the 3-phase primary lines. In such a case, it is rational modeling the series phase impedances of the lines in terms of self and mutual values. Additionally, the unbalanced loading will result in certain current flows in the ground/neutral return path, which should be considered also.

Back to Eq.3.2 of self and mutual inductances, the following equations of series phase impedances can be written,

$$z_{ii} = r_i + j\, 0.06285 \ln \frac{1}{GMR_i} \quad \Omega/km \tag{3.7}$$

$$z_{ij} = j\, 0.06285 \ln \frac{1}{D_{ij}} \quad \Omega/km \tag{3.8}$$

A derivation was given in [1] to calculate the self and mutual impedances of a line with ground return path. The derivation was developed based on Fig.3.2 illustrating two conductors with currents I_i and I_j connected to ground together from their ends. A virtual path 'd' is assumed carrying the return current I_d, resulting from the unbalance of I_i and I_j.

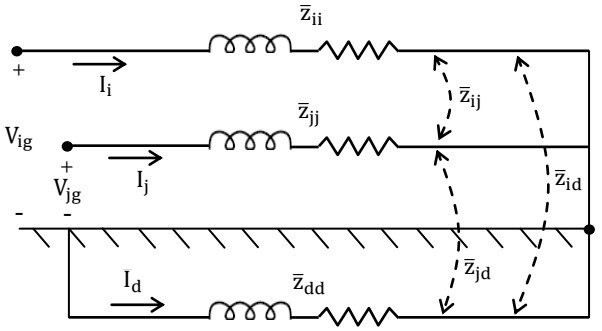

Figure 3.2 Two unbalanced conductors with virtual path for the return current flow

The application of Kirchhoff's voltage and current laws (KVL&KCL) for the voltage V_{ig} of Fig.3.2 can result in:

$$V_{ig} = \hat{z}_{ii} \times I_i + \hat{z}_{ij} \times I_j \tag{3.9}$$

Where,

$I_i + I_j = -I_d$

$$\hat{z}_{ii} = \bar{z}_{ii} + \bar{z}_{dd} - \bar{z}_{di} - \bar{z}_{id} \tag{3.10}$$

$$\hat{z}_{ij} = \bar{z}_{ij} + \bar{z}_{dd} - \bar{z}_{dj} - \bar{z}_{id} \tag{3.11}$$

Where $\hat{z}_{ii}$ and $\hat{z}_{ij}$ are called the primitive self and mutual impedances, which include the impact of the impedances in the virtual return path 'd'.

The impedance on the right hand side of Eq.3.10 and Eq.3.11 can be substituted by Eq.3.7 and Eq.3.8. Hence, the following derivations for the primitive impedances are expressed:

$$\hat{z}_{ii} = r_i + jx_{ii} + r_d + jx_{dd} - jx_{di} - jx_{id} \tag{3.12}$$

$$\hat{z}_{ii} = r_i + r_d + j0.06285 \left(\ln\frac{1}{GMR_i} + \ln\frac{1}{GMR_d} - \ln\frac{1}{D_{di}} - \ln\frac{1}{D_{id}}\right) \quad \Omega/km \tag{3.13}$$

$$\hat{z}_{ii} = r_i + r_d + j0.06285 \left(\ln\frac{1}{GMR_i} + \ln\frac{D_{di} \times D_{id}}{GMR_d}\right) \quad \Omega/km \tag{3.14}$$

Similarly,

$$\hat{z}_{ij} = r_d + j0.06285 \left(\ln\frac{1}{D_{ij}} + \ln\frac{D_{dj} \times D_{id}}{GMR_d}\right) \quad \Omega/km \tag{3.15}$$

However, applying Eqs.3.14 and 3.15 requires the values related to the virtual return path 'd' that are still unknown. In order to solve the problem, the work published by John Carson [2] is applied, where a technique was developed to determine the self and mutual impedances for an arbitrary number of conductors. The technique can be applied on both overhead and underground conductors.

According to the work in [1], the original Carson's equations for the self and mutual impedances are given as follows:

$$\hat{z}_{ii} = r_i + 4wP_{ii}G + j\left(X_i + 2wG.\ln\frac{S_{ii}}{RD_i} + 4wQ_{ii}G\right) \quad \Omega/mile \tag{3.16}$$

$$\hat{z}_{ij} = 4wP_{ij}G + j\left(2wG.\ln\frac{S_{ij}}{RD_{ij}} + 4wQ_{ij}G\right) \quad \Omega/mile \tag{3.17}$$

And,

$$X_i = 2wG.\ln\frac{RD_i}{GMR_i} \tag{3.18}$$

$$P_{ij} = P_{ii} = \pi/8 \tag{3.19}$$

$$Q_{ij} = -0.0386 + 0.5\ln\frac{2}{k_{ij}} \tag{3.20}$$

$$k_{ij} = 8.565 \times 10^{-4}.S_{ij}\sqrt{f/\rho} \tag{3.21}$$

$$Q_{ii} = 0.5 \times (7.6786 - \ln S_{ii} + 0.5\ln\frac{\rho}{f}) \tag{3.22}$$

Where,

$\hat{z}_{ii}$ - Self impedance of conductor i (Ω/mile),
$\hat{z}_{ij}$ - Mutual impedance between conductors i and j (Ω/mile),
r_i - resistance of conductor i (Ω/mile),
w = 2πf – angular frequency (rad/sec),
G = 0.1609344×10^{-3} (Ω/mile),
RD_i - Radius of conductor i (ft),
GMR_i - Geometric Mean Radius of conductor i (ft),
f - System frequency (Hz),
ρ - Resistivity of earth (Ω.meter),
D_{ij} - Distance between conductor i and j (ft),
S_{ij} - Distance between conductor i and the image of conductor j (ft),

Equations 3.18 to 3.22 are substituted wherever required into the original Carson's Eqs.3.16 and 3.17. The resulting expressions are solved and simplified accordingly giving the following equations of self and mutual primitive impedances (in Ω/mile) [1]:

$$\hat{z}_{ii} = r_i + 0.001588.f + j0.0020223.f\left(\ln\frac{1}{GMR_i} + 7.6786 + 0.5\ln\frac{\rho}{f}\right) \tag{3.23}$$

$$\hat{z}_{ij} = 0.001588.f + j0.0020223.f\left(\ln\frac{1}{D_{ij}} + 7.6786 + 0.5\ln\frac{\rho}{f}\right) \tag{3.24}$$

Where, ρ is the Earth resistivity = 100 Ω/meter,

The unit of Eqs.3.23 and 3.24 can be changed to Ω/km by multiply the two equations in (1/1.609344). Hence, for f=50Hz the equations are simplified in Ω/km as follows:

$$\hat{z}_{ii} = r_i + 0.04934 + j0.06285\left(\ln\frac{1}{GMR_i} + 8.02517\right) \quad \Omega/km \tag{3.25}$$

$$\hat{z}_{ij} = 0.04934 + j0.06285\left(\ln\frac{1}{D_{ij}} + 8.02517\right) \qquad \Omega/km \qquad (3.26)$$

As it can be seen, the Carson's modified Eqs.3.25 and 3.26 can solve for the primitive impedances of the lines without terms related to the virtual return path 'd'. Nevertheless, the impact of 'd' is included implicitly inside the terms of the two equations. It is worth mentioning that this impact can be recognized clearly by comparing the terms of Eqs.3.25 and 3.26 with their counterparts in Eqs.3.14 and 3.15.

Primitive Impedance Matrix:

At this stage, the Carson's modified Eqs.3.25 and 3.26 are used to build what is called a 'Primitive Impedance Matrix' of the line. As an example, the overhead four-wire line section with grounded Y results in 4x4 matrix. On the other hand, the grounded Y of underground line section with three concentric neutrals results in 6x6 matrix.

Based on the above, the primitive impedance matrix of unbalanced 3-phase line section with 'm' neutrals is formulated as follows:

$$[\hat{Z}_{Primitive}] = \begin{bmatrix} [\hat{Z}_{pp}] & [\hat{Z}_{pn}] \\ [\hat{Z}_{np}] & [\hat{Z}_{nn}] \end{bmatrix} \qquad (3.27)$$

And,

$$[\hat{Z}_{pp}] = \begin{bmatrix} \hat{z}_{aa} & \hat{z}_{ab} & \hat{z}_{ac} \\ \hat{z}_{ba} & \hat{z}_{bb} & \hat{z}_{bc} \\ \hat{z}_{ca} & \hat{z}_{cb} & \hat{z}_{cc} \end{bmatrix} \qquad (3.28.a) \qquad [\hat{Z}_{pn}] = \begin{bmatrix} \hat{z}_{a,n1} & \hat{z}_{a,n2} & \cdots & \hat{z}_{a,nm} \\ \hat{z}_{b,n1} & \hat{z}_{b,n2} & \cdots & \hat{z}_{b,nm} \\ \hat{z}_{c,n1} & \hat{z}_{c,n2} & \cdots & \hat{z}_{c,nm} \end{bmatrix} \qquad (3.28.b)$$

$$[\hat{Z}_{np}] = \begin{bmatrix} \hat{z}_{n1,a} & \hat{z}_{n1,b} & \hat{z}_{n1,c} \\ \cdots & \cdots & \cdots \\ \hat{z}_{nm,a} & \hat{z}_{nm,b} & \hat{z}_{nm,c} \end{bmatrix} \qquad (3.28.c) \qquad [\hat{Z}_{nn}] = \begin{bmatrix} \hat{z}_{n1,n1} & \hat{z}_{n1,n2} & \cdots & \hat{z}_{n1,nm} \\ \cdots & \cdots & \cdots & \cdots \\ \hat{z}_{nm,n1} & \hat{z}_{nm,n2} & \cdots & \hat{z}_{nm,nm} \end{bmatrix} \qquad (3.28.d)$$

Where,

$[\hat{Z}_{pp}]$ - Primitive impedance matrix of the three phases,

$[\hat{Z}_{pn}]$ - Primitive impedance matrix of the three phase conductors with the 'm' neutrals,

$[\hat{Z}_{np}]$ - Primitive impedance matrix of the 'm' neutrals with the three phases,

$[\hat{Z}_{nn}]$ - Primitive impedance matrix of the 'm' neutrals,

Phase Impedance Matrix:

To facilitate the three phase calculations it is very helpful if the primitive impedance matrix can be reduced to equivalent 3x3 matrix namely 'Phase Impedance Matrix'. In this case the effect of the neutral is included implicitly in the equivalent values of this matrix.

One of the potential methods that can realize this reduction is the *Korn reduction* [1]. To apply this method, a four-wire section with grounded Y system is assumed, as shown in Fig.3.3.

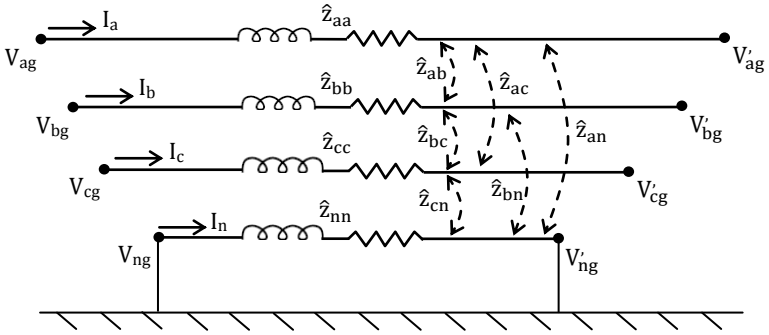

Figure 3.3 Four wire line section of grounded neutral

Application of KVL on the circuit of the figure yields:

$$\begin{bmatrix} V_{ag} \\ V_{bg} \\ V_{cg} \\ V_{ng} \end{bmatrix} = \begin{bmatrix} V'_{ag} \\ V'_{bg} \\ V'_{cg} \\ V'_{ng} \end{bmatrix} + \begin{bmatrix} \hat{Z}_{aa} & \hat{Z}_{ab} & \hat{Z}_{ac} & \hat{Z}_{an} \\ \hat{Z}_{ba} & \hat{Z}_{bb} & \hat{Z}_{bc} & \hat{Z}_{bn} \\ \hat{Z}_{ca} & \hat{Z}_{cb} & \hat{Z}_{cc} & \hat{Z}_{cn} \\ \hat{Z}_{na} & \hat{Z}_{nb} & \hat{Z}_{nc} & \hat{Z}_{nn} \end{bmatrix} \times \begin{bmatrix} I_a \\ I_b \\ I_c \\ I_n \end{bmatrix} \tag{3.29}$$

Comparing the sub-matrices of Eqs.3.27 with the primitive impedance matrix in Eq.3.29 shows that $[\hat{Z}_{pp}]$ consist of 3x3 elements, while $[\hat{Z}_{pn}], [\hat{Z}_{np}]$ and $[\hat{Z}_{nn}]$ consist of 3x1, 1x3 and 1x1 elements respectively. Accordingly, Eq.3.29 can be rewritten as follows:

$$\begin{bmatrix} [V_{abc}] \\ [V_{ng}] \end{bmatrix} = \begin{bmatrix} [V'_{abc}] \\ [V'_{ng}] \end{bmatrix} + \begin{bmatrix} [\hat{Z}_{pp}] & [\hat{Z}_{pn}] \\ [\hat{Z}_{np}] & [\hat{Z}_{nn}] \end{bmatrix} \text{ x } \begin{bmatrix} [I_{abc}] \\ [I_n] \end{bmatrix} \tag{3.30}$$

For grounded neutral, $[V_{ng}]$ and $[V'_{ng}]$ are equal to zero. Hence,

$$[V_{abc}] = [V'_{abc}] + [\hat{Z}_{pp}].[I_{abc}] + [\hat{Z}_{pn}] \text{ x } [I_n] \tag{3.31}$$

$$[0] = [0] + [\hat{Z}_{np}].[I_{abc}] + [\hat{Z}_{nn}] \text{ x } [I_n] \tag{3.32}$$

Solving Eq.3.32 for $[I_n]$ and substitute into Eq.3.31, gives:

$$[V_{abc}] = [V'_{abc}] + \left([\hat{Z}_{pp}] - [\hat{Z}_{pn}] . [\hat{Z}_{nn}]^{-1} . [\hat{Z}_{np}]\right) \text{ x } [I_{abc}] \tag{3.33}$$

Based on Eq.3.33, the equivalent 3x3 phase impedance matrix $[Z_{abc}]$ is given as follows:

$$[Z_{abc}] = [\hat{Z}_{pp}] - [\hat{Z}_{pn}] . [\hat{Z}_{nn}]^{-1} . [\hat{Z}_{np}] \tag{3.34}$$

And

$$[V_{abc}] = [V'_{abc}] + [Z_{abc}] . [I_{abc}] \tag{3.35}$$

It is important to mention that $[Z_{abc}]$ for three wire line section containing no neutral is determined with no need to Kron reduction. In other words, $[Z_{abc}]$ of such line section is directly equal to $[\hat{Z}_{pp}]$ of Eq.3.28.a.

3.2 Load and PVDG Production Curves

Connection of PVDG units to certain distribution feeders requires suitable modeling for the variations in feeders load demand and PVDG units production. This section deals with such modeling in terms of daily curves namely load curve and PVDG production curve.

3.2.1 Load Curve Modeling

The load curve of a certain feeder is usually divided into equal time intervals over certain time duration, usually daily. The intervals could be 15 min, 30 min, 1 hour, or even longer. To this end, the load demand of the feeder in each interval is normally determined as the average load over this interval. In other cases the load curve could be represented by the maximum or minimum load demand values recorded in each interval. The load curve values may be given in kilo/megaVoltampere (kVA/MVA), kilo/megaWatt (kW/MW), kilo/megaVAr (kVAr/MVAr), kilo/Amperes (kA/A), and per-unit. Regarding per-unit, the load curve values are expressed in per-unit of the peak load demand recorded over the total duration of the curve [3].

Table.3.1 shows an example on summer daily load demand of certain 11kV distribution feeder in Abu Dhabi city.

Table.3.1 Real and reactive daily load demands of actual 11kV distribution feeder

Time	MW	MVAr	Time	MW	MVAr
01:00	1.77	0.60	13:00	2.10	0.67
02:00	1.69	0.54	14:00	2.14	0.69
03:00	1.66	0.54	15:00	2.19	0.69
04:00	1.59	0.50	16:00	2.21*	0.69
05:00	1.63	0.55	17:00	2.14	0.69
06:00	1.54	0.56	18:00	2.06	0.69
07:00	1.47	0.63	19:00	1.86	0.65
08:00	1.57	0.63	20:00	2.14	0.73
09:00	1.73	0.67	21:00	2.17	0.77
10:00	1.87	0.67	22:00	2.12	0.79*
11:00	1.91	0.67	23:00	1.98	0.66
12:00	1.99	0.71	24:00	1.91	0.63

** MW & MVAr Peak load demands*

In the same connection, it is a usual practice representing the load curve in per-unit values. Thus, Eq.3.36 is applied to convert the actual load demand of certain distribution feeder into per-unit-values.

$$LD_{Fj-pu} = \frac{LD_{Fj}}{LD_{Fp}}\Bigg|_{j=1:24} \tag{3.36}$$

Where, LD_{Fj} – Load demand of the feeder at interval j,
LD_{Fp} – Peak load demand of the feeder,
$LD_{Fj\text{-}pu}$ – LD_{Fj} in per-unit of LD_{Fp},

Equation.3.36 is applied on the data of Table.3.1. The results are depicted in Fig.3.4.

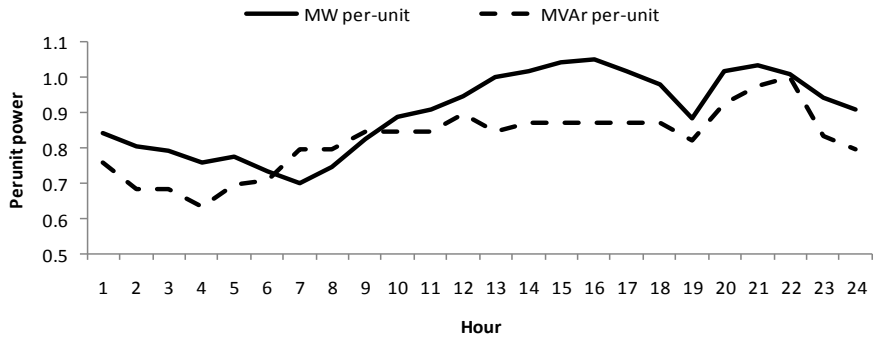

Figure 3.4 Daily load curve of certain 11kV distribution feeder in per-unit values

The farthest point on the distribution network monitored by the power distribution companies is most likely the input of distribution feeders. However, this work needs the load demand data along the feeder. To take over this, the load demand of each node along the feeder is assumed to vary in the same pattern of feeder load demand, but in a lower level [4, 5 & 6]. This assumption is reasonable in light that distribution feeders are likely to serve loads of similar nature in terms of residential, commercial and industrial loads. Hence, the actual load curve values at each node are leveled based on the values of Eq.3.36 and the peak load demand at that node, as follows:

$$LD_{ij} = LD_{ip} \times LD_{Fj\text{-}pu} \tag{3.37}$$

Where,
LD_{ij} – Load demand of node i at interval j,
LD_{ip} – Peak Load demand of node i,

Consequently, Eqs.3.36 and 3.37 are applied to generate reasonable load curves for the nodes along the feeder. Figure.3.5. shows example of real power load curves at the nodes of radial distribution feeder. Mind, whenever detailed load demands along the feeder are available; the relevant load curves are generated directly with no need to apply Eq.3.37.

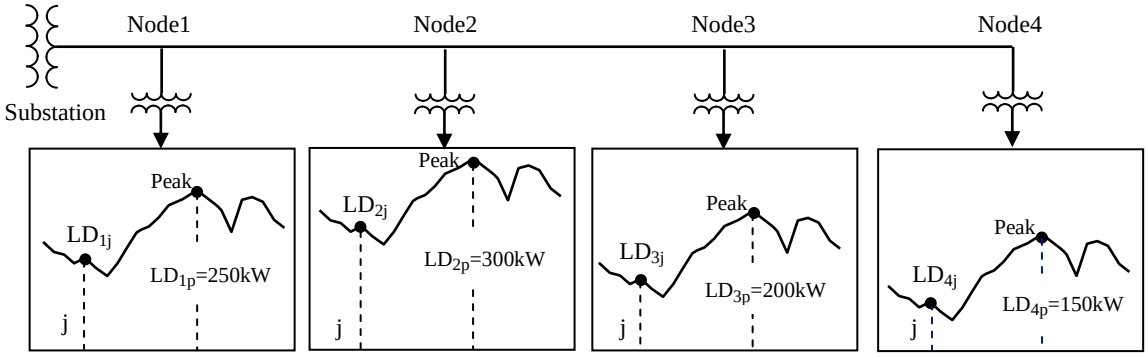

Figure 3.5 Simulation of load curves at the nodes of radial distribution feeder

At this stage, the load curves of all the nodes along the feeder are generated reasonably. Consequently, the currents and voltages along the feeder over the daily duration can be realized by applying power flow calculations in each time interval. In this case, the feeder nodes are considered as PQ buses in the calculation process, with their values of each interval to be substituted from the generated load curves.

3.2.2. PVDG Production Curve Modeling

The production of PVDG unit is directly proportional to the solar irradiance (SI) rates fall on the PV modules of the system [7]. The cell temperature of PV modules could be also an issue, but its impact is considerably small comparing to that of SI. Hence, the daily solar irradiance curve is resulting, to great extent, in a daily PVDG production curve of the same pattern.

Based on above, the values of SI curve is recalled and represented in per-unit of SI at standard conditions (SI_{STC}) as follows:

$$SI_{j-pu} = \frac{SI_j}{SI_{STC}}\Big|_{j=1:24} \tag{3.38}$$

Where,

SI_j – Solar irradiance at interval j,

SI_{STC} – Solar irradiance at standard conditions ($1kW/m^2$),

$SI_{j\text{-}pu}$ – Solar irradiance at interval j in per-unit of SI_{STC},

Thus, the results of Eq.3.38 are substituted directly to represent the daily PVDG production curve in per-unit of the PVDG output at SI_{STC}, as follows:

$$PVDG_{j-pu} = SI_{j-pu}\Big|_{j=1:24} \tag{3.39}$$

Where, $PVDG_{j\text{-}pu}$ is the output of the PVDG unit at j in per-unit of its output at SI_{STC}.

3.3 Application of Backward/Forward Sweep Power Flow

The main characteristics of radial distribution feeders are the radial structure, the multi-phase conductors and the unbalanced load operation. These features may cause the traditional power flow methods (of transmission systems) to return poor convergence characteristics and fail in meeting the distribution system requirements [8&9].

In the same connection, it is often possible to have the primary distribution feeder and all of its laterals consist of a 3-phase system. Such being the case, some power companies may consider the feeder operates in a balanced load condition.

Alternatively, suitable power flow methods specially designed for radial distribution systems are used. The backward/forward sweep and the ladder iterative methods are among the potential methods. The basic principle of each is similar [10], where the voltage magnitude and phase angle of the source should to be specified. Also the complex values of load demands at each node along the feeder should be given. Starting from the end of the feeder, the backward sweep calculates the line section currents and node voltages (by KCL and KVL) back to the source. The calculated voltage at the source is compared with its original specified value. If the error is beyond the limit the forward sweep is performed to update the node voltages along the feeder. In such a case, the specified source voltage and the line section currents already calculated in the previous backward sweep are used. The process keeps going back and forth until the voltage error at the source becomes within the limit.

3.3.1 Balanced Load Consideration

It has been mentioned that it is possible to consider the primary distribution feeder of 3-phase laterals operating in balanced load condition. It is deemed suitable to begin with the application of backward/forward power flow method on a 3-phase balanced load feeder. In this case the calculations are conducted in terms of line voltages and currents of single line diagram model, as in traditional power flow methods. Considering Fig.3.6, showing five nodes radial distribution feeder, the backward sweep begins from node 5 as follows:

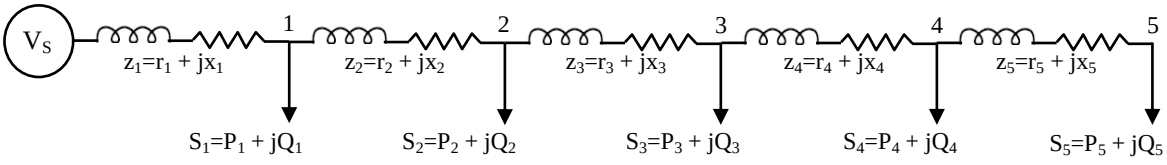

Figure 3.6 Single line diagram of 5-nodes radial distribution feeder

Backward Sweep

Before staring the backward sweep, an initial flat voltage equal to the specified substation voltage (V_{SS}) is assumed along the feeder.

The network is traced in the backward direction using KCL & KVL to calculate the currents and voltages in all sections and nodes respectively. Let the initial flat voltage is $V_{SS}\angle 0$; then the first iteration will start from node 5 calculating the relevant line current and voltage as follows:

$$I_5^1 = I_{45}^1 = \left(\frac{S_5}{\sqrt{3}\,V_5^1}\right)^* = \left(\frac{P_5 + jQ_5}{\sqrt{3}\,V_5^1}\right)^* \quad (3.40)$$

$$V_4^1 = V_5^1 + z_5 . I_{4,5}^1 \quad (3.41)$$

Setting initial voltage at node 5 as,

$$V_5^1 = V_{SS}\angle 0$$

Where, I_5^1 - Load current of node 5 at iteration 1

$I_{4,5}^1$ - Section current from node 4 to 5 at iteration 1

S_5 - Specified complex load demand of node 5

V_5^1 - Line voltage of node 5 at iteration 1

Then, in the upstream direction,

$$I_4^1 = \left(\frac{S_4}{\sqrt{3}\,V_4^1}\right)^* \quad (3.42)$$

$$I_{3,4}^1 = I_4^1 + I_{4,5}^1 \quad (3.43)$$

$$V_3^1 = V_4^1 + z_4 . I_{3,4}^1 \quad (3.44)$$

In general form; with i and t denoting the node and iteration numbers respectively,

$$I_i^t = \left(\frac{S_i}{\sqrt{3}\,V_i^t}\right)^* \quad (3.45)$$

$$I_{i-1,i}^t = I_i^t + I_{i,i+1}^t \quad (3.46)$$

$$V_{i-1}^t = V_i^t + z_i . I_{i-1,i}^t \quad (3.47)$$

Bearing in mind that z_i is determined in Ω/km by applying Eq.3.6

The procedure continues until V_{SS} is calculated. At that stage, if the difference between the calculated and specified V_{SS} is within the convergence tolerance, the procedure stops at the last calculated values in hand. Otherwise, it shall continue with the forward sweep.

Forward Sweep

The substation is set to its specified V_{SS} and the voltages of the downstream nodes are updated using the currents already calculated from the backward sweep. Thus, the updated voltages are calculated as follows:

$$V_1^2 = V_{SS} - z_1 . I_{SS.1}^1 \tag{3.48}$$

Where, V_1^2 - Updated line voltage of node 1 at iteration 2

$I_{SS.1}^1$ - Section current from the substation to node 1 calculated at iteration 1

Then, in the downstream direction,

$$V_2^2 = V_1^2 - z_2 . I_{1,2}^1 \tag{3.49}$$

In general form, with i and t denoting the node and iteration numbers respectively,

$$V_i^t = V_{i-1}^t - z_i . I_{i-1,i}^{t-1} \tag{3.50}$$

The procedure proceeds until V_5^2 is calculated initiating the next backward sweep. At the end of the next backward sweep, the most recent calculated V_{SS} is compared with its specified value. If the error is within the convergence tolerance the procedure stops, adopting the results of the last iteration. Otherwise, the procedure continues with new iteration and so on.

3.3.2 Unbalanced Load Consideration

Basically, the same procedure applied on 3-phase balanced load distribution feeder is also applied on unbalanced load feeder. However, in the case of an unbalanced load condition the calculations should be conducted by phase for each wire conductor along the feeder. In this course, the series impedances of the line sections are determined in terms of phase impedance matrix derived in Section.3.1.2. To this end, Fig.3.7 shows a line sections in certain four wires feeder of 3-phase unbalanced loads.

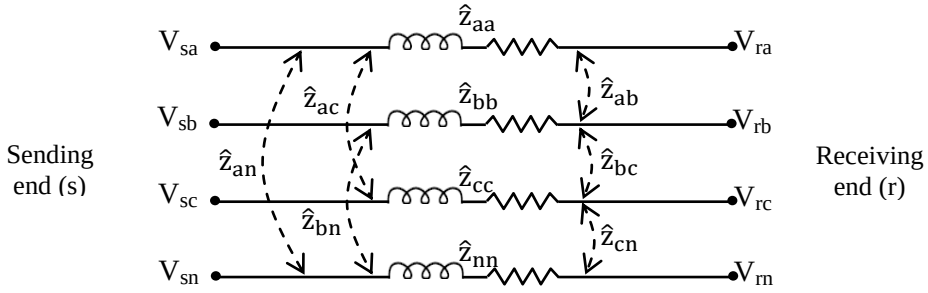

Figure 3.7 Line section in four wire feeder of 3-phase unbalanced loads

At the beginning, the primitive impedance matrix of the line section is formulated according to Eqs.3.27 & 3.28:

$$[Z_{primitive}] = \begin{bmatrix} \hat{z}_{aa} & \hat{z}_{ab} & \hat{z}_{ac} & \hat{z}_{an} \\ \hat{z}_{ba} & \hat{z}_{bb} & \hat{z}_{bc} & \hat{z}_{bn} \\ \hat{z}_{ca} & \hat{z}_{cb} & \hat{z}_{cc} & \hat{z}_{cn} \\ \hat{z}_{na} & \hat{z}_{nb} & \hat{z}_{nc} & \hat{z}_{nn} \end{bmatrix} \quad (3.51)$$

Then, the line section of Fig.3.7 is converted to equivalent three wires configuration by applying Korn's reduction method of Eq.3.34. This will result in the equivalent phase impedance matrix $[Z_{abc}]$ as follows:

$$[Z_{abc}] = \begin{bmatrix} \hat{z}_{aa} & \hat{z}_{ab} & \hat{z}_{ac} \\ \hat{z}_{ba} & \hat{z}_{bb} & \hat{z}_{bc} \\ \hat{z}_{ca} & \hat{z}_{cb} & \hat{z}_{cc} \end{bmatrix} - \begin{bmatrix} \hat{z}_{an} \\ \hat{z}_{bn} \\ \hat{z}_{cn} \end{bmatrix} . [\hat{z}_{nn}]^{-1} . \begin{bmatrix} \hat{z}_{na} & \hat{z}_{nb} & \hat{z}_{nc} \end{bmatrix} \quad (3.52)$$

Each of the elements on the right hand side of Eq.3.52 is determined by using Carson's modified Eqs.3.25 & 3.26 for the primitive impedance matrix. Hence, the resulting equivalent 3x3 phase impedance matrix of the line section is.

$$[Z_{abc}] = \begin{bmatrix} Z_{aa} & Z_{ab} & Z_{ac} \\ Z_{ba} & Z_{bb} & Z_{bc} \\ Z_{ca} & Z_{cb} & Z_{cc} \end{bmatrix} \quad (3.53)$$

Backward Sweep

The backward sweep starts with the setting of an initial flat voltage along the feeder, equal to the specified substation voltage by phase ($[V_{abc}]_{SS}$). The same procedure of tracing the feeder back and forth is applied until the error between the calculated and specified substation voltages becomes within the convergence tolerance.

Hence, back to Fig.3.6 assuming the 5 node radial distribution feeder is now operating under unbalanced load condition. Starting from the far end node,

$$[I_{abc}]_5^1 = \left(\frac{[S_{abc}]_5}{[V_{abc}]_5^1}\right)^* = \left(\frac{[(P + jQ)_{abc}]_5}{[V_{abc}]_5^1}\right)^* \xrightarrow{\text{yields}} \begin{bmatrix} I_a\angle\theta_a \\ I_b\angle\theta_b \\ I_c\angle\theta_c \end{bmatrix}_5^1 = [I_{abc}]_{4,5}^1 \quad (3.54)$$

$$[V_{abc}]_4^1 = [V_{abc}]_5^1 + [Z_{abc}]_5 . [I_{abc}]_{4,5}^1 \xrightarrow{\text{yields}} \begin{bmatrix} V_a\angle\alpha_a \\ V_b\angle\alpha_b \\ V_c\angle\alpha_c \end{bmatrix}_4^1 \quad (3.55)$$

Setting initial voltage at node 5,

$$[V_{abc}]_5^1 = [V_{abc}]_{SS} = \begin{bmatrix} V_a \\ V_b \\ V_c \end{bmatrix}_{SS} \xrightarrow{set} \left\{ \begin{array}{c} \text{At the substation the voltage is specified as} \\ |V_a| = |V_b| = |V_c| \text{ and} \\ \angle V_a = \theta,\ \angle V_b = (\theta - 120),\ \angle V_c = (\theta + 120) \end{array} \right\} \quad (3.56)$$

Where, $[I_{abc}]_5^1$ - Phase currents of node 5 at iteration 1

$[S_{abc}]_5$ - Specified complex load demands of node 5 by phase

$[V_{abc}]_5^1$ - Phase voltages of node 5 at iteration 1

$[I_{abc}]_{4,5}^1$ - Phase currents from node 4 to 5 at iteration 1

$[Z_{abc}]_5$ - Phase impedance matrix of line section 5

$[V_{abc}]_{SS}$ - Specified phase voltages of the substation

(*) - For conjugate complex values

In general form; with i and t denoting the node and iteration numbers respectively,

$$[I_{abc}]_i^t = \left(\frac{[S_{abc}]_i}{[V_{abc}]_i^t}\right)^* \tag{3.57}$$

$$[I_{abc}]_{i-1,i}^t = [I_{abc}]_i^t + [I_{abc}]_{i,i+1}^t \tag{3.58}$$

$$[V_{abc}]_{i-1}^t = [V_{abc}]_i^t + [Z_{abc}]_i \cdot [I_{abc}]_{i-1,i}^t \tag{3.59}$$

The procedure proceeds until $[V_{abc}]_{SS}$ is calculated. At that stage, if the difference between the calculated and specified $[V_{abc}]_{SS}$ is within the convergence tolerance, the procedure stops at the last calculated values in hand. Otherwise, it goes to the forward sweep

Forward Sweep

The forward sweep is commenced by setting the substation voltage to its specified value. The node voltages by phase are then updated in the downstream direction using the currents from the previous backward sweep. Thus, the updated voltages are calculated as follows:

$$[V_{abc}]_1^2 = [V_{abc}]_{SS} - [Z_{abc}]_1 \cdot [I_{abc}]_{SS.1}^1 \quad \xrightarrow{\text{yields}} \quad \begin{bmatrix} V_a\angle\alpha_a \\ V_b\angle\alpha_b \\ V_c\angle\alpha_c \end{bmatrix}_1^2 \tag{3.60}$$

Where,

$[I_{abc}]_{SS.1}^1$ - Phase currents from the substation to node 1 calculated at iteration 1

$[V_{abc}]_1^2$ - Updated voltages by phase of node 1 at iteration 2

Then, in the downstream direction,

$$[V_{abc}]_2^2 = [V_{abc}]_1^2 - [Z_{abc}]_2 \cdot [I_{abc}]_{1,2}^1 \tag{3.61}$$

In general form, with i and t denoting the node and iteration numbers respectively,

$$[V_{abc}]_i^t = [V_{abc}]_{i-1}^t - [Z_{abc}]_i \cdot [I_{abc}]_{i-1,i}^{t-1} \tag{3.62}$$

The procedure continues until $[V_{abc}]_5^2$ is calculated, initiating the next backward sweep. At the end of the next backward sweep, the most recent calculated $[V_{abc}]_{SS}$ is compared with its specified value. If the error is within the convergence tolerance the procedure stops adopting the results of the last iteration. Otherwise, the procedure continues with new iteration and so on.

3.4 Calculation of Line Power Loss

The calculation of line power loss along certain wire is easily determined by using the I^2R formula. However, for feeders of 3-phase system this formula is not always valid. Actually, it could work under 3-phase balanced load condition, as the series resistance per phase is determined individually for each section along the feeder. Consequently, the total line power loss is the summation of I^2R in the conductors of the three phases, assuming zero current in the neutral wire (in case of four wires system) [11].

Figure 3.8 shows a single line diagram of 3-phase four-wire distribution feeder of 'n' sections.

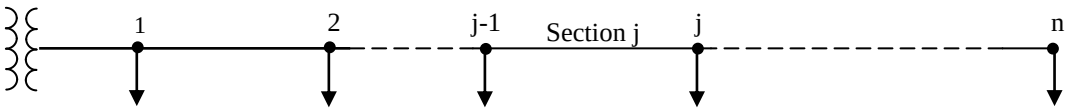

Figure 3.8 Single line diagram of 3-phase four-wire distribution feeder

The total line power loss (PL_T) along the feeder under balanced load condition is then:

$$PL_T = 3.\sum_{j=1}^{n} I_j^2 \ .R_j \tag{3.63}$$

Under unbalanced load condition, each four-wire line section is represented by equivalent 3x3 phase impedance matrix, by the means of Carson's equations and Korn's reduction. However, substituting the resistances of the equivalent 3x3 matrices into the I^2R formula will lead to incorrect results. Alternatively, the line power loss should be computed as the difference between the sending and receiving power of the line section by phase [8].

Assume the same 3-phase four-wire feeder is now operating under unbalanced load condition. The line power loss (PL_j) for line section j in this feeder is:

$$[PL_j]_{abc} = \begin{bmatrix} |(S_a)_{j-1} - (S_a)_j| \\ |(S_b)_{j-1} - (S_b)_j| \\ |(S_c)_{j-1} - (S_c)_j| \end{bmatrix} \tag{3.64}$$

$$\left[PL_j\right]_{abc} = \begin{bmatrix} \left|(V_a)_{j-1} \times (I_a)_j - (V_a)_j \times (I_a)_j\right| \\ \left|(V_b)_{j-1} \times (I_b)_j - (V_b)_j \times (I_b)_j\right| \\ \left|(V_c)_{j-1} \times (I_c)_j - (V_c)_j \times (I_c)_j\right| \end{bmatrix} = \left[\left|\Delta V_j \times I_j\right|\right]_{abc} \quad (3.65)$$

Where,

$(V_a)_{j-1}$ - Sending end voltage of section j at phase 'a'

$(V_a)_j$ - Receiving end voltage of section j at phase 'a'

$(I_a)_j$ - Current flows in section j at phase 'a'

ΔV_j - Voltage drop in section j by phase

I_j - Current flows in section j by phase

$|\ |$ - Gives positive power loss value even if the current flows from j to j-1

Hence, the total line power loss along the feeder (PL_T) is,

$$PL_T = \text{sum}\left(\sum_{j=1}^{n}\left[PL_j\right]_{abc}\right) \quad (3.66)$$

Where, 'sum' is the summation of line power loss across the three phases.

3.5 Summary

The sizing and location of PVDG units on distribution feeders require adequate modeling for the physical structure of the line sections along the feeder. The load curve of the feeder and the PVDG production curve are also matters of significant importance. Regarding the physical structure, the series impedances are modeled considering 3-phase balanced and unbalanced load conditions. For balanced load feeder, the self and mutual inductances of the conductors are combined in one formula. At the same time, the resistances are determined from the product specification sheet of the conductors.

However, the distribution feeders are most likely operated under unbalanced load conditions, which should be reflected in the modeling. Hence, a suitable procedure is applied to model the series impedances of unbalanced load feeder. The procedure calculates the self and mutual inductances of the line sections based on the Carson's equations. This will result in the 'primitive impedance matrix' for the conductors of each line section along the feeder. The work is improved further by using Korn's reduction method to generate equivalent 3x3 'phase impedance matrix' for any nxn 'primitive impedance matrix'.

Suitable modeling is developed for the load curve of the feeder. This is based on the assumption that the load demand of each node along the feeder is varied in the same pattern of feeder load demand. Hence, the feeder load curve is generated in per-unit of feeder peak load demand and then applied on each node in per-unit of the peak load demand of that node.

The modeling of the PVDG production is placed on the fact that the production is directly proportional to the solar irradiance (SI) rates fall on the PV modules of the system. Hence, the daily solar irradiance curve can result, to great extent, in a daily PVDG production curve of the same pattern. Based on that, the values of SI curve is recalled and represented in per-unit of SI at standard conditions. Consequently, the results will be true for the PVDG production in per-unit of the PVDG output due to SI at the standard condition.

At this stage, the aforementioned modeling components can be integrated together by the mean of suitable power flow. To this end, the backward/forward sweep power flow is used as one of the most potential techniques dealing with radial distribution feeders.

References

[1] W. H. Kersting, "Distribution System Modeling and Analysis," *Electric Power Engineering Series, CRC Press LLC*, USA, 2002, ch.4.

[2] J. R. Carson, "Wave Propagation in Overhead Wires with Ground Return," *Bell Systems Technical Journal*, vol.5, pp 539-554, Oct.1926.

[3] Turan Gonen, "Electric Power Distribution System Engineering," *McGraw-Hill Series in Electrical Engineering*, USA, 1986, ch.2.

[4] B. A. de Souza, H. N. Alves and H. A. Ferreira, "Microgenetic Algorithms and Fuzzy Logic Applied to the Optimal Placement of Capacitor Banks in Distribution Networks", IEEE Trans. Power Systems, vol,19, no.2, 2004, pp. 942-947.

[5] M.E. Baran and F.F. Wu, "Optimal Capacitor Placement On Radial Distribution Systems," *IEEE Transactions on Power Delivery*, vol. 4, no. 1, pages 725 – 734, Jan.1989.

[6] D.I.H. Sun, S. Abe, R.R. Shoults, M.S. Chen, P. Eichenberger, and D. Farris, "Calculation of Energy Losses in a Distribution System," *IEEE Transactions on Power Apparatus and Systems*," vol. PAS-99, No. 4, pp 1347-1356, July/Aug 1980.

[7] F.A. Viawan, F. Vuinovich, and A. Sannino, "Probabilistic Approach to the Design of Photovoltaic Distributed Generation in Low Voltage Feeder," *in Proc. Jun.2006 International Conference on Probabilistic Methods Applied to Power Systems*, pp.1–7.

[8] W. H. Kersting, "Distribution System Modeling and Analysis," *Electric Power Engineering Series, CRC Press LLC*, USA, 2002, ch.10.

[9] Jen-Hao Teng, "A Direct Approach for Distribution System Load Flow Solutions," *IEEE Transaction on Power Delivery*, vol.18, no.3, pp 882-887, Jul 2003.

[10] U. Eminoglu and M. H. Hocaoglu, "Three-Phase Voltage Regulator Modelling for Forward/ Backward sweep-Based Distribution Systems Power Flow Algorithms," *in Proc. Dec.2005 ELECO 5th International Conference on Electrical and Electronics Engineering*, vol. Electric-Control, pp.224-228.

[11] L. Ochoa, R. Ciric, A. Padiha-Feltrin, and G. Harrison, "Evaluation of Distribution System Losses due to Load Unbalance", *in Proc. August 2005 15th Power Systems Computation Conf., (PSCC'05)*, session 10, paper 6, page 4.

4 DERIVATIONS OF FEASIBLE OPTIMIZATION INTERVAL

Connection of PVDG units to certain distribution feeders requires correlation between the load curve of the feeder and the production curve of the PVDG units. The two curves are independent of each other. The peaks of the load and the PVDG production curves are therefore likely to occur at different intervals. With such peak mismatch, the PVDG unit can produce only part of its capacity at the time the feeder meets its peak load demand. To this end, connection of PVDG unit for benefits of peak power loss reduction is deemed not a feasible objective. Consideration of accumulated power loss reduction benefits over the day (line energy losses) is more appropriate in this application [1]. However, solution for energy-based benefits may require the repetition of the calculations on an hourly basis, or even shorter, after which the summation of the whole duration must be taken. To this end, determination of a certain time interval at which the whole energy-based benefits can be rated will be significantly helpful: this is the main objective of this chapter.

4.1 Peak Mismatch of Load and PVDG Production Curves

The amount of power generated by traditional DG units can be controlled according to the demand of the feeder to which it is connected. Thus, the production of such DG units can be easily regulated to serve at peak load intervals resulting in benefits of peak power loss reduction (ΔPPL). The case is different for PVDG units as the power they produce is driven by solar irradiance falling on the photovoltaic (PV) arrays. Thus, variations of PVDG power production curve track the variations of solar irradiance curve to a reasonable extent. Consequently, the per-unit values of PVDG production and solar irradiance curves are considered to have the same pattern. Figure A2.7 of Appendix 2 depicts the daily average solar irradiance curves of Abu Dhabi city. The curves show that the peak solar irradiance value resulting in peak PVDG power production is normally at noon. On the other hand, Fig.4.1 shows daily real power load curves in summer for six feeders existing at the 11kV level of the Abu Dhabi distribution network [2]. The curves are shown as per-unit of the relevant peak load demand values of the feeders.

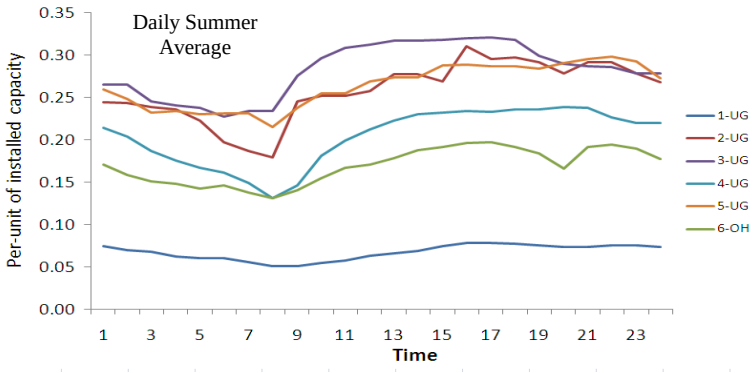

Figure 4.1 Summer daily real load curves for six 11kV feeders in Abu Dhabi

According to the six load curves, the peak load time intervals (PLT) are concluded in Fig.4.2, which shows PLT intervals occurring at different times than at noon. Moreover, two of the feeders (4-UG & 5-UG) meet their PLT after nightfall when the PVDG unit produces no power. Consequently, the average PLT interval for the six feeders is at around 5:30 pm.

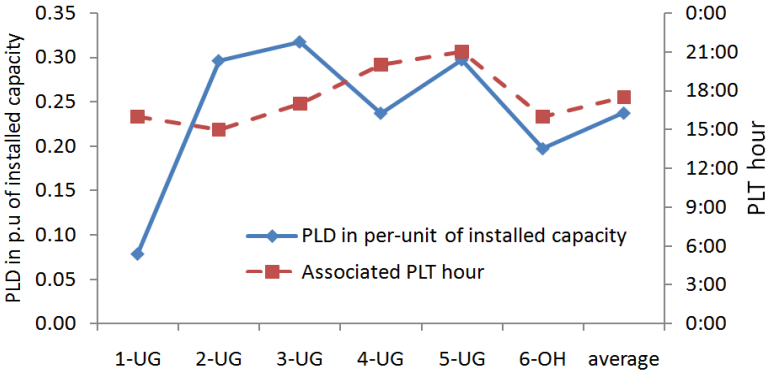

Figure 4.2 Peak load time hours of the six feeders in an August day

The peak mismatch of the load and the PVDG production curves results in the status that the PVDG unit produces only part of its capacity at the time the feeder meet its peak load demand. As example, Fig.4.3 correlates the summer daily load curve of two feeders with a virtual PVDG production curve tracking the pattern of summer solar irradiance curve in Abu Dhabi.

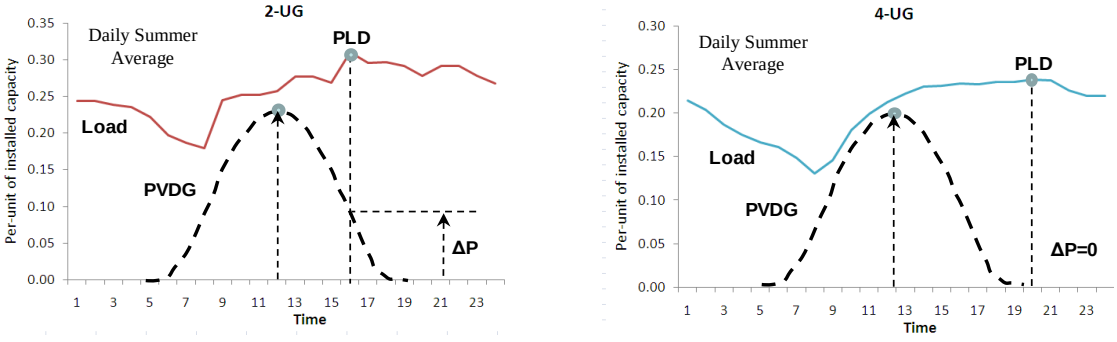

Figure 4.3 Load and PVDG production curves correlated on the same time axis

The aforementioned presentation suggests that the connection of the PVDG unit considering benefits of peak power loss reduction (ΔPPL) could make no sense. Alternatively, consideration of accumulated power loss reduction benefits over the day, so called energy loss reduction (ΔEL) is more appropriate in this application. Nevertheless, the ΔPPL benefits is still counted as an additional benefit provided that the PLT occurs during daylight time (as in the case of feeder 2-UG above) [1].

In this course, connection of PVDG unit at a certain coupling point (CP) along a radial distribution feeder will inject a certain amount of power in the feeder. Normally, the injected power flows in the downstream direction serving the loads between the CP and the end of the feeder. However, at any time if this power exceeds the demand, the surplus amount will flow in the reverse direction towards the substation. Referring to Fig.4.3, this mode of operation occurs when the maximum point of the PVDG curve increases penetrating the load curve of the feeder. If the reverse power flow (RPF) is to be avoided, the capacity of the PVDG unit should be sized in a way that its production not exceeds the load demand over the day.

In the same connection, the load curve levels over seasons change at different rates to the levels of PVDG production curves. Figure 4.4 represents the case showing actual daily load curves of real power for feeder 3-UG in each season. The figure shows a considerable drop in winter load curve as the high demand of air conditioning load in summer does no longer exist in winter. Note to mention that for spring and autumn, the load demand is almost the same in Abu Dhabi.

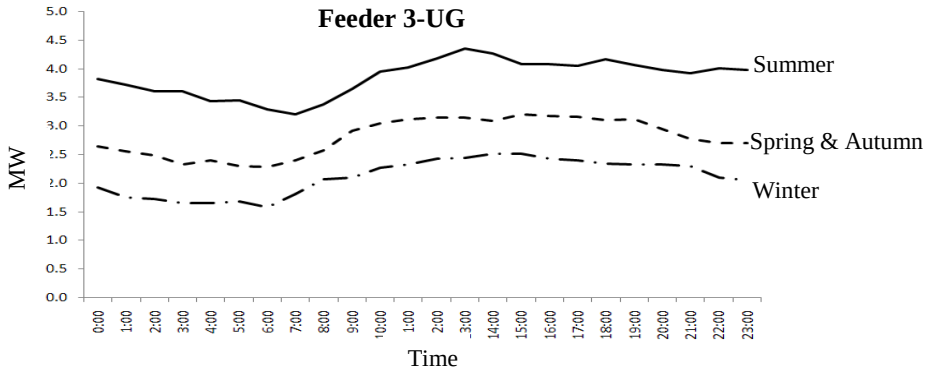

Figure 4.4 Samples of daily load curves for feeder 3-UG over the year

On the other hand, Fig.A2.7 of Appendix 2 shows that the change in PVDG production curves over seasons is mainly during the daily sunlight hours; while the peaks change is relatively small. Thus, sizing the PVDG unit based on the summer load curve may result in different behavior in other seasons. For clarity, Fig.4.5 correlates the load curves of Fig.4.4 with the power production curves of the PVDG unit sized based on summer load demand.

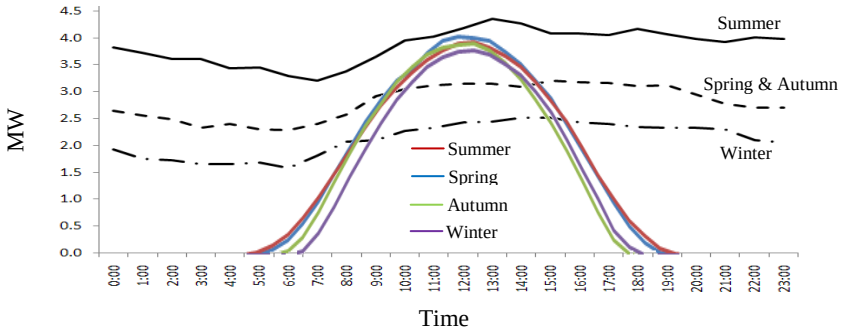

Figure 4.5 Correlation of feeder 3-UG daily load curves with the PVDG curves

Figure 4.5 indicates that sizing the PVDG unit based on the summer daily load curve will result in surplus PVDG power and consequently RPF during the other seasons.

To this end, in hot summer regions it is deemed more appropriate to size the PVDG unit based on the winter daily load curve. This way the RPF is avoided at most times. However, this conclusion is not necessarily applied in the event that RPF is allowed.

4.2 Determination of Feasible Optimization Interval

As mentioned earlier in Chapter.1 connection of DG units to radial distribution feeders can result in several benefits to the feeders and the distribution network as a whole. Determining the optimal sizing and/or location of DG units along radial distribution feeders has therefore become a matter of significant importance. The optimization process is generally solved for certain objectives relating to the minimization of losses in the line conductors of feeders. Consequently, the objectives are mostly placed in terms of line peak power loss reduction (ΔPPL) and/or accumulated line power loss reduction over the day, namely line energy loss reduction (ΔEL).

However, Section 4.1 has concluded that the consideration of ΔPPL benefits may make no sense in the case of PVDG application. This is due to the likely peak mismatch of the load together with PVDG production curves that limit the contribution of the PVDG unit during peak load time interval. Alternatively, consideration of ΔEL benefit perfectly fits the case where the accumulated line power loss reduction over the day is considered. Also it results in coincident benefit of CO_2 emission reduction. Chapter 2 stated that the trend of previous works dealing with ΔEL benefits is to calculate the line power loss reduction at each time interval then to take the overall summation of the whole daily duration. This is likely to end up with long calculations, especially with the connection of time-variant DG systems like PVDG.

In this section a certain time interval is identified at which the ΔEL can be rated. The interval is determined by correlating the load and PVDG production curves as shown in Fig.4.6. The figure shows interval 'A' at which the PVDG unit gives the highest possible compensation of the original power flow from the substation. This results in the highest possible line power loss reduction along the feeder. In such a case, if the PVDG curve touches the load curve, at PV2, the accumulated line power loss reduction over the day (ΔEL) is expected the highest subject to avoidance of RPF. In this essence, 'A' is called the Feasible Optimization Interval (FOI).

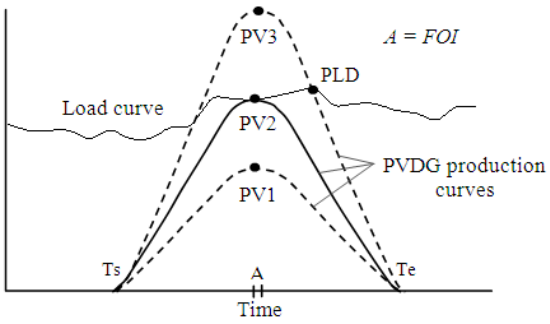

Figure 4.6 Correlation of load and PVDG production curves showing FOI

If the peak of the PVDG production curve increases to PV3 it will penetrate the load curve. This results in certain amount of surplus power production that turns in RPF, which drives the line losses going up again in the reverse direction. The possibility of rating ΔEL at the FOI is derived mathematically in Section 4.3.

It is important to mention that the PVDG power production is different from the capacity of the PV array. Commercially, the capacity of PV array is rated to its dc output power at solar irradiance equals to 1000w/m^2. On the other hand, the PVDG size is the ac power converted by the inverter at the FOI and injected in the feeder. Hence, the commercial PV array capacity (PV_{com}) that can afford for the PVDG power production at the FOI (PV_{FOI}) is expressed as:

$$PV_{com} = \frac{PV_{FOI}}{Eff_{Inv}} \times \frac{1000}{SI_{FOI}} \quad (4.1)$$

Where, Eff_{Inv} is the efficiency of the inverters interfacing the PV array with the grid, and SI_{FOI} is the solar irradiance at the FOI. The SI has the dominant impact over PV cell temperature on the performance of PV array. Thus, Eq.4.1 has been simplified by neglecting the temperature effect.

Power Flow Profile

The PVDG sizing and location that minimizes the power flow during an interval shall also minimize the line power loss along the feeder at that interval. The power flow profile of the

feeder is mainly driven by the load demands along the feeder. Hence, Fig.4.7 depicts the power flow profile along certain radial distribution feeder at the FOI, and this profile is for the real power flow. Note to mention that the load curve drawn at each power step represents the power flow along the line section corresponding to that step over the day. Bearing in mind that the FOI on each load curve is denoted by '•'. In other words, the accumulated area under the steps of Fig.4.7 represent the overall power flow along the feeder at the FOI. This area, namely power flow area, is mainly determined by the vertical lines representing the amount of power flow at the FOI in each line section along with the length of that section.

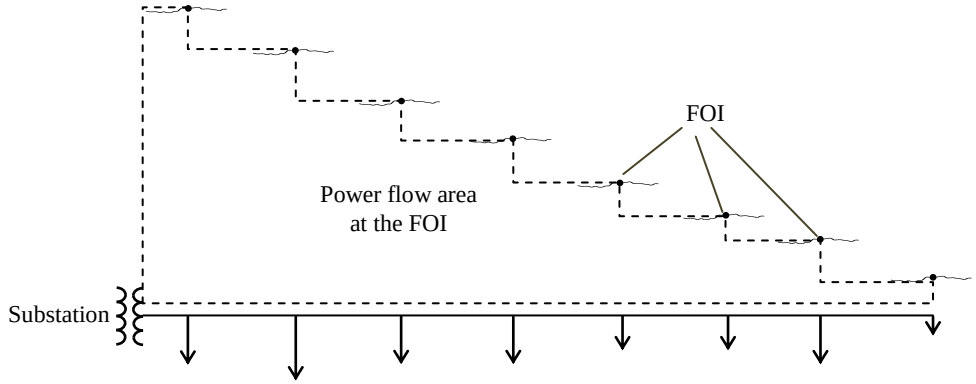

Figure 4.7 Power flow area along radial distribution feeder at the FOI

Now each of the vertical lines can be drawn at any point along the associated section as almost the same amount of power flows through that section. Since the locations of the nodes are fixed, then the power flow area is mainly dependent on the vertical lines. Consequently, the power flow area is represented by dragging these vertical lines to the ending node of each line section then joining the peaks of these lines together as shown in Fig.4.8.

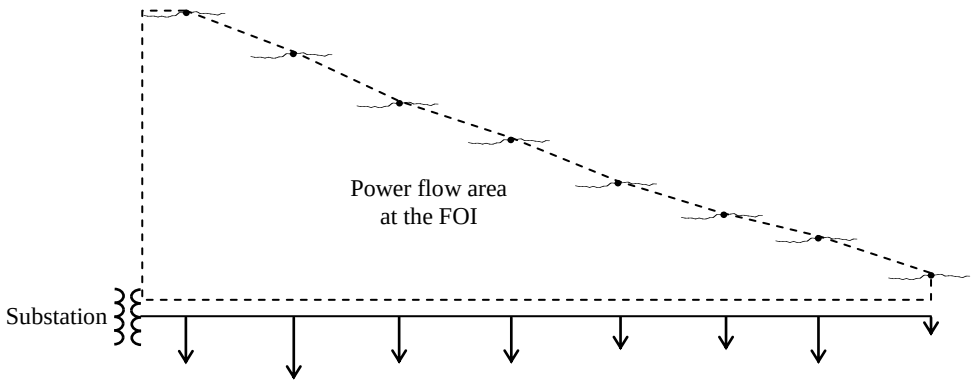

Figure 4.8 Approximated power flow area along radial distribution feeder at the FOI

4.3 Rating the Line Energy Loss at the FOI

It has been concluded in Section 4.1 that consideration of energy-based benefits is appropriate in solving for optimal sizing and location of PVDG units. Also Section 4.2 identified the FOI at which the PVDG unit performs its highest compensation to the original power flow from the substation. In this section a new method is derived to rate the ΔEL, arising from the connection of PVDG unit, by solving the optimization procedure only at the FOI. The method is significantly helpful in iterating the optimization procedure only at the FOI with no need to repeat the calculations on hourly basis, or even shorter intervals. Consequently, the method is integrated in the optimization procedures developed in this work. The procedures determine the optimal sizing and location of PVDG unit(s) that maximize ΔEL considering two scenarios; avoidance and allowance of RPF.

4.3.1 Connection of single PVDG unit with avoidance of reverse power flow

Connection of PVDG unit to node j of the feeder will inject a certain amount of power into the feeder through that node. If the injected power is less than the amount of power flow in section j (ends at node j), the PVDG power will flow in the downstream direction serving the loads between j and n. For maximum compensation of the original power flow from the substation, subject to no RPF, the peak of the PVDG production curve is sized up to touch the load curve of section j at the FOI.

Resulting power flow profile at the FOI

Connection of a PVDG unit at node j, avoiding RPF, divides the original power flow area into A^j and B^j as shown in Fig.4.9. Where $L_{j(FOI)}$ is the load curve value of section j at the FOI while $PV_{j(FOI)}$ is the amplitude of the PVDG production curve.

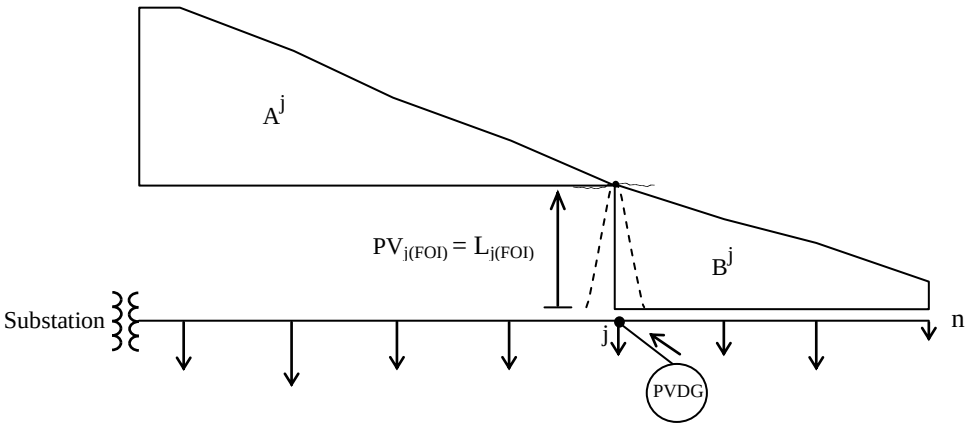

Figure 4.9 Power flow area with PVDG at j avoiding RPF

Moving the PVDG unit to node j-1 can raise the PVDG size to $L_{j-1(FOI)}$. This results in reducing A^j to A^{j-1} but increasing B^j to B^{j-1} as shown in Fig.4.10.

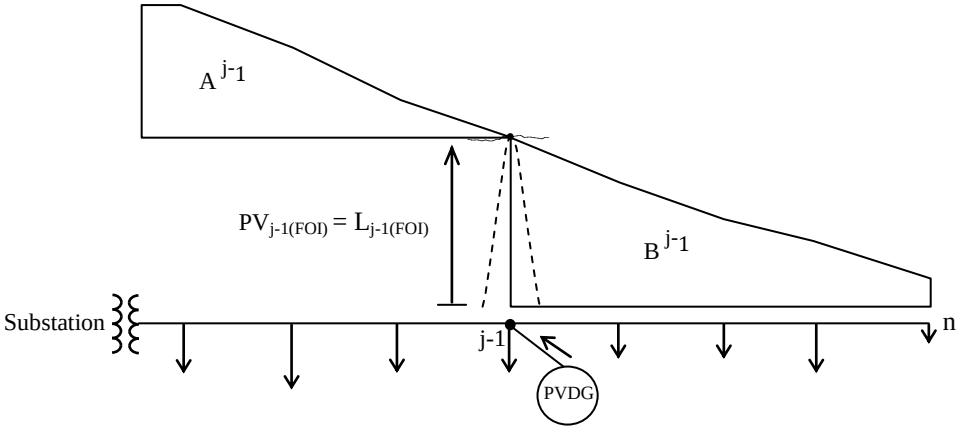

Figure 4.10 Power flow area with PVDG at j-1 avoiding RPF

Referring to Figs.4.9 and 4.10, the PVDG sizing and location that give smaller A+B area will consequently result in higher line power loss reduction at the FOI. Now let the optimal solution is associated with the coupling point (CP) node j-1, then:

$$A^{j-1} + B^{j-1} < A^j + B^j \tag{4.2}$$

As been mentioned earlier in this section, the power flow area is mainly determined by the vertical lines representing the amount of power flow at the FOI in each line section along with the length of that section. But the lengths of line sections are fixed all the time for the feeder. Based on that, the power flow area of a certain feeder can be rated by considering only the vertical lines of power flow along the feeder. Hence, the PVDG at node j is rated as,

$$A^j + B^j = \sum_{k=1}^{j} [L_{k(FOI)} - PV_{j(FOI)}] + \sum_{k=j+1}^{n} L_{k(FOI)} \tag{4.3}$$

And the PVDG at node j-1,

$$A^{j-1} + B^{j-1} = \sum_{k=1}^{j-1} [L_{k(FOI)} - PV_{j-1(FOI)}] + \sum_{k=j}^{n} L_{k(FOI)} \tag{4.4}$$

Where, $L_{k(FOI)}$ is the amount of power flow in section k at the FOI.

Substitution of Eqs.4.3 and 4.4 into Eq.4.2, with the PVDG production curve touching the load curve of the line section it is connected at, yields:

$$\sum_{k=1}^{j-1}(L_{k(FOI)} - L_{j-1(FOI)}) + \sum_{k=j}^{n} L_{k(FOI)} < \sum_{k=1}^{j}(L_{k(FOI)} - L_{j(FOI)}) + \sum_{k=j+1}^{n} L_{k(FOI)} \quad (4.5)$$

$$\sum_{k=1}^{j-1} L_{k(FOI)} - (j-1) \times L_{j-1(FOI)} + \sum_{k=j}^{n} L_{k(FOI)} < \sum_{k=1}^{j} L_{k(FOI)} - j \times L_{j(FOI)} + \sum_{k=j+1}^{n} L_{k(FOI)} \quad (4.6)$$

$$-(j-1) \times L_{j-1(FOI)} + \sum_{k=j}^{n} L_{k(FOI)} - \sum_{k=j+1}^{n} L_{k(FOI)} < -j \times L_{j(FOI)} + \sum_{k=1}^{j} L_{k(FOI)} - \sum_{k=1}^{j-1} L_{k(FOI)} \quad (4.7)$$

But the subtraction of the 2nd and 3rd terms on both sides of Eq.4.7 is equal, as follows:

$$\sum_{k=j}^{n} L_{k(FOI)} - \sum_{k=j+1}^{n} L_{k(FOI)} = \sum_{k=1}^{j} L_{k(FOI)} - \sum_{k=1}^{j-1} L_{k(FOI)} = L_{j(FOI)} \quad (4.8)$$

Substituting Eq.4.8 into Eq.4.7 yields,

$$(j-1) \times L_{j-1(FOI)} > j \times L_{j(FOI)} \quad (4.9)$$

Equation.4.9 compares the cut off area from the original power flow area due to the connection of the PVDG unit at node j and j-1. Hence, at the optimal solution, the difference between the two areas is deemed to be very small.

Resulting energy flow profile

The line energy loss through a line section during certain duration is proportional to the accumulated power flow through that section during the same duration. Accumulated power flow during certain duration is energy flow. Thus, the energy flow through the line section is determined based on the load curve of that section. According to Section.3.2.1, the load curves along the feeder are assumed to vary in a similar pattern to that of the feeder input, but at different levels. Hence, the energy flow of a line section j (E_j) is expressed below in terms of the section load demand at the FOI.

$$E_j = L_{j(FOI)} \times \sum_{i=T1}^{T2} L_{1(i)pu} \quad (4.10)$$

$$L_{1(i)pu} = \frac{L_{1(i)}}{L_{1(FOI)}} \quad (4.11)$$

Where, $L_{j(FOI)}$ - Load demand of section j at the FOI,
$L_{1(i)}$ - Feeder load demand (through section 1) at interval i,
$L_{1(FOI)}$ - Feeder load demand at the FOI,
$L_{1(i)pu}$ - Feeder load demand at interval i in per-unit of that at the FOI,

The influence of PVDG sizing and location on the energy flow through a feeder is depicted in Fig.4.11. For maximum line loss reduction, avoiding RPF, the peak of the PVDG production curve ($PV_{j(FOI)}$) is sized so as to allow the maximum point to touch the load curve of section j at the FOI. Consequently, the area under this PVDG curve will be deducted from each area under the load curves of line sections between the substation and j.

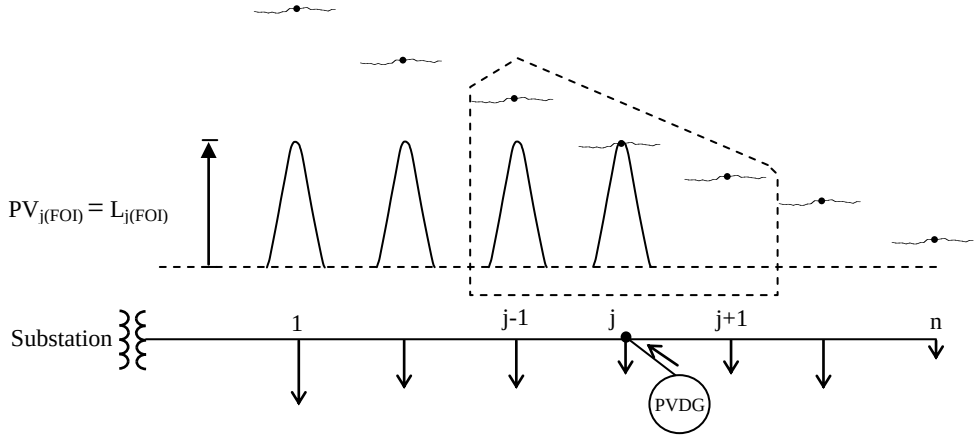

Figure 4.11 Connection of a PVDG unit to node j and its influence on the feeder

In order to analyze the case in more details, the part enclosed by the dotted line in Fig.4.11 is zoomed-in in Fig.4.12.

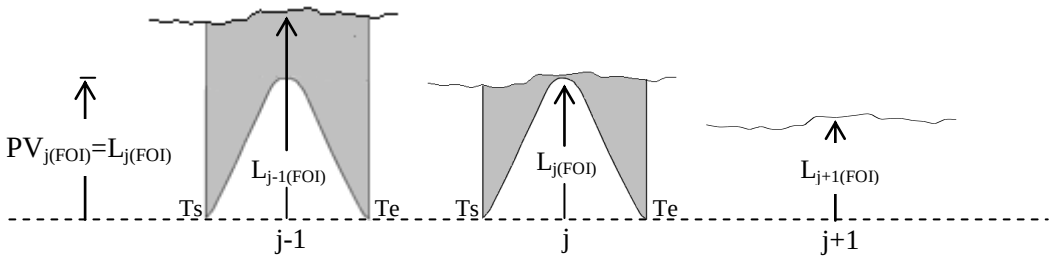

Figure 4.12 Zooming of Fig.4.11

Figure 4.12 shows that the PVDG unit results in zero power flow through section j (ends at node j) at the FOI. However, still there is residual energy flow represented by the shaded area under the load curve of j on the PVDG production curve shoulders. Note that the PVDG unit causes the change only between the start and end of the daytime (Ts-Te). Therefore, the energy-based benefits in this work are considered during this duration.

The energy flow in any line section between the substation and j is rated by subtracting the area under the PVDG curve from the area under the load curve. Taking the line section j-1 as example, the energy flow (E_{j-1}^{j}) is calculated below.

Let,

$$D = \sum_{i=Ts}^{Te} L_{1(i)pu} \qquad \text{and} \qquad S = \sum_{i=Ts}^{Te} PV_{(i)pu} \tag{4.12}$$

Where $L_{1(i)pu}$ and $PV_{(i)pu}$ are in per-unit of their values at the FOI. Then,

$$E_{j-1}^{j} = L_{j-1(FOI)} \times D - L_{j(FOI)} \times S \tag{4.13}$$

Where, superscript j defines the energy terms associated with the PVDG unit at node j.

The energy flow in the downstream sections after j is not affected by the PVDG unit. Taking the line section j+1 as example, the energy flow (E_{j+1}^{j}) over the same duration is rated as:

$$E_{j+1}^{j} = L_{j+1(FOI)} \times D \tag{4.14}$$

Consequently, the total energy flow area along the feeder, with the PVDG unit connected to node j (ET^{j}) is rated below:

$$ET^{j} = \ ET_{1\to j}^{j} + \ ET_{(j+1)\to n}^{j} \tag{4.15}$$

Where $ET_{1\to j}^{j}$ is the summation of energy flow through line section 1 up to j, while $ET_{(j+1)\to n}^{j}$ is the same for the downstream line sections after j up to the end of the feeder. Based on the above, the terms of Eq.4.15 are expressed in terms of Eqs.4.13 and 4.14 as follows:

$$ET_{1\to j}^{j} = \sum_{k=1}^{j} \left(L_{k(FOI)} \times D - L_{j(FOI)} \times S\right) = \sum_{k=1}^{j} L_{k(FOI)} \times D - j \times L_{j(FOI)} \times S \tag{4.16}$$

And,

$$ET_{(j+1)\to n}^{j} = \sum_{k=j+1}^{n} L_{k(FOI)} \times D \tag{4.17}$$

Then,

$$ET^{j} = \sum_{k=1}^{j} L_{k(FOI)} \times D - j \times L_{j(FOI)} \times S + \sum_{k=j+1}^{n} L_{k(FOI)} \times D \tag{4.18}$$

In the same way, the energy flow area associated with the connection of the PVDG unit to node j-1 can be expressed as follows:

$$ET^{j-1} = \sum_{k=1}^{j-1} L_{k(FOI)} \times D - (j-1) \times L_{j-1(FOI)} \times S + \sum_{k=j}^{n} L_{k(FOI)} \times D \tag{4.19}$$

The **s**uperscript 'j-1' defines the energy terms with the PVDG unit connected to node j-1.

Matching of optimal solutions considering energy and power flow at the FOI

The solution associated with the CP node j-1 will be also optimal, considering minimization of energy flow, if the following relation is realized:

$$ET^{j-1} < ET^{j} \tag{4.20}$$

Substituting Eqs.4.18 & 4.19 into Eq.4.20 them multiplying by '-1', yields:

$$-\sum_{k=1}^{j-1} L_{k(FOI)} \times D + (j-1) \times L_{j-1(FOI)} \times S - \sum_{k=j}^{n} L_{k(FOI)} \times D \; > \; -\sum_{k=1}^{j} L_{k(FOI)} \times D + j \times L_{j(FOI)} \times S - \sum_{k=j+1}^{n} L_{k(FOI)} \times D \tag{4.21}$$

On the other hand, the original energy flow area along the feeder is rated as follows:

$$\sum_{k=1}^{n} L_{k(FOI)} \times D = \left(\sum_{k=1}^{j-1} L_{k(FOI)} + \sum_{k=j}^{n} L_{k(FOI)} \right) \times D \tag{4.22.a}$$

Or

$$\sum_{k=1}^{n} L_{k(FOI)} \times D = \left(\sum_{k=1}^{j} L_{k(FOI)} + \sum_{k=j+1}^{n} L_{k(FOI)} \right) \times D \tag{4.22.b}$$

Now, add the right hand sides of Eqs.4.22.a and 4.22.b to the relevant sides of Eq.4.21 and simplify the results in the following equation:

$$(j-1) \times L_{j-1(FOI)} > \; j \times L_{j(FOI)} \tag{4.23}$$

But Eq.4.23 is exactly the same like Eq.4.9, which was already associated with the optimal solution of node j-1 minimizing the power flow at the FOI. In other words, the optimal sizing and location of the PVDG unit that results in the minimum power flow at the FOI also results in the minimum energy flow. Hence, it is enough to run the optimization procedure only at the FOI with no need to go through the long energy-based calculations. This is deemed to be significantly helpful in solving for maximum energy-based benefits along the feeder considering only one interval, which is the FOI.

4.3.2 Connection of multiple PVDG units with avoidance of reverse power flow

Connection of multiple PVDG units on the same feeder can be treated using the aforementioned derivation concept. For simplicity, the derivations will be conducted considering two PVDG units on the feeder. However, the same process is applicable on any number of units.

Resulting power flow profile at the FOI

Figure 4.13 illustrates certain radial distribution feeder with PVDG units at nodes 'X_1' and 'X_2'. The resulting power flow profile at the FOI is rated by the areas A, B and C.

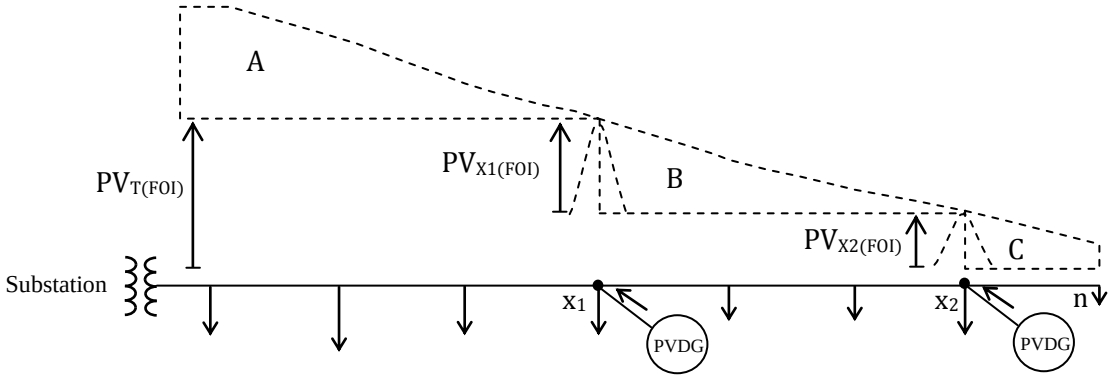

Figure 4.13 Power flow profile with two PVDG units avoiding RPF

Based on Fig.4.13, the two PVDG units are sized as follows:

$$\left.\begin{aligned} PV_{X2(FOI)} &= L_{X2(FOI)} \\ PV_{X1(FOI)} &= L_{X1(FOI)} - L_{X2(FOI)} \\ PV_{T(FOI)} &= PV_{X1(FOI)} + PV_{X2(FOI)} = L_{X1(FOI)} \end{aligned}\right\} \quad (4.24)$$

Where $L_{X1(FOI)}$ and $L_{X2(FOI)}$ are the power flow in line sections 'X_1' and 'X_2' at the FOI.

The total power flow area with the PVDG units at node 'X_1' and 'X_2' is rated as follows:

$$\begin{aligned} (A+B+C)_{X_1}^{X_2} &= \sum_{k=1}^{X_1}(L_{k(FOI)} - L_{X_1(FOI)}) + \sum_{k=X_1+1}^{X_2}(L_{k(FOI)} - L_{X_2(FOI)}) + \sum_{k=X_2+1}^{n} L_{k(FOI)} \\ &= \sum_{k=1}^{X_1} L_{k(FOI)} - x_1 \times L_{X_1(FOI)} + \sum_{k=X_1+1}^{X2} L_{k(FOI)} - (x_2 - x_1) \times L_{X_2(FOI)} + \\ &\quad \sum_{k=X_2+1}^{n} L_{k(FOI)} \end{aligned} \quad (4.25)$$

If the PVDG unit at node 'X_1' is moved one step back to node 'X_1-1'; then power flow area is similarly rated as follows:

$$(A+B+C)_{X_1-1}^{X_2} = \sum_{k=1}^{X_1-1}(L_{k(FOI)} - L_{X_1-1(FOI)}) + \sum_{k=X_1}^{X2}(L_{k(FOI)} - L_{X_2(FOI)}) + \sum_{k=X2+1}^{n} L_{k(FOI)}$$

$$= \sum_{k=1}^{X_1-1} L_{k(FOI)} - (x_1 - 1) \times L_{X_1-1(FOI)} +$$

$$\sum_{k=X_1}^{X_2} L_{k(FOI)} - (x_2 - (x_1 - 1)) \times L_{X_2(FOI)} + \sum_{k=X_2+1}^{n} L_{k(FOI)} \quad (4.26)$$

Now, let the optimal solution is associated with the CP node 'X_1-1' and 'X_2'; thus,

$$(A+B+C)_{X_1-1}^{X_2} < (A+B+C)_{X_1}^{X_2} \quad (4.27)$$

Expand Eq.4.27 then move each of $\sum_{k=1}^{X_1-1} L_{k(FOI)}$ and $\sum_{k=X_1+1}^{X_2} L_{k(FOI)}$ from its side to the other side, as follows:

$$-(x_1 - 1) \times L_{X_1-1(FOI)} + \sum_{k=X_1}^{X_2} L_{k(FOI)} - \sum_{k=X_1+1}^{X_2} L_{k(FOI)} - (x_2 - (x_1 - 1)) \times L_{X_2(FOI)} <$$

$$\sum_{k=1}^{X_1} L_{k(FOI)} - \sum_{k=1}^{X_1-1} L_{k(FOI)} - x_1 \times L_{X_1(FOI)} - (x_2 - x_1) \times L_{X_2(FOI)} \quad (4.28)$$

But

$$\sum_{k=X_1}^{X_2} L_{k(FOI)} - \sum_{k=X_1+1}^{X_2} L_{k(FOI)} = \sum_{k=1}^{X_1} L_{k(FOI)} - \sum_{k=1}^{X_1-1} L_{k(FOI)} = L_{X_1(FOI)} \quad (4.29)$$

Hence,

$$(x_1 - 1) \times L_{X_1-1(FOI)} + (x_2 - (x_1 - 1)) \times L_{X_2(FOI)} > x_1 \times L_{X_1(FOI)} + (x_2 - x_1) \times L_{X_2(FOI)} \quad (4.30)$$

The derivation concept above can be applied in the case of moving the PVDG unit at node 'X_2' to node 'X_2-1' while keeping the PVDG at 'X_1' as is. Assume this will be the optimal solution, the derivation will result in:

$$x_1 \times L_{X_1(FOI)} + ((x_2 - 1) - x_1) \times L_{X_2-1(FOI)} > x_1 \times L_{X_1(FOI)} + (x_2 - x_1) \times L_{X_2(FOI)} \quad (4.31)$$

Resulting energy flow profile

The energy flow profile along the feeder due to the connection of the same two PVDG units at node 'X_1' and 'X_2' is illustrated in Fig.4.14.

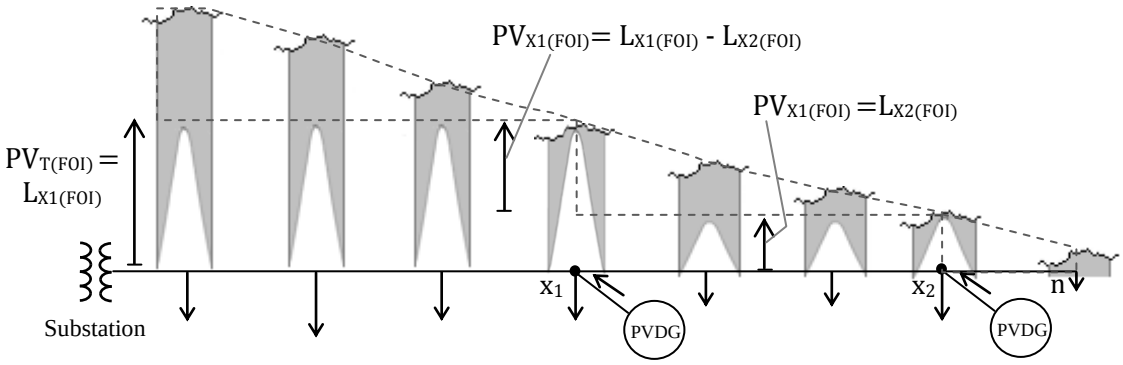

Figure 4.14 Energy flow profile with two PVDG units avoiding RPF

Based on the figure above, the total energy flow area along the feeder with the two PVDG units connected to node 'X_1' and 'X_2' ($ET_{X_1}^{X_2}$) is rated below. Note to mention that the amplitudes of the PVDG production curves are given by Eq.4.24:

$$ET_{X_1}^{X_2} = ET_{1\rightarrow X_1} + ET_{(X_1+1)\rightarrow X_2} + ET_{(X_2+1)\rightarrow n} \tag{4.32}$$

Where,

$$ET_{1\rightarrow X_1} = \sum_{k=1}^{X_1}\left(L_{k(FOI)} \times D - L_{X_1(FOI)} \times S\right) \tag{4.33}$$

$$ET_{(X_1+1)\rightarrow X_2} = \sum_{k=X_1+1}^{X_2}\left(L_{k(FOI)} \times D - L_{X_2(FOI)} \times S\right) \tag{4.34}$$

$$ET_{(X_2+1)\rightarrow n} = \sum_{k=X_{1+1}}^{n} L_{k(FOI)} \times D \tag{4.35}$$

Substitute Eqs.4.33, 4.34 and 4.35 into Eq.4.32 then solve; yields:

$$ET_{X_1}^{X_2} = \sum_{k=1}^{X_1} L_{k(FOI)} \times D - x_1 \times L_{X_1(FOI)} \times S + \sum_{k=X_1+1}^{X_2} L_{k(FOI)} \times D - (x_2 - x_1) \times L_{X_2(FOI)} \times S + \sum_{k=X_2+1}^{n} L_{k(FOI)} \times D \tag{4.36}$$

Similarly; moving the PVDG unit at node 'X_1' back to node 'X_1-1' with the one at 'X_2'is kept as is will result in the following expression for total energy flow area ($ET_{X_1-1}^{X_2}$):

$$ET_{X_1-1}^{X_2} = \sum_{k=1}^{X_1-1} L_{k(FOI)} \times D - (x_1 - 1) \times L_{X_1(FOI)} \times S + \sum_{k=X_1}^{X_2} L_{k(FOI)} \times D - (x_2 - (x_1 - 1)) \times L_{X_2(FOI)} \times S + \sum_{k=X_2+1}^{n} L_{k(FOI)} \times D \quad (4.37)$$

If the optimal solution is associated with the CP node 'X_1-1' and 'X_2', the following relation should be realized:

$$ET_{X_1-1}^{X_2} < ET_{X_1}^{X_2} \quad (4.38)$$

On the other hand, the original energy flow area along the feeder can be expressed as follows:

$$\sum_{k=1}^{n} L_{k(FOI)} \times D = \left(\sum_{k=1}^{X_1} L_{k(FOI)} + \sum_{k=X_1+1}^{X_2} L_{k(FOI)} + \sum_{k=X_2+1}^{n} L_{k(FOI)} \right) \times D \quad (4.39.a)$$

Or

$$\sum_{k=1}^{n} L_{k(FOI)} \times D = \left(\sum_{k=1}^{X_1-1} L_{k(FOI)} + \sum_{k=X_1}^{X_2} L_{k(FOI)} + \sum_{k=X_2+1}^{n} L_{k(FOI)} \right) \times D \quad (4.39.b)$$

At this point, Eqs.4.36 and 4.37 are substituted into Eq.4.38 with both sides of the resulting equation are multiplied by '-1'. Then, adding the term of original energy flow area to each side using Eq.4.39.a for the right hand side and Eq.4.39.b for left hand side results in:

$$(x_1 - 1) \times L_{X_1-1(FOI)} \times S + (x_2 - (x_1 - 1)) \times L_{X_2(FOI)} \times S > x_1 \times L_{X_1(FOI)} \times S + (x_2 - x_1) \times L_{X_2(FOI)} \times S \quad (4.40)$$

Division of Eq.4.40 by S gives:

$$(x_1 - 1) \times L_{X_1-1(FOI)} + (x_2 - (x_1 - 1)) \times L_{X_2(FOI)} > x_1 \times L_{X_1(FOI)} + (x_2 - x_1) \times L_{X_2(FOI)} \quad (4.41)$$

Equation 4.41 is exactly the same as Eq.4.30 realized when the optimal solution associated to node 'X_1-1' and 'X_2' resulted in minimum power flow at the FOI. In the same course, solving the derivations with the PVDG unit at node 'X_2' is moved back to X_2-1 while the one at the 'X_2' is kept as is will yield the same equation as Eq.4.31.

Hence, the optimal solution that results in minimum power flow along the feeder at the FOI also results in minimum energy flow. The derivation concept can be applied easily on any number of PVDG units to yield the same optimal solution.

4.3.3 Connection of single PVDG unit with allowance of reverse power flow

Some power distribution companies upgrade their networks with smart protection and control systems equipped with microprocessor units. These systems are supposed to deal reasonably with RPF conditions. In such a case, setting the RPF as a constraint is no longer valid. Consequently, the optimization procedure is developed further allowing RPF to the extent that it does not reach the substation. This way, the voltage profile is deemed not to exceed the voltage level at the s/s. Besides, the current flow will be complied with the ampacity of the feeder.

In light of allowing reverse power flow, a new variable related to the PVDG sizing is added to the optimization process. This variable arises because the PVDG sizing at certain locations is no longer limited to the amount of power flow to that location. As a matter of fact, each location is now eligible to install PVDG units of different capacity and produce different amounts of reverse power flow. To this end, the optimization procedure is further developed to determine the local optimal capacity for the PVDG unit at each location. In this section, the local optimal sizing is assumed at a value that avoids the reverse power flow from reaching the substation. However, determination of the local optimal sizing will be explained in Section 5.3.

Resulting power flow profile at the FOI

Using the same concept of Sections 4.3.1 and 4.3.2, Figs.4.15 and 4.16 illustrate the power flow area along the feeder with the PVDG unit connected to nodes j and j-1. The PVDG size in both cases exceeds the original power flow of the location they are connected at, resulting in certain amount of RPF. However, the size is set in a way that the RPF does not reach the substation. Note to mention that m^j represents the node at which the RPF ends, and $L_{m^j(FOI)}$ is the original power flow in line section m^j at the FOI.

The power flow area resulting from the connection of the PVDG unit at j is rated, based on Fig.4.15, as follows:

$$A^j = \sum_{k=1}^{m^j} (L_{k(FOI)} - L_{m^j(FOI)}) = \sum_{k=1}^{m^j} L_{k(FOI)} - m^j \times L_{m^j(FOI)} \quad (4.42.a)$$

$$B^j = \sum_{k=m^j+1}^{j} (L_{m^j(FOI)} - L_{k(FOI)}) = (j - m^j) \times L_{m^j(FOI)} - \sum_{k=m^j+1}^{j} L_{k(FOI)} \quad (4.42.b)$$

$$C^j = \sum_{k=j+1}^{n} L_{k(FOI)} \quad (4.42.c)$$

Similarly,

$$A^{j-1} = \sum_{k=1}^{m^{j-1}} (L_{k(FOI)} - L_{m^{j-1}(FOI)}) = \sum_{k=1}^{m^{j-1}} L_{k(FOI)} - m^{j-1} \times L_{m^{j-1}(FOI)} \quad (4.43.a)$$

$$B^{j-1} = \sum_{k=m^{j-1}+1}^{j-1} (L_{m^{j-1}(FOI)} - L_{k(FOI)})$$

$$= ((j-1) - m^{j-1}) \times L_{m^{j-1}(FOI)} - \sum_{k=m^{j-1}+1}^{j-1} L_{k(FOI)} \quad (4.43.b)$$

$$C^{j-1} = \sum_{k=j}^{n} L_{k(FOI)} \quad (4.43.c)$$

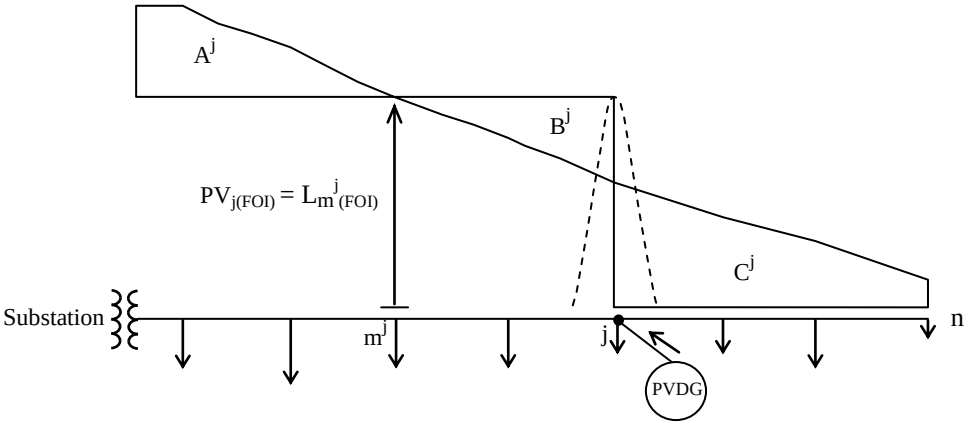

Figure 4.15 Power flow profile with PVDG at j allowing reverse power flow

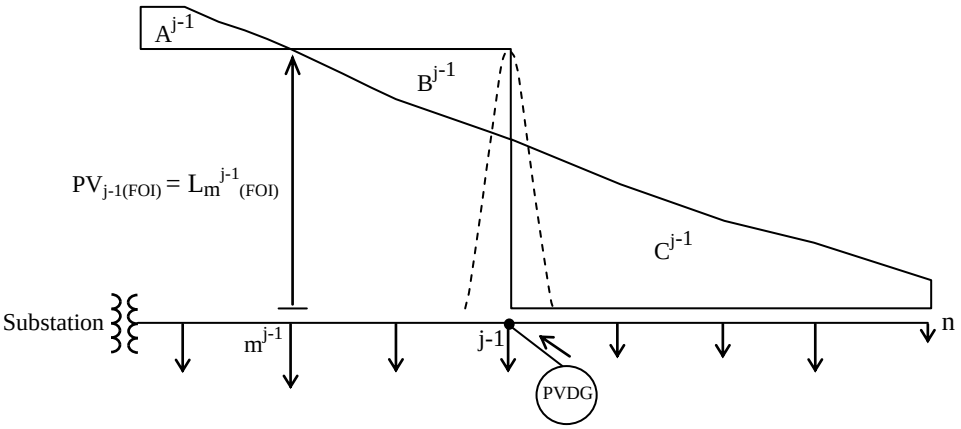

Figure 4.16 Power flow profile with PVDG at j-1 allowing reverse power flow

Let the optimal solution be associated with the CP node j-1, then:

$$A^{j-1} + B^{j-1} + C^{j-1} < A^j + B^j + C^j \quad (4.44)$$

Multiply Eq.4.44 by '-1' then add $\sum_{k=1}^{n} L_{k(FOI)}$ to both sides, yields:

$$\sum_{k=1}^{n} L_{k(FOI)} - \left(A^{j-1} + B^{j-1} + C^{j-1}\right) > \sum_{k=1}^{n} L_{k(FOI)} - \left(A^{j} + B^{j} + C^{j}\right) \quad (4.45)$$

But

$$\sum_{k=1}^{n} L_{k(FOI)} = \sum_{k=1}^{m^{j-1}} L_{k(FOI)} + \sum_{k=m^{j-1}+1}^{j-1} L_{k(FOI)} + \sum_{k=j}^{n} L_{k(FOI)} \quad (4.46.a)$$

Or,

$$\sum_{k=1}^{n} L_{k(FOI)} = \sum_{k=1}^{m^{j}} L_{k(FOI)} + \sum_{k=m^{j}+1}^{j} L_{k(FOI)} + \sum_{k=j+1}^{n} L_{k(FOI)} \quad (4.46.b)$$

Eqs.4.46.a and 4.46.b were substituted into the left and right hand sides of Eq.4.45 respectively, then A, B, and C were expressed in their forms of Eqs.4.42 and 4.43. Solving the resulting expression yields:

$$m^{j-1} \times L_{m^{j-1}(FOI)} - \left(j - 1 - m^{j-1}\right) \times L_{m^{j-1}(FOI)} + 2 \times \sum_{k=m^{j-1}+1}^{j-1} L_{k(FOI)} \; > \; m^{j} \times L_{m^{j}(FOI)} - (j - m^{j}) \times L_{m^{j}(FOI)} + 2 \times \sum_{k=m^{j}+1}^{j} L_{k(FOI)} \quad (4.47)$$

Matching Eq.4.47 with Figs.4.15 & 4.16 shows that it compares the cut off area from the original power flow area due to the connection of the PVDG unit at node j and j-1.

Resulting energy flow profile

The energy flow associated with RPF adds complexity to the derivation process. The reason is that the direction of energy flow will not be the same in all the line sections along the feeder. Moreover, in some line sections the energy flow will change its direction during the same day. The shaded areas in Fig.4.17 show the energy flow profile along the distribution feeder with a PVDG unit connected to node j, allowing RPF.

The energy flow area along the feeder between the substation and node m^j due to connection of PVDG unit at j ($ET^{j}_{1\rightarrow m^{j}}$) is rated below. Note that the superscript j defines the terms associated with the connection of the PVDG unit at j.

$$ET^{j}_{1\rightarrow m^{j}} = \sum_{k=1}^{m^{j}} (L_{k(FOI)} \times D - L_{m^{j}(FOI)} \times S) = \sum_{k=1}^{m^{j}} L_{k(FOI)} \times D \; - m^{j} \times \; L_{m^{j}(FOI)} \times S \quad (4.48)$$

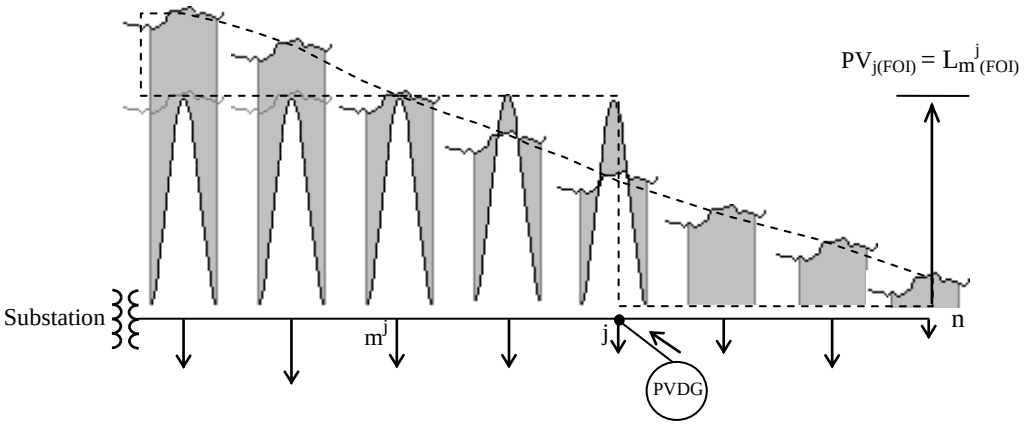

Figure 4.17 Power flow profile with PVDG at j allowing reverse power flow

The feeder sections between nodes m^j and j encounters RPF during the times the PVDG production exceeds the load demand. Thus, the energy flow area in any line sections, k, of these is represented by the portions 1, 2 and 3; which are illustrated in Fig.4.18.

Portion 1 exceeds the load demand so it flows in the reverse direction. At the same time, portions 2 and 3 represent the residual energy flow in the forward direction that cannot be compensated by the PVDG production.

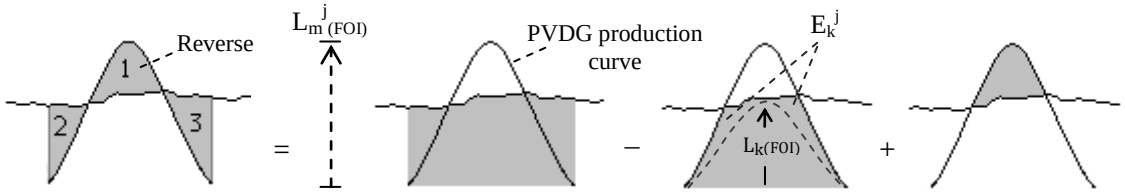

Figure 4.18 Determination of energy flow in line section between node m^j and j

Referring to Fig.4.18, the shaded areas b, c and d along the feeder between nodes m^j and j are expressed as follows:

$$b = \sum_{k=m^j+1}^{j} L_{k(FOI)} \times D \qquad (4.49.a)$$

$$c = \sum_{k=m^j+1}^{j} \left(L_{k(FOI)} \times S + E_k^j \right) \qquad (4.49.b)$$

$$d = \sum_{k=m^j+1}^{j} \left(L_{m^j(FOI)} \times S - \left(L_{k(FOI)} \times S + E_k^j \right) \right) \qquad (4.49.c)$$

Where, E_k^j is the energy portion under the load curve enclosed between the actual PVDG curve and a virtual PVDG curve of amplitude equals to $L_{k(FOI)}$.

According to Fig.4.18, the energy flow area along the feeder between node m^j and j due to connection of PVDG unit at j ($ET^j_{(m^j+1)\to j}$) is rated as follows:

$$ET^j_{(m^j+1)\to j} = \sum_{k=m^j+1}^{j} (b - c + d) \tag{4.50}$$

Substituting Eq.4.49 into Eq.4.50 yields:

$$ET^j_{(m^j+1)\to j} = \sum_{k=m^j+1}^{j} L_{k(FOI)} \times D - \sum_{k=m^j+1}^{j} \left(L_{k(FOI)} \times S + E_k^j\right) + \sum_{k=m^j+1}^{j} \left(L_{m^j(FOI)} \times S - \left(L_{k(FOI)} \times S + E_k^j\right)\right) \tag{4.51}$$

The energy flow area along the feeder between node j and n ($ET^j_{(j+1)\to n}$) is not affected by the connection of PVDG unit. Hence, the energy flow is rated as follows:

$$ET^j_{(j+1)\to n} = \sum_{k=j+1}^{n} L_{k(FOI)} \times D \tag{4.52}$$

Consequently, the total energy flow along the feeder, with the PVDG unit connected to node j (ET^j) is rated below:

$$ET^j = \{ET^j_{1\to m^j}\} + \{ET^j_{(m^j+1)\to j}\} + \{ET^j_{(j+1)\to n}\} \tag{4.53}$$

Substitution of Eqs.4.48, 4.51 and 4.52 into Eq.4.53, gives:

$$ET^j = \left\{ \sum_{k=1}^{m^j} L_{k(FOI)} \times D - m^j \times L_{m^j(FOI)} \times S \right\} + \left\{ \sum_{k=m^j+1}^{j} L_{k(FOI)} \times D - 2 \sum_{k=m^j+1}^{j} L_{k(FOI)} \times S - 2 \sum_{k=m^j+1}^{j} E_k^j + (j - m^j) \times L_{m^j(FOI)} \times S \right\} + \left\{ \sum_{k=j+1}^{n} L_{k(FOI)} \times D \right\} \tag{4.54}$$

Similarly, moving the PVDG unit back to node j-1 will result in the following energy flow:

$$ET^{j-1} = \left\{ \sum_{k=1}^{m^{j-1}} L_{k(FOI)} \times D - m^{j-1} \times L_{m^{j-1}(FOI)} \times S \right\} + \left\{ \sum_{k=m^{j-1}+1}^{j-1} L_{k(FOI)} \times D - 2 \sum_{k=m^{j-1}+1}^{j-1} L_{k(FOI)} \times S - 2 \sum_{k=m^{j-1}+1}^{j-1} E_k^{j-1} + (j - 1 - m^{j-1}) \times L_{m^{j-1}(FOI)} \times S \right\} + \left\{ \sum_{k=j}^{n} L_{k(FOI)} \times D \right\} \quad (4.55)$$

Matching of optimal solutions considering energy and power flow at the FOI

Let the solution associated with the CP node j-1 be the optimal solution; then

$$ET^{j-1} < ET^{j} \quad (4.56)$$

Substituting Eqs.4.54 and 4.55 into Eq.5.56 and multiplying both sides by '-1' yields:

$$-\sum_{k=1}^{m^{j-1}} L_{k(FOI)} \times D + m^{j-1} \times L_{m^{j-1}(FOI)} \times S - \sum_{k=m^{j-1}+1}^{j-1} L_{k(FOI)} \times D + 2 \sum_{k=m^{j-1}+1}^{j-1} L_{k(FOI)} \times S + 2 \sum_{k=m^{j-1}+1}^{j-1} E_k^{j-1} - (j - 1 - m^{j-1}) \times L_{m^{j-1}(FOI)} \times S - \sum_{k=j}^{n} L_{k(FOI)} \times D$$

$$> -\sum_{k=1}^{m^{j}} L_{k(FOI)} \times D + m^{j} \times L_{m^{j}(FOI)} \times S - \sum_{k=m^{j}+1}^{j} L_{k(FOI)} \times D + 2 \sum_{k=m^{j}+1}^{j} L_{k(FOI)} \times S + 2 \sum_{k=m^{j}+1}^{j} E_k^{j} - (j - m^{j}) \times L_{m^{j}(FOI)} \times S - \sum_{k=j+1}^{n} L_{k(FOI)} \times D \quad (4.57)$$

Adding $\sum_{k=1}^{n} L_{k(FOI)} \times D$ to both sides of Eq.4.57 while considering the following breakdown expressions,

$$\sum_{k=1}^{n} = \left(\sum_{k=1}^{m^{j-1}} + \sum_{k=m^{j-1}+1}^{j-1} + \sum_{j}^{n} \right) = \left(\sum_{k=1}^{m^{j}} + \sum_{k=m^{j}+1}^{j} + \sum_{j+1}^{n} \right) \quad (4.58)$$

allows, Eq.4.57 to be simplified to,

$$m^{j-1} \times L_{m^{j-1}(FOI)} \times S - (j - 1 - m^{j-1}) \times L_{m^{j-1}(FOI)} \times S + 2 \sum_{k=m^{j-1}+1}^{j-1} L_{k(FOI)} \times S + 2 \sum_{k=m^{j-1}+1}^{j-1} E_k^{j-1}$$

$>$

$$m^{j} \times L_{m^{j}(FOI)} \times S - (j - m^{j}) \times L_{m^{j}(FOI)} \times S + 2 \sum_{k=m^{j}+1}^{j} L_{k(FOI)} \times S + 2 \sum_{k=m^{j}+1}^{j} E_k^{j} \quad (4.59)$$

Dividing both sides by S, yields:

$$m^{j-1} \times L_{m^{j-1}(FOI)} - (j - 1 - m^{j-1}) \times L_{m^{j-1}(FOI)} + 2 \sum_{k=m^{j-1}+1}^{j-1} L_{k(FOI)} + \left(\frac{2}{S} \times \sum_{k=m^{j-1}+1}^{j-1} E_k^{j-1} \right)$$

$>$

$$m^{j} \times L_{m^{j}(FOI)} - (j - m^{j}) \times L_{m^{j}(FOI)} + 2 \sum_{k=m^{j}+1}^{j} L_{k(FOI)} + \left(\frac{2}{S} \times \sum_{k=m^{j}+1}^{j} E_k^{j} \right) \quad (4.60)$$

Equqtion.4.60 is similar to Eq.4.47 when the optimal solution at node j-1 resulted in the maximum ΔPL_{FOI}. The only difference is the terms of E_k on both side of Eq.4.60. Figure.4.18.c illustrated that E_k is part of the area cut off from the original energy flow area due to the connection of the PVDG unit. It shows also that E_k is proportional to the amplitude of the PVDG production curve, which is also the case with the total cut off area. Consequently, to a reasonable approximation the E_k term on both sides of Eq.4.60 are assumed not to change the balance of the equation.

As a conclusion, the optimal solution that maximizing the ΔPL_{FOI} benefit is to great extent the optimal solution maximizing the ΔEL, even with the allowance of RPF.

4.3.4 Connection of multiple PVDG units with allowance of reverse power flow

The application set is completed by considering the scenario of RPF allowance with multiple PVDG units on the same radial feeder. From the experience of the previous sections, the same derivations of Section 4.3.3 can be extended to tackle this scenario with no need to go through new detailed derivations.

Reduction in power flow profile at the FOI

For simplicity, the derivation is conducted considering two PVDG units, but the same concept can be applied on any number of units. Thus, Fig.4.19 shows the power flow profile at the FOI with two PVDG units connected at the CP node X_1 and X_2. On the same concept of Eq.4.47, the total reduction in power flow area is represented directly by the area cut off from the original power flow area minus the power flow area added in the sections witnessing RPF.

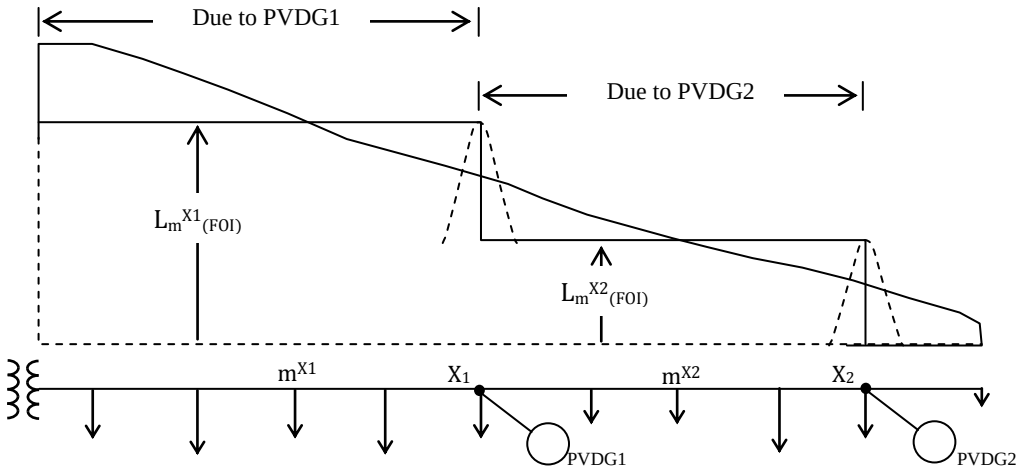

Figure 4.19 Power flow profile with two PVDG units allowing RPF

Also it is noticed that the power flow area along the line sections affected by the PVDG units in Fig.4.19 (from the s/s to X_2) have the same trend of that in Fig.4.15 (or Fig.4.16). As a matter of fact, the trend associated with single PVDG unit in Fig.4.15 is repeated in Fig.4.19 number of times equal the number of PVDG units. Hence, the reduction in power flow area due to the PVDG units at X_1 and X_2 ($\Delta PA_{X_1}^{X_2}$) can be expressed directly, based on Eq.4.47, as follows:

$$\Delta PA_{X_1}^{X_2} = m^{X_1} \cdot L_{m^{X_1}(FOI)} - (X_1 - m^{X_1}) \cdot L_{m^{X_1}(FOI)} + 2 \sum_{k=m^{X_1}+1}^{X_1} L_{k(FOI)}$$
$$+(m^{X_2} - X_1) \cdot L_{m^{X_2}(FOI)} - (X_2 - m^{X_2}) \cdot L_{m^{X_2}(FOI)} + 2 \sum_{k=m^{X_2}+1}^{X_2} L_{k(FOI)} \quad (4.61)$$

On the same basis, if the PVDG unit at node X_2 is moved back to node X_2-1, the reduction in power flow area is expressed as:

$$\Delta PA_{X_1}^{X_2-1} = m^{X_1} \cdot L_{m^{X_1}(FOI)} - (X_1 - m^{X_1}) \cdot L_{m^{X_1}(FOI)} + 2 \sum_{k=m^{X_1}+1}^{X_1} L_{k(FOI)}$$
$$+(m^{X_2-1} - X_1) \cdot L_{m^{X_2-1}(FOI)} - ((X_2 - 1) - m^{X_2-1}) \cdot L_{m^{X_2-1}(FOI)} + 2 \sum_{k=m^{X_2-1}+1}^{X_2-1} L_{k(FOI)} \quad (4.62)$$

Now, let the optimal solution is associated with the CP node 'X_1' and 'X_2-1'; thus,

$$\Delta PA_{X_1}^{X_2-1} > \Delta PA_{X_1}^{X_2} \quad (4.63)$$

Substituting Eqs.4.61 and 4.62 into Eq.4.63 then canceling the similar terms yields:

$$(m^{X_2-1} - X_1) \cdot L_{m^{X_2-1}(FOI)} - ((X_2 - 1) - m^{X_2-1}) \cdot L_{m^{X_2-1}(FOI)} + 2 \sum_{k=m^{X_2-1}+1}^{X_2-1} L_{k(FOI)}$$

>

$$(m^{X_2} - X_1) \cdot L_{m^{X_2}(FOI)} - (X_2 - m^{X_2}) \cdot L_{m^{X_2}(FOI)} + 2 \sum_{k=m^{X_2}+1}^{X_2} L_{k(FOI)} \quad (4.64)$$

Resulting energy flow profile

The resulting energy flow profile due to the PVDG units at the CP nodes X_1 and X_2 is represented by the shaded areas of Fig.4.20. Similar to the power flow reduction of Fig.4.19, the trend associated with single PVDG unit in Fig.4.17 is repeated in Fig.4.20 by the number of PVDG units. Hence, the reduction in energy flow area due to the PVDG units at X_1 and X_2 ($\Delta EA_{X_1}^{X_2}$) can be expressed directly, based on Eq.4.60, as follows:

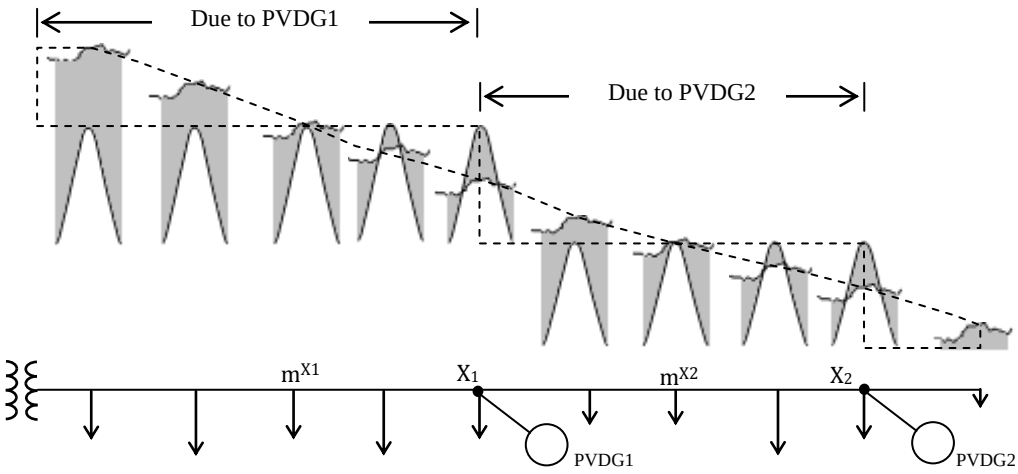

Figure 4.20 Energy flow profile with two PVDG units allowing RPF

$$\Delta EA_{X_1}^{X_2} = m^{X_1} \cdot L_{m^{X_1}(FOI)} - (X_1 - m^{X_1}) \cdot L_{m^{X_1}(FOI)} + 2 \sum_{k=m^{X_1}+1}^{X_1} L_{k(FOI)} + \frac{2}{S} \times \sum_{k=m^{X_1}+1}^{X_1} E_k^{X_1} +$$

$$(m^{X_2} - X_1) \cdot L_{m^{X_2}(FOI)} - (X_2 - m^{X_2}) \cdot L_{m^{X_2}(FOI)} + 2 \sum_{k=m^{X_2}+1}^{X_2} L_{k(FOI)} +$$

$$\frac{2}{S} \times \sum_{k=m^{X_2}+1}^{X_2} E_k^{X_2} \quad (4.65)$$

On the same basis, if the PVDG unit at node X_2 is moved back to node X_2-1, the reduction in power flow area is expressed as:

$$\Delta EA_{X_1}^{X_2-1} = m^{X_1} \cdot L_{m^{X_1}(FOI)} - (X_1 - m^{X_1}) \cdot L_{m^{X_1}(FOI)} + 2 \sum_{k=m^{X_1}+1}^{X_1} L_{k(FOI)} + \frac{2}{S} \sum_{k=m^{X_1}+1}^{X_1} E_k^{X_1} +$$

$$(m^{X_2-1} - X_1) \cdot L_{m^{X_2-1}(FOI)} - \left((X_2 - 1) - m^{X_2-1}\right) \cdot L_{m^{X_2-1}(FOI)} + 2 \sum_{k=m^{X_2-1}+1}^{X_2-1} L_{k(FOI)} +$$

$$\frac{2}{S} \times \sum_{k=m^{X_2-1}+1}^{X_2-1} E_k^{X_2-1} \quad (4.66)$$

Now, let the optimal solution is associated with the CP node 'X_1' and 'X_2-1'; thus,

$$\Delta EA_{X_1}^{X_2-1} > \Delta EA_{X_1}^{X_2} \quad (4.67)$$

Substituting Eqs.4.65 and 4.66 into Eq.4.67 then canceling the similar terms yields:

$$(m^{X_2-1} - X_1) \cdot L_{m^{X_2-1}(FOI)} - \left((X_2 - 1) - m^{X_2-1}\right) \cdot L_{m^{X_2-1}(FOI)} + 2 \sum_{k=m^{X_2-1}+1}^{X_2-1} L_{k(FOI)} +$$

$$\frac{2}{S} \times \sum_{k=m^{X_2-1}+1}^{X_2-1} E_k^{X_2-1}$$

$>$

$$(m^{X_2} - X_1) \cdot L_{m^{X_2}(FOI)} - (X_2 - m^{X_2}) \cdot L_{m^{X_2}(FOI)} + 2 \sum_{k=m^{X_2}+1}^{X_2} L_{k(FOI)} +$$

$$\frac{2}{S} \times \sum_{k=m^{X_2}+1}^{X_2} E_k^{X_2} \quad (4.68)$$

The detailed terms of Eq.4.68 are similar that of Eq.4.64 related to power flow reduction. The only difference is the terms of E_k on both side of Eq.4.68, which can be reasonably assumed not to change the balance of the equation.

As a conclusion, the optimal solution that maximizes the power flow reduction at the FOI to great extent maximizes the energy flow reduction. But the power and energy flow n is directly proportional to the power and energy losses in the lines. Hence, the optimal solution maximizes ΔPL_{FOI} is also considered to maximize ΔEL.

4.4 Summary

Connection of PVDG units to distribution feeders brings several benefits to the feeders and the distribution network as a whole. The degree of benefit depends on the sizing and location of these units. A suitable procedure for optimal sizing and location of certain PVDG unit on radial distribution feeder has been developed. Due to the peak mismatch of load and PVDG production curves, the procedure is placed considering maximum line energy loss reduction (ΔEL) rather than maximum line peak power loss reduction (ΔPPL).

However, solving for maximum ΔEL requires the calculation of accumulated line power loss reduction throughout the intervals of the daily duration. This is deemed to need long calculations especially with the connection of time-variant DG systems like PVDG units. In this course a certain time interval, namely feasible optimization interval (FOI), is determined at which the ΔEL can be rated. The FOI corresponds to the time at which the PVDG unit gives the highest possible compensation of the original power flow from the substation.

As a conclusion, the optimal sizing and location of a PVDG unit that results in maximum line power loss reduction at the FOI also found to result in maximum ΔEL. Hence, it is enough to run the optimization procedure only at the FOI with no need to go through the lengthy energy-based calculations. Detailed mathematical derivations have been developed to prove the concept considering single and multiple PVDG units on radial distribution feeder. The derivations have been placed in a way that avoids RPF along the feeder. However, the derivations have been extended further considering the case of connecting single and multiple PVDG unit with the allowance of RPF.

In the same connection, the variations of load curves and PVDG production curves over seasons have been also taken into account. In hot summer regions, like Abu Dhabi, the sizing of a PVDG unit based on summer daily load curve may result in surplus PVDG power, and consequently RPF, during the other seasons. Thus, if the avoidance of RPF is required in such regions, it is recommended to size the PVDG unit(s) based on winter daily load curve.

References

[1] A. Al-Sabounchi, J. Gow, M. Al-Akaidi, and H. Al-Thani "Optimal Sizing and Location of PVDG Unit on Radial Distribution Feeder Avoiding Reverse Current Flow," *in Proc. Dec.2010 GAMEON-ARABIA'2010, Egypt,* pp.1-7

[2] Sauli Jäntti (Editor), "Connection of Distributed Energy Generation Units in the Distribution Network and Grid," *CODGUNet final report, Issued by Merinova Ab on behalf of four Nordic countries,* Finland, Sep. 2003.

5 OPTIMAL SIZING & LOCATION OF PVDG UNITS

As has been mentioned earlier in previous chapters, connection of PVDG unit(s) to radial distribution feeder results in several benefits to the feeder and the distribution network. The level of benefits is driven by the sizing and location of the connected PVDG units. A suitable optimization procedure determining the optimal sizing and location of these units on a radial distribution feeder has been developed in this section. The main objective of the optimization problem is to maximize the accumulated line power loss reduction along the feeder over the day, namely line energy loss reduction (ΔEL). Due to the peak mismatch of the load and PVDG production curves, the line peak power loss reduction is considered as an additional benefit provided that the peak load time occurs during daylight hours.

The connection of PVDG units to radial distribution feeders injects a certain amount of power into the feeder. If the injected power exceeds the load demand at the coupling point, the surplus power will flow in the reverse direction towards the substation. Due to the inconveniences of reverse power flow (RPF), stated in Chapter 1, the optimization procedure is solved subject to avoidance of surplus PVDG power production over the day. For a wider range of applications, suitable optimization procedures have been developed considering single and multiple PVDG units on the same feeder.

Nevertheless, some distribution companies upgrade their networks with advanced protection and control systems that can deal with RPF. To this end, the work has been extended further dealing with the optimal sizing and location PVDG units with the allowance of RPF. Suitable procedures have been developed considering single and multiple PVDG units.

5.1 Optimization Procedures Avoiding RPF

This section presents the procedures developed for the optimal sizing and location of single and multiple PVDG units on a radial distribution feeder. Surplus PVDG power production and consequent RPF are set as constraints.

5.1.1 Single PVDG units on balanced 3-phase feeder avoiding RPF

Primary distribution feeders are usually installed as a 3-phase system. However, lateral feeders of 1-phase, 2-phase, and 3-phase systems maybe branched out from them. At the same time,

loads of different characteristics and demands are served by the phases of the feeders and laterals. As a result, the distribution feeders are most likely to operate in an unbalanced load condition [1].

Nevertheless, the primary feeders and laterals in many distribution networks, such as those in Abu Dhabi, consist of 3-phase systems. In such cases the distribution companies may generally consider the feeders to operate under 3-phase balanced load condition.

Based on the above, this section is dedicated to develop the optimization procedure considering a 3-phase balanced load feeder. This will be helpful in presenting the concept and setting recommendations for the following sections dealing with unbalanced load feeder. The procedure is applied on the two 11kV feeders specified in Appendix 2.

Modeling of line impedance in 3-phase balanced load feeder

In order to apply the optimization procedure it is important to model the line impedance of the distribution feeder along with the load and PVDG production curves. Note that the load curve of active power demand has been considered. This is due the assumption that the PVDG unit is working at unity power factor. However, all the power flow calculations are run using complex numbers so that the impact of reactive power on the line losses is included.

The line impedance (z_i) of the feeder sections along the feeder is modeled based on the type and geometric parameters of the conductors and the length of sections. The resistance (r) per-unit length is obtained from the conductor data sheet. As for the line impedance (z), Eq.3.6 is applied with D_{eq} is calculated from Eq.3.4 and GMR is determined from the data sheet or by multiplying the radius of the conductor by 0.7788 [2]. Table 5.1 and Table 5.2 state the results from the two feeders after having been multiplied by the length of feeder sections.

Table 5.1 Line impedance of feeder F1 considering 3-phase balanced load condition

Send node	Receive node	Line section	Impedance (z) in Ω
S.S	1	1	0.15360 + j0.10793
1	2	2	0.07936 + j0.05577
2	3	3	0.00519 + j0.00461
3	4	4	0.05248 + j0.03688
4	5	5	0.19200 + j0.13492
5	6	6	0.06174 + j0.05479
6	7	7	0.07840 + j0.06958
7	8	8	0.07840 + j0.06958
8	9	9	0.06246 + j0.04389
9	10	10	0.12480 + j0.08770
10	11	11	0.15043 + j0.13350
11	12	12	0.10880 + j0.07645
12	13	13	0.02842 + j0.02522
13	14	14	0.02842 + j0.02522

Table 5.2 Line impedance of feeder F2 considering 3-phase balanced load condition

From node	Receive node	Line section	Impedance (z) in Ω
S.S	1	1	$0.35045 + j0.31101$
1	2	2	$0.00980 + j0.00870$
2	3	3	$0.10398 + j0.13001$
3	4	4	$0.09235 + j0.11546$
4	5	5	$0.18191 + j0.22745$
5	6	6	$0.25958 + j0.32456$
6	7	7	$0.26438 + j0.33057$
7	8	8	$0.18317 + j0.22903$
8	9	9	$0.22770 + j0.28470$
9	10	10	$0.18596 + j0.23251$
10	11	11	$0.09285 + j0.11610$
11	12	12	$0.11081 + j0.13856$
12	13	13	$0.17710 + j0.22144$
13	14	14	$0.29146 + j0.36442$
14	15	15	$0.18621 + j0.23282$
15	16	16	$0.24516 + j0.30653$
16	17	17	$0.32890 + j0.41124$
17	18	18	$0.17710 + j0.22144$
18	19	19	$0.16723 + j0.20910$
19	20	20	$0.14345 + j0.17936$
20	21	21	$0.09892 + j0.12369$
21	22	22	$0.18241 + j0.22808$
22	23	23	$0.28032 + j0.35050$
23	24	24	$0.18697 + j0.23377$
24	25	25	$0.07752 + j0.06880$
25	26	26	$0.14700 + j0.13046$
26	27	27	$0.00147 + j0.00130$
27	28	28	$0.07350 + j0.06523$
28	29	29	$0.00147 + j0.00130$

PVDG production curve modeling

At this time the optimization procedure is run based on summer daily demand. Thus the average daily solar irradiance (SI) curve of Abu Dhabi city is recalled. The SI curve is modeled in per-unit of the SI at the FOI and then used to represent the per-unit PVDG production curve according to Eq.3.39. Fig.5.1 depicts the resulting per-unit curve, showing that the FOI corresponds to the time 12:00 noon.

Load curve modeling

The relevant load curve of feeder F1 and F2, illustrated in Figs.A2.1 and A2.4 of Appendix 2 respectively are recalled. Corresponding daily load curves are generated for each node along the feeders by applying Eqs.3.36 and 3.37. Based on the generated load curves, the real (P) and reactive (Q) load demands of each node at the FOI are stated in Table 5.3.

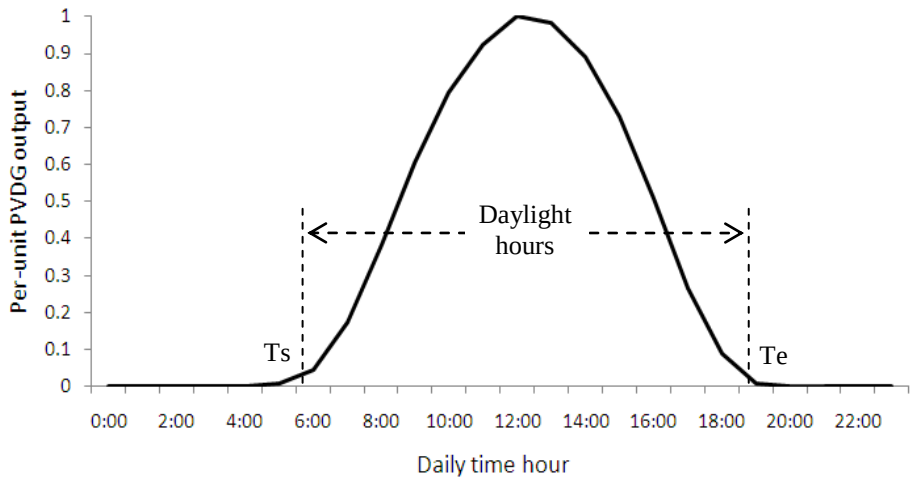

Figure 5.1 Daily summer PVDG production curve (per-unit) of the production at the FOI

Table 5.3 Real (P) and reactive (Q) load demand of the nodes at the FOI in summer day

Node	Feeder F1		Feeder F2	
	P (MW)	Q (MVAR)	P (MW)	Q (MVAR)
1	0.33405	0.18568	0.08884	0.03170
2	0.33405	0.18568	0.17768	0.06340
3	0.33405	0.18568	0.03554	0.01268
4	0.11135	0.06189	0.03554	0.01268
5	0.33405	0.18568	0.03554	0.01268
6	0.33405	0.18568	0.03554	0.01268
7	0.33405	0.18568	0.03554	0.01268
8	0.33405	0.18568	0.03554	0.01268
9	0.33405	0.18568	0.03554	0.01268
10	0.33405	0.18568	0.03554	0.01268
11	0.22270	0.12378	0.03554	0.01268
12	0.33405	0.18568	0.03554	0.01268
13	0.22270	0.12378	0.03554	0.01268
14	0.22270	0.12378	0.08885	0.03170
15	Feeder F1 consists of 14 nodes		0.03554	0.01270
16			0.03554	0.01270
17			0.17768	0.06340
18			0.03554	0.01268
19			0.03554	0.01268
20			0.03554	0.01268
21			0.03554	0.01268
22			0.03554	0.01268
23			0.03554	0.01268
24			0.03554	0.01268
25			0.03554	0.01268
26			0.17768	0.06340
27			0.17768	0.06340
28			0.17768	0.06340
29			0.17768	0.06340

The optimization procedure

Based on the derivations of Chapter 4, there will be one local optimal size for the PVDG unit at each location. The local optimal size is set so that the peak of the ac PVDG production curve equals the amount of power flow, at the FOI, in the line section at which the PVDG unit is connected. Of course this is considering the avoidance of RPF along the feeder.

Consequently, the optimization problem has ended up with one PVDG size at each location and one interval, which is the FOI, at which the total line energy loss reduction (ΔEL) is rated.

Thus, at every node the PVDG unit is sized up according to the power flow at that location and then the ΔEL is checked. The calculations are iterated at each node and the one resulting in the maximum ΔEL is selected.

In the event of more than one PVDG unit, the optimization procedure is implemented using a method based upon the selection of the feasible locations of the units per iteration. This method will be explained later on in Sections 5.1.3 and 5.1.4.

For a single PVDG unit, it would appear better to place it at the far end of the radial distribution feeder. This way, all of the line sections benefit from the reduction in power flow along the feeder. On this basis, the iterations of the optimization procedure are set to commence from the far end of the feeder. As example, Fig.5.2 illustrates the iteration process starting from the end of a 5-node radial distribution feeder. In the first iteration the PVDG unit is connected to node 5 and the peak of the ac PVDG production curve is sized up to PV_5, touching the load curve at the FOI. Then, the ΔEL along the feeder is checked. The same steps are applied on the successive nodes in the upstream direction one after one. At the end, the optimal solution is realized at the node and associated PVDG size resulting in maximum ΔEL.

Emphasis is placed upon the determination of the commercial capacity of the PV array (PV_{com}), corresponding to the optimal sizing of the PVDG unit, by applying Eq.4.1.

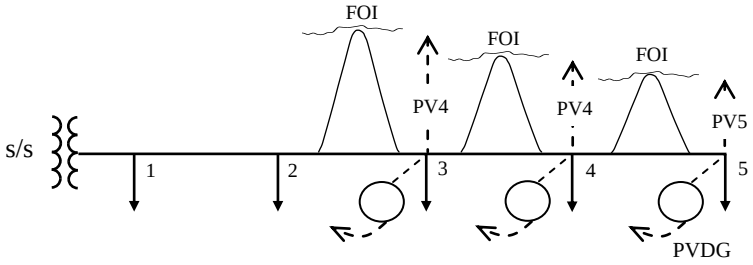

Figure 5.2 Iteration process with single PVDG unit, with avoidance of RPF

Back to the optimization procedure; the calculation of ΔEL requires power flow application along the feeder at each time interval. Knowing that this process is repeated for each section on the feeder may give an idea of the computational requirements.. Thus, the concept of rating the energy flow along the feeder by the power flow at the FOI, derived in Section 4.3.1, is integrated in the procedure. This can be put into effect by calculating the line power loss at the FOI (PL_{FOI}) along with the associated line power loss reduction (ΔPL_{FOI}) due to the connection of the PVDG unit. Consequently, the optimal PVDG sizing and location that result in maximum ΔPL_{FOI} also results in maximum ΔEL. However, just in this section, the optimization procedure will be solved twice for maximum ΔPL_{FOI} and ΔEL separately. The matching of the two optimal solutions will be checked in order to validate the derivations of rating the ΔEL benefit by the ΔPL_{FOI} benefit.

Solving for maximum ΔPL_{FOI}

The procedure is applied on feeders F1 & F2 specified in Table A2.1 and A2.3 of Appendix 2 These feeders are considered by the distribution company to be balanced 3-phase feeders, which is the model used in this section. However, a model for the unbalanced 3-phase condition will be worked out in following sections.

A suitable MATLAB program has been designed putting together the aforementioned dealings related to the ΔPL_{FOI} benefit. The general flow of program is illustrated in Fig.5.3.

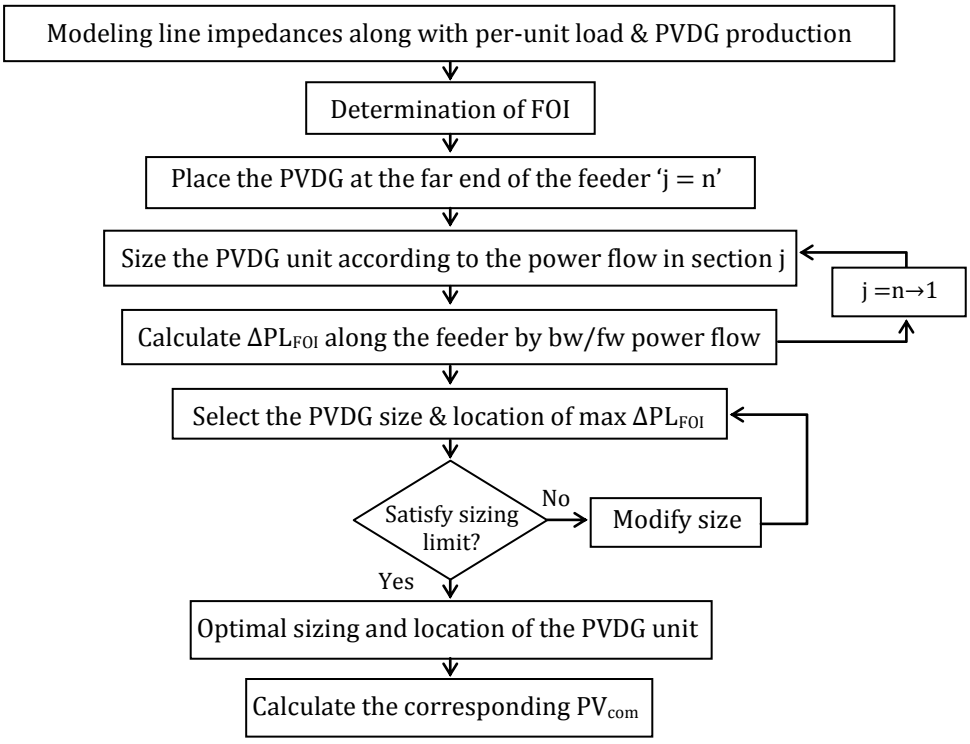

Figure 5.3 Optimization of single PVDG unit considering ΔPL_{FOI} with avoidance of RPF

At this point, the load demand of the nodes at the FOI and the impedance of line sections along the feeder are known. Thus, the backward/forward power flow explained in Section 3.3.1 can be applied by setting the line voltage at substation (V_{ss}) equal to 11kV. Note that the nodes are considered as PQ buses. The results of line voltage (V_L) at the nodes and line current (I_L) in the feeder sections, at the FOI, are stated in Table 5.4.

Table 5.4 Line voltages and currents along the feeders, at the FOI, without PVDG unit

Node/ Section	Feeder F1		Feeder F2	
	Node V_L (kV)	Section I_L (A)	Node V_L (kV)	Section I_L (A)
1	10.953 - j0.00486	218.940 - j122.18	10.950 - j0.01915	107.080 - j40.392
2	10.931 - j0.00717	201.330 - j112.38	10.949 - j0.01966	102.400 - j38.712
3	10.930 - j0.00749	183.690 - j102.57	10.934 - j0.02808	93.039 - j35.353
4	10.917 - j0.00874	166.050 - j92.746	10.922 - j0.03541	91.165 - j34.678
5	10.875 - j0.01317	160.170 - j89.468	10.898 - j0.04953	89.288 - j34.002
6	10.861 - j0.01607	142.440 - j79.589	10.864 - j0.06925	87.409 - j33.322
7	10.847 - j0.01928	124.700 - j69.693	10.831 - j0.08890	85.525 - j32.636
8	10.830 - j0.02295	106.940 - j59.778	10.808 - j0.10219	83.636 - j31.945
9	10.822 - j0.02375	89.151 - j49.842	10.781 - j0.11835	81.745 - j31.250
10	10.810 - j0.02503	71.352 - j39.897	10.759 - j0.13124	79.849 - j30.550
11	10.798 - j0.02768	53.533 - j29.939	10.748 - j0.13751	77.951 - j29.846
12	10.792 - j0.02832	41.643 - j23.290	10.736 - j0.14482	76.051 - j29.141
13	10.790 - j0.02855	23.797 - j13.310	10.716 - j0.15621	74.149 - j28.433
14	10.790 - j0.02866	11.899 - j06.655	10.685 - j0.17445	72.245 - j27.723
15	Feeder F1 consists of 14 nodes		10.667 - j0.18534	67.474 - j25.932
16			10.643 - j0.19925	65.563 - j25.213
17			10.612 - j0.21737	63.649 - j24.489
18			10.598 - j0.22565	54.057 - j20.843
19			10.585 - j0.23319	52.136- j20.112
20			10.574 - j0.23942	50.214 - j19.378
21			10.567 - j0.24354	48.291 - j18.642
22			10.554 - j0.25085	46.366 - j17.905
23			10.536 - j0.26162	44.440 - j17.166
24			10.524 - j0.26848	42.511 – j16.423
25			10.520 - j0.27006	40.580 –j15.678
26			10.512 - j0.27291	38.649 –j14.933
27			10.512 - j0.27293	28.988 –j11.200
28			10.510 - j0.27364	19.326 –j07.467
29			10.510 - j0.27365	09.633 –j03.733

Based on the above, the line power loss at the FOI (PL_{FOI}) is computed. Considering the balanced load condition of the case study, the PL_{FOI} is calculated with Eq.5.1 by the I^2R concept. However, in the event of an unbalanced load condition of the following sections, the losses are computed as the difference in input & output power by phase [3].

$$PL_{FOI} = 3 \times \sum_{k=1}^{n} I_{L(FOI)k}^2 \times r_k \quad (5.1)$$

Where, $I_{L(FOI)k}$ and r_k are the line current at the FOI and the total resistance of section k respectively.

Consequently, the resulting PL_{FOI} in the two feeders without connection of PVDG unit is:

Feeder F1	Feeder F2
$PL_{FOI} = 88.817$ kW	$PL_{FOI} = 86.988$ kW

The PVDG unit connected to certain coupling point (CP) on the feeder can be modeled by a PQ bus delivering negative power at unity power factor [4]. Thus, for maximum ΔPL_{FOI} and ΔEL, avoiding RPF, the size of the PVDG unit is equaled to the power flow at the FOI of the line section ends by the CP node. This can be expressed as follows:

$$PV_{cp(FOI)} = \mathrm{Re}\left\{\sum_{k=cp}^{n} LD_{k(FOI)}\right\} \tag{5.2}$$

Where,

$PV_{cp(FOI)}$ - Peak of the ac PVDG production curve placed at the CP node,
$LD_{k(FOI)}$ - Load demand at the FOI of node k, at or after the CP node,
$\mathrm{Re}\{\bullet\}$ - Real component of the complex quantity,

The new load demand of the CP node ($nLD_{cp(FOI)}$), after connecting the PVDG unit is then updated before running the backward/forward power flow. Note that the superscripts P & Q define the real and reactive power components respectively.

$$nLD_{cp(FOI)} = \left(LD^{P}_{cp(FOI)} + jLD^{Q}_{cp(FOI)}\right) - \left(PV_{cp(FOI)} + j0\right) \tag{5.3}$$

Iteration1:

In the first iteration, the PVDG unit is located at the far end of feeders F1 and F2. The unit is then sized by substituting the load demand of the relevant nodes, stated in Table 5.3, in Eq.5.2. This results in:

Feeder F1	Feeder F2
$PV^{(1)}_{14(FOI)} = 0.2227 + j0$ MW	$PV^{(1)}_{29(FOI)} = 0.17768 + j0$ MW
$nLD_{14(FOI)} = 0 + j0.1238$ MVA	$nLD_{29(FOI)} = 0 + j0.0634$ MVA

Where the superscript 1 denotes the first iteration in the optimization procedure, and 14 and 29 are the CP nodes on feeders F1 and F2 respectively.

The line voltages and currents at the FOI along the feeder are computed by the means of backward/forward power flow, using the new load demand at the CP nodes. The resulting PL_{FOI} of the first iteration is calculated for the two feeders by applying Eq.5.1, which gives:

Feeder F1	Feeder F2
$PL^{(1)}_{FOI} = 78.619$ kW	$PL^{(1)}_{FOI} = 68.018$ kW
$\Delta PL^{(1)}_{FOI} = 11.482\%$	$\Delta PL^{(1)}_{FOI} = 21.808\%$

Iteration2:

The computations are repeated with the moving of the PVDG unit back to the next upstream node on the feeders. Below are the counterpart results of the second iteration:

Feeder F1	Feeder F2
$PV_{13(FOI)}^{(2)} = 0.44541+j0$ MW	$PV_{28(FOI)}^{(2)} = 0.35536+j0$ MW
$nLD_{13(FOI)} = -0.2227+j0.12378$ MVA	$nLD_{28(FOI)} = -0.17768+j0.0634$ MVA
$PL_{FOI}^{(2)} = 69.515$ kW	$PL_{FOI}^{(2)} = 52.094$ kW
$\Delta PL_{FOI}^{(2)} = 21.732\%$	$\Delta PL_{FOI}^{(2)} = 40.114\%$

The process is continued in the upstream direction up to the CP node 1. The results of PV_{FOI} vs. PL_{FOI} and ΔPL_{FOI} in per-unit of the original PL_{FOI} are illustrated in Figs.5.4 & 5.5.

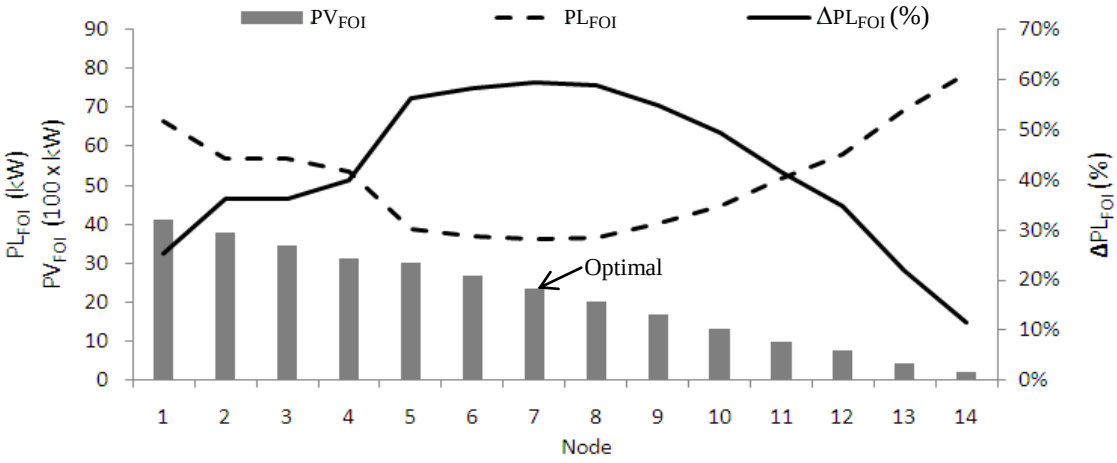

Figure 5.4 Single PVDG unit on feeder F1 considering ΔPL_{FOI} with the avoidance of RPF

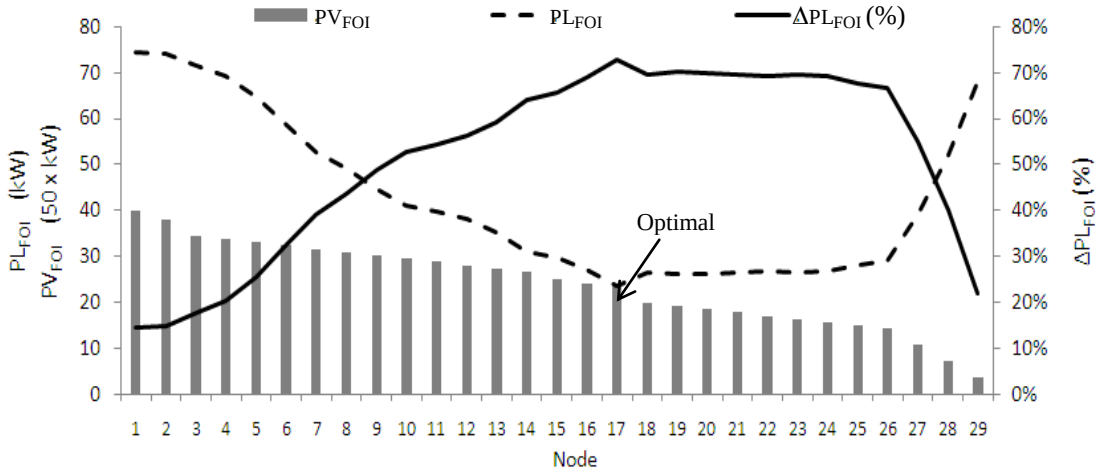

Figure 5.5 Single PVDG unit on feeder F2 considering ΔPL_{FOI} with the avoidance of RPF

According to the figures, the optimal PVDG size and location maximizing ΔPL_{FOI}, with the avoidance of RPF, are stated below. Note to mention that the optimal size is given in term of peak of the ac PVDG production curve concurred at the FOI.

Feeder F1	Feeder F2
Optimal location (CP node) = 7	Optimal location (CP node) = 17
Optimal size ($PV_{cp(FOI)}$)= 2.3384+j0 MW	Optimal size ($PV_{cp(FOI)}$)=1.1727+j0 MW
$PL_{FOI} = 36.152$ kW	$PL_{FOI} = 23.656$ kW
$\Delta PL_{FOI} = 59.297\%$	$\Delta PL_{FOI} = 72.805\%$

Solving for maximum ΔEL

In order to validate the derivations of rating the ΔEL by the ΔPL_{FOI}, the MATLAB program is extended to solve for maximum ΔEL by actual calculations. The flowchart of the program is illustrated generally in Fig.5.6.

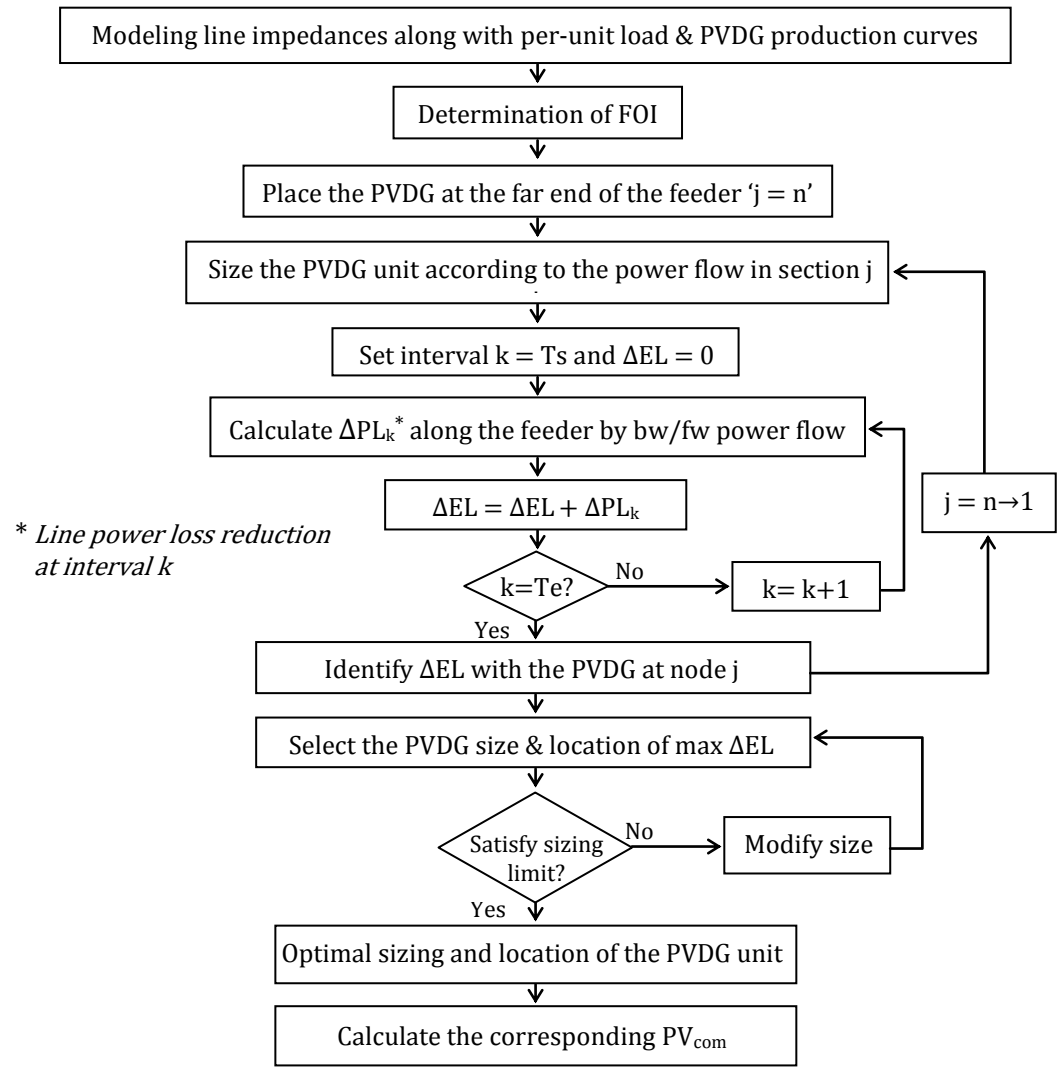

Figure 5.6 Optimization of single PVDG unit considering ΔEL with the avoidance of RPF

The line energy loss of the feeder (EL) is realized by taking the summation of line power loss (PL) over the daily duration along the feeder sections. The calculations can be reduced by narrowing the daily duration to the daylight hours during which the PVDG unit can work. According to Fig.5.1, the summer daylight hours in Abu Dhabi starts at Ts=6:00 and ends at Te =19:00.

The backward/forward power flow, explained in Section 3.3.1, is applied to generate the line voltage of nodes and line current of sections over the intervals Ts to Te. Thus, the load demand of the nodes (PQ busses) at each interval is required, which is generated as follows:

$$[\mathrm{LD}] = \begin{bmatrix} \mathrm{LD}_{1(\mathrm{Ts})} & \cdots & \mathrm{LD}_{\mathrm{n}(\mathrm{Ts})} \\ \vdots & \ddots & \vdots \\ \mathrm{LD}_{1(\mathrm{Te})} & \cdots & \mathrm{LD}_{\mathrm{n}(\mathrm{Te})} \end{bmatrix} \tag{5.4}$$

Where the elements of [LD] are determined by applying Eq.3.37. Then,

$$[\mathrm{P}] = \mathrm{Re}[\mathrm{LD}] \quad \text{and} \quad [\mathrm{Q}] = \mathrm{Im}[\mathrm{LD}] \tag{5.5}$$

Setting the substation line voltage (V_{ss}) to 11kV, the backward/forward power flow can be applied resulting in the line voltage of nodes (V_L) and line current of sections (I_L). The results are generated in the form below, where the elements of $[V_L]$ and $[I_L]$ are complex numbers:

$$[\mathrm{V_L}] = \begin{bmatrix} \mathrm{V}_{\mathrm{L1}(\mathrm{Ts})} & \cdots & \mathrm{V}_{\mathrm{Ln}(\mathrm{Ts})} \\ \vdots & \ddots & \vdots \\ \mathrm{V}_{\mathrm{L1}(\mathrm{Te})} & \cdots & \mathrm{V}_{\mathrm{Ln}(\mathrm{Te})} \end{bmatrix} \tag{5.6}$$

$$[\mathrm{L_L}] = \begin{bmatrix} \mathrm{L}_{\mathrm{L1}(\mathrm{Ts})} & \cdots & \mathrm{I}_{\mathrm{Ln}(\mathrm{Ts})} \\ \vdots & \ddots & \vdots \\ \mathrm{I}_{\mathrm{L1}(\mathrm{Te})} & \cdots & \mathrm{I}_{\mathrm{Ln}(\mathrm{Te})} \end{bmatrix} \tag{5.7}$$

The line energy loss along the feeder is then computed by applying Eq.5.8, where, $[\mathrm{r}]^{\mathrm{T}}$ is the transpose vector of line resistance along the feeder.

$$\mathrm{EL} = \sum \left(3 \times \left[\mathrm{I_L^2}\right] \times [\mathrm{r}]^{\mathrm{T}} \right) \tag{5.8}$$

Based on the above, the EL along feeders F1 and F2 without PVDG unit is:

Feeder F1	Feeder F2
$\mathrm{EL} = 1089.1$ kWh	$\mathrm{EL} = 1101.3$ kWh

Connection of PVDG unit with suitable size at some CP node on the feeder results in certain amount of line energy loss reduction (ΔEL). For maximum ΔEL, avoiding RPF, the peak of the ac PVDG production curve ($PV_{cp(FOl)}$) is sized up according to Eq.5.2.

In order to run the backward/forward power flow, the load demand of the CP node is updated to its new values (using the concept of Eq.5.3) for each time interval as follows:

$$[\mathrm{nLD}]_{\mathrm{cp}} = \left(\begin{bmatrix} \mathrm{LD}^{\mathrm{P}}_{(\mathrm{Ts})} \\ \vdots \\ \mathrm{LD}^{\mathrm{P}}_{(\mathrm{i})} \\ \vdots \\ \mathrm{LD}^{\mathrm{P}}_{(\mathrm{Te})} \end{bmatrix}_{\mathrm{cp}} + \mathrm{j} \begin{bmatrix} \mathrm{LD}^{\mathrm{Q}}_{(\mathrm{Ts})} \\ \vdots \\ \mathrm{LD}^{\mathrm{Q}}_{(\mathrm{i})} \\ \vdots \\ \mathrm{LD}^{\mathrm{Q}}_{(\mathrm{Te})} \end{bmatrix}_{\mathrm{cp}} \right) - \left(\mathrm{PV}_{\mathrm{cp(FOI)}} \times \begin{bmatrix} \mathrm{PVDG}_{(\mathrm{Ts})\mathrm{pu}} \\ \vdots \\ \mathrm{PVDG}_{(\mathrm{i})\mathrm{pu}} \\ \vdots \\ \mathrm{PVDG}_{(\mathrm{Te})\mathrm{pu}} \end{bmatrix}_{\mathrm{cp}} + \mathrm{j}[0] \right) \tag{5.9}$$

Where, $\mathrm{PVDG}_{(\mathrm{i})\mathrm{pu}}$ is the output of the PVDG unit at interval i in per-unit of its output at $\mathrm{SI}_{(\mathrm{FOI})}$, which can be determined by applying Eqs.3.38 and 3.39. Also the superscripts P and Q define the real and reactive components of the load demand.

Iteration1:

In the first iteration, the PVDG unit is located at the far end of feeder F1 and F2. The peak of the ac PVDG production curve ($\mathrm{PV}_{\mathrm{cp(FOI)}}$) is sized up according to Eq.5.2. The output of the PVDG unit over the daylight duration and the resulting new load demand of the CP node are calculated based on Eq.5.9.

Feeder F1:

$\mathrm{PV}^{(1)}_{14(\mathrm{FOI})} = 0.2227 + \mathrm{j}0\ \mathrm{MW}$

$$[\mathrm{PVDG}]^{(1)}_{14} = \mathrm{PV}_{14(\mathrm{FOI})} \times \begin{bmatrix} \mathrm{PVDG}_{(\mathrm{Ts})\mathrm{pu}} \\ \vdots \\ \mathrm{PVDG}_{(\mathrm{Te})\mathrm{pu}} \end{bmatrix}$$

$$[\mathrm{nLD}]_{14} = \left(\begin{bmatrix} \mathrm{P}_{(\mathrm{Ts})} \\ \vdots \\ \mathrm{P}_{(\mathrm{Te})} \end{bmatrix}_{14} + \mathrm{j} \begin{bmatrix} \mathrm{Q}_{(\mathrm{Ts})} \\ \vdots \\ \mathrm{Q}_{(\mathrm{Te})} \end{bmatrix}_{14} \right) - \left(\mathrm{PV}_{14(\mathrm{FOI})} \times \begin{bmatrix} \mathrm{PVDG}_{(\mathrm{Ts})\mathrm{pu}} \\ \vdots \\ \mathrm{PVDG}_{(\mathrm{Te})\mathrm{pu}} \end{bmatrix} + \mathrm{j}[0] \right)$$

Feeder F2:

$\mathrm{PV}^{(1)}_{29(\mathrm{FOI})} = 0.17768 + \mathrm{j}0\ \mathrm{MW}$

$$[\mathrm{PVDG}]^{(1)}_{29} = \mathrm{PV}_{29(\mathrm{FOI})} \times \begin{bmatrix} \mathrm{PVDG}_{(\mathrm{Ts})\mathrm{pu}} \\ \vdots \\ \mathrm{PVDG}_{(\mathrm{Te})\mathrm{pu}} \end{bmatrix}$$

$$[\mathrm{nLD}]_{29} = \left(\begin{bmatrix} \mathrm{P}_{(\mathrm{Ts})} \\ \vdots \\ \mathrm{P}_{(\mathrm{Te})} \end{bmatrix}_{29} + \mathrm{j} \begin{bmatrix} \mathrm{Q}_{(\mathrm{Ts})} \\ \vdots \\ \mathrm{Q}_{(\mathrm{Te})} \end{bmatrix}_{29} \right) - \left(\mathrm{PV}_{29(\mathrm{FOI})} \times \begin{bmatrix} \mathrm{PVDG}_{(\mathrm{Ts})\mathrm{pu}} \\ \vdots \\ \mathrm{PVDG}_{(\mathrm{Te})\mathrm{pu}} \end{bmatrix} + \mathrm{j}[0] \right)$$

Setting the substation line voltage (V_{ss}) equal to 11kV, the line voltage of the nodes [V_L] and line current of the sections [I_L] are calculated in the form of Eqs.5.6 and 5.7. Then the EL is calculated by applying Eq.5.8 to give:

Feeder F1	Feeder F2
$\mathrm{EL}^{(1)} = 1015.4$ kWh	$\mathrm{EL}^{(1)} = 958.52$ kWh
$\Delta\mathrm{EL}^{(1)} = 6.762\%$	$\Delta\mathrm{EL}^{(1)} = 12.964\%$

Iteration2:

The computations are repeated with the PVDG unit moved back to the following upstream node on the feeder F1 and F2. Below are the results of the new line energy loss:

Feeder F1:

$\mathrm{PV}_{13(\mathrm{FOI})}^{(2)} = 0.44541 + \mathrm{j}0$ MW

$$[\mathrm{PVDG}]_{13}^{(2)} = \mathrm{PV}_{13(\mathrm{FOI})} \times \begin{bmatrix} \mathrm{PVDG}_{(\mathrm{Ts})\mathrm{pu}} \\ \vdots \\ \mathrm{PVDG}_{(\mathrm{Te})\mathrm{pu}} \end{bmatrix}$$

$$[\mathrm{nLD}]_{13} = \left(\begin{bmatrix} \mathrm{P}_{(\mathrm{Ts})} \\ \vdots \\ \mathrm{P}_{(\mathrm{Te})} \end{bmatrix}_{13} + \mathrm{j} \begin{bmatrix} \mathrm{Q}_{(\mathrm{Ts})} \\ \vdots \\ \mathrm{Q}_{(\mathrm{Te})} \end{bmatrix}_{13} \right) - \left(\mathrm{PV}_{13(\mathrm{FOI})} \times \begin{bmatrix} \mathrm{PVDG}_{(\mathrm{Ts})\mathrm{pu}} \\ \vdots \\ \mathrm{PVDG}_{(\mathrm{Te})\mathrm{pu}} \end{bmatrix} + \mathrm{j}[0] \right)$$

$\mathrm{EL}^{(2)} = 948.06$ kWh

$\Delta\mathrm{EL}^{(2)} = 12.947\%$

Feeder F2:

$\mathrm{PV}_{28(\mathrm{FOI})}^{(3)} = 0.35536 + \mathrm{j}0$ MW

$$[\mathrm{PVDG}]_{28}^{(2)} = \mathrm{PV}_{28(\mathrm{FOI})} \times \begin{bmatrix} \mathrm{PVDG}_{(\mathrm{Ts})\mathrm{pu}} \\ \vdots \\ \mathrm{PVDG}_{(\mathrm{Te})\mathrm{pu}} \end{bmatrix}$$

$$[\mathrm{nLD}]_{28} = \left(\begin{bmatrix} \mathrm{P}_{(\mathrm{Ts})} \\ \vdots \\ \mathrm{P}_{(\mathrm{Te})} \end{bmatrix}_{28} + \mathrm{j} \begin{bmatrix} \mathrm{Q}_{(\mathrm{Ts})} \\ \vdots \\ \mathrm{Q}_{(\mathrm{Te})} \end{bmatrix}_{28} \right) - \left(\mathrm{PV}_{28(\mathrm{FOI})} \times \begin{bmatrix} \mathrm{PVDG}_{(\mathrm{Ts})\mathrm{pu}} \\ \vdots \\ \mathrm{PVDG}_{(\mathrm{Te})\mathrm{pu}} \end{bmatrix} + \mathrm{j}[0] \right)$$

$\mathrm{EL}^{(2)} = 833.1$ kWh

$\Delta\mathrm{EL}^{(2)} = 24.353\%$

The process is continued in the upstream direction up to the CP node 1. The results of PV_{FOI} and EL along with ΔEL, in per-unit of the original EL without PVDG unit, are illustrated in Figs.5.7 and 5.8.

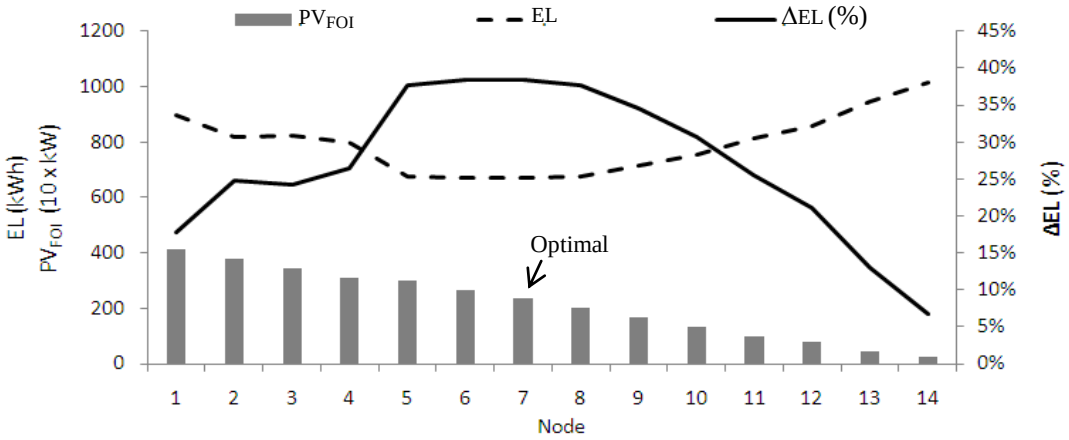

Figure 5.7 Single PVDG unit on feeder F1 considering ΔPL with RPF avoidance

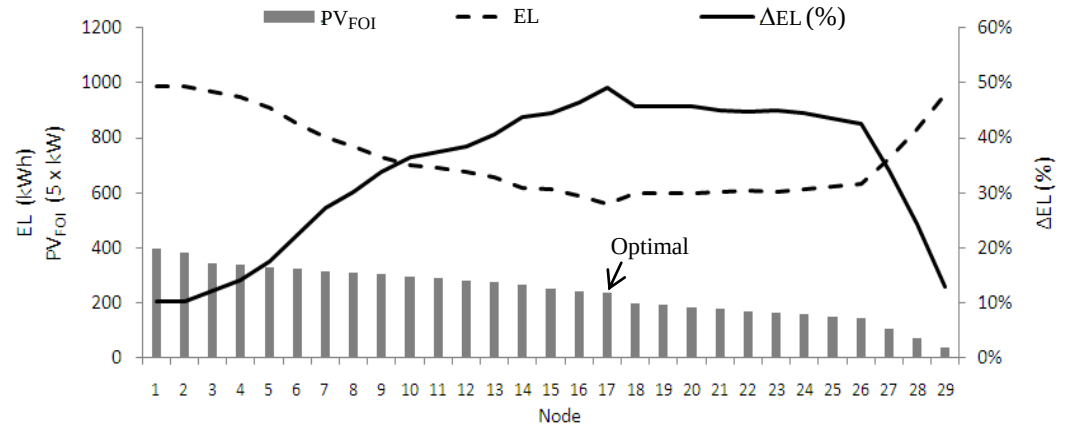

Figure 5.8 Single PVDG unit on feeder F2 considering ΔPL with the avoidance of RPF

According to the figures, the optimal PVDG size and location maximizing ΔEL, avoiding RPF, are stated below. Note to mention that the optimal size is given in terms of peak of the ac PVDG production curve concurrent with the FOI.

Feeder F1	Feeder F2
Optimal location (CP node) = 7	Optimal location (CP node) = 17
Optimal size ($PV_{CP(FOI)}$)= 2.3384+j0 MW	Optimal size ($PV_{CP(FOI)}$)=1.1727+j0 MW
EL = 669.72 kWh	EL = 561.31 kWh
ΔEL = 38.505 %	ΔEL= 49.032 %

Comparing the results of Figs.5.7 and 5.8 with those of Figs.5.4 and 5.5 shows that the optimal PVDG size and location that maximize ΔPL_{FOI} also maximize ΔEL. This comes from the mathematical derivations, in Section 4.3, of rating the line energy loss reduction by the line power loss reduction at the FOI. Hence the optimal procedures in the following sections are solved only for maximum ΔPL_{FOI} without going through the long energy-based calculations.

Modifying optimal size considering the four seasons

In places like Abu Dhabi, the benefits of PVDG placement are anticipated to be maximized in summer where the PV array yields higher production rates. Thus, the optimization procedure is so far run based on summer data. However, both load and PVDG production curves may vary in different rates over other seasons [5]. In view of that, it is possible that the load curves in other seasons go down lower than the PVDG curves do. Such being the case, considerable reverse power will flow during the times that the PVDG curve penetrates the load curve.

Taking the results of feeder F1 as example, Fig.5.9 depicts the daily load curves over seasons of line section 7 (ends with the CP node 7). The curves are correlated, with the corresponding PVDG production curves resulting from the PVDG size optimized based on summer.

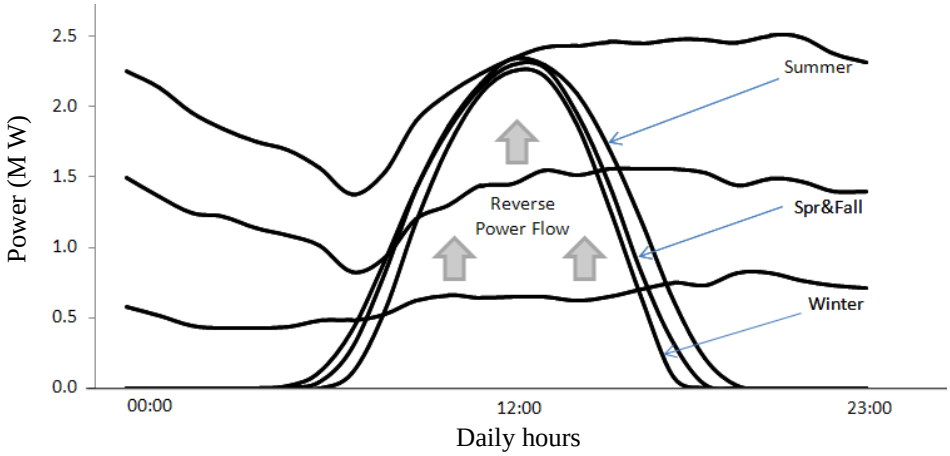

Figure 5.9 Load curves of the CP section and PVDG curves of feeder F1 over seasons

The figure shows considerable drop in winter load curve with an almost insignificant drop in winter PV_{FOI}. The reason is that the high demand of air conditioning load in summer no longer exists in winter. The figure shows also that the main change in the PVDG production curve is not in its peak but in the daylight duration. The same is said for spring and autumn, but in a lower degree.

As a conclusion, it is recommended to solve the optimization procedure based on winter data so that RPF is avoided over the year. This recommendation is applied in solving the optimization procedures of the following sections.

In the meantime, the $PV_{cp(FOI)}$ size, optimized in summer, can be modified in this section to consider winter data. The modification is done by reducing the optimal $PV_{cp(FOI)}$ in a way that the peak of the re sulting PVDG production curve in winter does not exceed the power flow in line section7. Hence, the modified optimal size ($mPV_{cp(FOI)}$) is realized as follows:

$$mPV_{CP(FOI)} = \mathrm{Re}\left\{\sum_{k=CP}^{n} LD_{k(FOI)}\right\}_{winter} \quad (5.10)$$

Where,

CP - Optimal location node of the PVDG unit,

$LD_{k(FOI)}$ - Load demand of node k upstream to CP at the FOI in a winter day,

According to Fig.5.9, the real power flow in line section 7 at the FOI in a winter day is 0.6468 MW; which is the modified size of the PVDG unit according to winter daily load curve.

Recalling Eq.4.1, the dc commercial capacity of the PV array (PV_{com}) for the required $PV_{CP(FOI)}$ is calculated. Assuming the average conversion efficiency of the inverters interfacing the PV array with the grid is 0.9, the resulting PV_{com} is in the range of 0.85 MWp.

It is worth mentioning that the voltage profile along the feeder is expected to improve all the time as the power and energy flow are reduced. At the same time, the avoidance of RPF diffuses the concern of exceeding the maximum voltage limit of the feeder. This might be additional benefit of the proposed procedure.

5.1.2 Single PVDG units on unbalanced 3-phase feeder avoiding RPF

The proposed optimization procedure is developed further to deal with the optimal sizing and location of single PVDG unit on a 3-phase unbalanced load feeder. The procedure solves for maximum line energy loss reduction (ΔEL) with the avoidance of RPF over the day. Based on the findings of Section 5.1.1 and the derivations of Section 4.3.1, the ΔEL will be rated in terms of the line power loss reduction at the FOI (ΔPL_{FOI}). According to the same findings, the optimization problem will be solved considering winter load demand data.

Starting from this section, the feeder F2 specified in Table A2.2 will be taken as the case study for the developed optimization procedures. This brings the opportunity of comparing the optimization results coming from each of the procedures.

Modeling of line impedance in 3-phase unbalanced load feeder

Based on Carson equations of Section 3.1.2, the elements of the phase impedance matrix for each line section are generated directly by applying Eqs.3.25 and 3.26. The absence of the neutral return path in the case study feeder generates a 3x3 matrix so there is no need to use Korn's reduction method [6].

According to Table A2.2, the spacing and specification of the three wire conductors are the same per line section. Therefore, the diagonal elements of the matrix, on one side, and the off diagonal elements, on the other side, have the same values. The results are stated in Table 5.5.

Table 5.5 Phase impedance matrix of the line sections along feeder F2

Section	$Z_{aa} = Z_{bb} = Z_{cc}$	$Z_{ab} = Z_{ba} = Z_{ac} = Z_{ca} = Z_{bc} = Z_{cb}$
1	$0.5269 + j2.6459\ \Omega$	$0.1765 + j2.3349\ \Omega$
2	$0.0147 + j0.0740\ \Omega$	$0.0049 + j0.0653\ \Omega$
3	$0.1243 + j0.3158\ \Omega$	$0.0203 + j0.1858\ \Omega$
4	$0.1104 + j0.2804\ \Omega$	$0.0180 + j0.1650\ \Omega$
5	$0.2174 + j0.5524\ \Omega$	$0.0355 + j0.3250\ \Omega$
6	$0.3102 + j0.7883\ \Omega$	$0.0506 + j0.4638\ \Omega$
7	$0.3160 + j0.8029\ \Omega$	$0.0516 + j0.4724\ \Omega$
8	$0.2189 + j0.5563\ \Omega$	$0.0357 + j0.3273\ \Omega$
9	$0.2721 + j0.6915\ \Omega$	$0.0444 + j0.4068\ \Omega$
10	$0.2222 + j0.5647\ \Omega$	$0.0363 + j0.3322\ \Omega$
11	$0.1110 + j0.2820\ \Omega$	$0.0181 + j\ 0.1659\ \Omega$
12	$0.1324 + j0.3365\ \Omega$	$0.0216 + j0.1980\ \Omega$
13	$0.2116 + j0.5378\ \Omega$	$0.0345 + j0.3164\ \Omega$
14	$0.3483 + j0.8851\ \Omega$	$0.0568 + j0.5207\ \Omega$
15	$0.2225 + j0.5655\ \Omega$	$0.0363 + j0.3327\ \Omega$
16	$0.2930 + j0.7445\ \Omega$	$0.0478 + j0.4380\ \Omega$
17	$0.3931 + j0.9989\ \Omega$	$0.0642 + j0.5876\ \Omega$
18	$0.2116 + j0.5378\ \Omega$	$0.0345 + j0.3164\ \Omega$
19	$0.1999 + j0.5079\ \Omega$	$0.0326 + j0.2988\ \Omega$
20	$0.1714 + j0.4357\ \Omega$	$0.0280 + j0.2563\ \Omega$
21	$0.1182 + j0.3004\ \Omega$	$0.0193 + j0.1767\ \Omega$
22	$0.2180 + j0.5540\ \Omega$	$0.0356 + j0.3259\ \Omega$
23	$0.3350 + j0.8513\ \Omega$	$0.0547 + j0.5008\ \Omega$
24	$0.2234 + j0.5678\ \Omega$	$0.0365 + j0.3340\ \Omega$
25	$0.1166 + j0.5853\ \Omega$	$0.0390 + j0.5165\ \Omega$
26	$0.2210 + j1.1099\ \Omega$	$0.0740 + j0.9794\ \Omega$
27	$0.0022 + j0.0111\ \Omega$	$0.0007 + j0.0098\ \Omega$
28	$0.1105 + j0.5549\ \Omega$	$0.0370 + j0.4897\ \Omega$
29	$0.0022 + j0.0111\ \Omega$	$0.0007 + j0.0098\ \Omega$

PVDG production curve modeling

The optimization procedure is run based on winter daily demand. Similar to Section 5.1.1, the per-unit PVDG production curve can be modeled based on Eq.3.39, this time using the SI rates of winter. However, the optimization procedure is run only at the FOI, so there is no need to model the PVDG production curve over the day. To this end, it is enough to model the PVDG unit by its amplitude coincident with the FOI. This amplitude is equaled to the power flow at the FOI in the line section that the PVDG unit connected at.

Load curve modeling

The data of daily load curves by phase for the feeder was found not to be available at the local power company. They deal with total load curve values for the three phases together. As an alternative, the company provided the figures of Table 5.6 on the rates of feeder real power demand (P) and power factor (PF), by phase, based on previous measurements. The rates (R) are given in per unit of the total MW demand of the feeder.

Table 5.6 Feeder real power demand and power factors by phase

	Phase 'a'	Phase 'b'	Phase 'c'
Rate (R)	0.35	0.31	0.34
PF	0.80	0.84	0.82

Considering the concept of rating the line energy loss by the line power loss at the FOI, it is enough to model the power flow quantities only at the FOI. Hence, the rates of Table 5.6 are applied to the total daily demand of the feeder at the FOI to generate corresponding values by phase. Thus the real and reactive load demands of the feeder are generated as follows:

$$[\mathrm{LD}_{\mathrm{F(FOI)}}]^{\mathrm{P}}_{\mathrm{abc}} = \begin{bmatrix} \mathrm{R_a} \\ \mathrm{R_b} \\ \mathrm{R_c} \end{bmatrix} \times \left[\mathrm{LD}_{\mathrm{F(FOI)}}\right]^{\mathrm{P}} \tag{5.11}$$

Then by taking the following array product (element by element),

$$[\mathrm{LD}_{\mathrm{F(FOI)}}]^{\mathrm{Q}}_{\mathrm{abc}} = [\mathrm{LD}_{\mathrm{F(FOI)}}]^{\mathrm{P}}_{\mathrm{abc}} \times \begin{bmatrix} \tan\left(\cos^{-1}\mathrm{PF_a}\right) \\ \tan\left(\cos^{-1}\mathrm{PF_b}\right) \\ \tan\left(\cos^{-1}\mathrm{PF_c}\right) \end{bmatrix} \tag{5.12}$$

Where, P & Q - Symbols of real and reactive power respectively,
$[\mathrm{LD}_{\mathrm{F(FOI)}}]^{\mathrm{P}}_{\mathrm{abc}}$ - Feeder load demand of P at the FOI by phase,
$\left[\mathrm{LD}_{\mathrm{F(FOI)}}\right]^{\mathrm{P}}$ - Feeder load demand of P at the FOI for the three phases altogether,
$[\mathrm{LD}_{\mathrm{F(FOI)}}]^{\mathrm{Q}}_{\mathrm{abc}}$ - Feeder load demand of Q at the FOI by phase,
$\mathrm{R_a}$ - Rate of phase 'a' real power in per-unit of total 3-phase real power,
$\mathrm{PF_a}$ - Power factor of phase 'a',

Note that the feeder load demand can be represented by the relevant values of power flow in line section 1.

Equations 5.11 and 5.12 are applied on the winter load demand of feeder F2 illustrated earlier in A2.5 of Appendix 2. The results are stated in Table 5.7 below.

Table 5.7 Real and reactive load demand of feeder F2, at the FOI by phase

	Phase 'a'	Phase 'b'	Phase 'c'
$[\mathrm{LD}_{\mathrm{F(FOI)}}]^{\mathrm{P}}_{\mathrm{abc}}$ (MW)	0.1855	0.1643	0.1802
$[\mathrm{LD}_{\mathrm{F(FOI)}}]^{\mathrm{Q}}_{\mathrm{abc}}$ (MVAr)	0.1391	0.1061	0.1258

After getting the P and Q load curve values of the feeder at the FOI, the counterpart values for the nodes along the feeder are determined. At the beginning the feeder load curve values at the FOI are given in per-unit (pu) of feeder peak load demand by phase. This can be realized by taking the array product below.

$$[\mathrm{LD}_{\mathrm{F(FOI)pu}}]^{\mathrm{P}}_{\mathrm{abc}} = [\mathrm{LD}_{\mathrm{F(FOI)}}]^{\mathrm{P}}_{\mathrm{abc}} \times \left[\frac{1}{\mathrm{LD}_{\mathrm{F(pk)}}}\right]^{\mathrm{P}}_{\mathrm{abc}} \quad (5.13)$$

And,

$$[\mathrm{LD}_{\mathrm{F(FOI)pu}}]^{\mathrm{Q}}_{\mathrm{abc}} = [\mathrm{LD}_{\mathrm{F(FOI)}}]^{\mathrm{Q}}_{\mathrm{abc}} \times \left[\frac{1}{\mathrm{LD}_{\mathrm{F(pk)}}}\right]^{\mathrm{Q}}_{\mathrm{abc}} \quad (5.14)$$

Where,

P and Q - Real and reactive power components respectively
$[\mathrm{LD}_{\mathrm{F(pk)}}]_{\mathrm{abc}}$ - Feeder peak load demand, by phase
$[\mathrm{LD}_{\mathrm{F(FOI)}}]_{\mathrm{abc}}$ - Feeder load demand by phase, at the FOI,
$\mathrm{LD}_{\mathrm{F(FOI)pu}}$ - $\mathrm{LD}_{\mathrm{F(FOI)}}$ in per unit of $\mathrm{LD}_{\mathrm{F(pk)}}$,

But the load curves of nodes are assumed to vary in the same pattern as the feeder load curve [7-9]. Thus, the same per-unit values of the feeder can be applied to the nodes. Hence,

$$[\mathrm{LD}_{\mathrm{k(FOI)}}]^{\mathrm{P}}_{\mathrm{abc}} = [\mathrm{LD}_{\mathrm{F(FOI)pu}}]^{\mathrm{P}}_{\mathrm{abc}} \times [\mathrm{LD}_{\mathrm{k(pk)}}]^{\mathrm{P}}_{\mathrm{abc}} \quad (5.15)$$

And,

$$[\mathrm{LD}_{\mathrm{k(FOI)}}]^{\mathrm{Q}}_{\mathrm{abc}} = [\mathrm{LD}_{\mathrm{F(FOI)pu}}]^{\mathrm{Q}}_{\mathrm{abc}} \times [\mathrm{LD}_{\mathrm{k(pk)}}]^{\mathrm{Q}}_{\mathrm{abc}} \quad (5.16)$$

Where,

$[\mathrm{LD}_{\mathrm{k(FOI)}}]^{\mathrm{P}}_{\mathrm{abc}}$ – Real load demand of node k at the FOI, by phase
$[\mathrm{LD}_{\mathrm{k(FOI)}}]^{\mathrm{Q}}_{\mathrm{abc}}$ – Reactive load demand of node k at the FOI, by phase

Substituting Eqs.5.13 & 5.14 into Eqs.5.15 & 5.16 then applying at each node yields the real and reactive load demands by phase of each node at the FOI. The results are stated in Table 5.8.

Table 5.8 Load demand of the nodes along feeder F2 at the FOI, by phase

Node	$P_a + jQ_a$ (MVA)	$P_b + jQ_b$ (MVA))	$P_c + jQ_c$ (MVA)
1	0.0083 + j0.0062	0.0073 + j0.0047	0.0080 + j0.0056
2	0.0166 + j0.0124	0.0147 + j0.0095	0.0161 + j0.0112
3	0.0033 + j0.0025	0.0029 + j0.0019	0.0032 + j0.0022
4	0.0033 + j0.0025	0.0029 + j0.0019	0.0032 + j0.0022
5	0.0033 + j0.0025	0.0029 + j0.0019	0.0032 + j0.0022
6	0.0033 + j0.0025	0.0029 + j0.0019	0.0032 + j0.0022
7	0.0033 + j0.0025	0.0029 + j0.0019	0.0032 + j0.0022
8	0.0033 + j0.0025	0.0029 + j0.0019	0.0032 + j0.0022
9	0.0033 + j0.0025	0.0029 + j0.0019	0.0032 + j0.0022
10	0.0033 + j0.0025	0.0029 + j0.0019	0.0032 + j0.0022
11	0.0033 + j0.0025	0.0029 + j0.0019	0.0032 + j0.0022
12	0.0033 + j0.0025	0.0029 + j0.0019	0.0032 + j0.0022
13	0.0033 + j0.0025	0.0029 + j0.0019	0.0032 + j0.0022
14	0.0083 + j0.0062	0.0073 + j0.0047	0.0080 + j0.0056
15	0.0033 + j0.0025	0.0029 + j0.0019	0.0032 + j0.0022
16	0.0033 + j0.0025	0.0029 + j0.0019	0.0032 + j0.0022
17	0.0166 + j0.0124	0.0147 + j0.0095	0.0161 + j0.0112
18	0.0033 + j0.0025	0.0029 + j0.0019	0.0032 + j0.0022
19	0.0033 + j0.0025	0.0029 + j0.0019	0.0032 + j0.0022
20	0.0033 + j0.0025	0.0029 + j0.0019	0.0032 + j0.0022
21	0.0033 + j0.0025	0.0029 + j0.0019	0.0032 + j0.0022
22	0.0033 + j0.0025	0.0029 + j0.0019	0.0032 + j0.0022
23	0.0033 + j0.0025	0.0029 + j0.0019	0.0032 + j0.0022
24	0.0033 + j0.0025	0.0029 + j0.0019	0.0032 + j0.0022
25	0.0033 + j0.0025	0.0029 + j0.0019	0.0032 + j0.0025
26	0.0166 + j0.0124	0.0147 + j0.0095	0.0161 + j0.0112
27	0.0166 + j0.0124	0.0147 + j0.0095	0.0161 + j0.0112
28	0.0166 + j0.0124	0.0147 + j0.0095	0.0161 + j0.0112
29	0.0166 + j0.0124	0.0147 + j0.0095	0.0161 + j0.0112

Based on the findings of Section 5.1.1 and the derivations of Section 4.3.1, the ΔEL will be rated in terms of the line power loss reduction at the FOI (ΔPL_{FOI}). Consequently, the optimization procedure is similar to that solving for maximum ΔPL_{FOI} in Section 5.1.1. However, the sizing of the PVDG units and the power flow analysis along with line power loss calculations should be carried out considering a 3-phase unbalanced load condition.

Power flow calculations

At this point, the load demands of the nodes are determined from Table 5.8, while the phase impedance matrix of each line section is known from Table 5.5. On the other hand, the phase voltage at the substation (V_{ss}) is set to is set to $11/\sqrt{3} = 6.35085$kV. Then,

$$[V_{ss}]_{abc} = \begin{bmatrix} 6.35085 \measuredangle 0 \\ 6.35085 \measuredangle -120 \\ 6.35085 \measuredangle 120 \end{bmatrix} \text{ kV}$$

The backward/forward power flow considering a 3-phase unbalanced load feeder can be applied as explained in Section 3.3.1. The results of phase voltage (VP) at the nodes and current (I) in the phase conductors, at the FOI, without PVDG unit are stated in Tables 5.9 and 5.10.

Table 5.9 Phase voltage of nodes along feeder F2, at the FOI, without PVDG unit

Node	Node phase voltage (VP) in kV		
	$VP_a \measuredangle degree^o$	$VP_b \measuredangle degree^o$	$VP_c \measuredangle degree^o$
s.s	6.3509 ∠0	6.3509 ∠-120	6.3509 ∠120
1	6.3290 ∠-0.0404	6.3484 ∠-119.9309	6.3269 ∠120.1411
2	6.3284 ∠-0.0435	6.3483 ∠-119.9310	6.3262 ∠120.1429
3	6.3229 ∠-0.0622	6.3449 ∠-119.9428	6.3208 ∠120.1361
4	6.3180 ∠-0.0786	6.3419 ∠-119.9531	6.3161 ∠120.1301
5	6.3087 ∠-0.1102	6.3361 ∠-119.9729	6.3070 ∠120.1186
6	6.2956 ∠-0.1546	6.3281 ∠-120.0006	6.2944 ∠120.1024
7	6.2826 ∠-0.1989	6.3200 ∠-120.0283	6.2817 ∠120.0862
8	6.2738 ∠-0.2291	6.3146 ∠-120.0470	6.2732 ∠120.0753
9	6.2632 ∠-0.2658	6.3080 ∠-120.0699	6.2628 ∠120.0619
10	6.2546 ∠-0.2952	6.3027 ∠-120.0881	6.2545 ∠120.0512
11	6.2505 ∠-0.3095	6.3002 ∠-120.0971	6.2504 ∠120.0460
12	6.2456 ∠-0.3262	6.2972 ∠-120.1074	6.2457 ∠120.0399
13	6.2381 ∠-0.3523	6.2925 ∠-120.1236	6.2384 ∠120.0304
14	6.2260 ∠-0.3943	6.2851 ∠-120.1496	6.2266 ∠120.0151
15	6.2188 ∠-0.4194	6.2806 ∠-120.1651	6.2196 ∠120.0060
16	6.2096 ∠-0.4516	6.2749 ∠-120.1850	6.2106 ∠119.9943
17	6.1976 ∠-0.4937	6.2675 ∠-120.2109	6.1989 ∠119.9790
18	6.1921 ∠-0.5130	6.2642 ∠-120.2228	6.1936 ∠119.9720
19	6.1871 ∠-0.5306	6.2611 ∠-120.2336	6.1887 ∠119.9656
20	6.1830 ∠-0.5451	6.2585 ∠-120.2425	6.1847 ∠119.9603
21	6.1802 ∠-0.5548	6.2568 ∠-120.2485	6.1820 ∠119.9568
22	6.1754 ∠-0.5719	6.2539 ∠-120.2590	6.1773 ∠119.9505
23	6.1682 ∠-0.5972	6.2495 ∠-120.2745	6.1703 ∠119.9414
24	6.1637 ∠-0.6133	6.2467 ∠-120.2844	6.1659 ∠119.9355
25	6.1619 ∠-0.6233	6.2465 ∠-120.2846	6.1639 ∠119.9414
26	6.1586 ∠-0.6412	6.2461 ∠-120.2851	6.1602 ∠119.9520
27	6.1585 ∠-0.6414	6.2461 ∠-120.2851	6.1602 ∠119.9520
28	6.1577 ∠-0.6459	6.2460 ∠-120.2852	6.1593 ∠119.9547
29	6.1577 ∠-0.6459	6.2460 ∠-120.2852	6.1593 ∠119.9547

Table 5.10 Current in line sections along feeder F2, at the FOI, without PVDG unit

Section	Section current (I) in A		
	$I_a \measuredangle$degree^o	$I_b \measuredangle$degree^o	$I_c \measuredangle$degree^o
1	37.3089 ∡-37.3830	31.1484 ∡-153.1023	35.3557 ∡85.0211
2	35.6734 ∡-37.4013	29.7729 ∡-153.1134	33.8051 ∡85.0151
3	32.4020 ∡-37.4432	27.0220 ∡-153.1388	30.7035 ∡85.0009
4	31.7472 ∡-37.4523	26.4715 ∡-153.1443	30.0827 ∡84.9979
5	31.0918 ∡-37.4613	25.9208 ∡-153.1498	29.4614 ∡84.9948
6	30.4355 ∡-37.4701	25.3696 ∡-153.1551	28.8392 ∡84.9919
7	29.7778 ∡-37.4784	24.8176 ∡-153.1601	28.2158 ∡84.9892
8	29.1188 ∡-37.4860	24.2650 ∡-153.1646	27.5910 ∡84.9867
9	28.4588 ∡-37.4932	23.7118 ∡-153.1689	26.9655 ∡84.9844
10	27.7977 ∡-37.5000	23.1581 ∡-153.1729	26.3389 ∡84.9823
11	27.1357 ∡-37.5063	22.6040 ∡-153.1766	25.7115 ∡84.9803
12	26.4732 ∡-37.5127	22.0496 ∡-153.1803	25.0836 ∡84.9784
13	25.8103 ∡-37.5189	21.4949 ∡-153.1840	24.4553 ∡84.9765
14	25.1465 ∡-37.5248	20.9398 ∡-153.1873	23.8263 ∡84.9748
15	23.4839 ∡-37.5380	19.5505 ∡-153.1948	22.2507 ∡84.9711
16	22.8181 ∡-37.5431	18.9944 ∡-153.1976	21.6198 ∡84.9697
17	22.1513 ∡-37.5475	18.4378 ∡-153.2000	20.9879 ∡84.9686
18	18.8108 ∡-37.5670	15.6514 ∡-153.2100	17.8227 ∡84.9647
19	18.1421 ∡-37.5710	15.0938 ∡-153.2120	17.1891∡84.9640
20	17.4728 ∡-37.5747	14.5360 ∡-153.2138	16.5550 ∡84.9635
21	16.8032 ∡-37.5781	13.9779 ∡-153.2153	15.9205 ∡84.9632
22	16.1332 ∡-37.5813	13.4196 ∡-153.2167	15.2857 ∡84.9630
23	15.4627 ∡-37.5841	12.8611 ∡-153.2178	14.6505 ∡84.9630
24	14.7914 ∡-37.5861	12.3023 ∡-153.2182	14.0145 ∡84.9635
25	14.1196 ∡-37.5874	11.7431 ∡-153.2183	13.3781∡84.9643
26	13.4476 ∡-37.5884	11.1839 ∡-153.2183	12.7414 ∡84.9649
27	10.0860 ∡-37.5892	08.3880 ∡-153.2183	09.5563 ∡84.9653
28	06.7243 ∡-37.5907	05.5920 ∡-153.2184	06.3712 ∡84.9662
29	03.3621 ∡-37.5907	02.7960 ∡-153.2184	03.1856 ∡84.9662

The concept of I^2R is no longer valid in calculating the line power loss of an unbalanced load feeder [3]. Alternatively, the line power loss at the FOI (PL_{FOI}) is computed below as the difference between total input & output power in each line section [10].

$$\left[PL_{k(FOI)}\right]_{abc} = \left\{\left[VP_{k-1(FOI)}\right]_{abc} - \left[VP_{k(FOI)}\right]_{abc}\right\} \times [I_k]_{abc} \quad (5.17)$$

Where,

$PL_{k(FOI)}$ - Power loss of line section k at the FOI per phase,

$VP_{k(FOI)}$ - Phase voltage of node k at the FOI per phase

$I_{k(FOI)}$ - Current flows in line section k at the FOI per phase

The total PL_{FOI} ($PL_{T(FOI)}$) along the feeder for the phases altogether is computed as follows:

$$PL_{T(FOI)} = \sum\sum_{k=1}^{n} \left[PL_{k(FOI)}\right]_{abc} \tag{5.18}$$

Applying Eqs.5.17 and 5.18, using the values in Tables 5.9 & 5.10, results in the following total line power loss at the FOI in feeder F2, without connection of PVDG unit,

$$PL_{T(FOI)} = \sum \begin{bmatrix} 5.4975 \\ 2.3759 \\ 4.8672 \end{bmatrix} = 12.7408 \text{ kW}$$

The optimization procedure

The optimization procedure is commenced by connecting the PVDG unit to the nodes of feeder F2, one by one, starting from the far end. As been practiced earlier, the unit is modeled as a PQ bus operating at unity power factor, thus it is sized according to the real power flow in the line section that is connected.

Considering the 3-phase unbalanced load condition, it seems suitable to size the PVDG unit to the phase of lowest load demand, which is 'b' according to Table 5.7. This avoids the RPF in all of the three phases. Hence,

$$\left[PV_{CP(FOI)}\right]_{abc} = \sum_{k=CP}^{n} \begin{bmatrix} LD^{b}_{k(FOI)} \\ LD^{b}_{k(FOI)} \\ LD^{b}_{k(FOI)} \end{bmatrix}^{P} \tag{5.19}$$

Where,

CP	- The coupling point node of the PVDG unit,
b	- The phase of the lowest load demand among the three phases,
P	- Real power component of the load demand,
k	- Any node between the CP and far end node (n) of the feeder,
$\left[PV_{CP(FOI)}\right]_{abc}$	- Peak of the ac PVDG production curve at the CP node, by phase,
$LD^{b}_{k(FOI)}$	- Load demand of phase b of node k at the FOI

The new load demand of the CP node after connecting the PVDG unit is then updated below.

$$\left[nLD_{CP(FOI)}\right]_{abc} = \left(\left[LD_{CP(FOI)}\right]^{P}_{abc} + j\left[LD_{CP(FOI)}\right]^{Q}_{abc}\right) - \left(\left[PV_{CP(FOI)}\right]_{abc} + j[0]\right) \tag{5.20}$$

Iteration1:

In the first iteration, the PVDG unit is located at the far end of feeder F2, corresponding to node 29. The unit is then sized up by substituting the load demand of the relevant node by phase, stated in Table 5.8, into Eq.5.19. This results in:

$$\left[\mathrm{PV}_{29(\mathrm{FOI})}^{(1)}\right]_{\mathrm{abc}} = \begin{bmatrix}0.0147\\0.0147\\0.0147\end{bmatrix} + \mathrm{j}\,[0] = 0.441\ \mathrm{MW}$$

$$\left[\mathrm{nLD}_{29(\mathrm{FOI})}\right]_{\mathrm{abc}} = \left(\begin{bmatrix}0.0166\\0.0147\\0.0161\end{bmatrix} + \mathrm{j}\begin{bmatrix}0.0124\\0.0095\\0.0112\end{bmatrix}\right) - \left(\begin{bmatrix}0.0147\\0.0147\\0.0147\end{bmatrix} + \mathrm{j}\,[0]\right) \ \mathrm{MVA}$$

$$= \begin{bmatrix}0.0019\\0\\0.0014\end{bmatrix} + \mathrm{j}\begin{bmatrix}0.0124\\0.0095\\0.0112\end{bmatrix} \ \mathrm{MVA}$$

Where the superscript (1) denotes the first iteration in the optimization procedure; while 29 is the CP nodes on feeder F2.

The line voltages and currents at the FOI along the feeder are computed by the means of backward/forward power flow, using the new load demand at the CP node. The resulting $\mathrm{PL}_{\mathrm{FOI}}$ over the first iteration is calculated by applying Eqs.5.17 and 5.18, which gives:

$$\mathrm{PL}_{\mathrm{T(FOI)}}^{(1)} = \sum \begin{bmatrix}4.7464\\1.8914\\4.2238\end{bmatrix} = 10.8616\ \mathrm{kW}$$

$$\Delta\mathrm{PL}_{\mathrm{T(FOI)}}^{(1)} = 14.746\%$$

Iteration2:

The computations are repeated with the PVDG unit is moved back to the next upstream node on feeder F2. Below are the counterpart results of the second iteration:

$$\mathrm{PV}_{28(\mathrm{FOI})}^{(2)} = \begin{bmatrix}0.0294\\0.0294\\0.0294\end{bmatrix} + \mathrm{j}\,[0]\ \mathrm{MW}$$

$$\left[\mathrm{nLD}_{28(\mathrm{FOI})}\right]_{\mathrm{abc}} = \left(\begin{bmatrix}0.0166\\0.0147\\0.0161\end{bmatrix} + \mathrm{j}\begin{bmatrix}0.0124\\0.0095\\0.0112\end{bmatrix}\right) - \left(\begin{bmatrix}0.0294\\0.0294\\0.0294\end{bmatrix} + \mathrm{j}\,[0]\right) \ \mathrm{MVA}$$

$$\left[\mathrm{nLD}_{28(\mathrm{FOI})}\right]_{\mathrm{abc}} = \begin{bmatrix}-0.0128\\-0.0147\\-0.0133\end{bmatrix} + \mathrm{j}\begin{bmatrix}0.0124\\0.0095\\0.0112\end{bmatrix} \ \mathrm{MVA}$$

$$\mathrm{PL}_{\mathrm{T(FOI)}}^{(2)} = \sum \begin{bmatrix}4.0875\\1.5065\\3.6699\end{bmatrix} = 9.2639\ \mathrm{kW}$$

$$\Delta\mathrm{PL}_{\mathrm{T(FOI)}}^{(2)} = 27.290\%$$

The process is continued in the upstream direction up to the CP node 1. The total results for the three phases altogether, in terms of $\mathrm{PV}_{\mathrm{FOI}}$ and $\mathrm{PL}_{\mathrm{T(FOI)}}$ along with $\Delta\mathrm{PL}_{\mathrm{T(FOI)}}$ in per-unit of the original $\mathrm{PL}_{\mathrm{T(FOI)}}$, are illustrated in Fig.5.10.

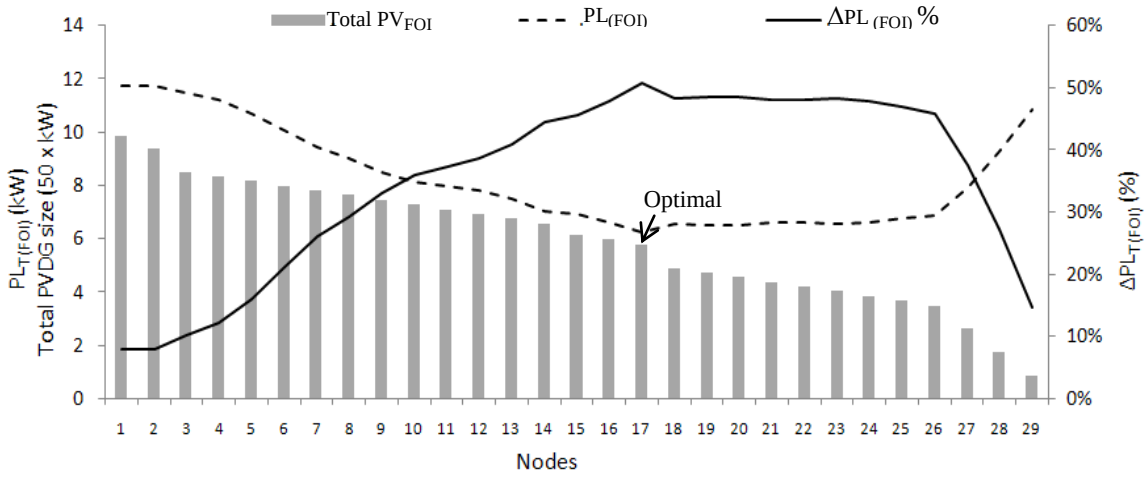

Figure 5.10 Single PVDG unit on unbalanced feeder F2 with the avoidance of RPF

According to the figure, the optimal PVDG size and location maximizing ΔPL_{FOI}, with the avoidance RPF, are stated below.

Optimal location (CP node) = 17

$$\text{Optimal } PV_{cp(FOI)} = \begin{bmatrix} 0.0968 \\ 0.0968 \\ 0.0968 \end{bmatrix} + j\,[0] = 0.2905 \text{ MW}$$

$$PL_{T(FOI)} = \sum \begin{bmatrix} 2.6824 \\ 0.9938 \\ 2.5831 \end{bmatrix} = 6.2593 \text{ kW}$$

$\Delta PL_{T(FOI)}$ = 50.872%

Recalling Eq.4.1, the dc commercial capacity of the PV array (PV_{com}) that can afford for this production is calculated. Assuming the average conversion efficiency of the grid-tied inverters is 0.9, and SI at the FOI is 850 W/m^2, the resulting PV_{com} is,

$$PV_{com} = \sum \begin{bmatrix} 0.1265 \\ 0.1265 \\ 0.1265 \end{bmatrix} = 0.3795 \text{ MW}$$

Figure 5.11 compares the voltage profile at the FOI along the feeder with and without the single PVDG unit at the optimal solution. It shows obvious improvement in the voltage profile for the three phases.

Also Fig.5.12 illustrates the same comparison for the current flow profile along the feeder. It shows considerable current flow reduction in the upstream line sections before the CP node 17. However, the rest of line sections after node 17 are not affected by the PVDG unit.

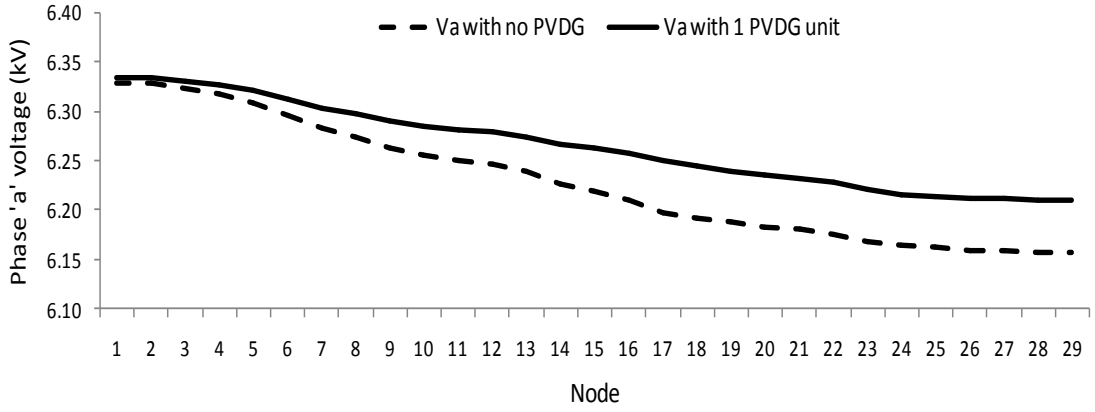

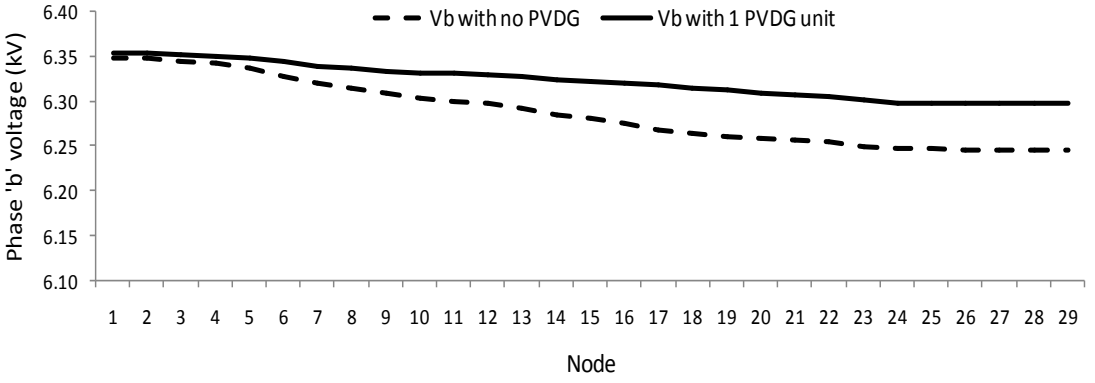

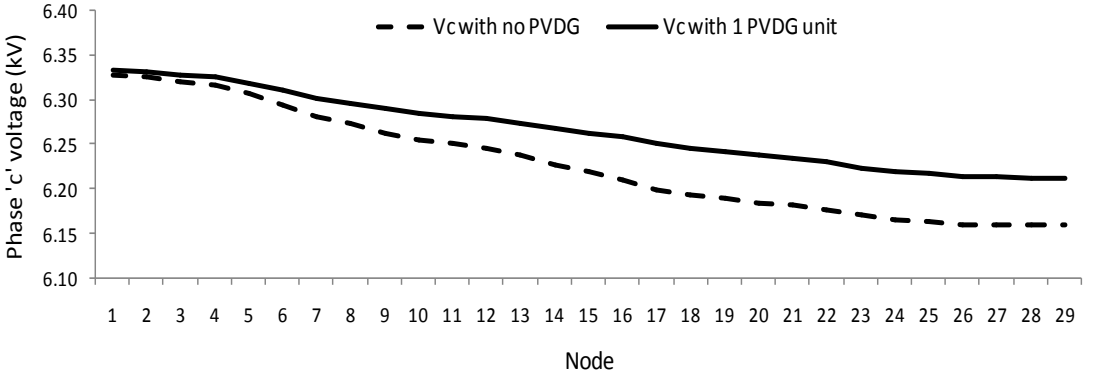

Figure 5.11 Feeder F2 phase voltage at the FOI with optimal single PVDG unit, avoiding RPF

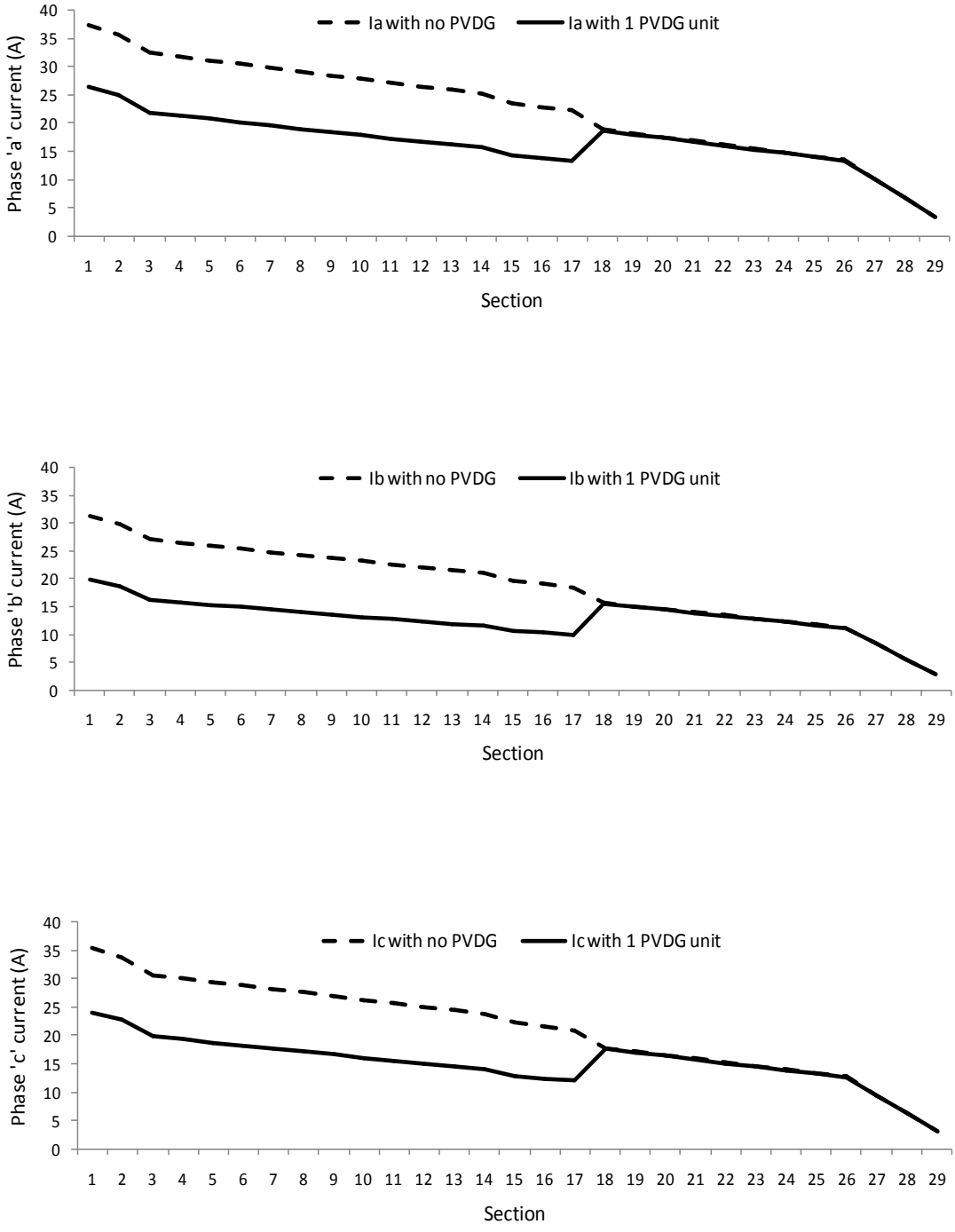

Figure 5.12 Feeder F2 current at the FOI with optimal single PVDG unit, avoiding RPF

5.1.3 Multiple PVDG units on unbalanced 3-phase feeder avoiding RPF

The previous sections tackled the case of a single PVDG unit connected to a radial distribution feeder. It showed that the PVDG unit affects the power flow in the line sections from the substation (s/s) up to the coupling point (CP) node. However, when multiple PVDG units are connected to the same feeder, the closest one to the end will affect all the other units but not the opposite. Consequently, the size of a PVDG unit at certain CP node should be considered when sizing any unit in the upstream direction to this CP.

Additionally, with the installation of multiple PVDG units it is deemed not feasible to iterate the optimization procedure in the same way as with a single PVDG unit. Doing this will yield hundreds, or even thousands of possible PVDG locations.

The two points above have been considered in this section to develop the optimization procedure in a way that deals with multiple PVDG units on the same feeder. Cases with two and three PVDG units are considered as examples in this application. The developed procedure is applied on the feeder F2, considering winter load demand and assuming unbalanced load condition. Hence, the results of phase impedance matrix stated in Table 5.5 are applied. Also the load demand of nodes, phase voltage and current along the feeder before connecting the PVDG unit are substituted from Tables 5.8, 5.9 and 5.10 respectively.

The optimization procedure

With multiple PVDG units on one radial feeder, it is suitable to commence the optimization process with an initial feasible location for the units. The initial locations are determined so that the overall impact of the PVDG units covers as much as possible of the feeder length. The size of the units is then set according to the location of each one of them. Figure 5.13 shows the sizing concept with three PVDG units on 10-node radial distribution feeder.

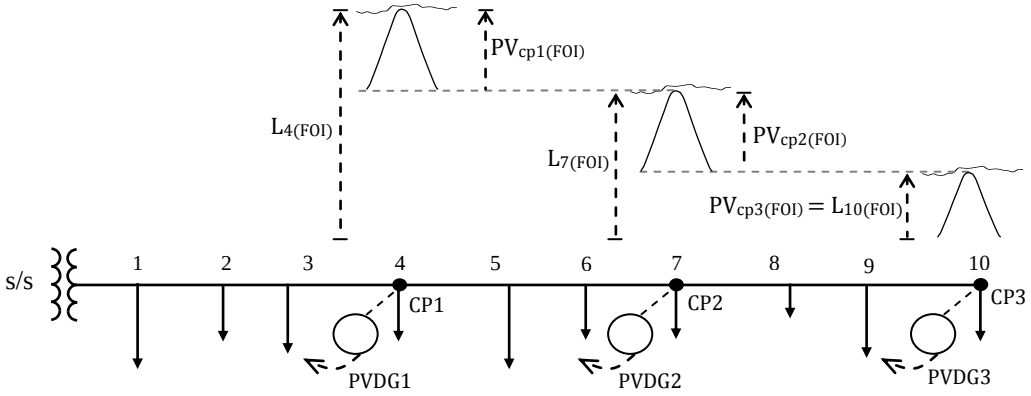

Figure 5.13 Optimization of three PVDG units with the avoidance of RPF

Sizing the PVDG units:

The sizing of the PVDG units is carried out based on Eq.5.19 considering that each unit is affected by the size of the units on its downstream direction. Thus, the sizing of 'x' PVDG units is shown below, assuming phase 'b' carries the lowest power flow among the three phases. The load demand of nodes by phase is realized by applying Eq.5.15.

$$\left[PV_{CPj(FOI)}\right]_{abc} = \sum_{k=CPj}^{n} \begin{bmatrix} LD^{b}_{k(FOI)} \\ LD^{b}_{k(FOI)} \\ LD^{b}_{k(FOI)} \end{bmatrix}^{P} - \sum_{u=CP(j+1)}^{\times} \left[PV_{u(FOI)}\right]_{abc} \quad (5.21)$$

Where,

x - Number of multiple PVDG units,

CPj - Coupling point node at which the j^{th} PVDG unit is located,

u - Index of the PVDG units on the downstream side of CPj,

$PV_{CPj(FOI)}$ - Peak of the ac PVDG production curve of j^{th} PVDG unit,

$LD^{b}_{k(FOI)}$ - Phase b load demand of node k at the FOI,

In the same connection, the load demand at each CP node after the connection of the PVDG unit is then updated by applying Eq.5.20.

Equation 5.21 and 5.20 are applied to the multiple PVDG units along the feeder over the iterations of the optimization procedure. However, initial feasible locations should be determined for the units before the iteration process is commenced.

Determination of initial feasible locations

A suitable method has been developed to determine the initial feasible location (ini_CP) for any number of PVDG units on radial distribution feeder. In this course, a uniform load distribution feeder equivalent to the actual feeder is modeled. The initial feasible locations are determined on the uniform feeder, and then returned to their equivalent ini_CP nodes on the actual feeder.

However, one should be aware that line sections of actual distribution feeders are of different lengths. Additionally, they are possibly constructed in different wire sizes and consequently different resistances per unit length (r). Hence, the lengths of the actual line sections are normalized to one reference 'r' (r_{ref}) along the feeder, as follows [11]:

$$Le_{k\_norm} = Le_{k\_org} \times \frac{r_k}{r_{ref}} \quad (5.22)$$

Where,

Le_{k_norm} - Normalized length of line section k (km),
Le_{k_act} - Actual length of line section k (km),
r_k - Wire conductor resistance of the actual line section k (Ω/km),
r_{ref} - Reference wire conductor resistance (Ω/km),

At this point, the power flow area along the feeder at the FOI ($PF_{F(FOI)}$) can be represented by applying Eq.5.23. Note to mention that $LD_{i(FOI)}$ is the load demand at the FOI of node i:

$$PF_{F(FOI)} = \sum_{k=1}^{n} \left(Le_{k\_norm} \times \sum_{i=k}^{n} LD_{i(FOI)} \right) \quad (5.23)$$

The power flow area at the FOI and the normalized feeder are represented in Figure 5.14. Note to mention that $LD_{F(FOI)}$ is the total load demand of the feeder at the FOI, and n=10.

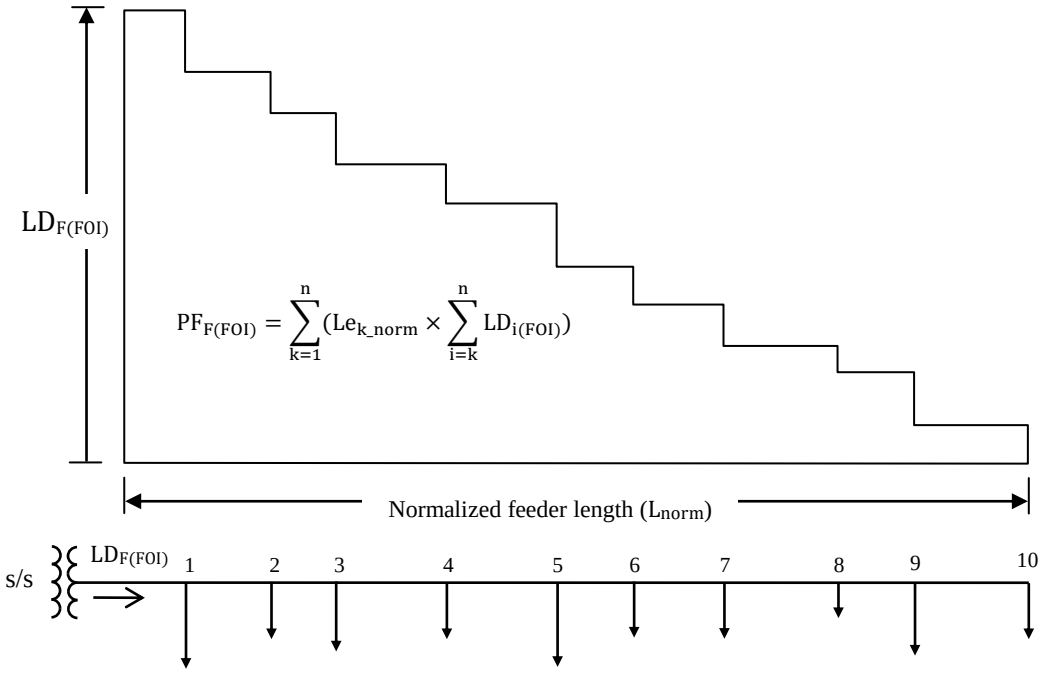

Figure 5.14 Power flow area/profile at the FOI along the normalized feeder

In a uniform feeder the load is distributed uniformly per unit length along the feeder. Thus, its power flow area is represented by a right triangle shape rather than ladder shape [12&13]. Based on that, an equivalent uniformly distributed feeder is generated whose $LD_{F(FOI)}$ and $PL_{F(FOI)}$ equal those of the normalized feeder. Figure 5.15 represents the equivalent feeder.

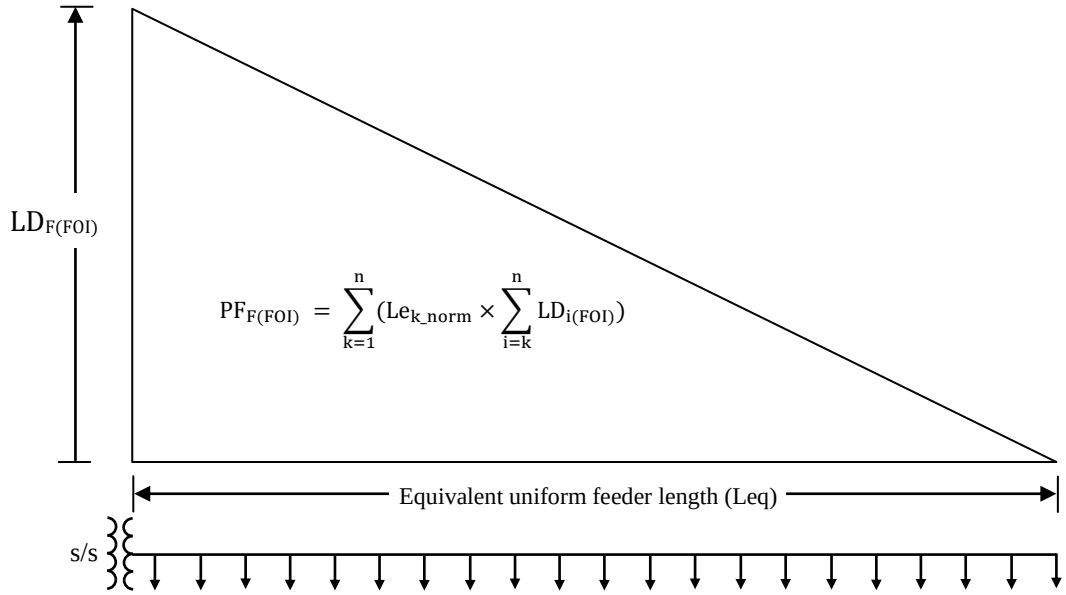

Figure 5.15 Equivalent uniformly distributed feeder to the normalized feeder

Connection of PVDG units of a suitable size and location on the uniform feeder will compensate part of the power flow area shown in Fig.5.15. Assume three PVDG units are connected on the feeder, as in Figure 5.16. The PVDG units are sized according to the power flow in the sections they are connected to.

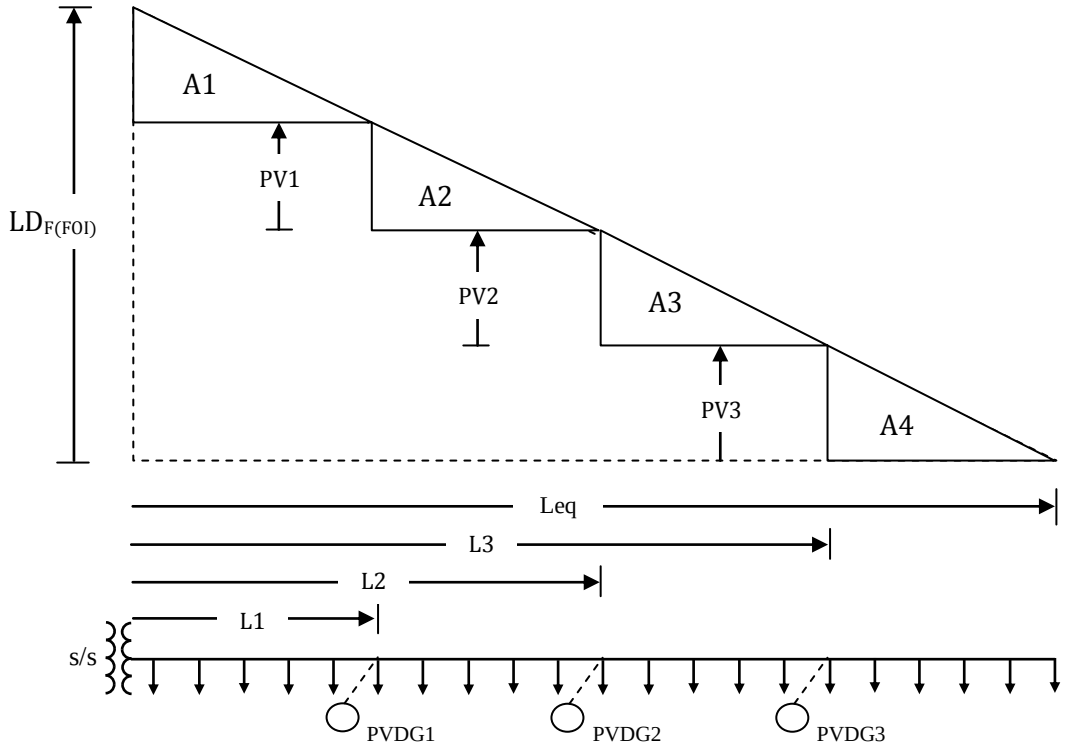

Figure 5.16 Power flow profile of uniform feeder with 3 PVDG units avoiding RPF

Based on Fig.5.15, the equivalent length of the uniform feeder (Leq) is determined as follows:

$$\mathrm{Leq} = \frac{\mathrm{PF_{F(FOI)}}}{0.5 \times \mathrm{LD_{F(FOI)}}} \tag{5.24}$$

Then, the derivations below are expressed based on Fig.5.16,

$$\mathrm{A1} = 0.5 \times \left(\mathrm{LD_{F(FOI)}} - \mathrm{PV1} - \mathrm{PV2} - \mathrm{PV3}\right) \times \mathrm{L1} \tag{5.25.a}$$

$$\mathrm{A2} = 0.5 \times \mathrm{PV1} \times (\mathrm{L2} - \mathrm{L1}) \tag{5.25.b}$$

$$\mathrm{A3} = 0.5 \times \mathrm{PV2} \times (\mathrm{L3} - \mathrm{L2}) \tag{5.25.c}$$

$$\mathrm{A4} = 0.5 \times \mathrm{PV3} \times (\mathrm{Leq} - \mathrm{L3}) \tag{5.25.d}$$

$$\mathrm{A} = \mathrm{A1} + \mathrm{A2} + \mathrm{A3} + \mathrm{A4} \tag{5.25.e}$$

Based on above, minimum 'A' shall result in minimum power flow area along the feeder. But minimum 'A' can be realized by setting the first derivative of 'A' with respect to each of PV1-PV3 equals to zero as follows:

$$\frac{\mathrm{dA}}{\mathrm{dPV1}} = 0 \;\rightarrow\; 0.5 \times\; (\mathrm{L2} - 2\,\mathrm{L1}) = 0$$

$$\therefore \mathrm{L2} = 2\,\mathrm{L1} \tag{5.26.a}$$

$$\frac{\mathrm{dA}}{\mathrm{dPV2}} = 0 \;\rightarrow\; 0.5 \times\; (\mathrm{L3} - \mathrm{L1} - \mathrm{L2}) = 0$$

$$\therefore \mathrm{L3} = \mathrm{L1} + \mathrm{L2} \tag{5.26.b}$$

$$\frac{\mathrm{dA}}{\mathrm{dPV3}} = 0 \;\rightarrow\; 0.5 \times\; (\mathrm{Leq} - \mathrm{L1} - \mathrm{L3}) = 0$$

$$\therefore \mathrm{Leq} = \mathrm{L1} + \mathrm{L3} \tag{5.26.c}$$

Solving Eq.5.26 shows that the three PVDG units divide the 'Leq' into four equal parts that each one them equals the length span L1. In general form, the length span on the equivalent uniform ($\mathrm{Leq_{span}}$) feeder with 'x' PVDG units is expressed as follows:

$$\mathrm{Leq_{span}} = \frac{\mathrm{Leq}}{\mathrm{x} + 1} \tag{5.27}$$

To this end, the initial feasible locations (ini_CP) are determined based on the corresponding multiples of $\mathrm{Leq_{span}}$. In other words, ini_CP1 is referenced to $1\times\mathrm{Leq_{span}}$ and ini_CP2 to $2\times\mathrm{Leq_{span}}$, and so on. Once the ini_CP nodes are determined, the optimization process is iterated by moving the PVDG units in the upstream direction according to certain steps formula.

However, it is known that the equivalent uniform feeder is modeled by approximation. Consequently, the corresponding multiples of Leq_{span} will return approximated locations for the counterpart ini_CP nodes on the normalized feeder. To this end, if the ini_CP node is located on the downstream side of the actual optimal locations then there will be no problem. The reason is that the optimization process is set to move in the upstream direction so the optimal location will come in its way. On the contrary, if it happened that the ini_CP node is located on the upstream side of the actual optimal location, even by one node, then the optimization procedure will miss it.

Based on the above, the optimization results can be enhanced further by shifting the initial locations, to some extent, in the downstream direction. In this work, each of the ini_CP locations on the uniform feeder is shifted by one Leq_{span} as follows:

$$Leq\_CPj = Leq_{span} \times (j + 1) \tag{5.28}$$

Where Leq_CPj is the length on the equivalent uniform feeder at which the jth PVDG unit is connected.

The Leq_CPj is returned to its equivalent node (ini_CPj) on the normalized feeder by solving the following formula for the node Nj,

$$\sum_{k=1}^{N_{CPj}} Le_{k\_norm} \approxeq Leq\_CPj \times \frac{L_{norm}}{Leq} \tag{5.29.a}$$

Where L_{norm} is the length of the normalized feeder,

Then,

$$ini\_CPj = N_{CPj}\big|_{j=1:x} \tag{5.29.b}$$

Where N_{CPj} is the node on the normalized feeder satisfies Eq.5.29, at which the CPj is located. While 'x' is the number of installed PVDG units.

Feasible iterative steps formula:

The running of the iterative steps for multiple PVDG units the same way as that for single PVDG unit will yield hundreds or even thousands of iterations. Hence, a suitable formula to reduce the number of iterative steps considerably is developed. The formula checks the possible moving steps of the multiple units and then selects the more feasible one.

Assuming three PVDG units; the stepping possibilities per iteration are taken as in Table 5.11 below:

Table 5.11 Determining feasible iterative steps with three PVDG units avoiding RPF

		Iteration 1	
Poss.1	$CP1^{(1)} = ini\_CP1$	$CP2^{(1)} = ini\_CP2$	$CP3^{(1)} = ini\_CP3$
		Iteration 2	
Poss.1	$CP1^{(2)} = CP1^{(1)} - 1$	$CP2^{(2)} = CP2^{(1)}$	$CP3^{(2)} = CP3^{(1)}$
Poss.2	$CP1^{(2)} = CP1^{(1)}$	$CP2^{(2)} = CP2^{(1)} - 1$	$CP3^{(2)} = CP3^{(1)}$
Poss.3	$CP1^{(2)} = CP1^{(1)}$	$CP2^{(2)} = CP2^{(1)}$	$CP3^{(2)} = CP3^{(1)} - 1$
		Iteration 3	
Poss.1	$CP1^{(3)} = CP1^{(2)} - 1$	$CP2^{(3)} = CP2^{(2)}$	$CP3^{(3)} = CP3^{(2)}$
Poss.2	$CP1^{(3)} = CP1^{(2)}$	$CP2^{(3)} = CP2^{(2)} - 1$	$CP3^{(3)} = CP3^{(2)}$
Poss.3	$CP1^{(3)} = CP1^{(2)}$	$CP2^{(3)} = CP2^{(2)}$	$CP3^{(3)} = CP3^{(2)} - 1$
⋮	⋮	⋮	⋮
⋮	⋮	⋮	⋮
		Iteration t	
Poss.1	$CP1^{(t)} = CP1^{(t-1)} - 1$	$CP2^{(t)} = CP2^{(t-1)}$	$CP3^{(t)} = CP3^{(t-1)}$
Poss.2	$CP1^{(t)} = CP1^{(t-1)}$	$CP2^{(t)} = CP2^{(t-1)} - 1$	$CP3^{(t)} = CP3^{(t-1)}$
Poss.3	$CP1^{(t)} = CP1^{(t-1)}$	$CP2^{(t)} = CP2^{(t-1)}$	$CP3^{(t)} = CP3^{(t-1)} - 1$

Where the superscripts define the iteration number,

For iteration t, the resulting power flow area along the feeder at the FOI is illustrated in Fig.5.17. The shaded areas in the figure represent the compensated power flow areas due to the connection of the PVDG units at the nodes of CP1, CP2 and CP3.

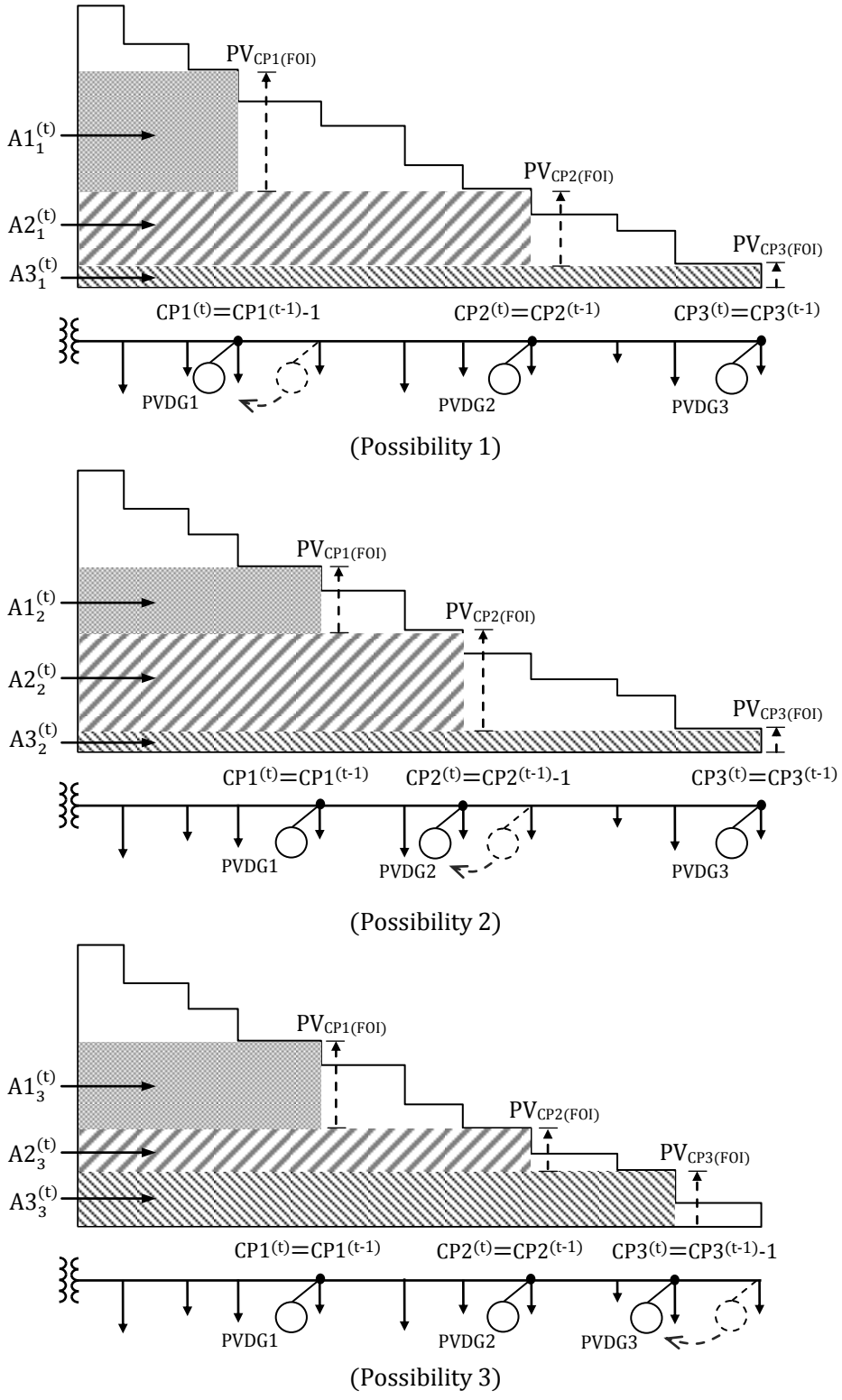

Aj_p^t - *Compensated power flow area due to the connection of the jth PVDG unit at the location associated with possibility p over iteration t*

Figure 5.17 Possible steps of three PVDG units at iteration avoiding RPF

The three PVDG units are sized according to the amount of power flow, at the FOI, in the line sections they are connected at. Hence, Eq.5.30 is applied to calculate the total compensated power flow area associated with each of the three possibilities (A_{Poss}). Note to mention that the line sections along the feeder are now already normalized to one wire size

$$A_{Poss} = \sum_{j=1}^{x} PV_{CPj(FOI)} \times \sum_{k=1}^{CPj} Le_{k\_norm} \tag{5.30}$$

But the amount of power flow is directly proportional to the amount of line power loss. Therefore, as high is the compensated power flow area as low is the resulting power flow and high the ΔPL_{FOI} along the feeder. In this course, Eq.5.30 is applied to calculate the total compensated power flow area for each of the three possibilities illustrated in Fig.5.17. Then, the feasible CP nodes at the relevant iteration 't' are determined as follows:

$$\text{If} \quad A^{(t)}_{Poss.1} > A^{(t)}_{Poss.2} \quad \text{and} \quad A^{(t)}_{Poss.1} > A^{(t)}_{Poss.3}, \quad \text{then,}$$
$$CP1^{(t)} = CP1^{(t-1)} - 1, \quad CP2^{(t)} = CP2^{(t-1)}, \quad CP3^{(t)} = CP3^{(t-1)}$$

$$\text{If} \quad A^{(t)}_{Poss.2} > A^{(t)}_{Poss.1} \quad \text{and} \quad A^{(t)}_{Poss.2} > A^{(t)}_{Poss.3}, \quad \text{then,} \tag{5.31}$$
$$CP1^{(t)} = CP1^{(t-1)}, \quad CP2^{(t)} = CP2^{(t-1)} - 1, \quad CP3^{(t)} = CP3^{(t-1)}$$

$$\text{If} \quad A^{(t)}_{Poss.3} > A^{(t)}_{Poss.1} \quad \text{and} \quad A^{(t)}_{Poss.3} > A^{(t)}_{Poss.2}, \quad \text{then,}$$
$$CP1^{(t)} = CP1^{(t-1)}, \quad CP2^{(t)} = CP2^{(t-1)}, \quad CP3^{(t)} = CP3^{(t-1)} - 1$$

Hence, applying Eqs.5.30 and 5.31 will significantly reduce the number of iterations over the optimization process. To have an idea on the possible reduction in the number of iterations, feeder F2 has been taken as example with and without applying the two equations. At a certain CP3 node on the feeder, all of the nodes in the upstream direction could come as CP2. Then, at each CP2 node of these all of the nodes in the upstream direction again could come as CP1. Locating CP3 at node 29 and CP2 at node 28 will result in another 27 possibilities of CP1 locations, and so on. At the end, it took 3654 iterations to check all the available possibilities of the three PVDG units on feeder F2. On the other hand, the application of Eqs.5.30 and 5.31 has reduced the possible locations of the three units to 29 utmost.

Applications considering two and three PVDG units

The developed procedure was applied on feeder F2 under unbalanced load conditions and considering winter load demand. The line impedance of the feeder was taken from the phase impedance matrix stated in Table 5.5. Also the load demand of nodes, phase voltage and current along the feeder were substituted from Tables 5.8, 5.9 and 5.10 respectively.

The steps of the optimization procedure are illustrated below in Fig.5.18.

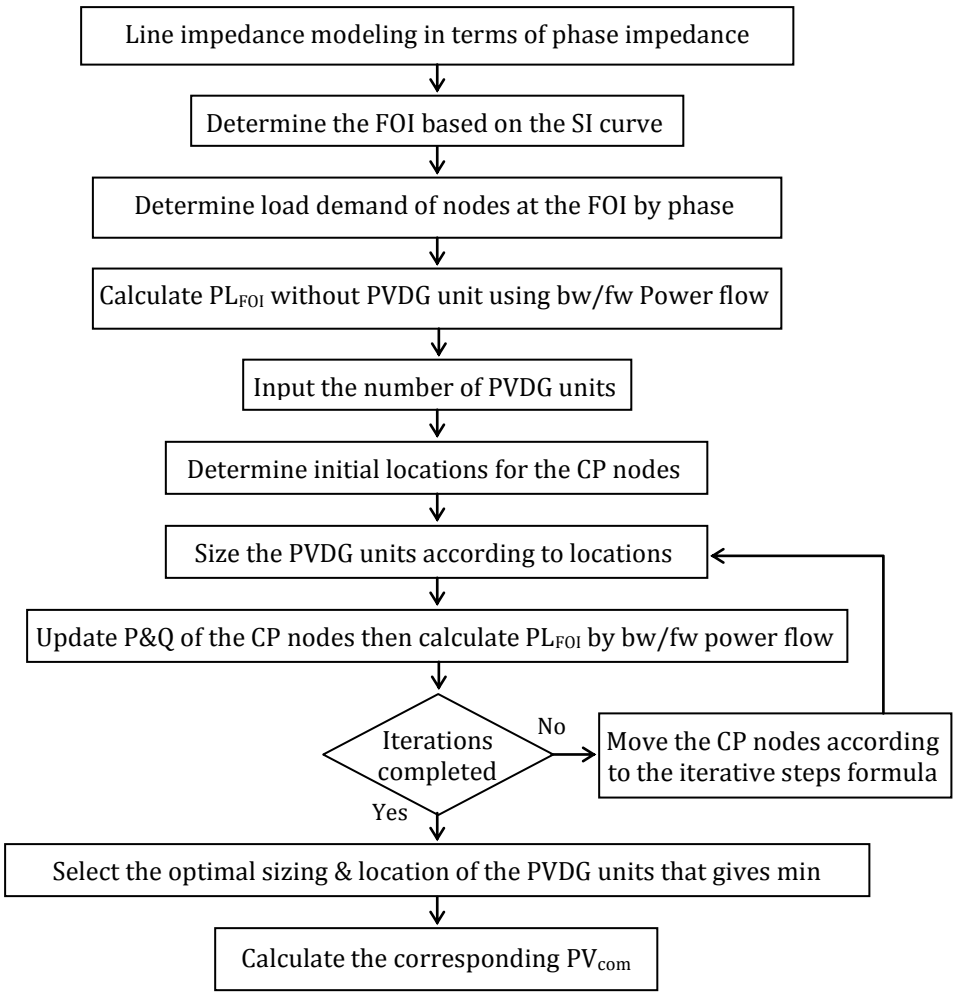

Figure 5.18 Optimization procedure of multi PVDG units avoiding RPF

The first four blocks in the flow chart of Fig.5.18 are similar to that of the flowchart in Section 5.1.2. Starting from there, the normalized length of line sections along the feeder are generated by applying Eq.5.22. The wire conductor resistance of line section 1, equaling 0.098 (Ω/km), is taken as the reference of the normalized lengths. After that, Eqs.5.23 and 5.24 are applied to model the length of the equivalent uniform feeder. The original, normalized and equivalent uniform lengths related to feeder F2 are stated below.

Original length (Le) of F2	Normalized length (Le$_{norm}$)	Equivalent uniform length (Leq)
23.221 km	49.2768 km	63.1491 km

The length span and the resulting CP lengths on the uniform feeder are then computed according to the number of PVDG units, using Eqs.5.27 and 5.28 respectively. At this stage, the initial locations of the CP nodes can be determined by applying Eq.5.29.

The result considering two and three PVDG units on feeder F2 are stated below.

	Two PVDG units (x = 2)		Three PVDG units (x = 3)		
	PVDG 1	PVDG 2	PVDG 1	PVDG 2	PVDG 3
Leq_CPj (km)	42.0994 km	63.1491 km	31.5746 km	47.3619 km	63.149 km
Ini_CPj (node)	17	29	14	19	29

Leq_CPj is from the substation up to the CP location on the equivalent uniform feeder

The optimization procedure is then iterated from the initial locations of the PVDG units stated in the above table. The results of the first two iterations are given below, with the results over the whole iteration set being graphed separately for the cases of two and three PVDG units.

Iteration1:

In the first iteration, the PVDG units are located at the initial CP nodes and then sized according to their locations by applying Eq.5.21. The load demands of the CP nodes are then updated by using Eq.5.20. The resulting line power loss at the FOI (PL_{FOI}) is calculated by the means of backward/forward power flow then applying Eqs.5.17 and 5.18. The results of iteration 1 are as tabulated below.

	Two PVDG units (x = 2)		Three PVDG units (x = 3)		
	PVDG 1	PVDG 2	PVDG 1	PVDG 2	PVDG 3
$CP^{(1)}$ node	17	29	14	19	29
$PV_{FOI}^{(1)}$ size (MW)	0.247	0.044	0.0932	0.1940	0.0440
$PL_{FOI}^{(1)}$ (kW)	5.8846		5.4335		
$\Delta PL_{FOI}^{(1)}$	53.8%		57.353%		

PV_{F0I} size is stated in terms of total sizes for the three phases altogether,
ΔPL_{F0I} is in percentage of the PL_{FOI} without PVDG units,

Iteration2:

	Two PVDG units (x = 2)		Three PVDG units (x = 3)		
	PVDG 1	PVDG 2	PVDG 1	PVDG 2	PVDG 3
$CP^{(2)}$ node	17	28	14	19	28
$PV_{FOI}^{(2)}$ size (MW)	0.203	0.088	0.0932	0.15	0.088
$PL_{FOI}^{(2)}$ (kW)	5.5998		5.232		
$\Delta PL_{FOI}^{(2)}$	56.05%		58.953%		

Figures 5.19 & 5.20 shows the feasible CP nodes and sizes over iterations for two PVDG units on feeder F2. At the same time, Fig.5.21 illustrates the line power loss and the line power loss reduction at the FOI (PL_{F0I} & ΔPL_{F0I}) associated with each of these iterations. Figures 5.22 to 5.24 depict the same results considering three PVDG units.

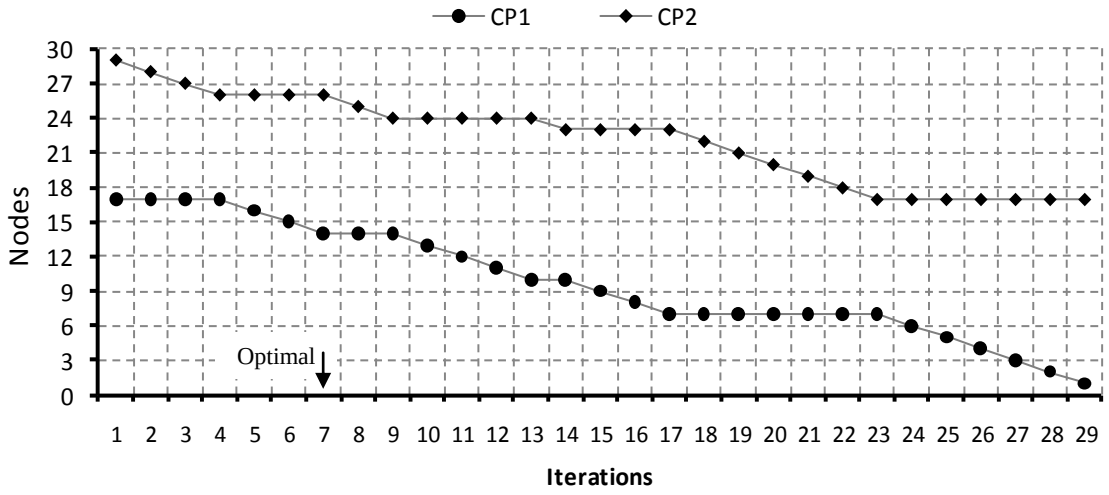

Figure 5.19 CP nodes vs. iterations of two PVDG units on feeder F2, avoiding RPF

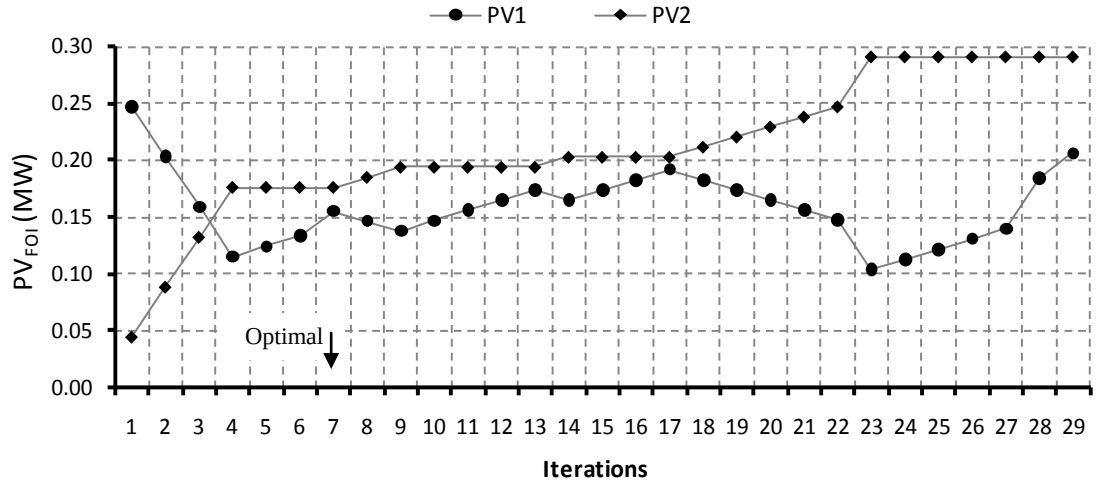

Figure 5.20 PV_{FOI} vs. iterations of two PVDG units of feeder F2, avoiding RPF

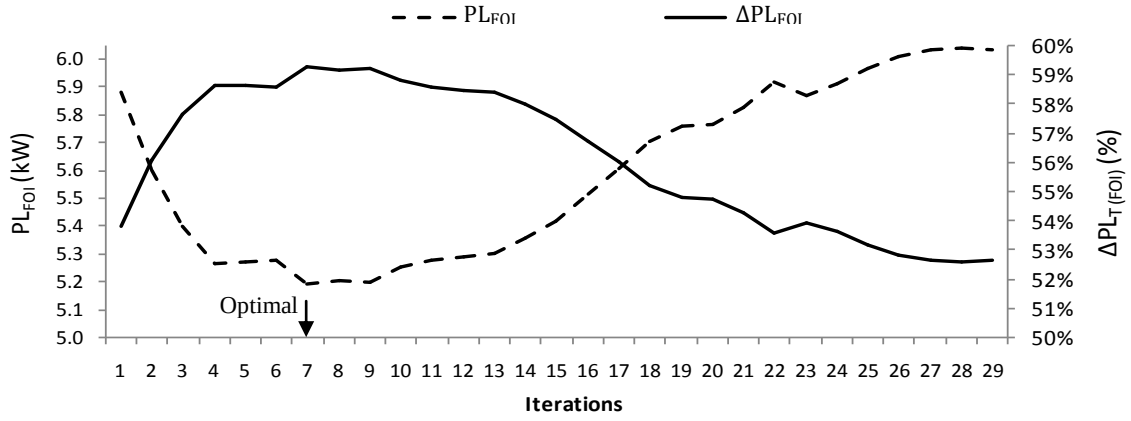

Figure 5.21 PL_{FOI} & ΔPL_{FOI} with two PVDG units of feeder F2, avoiding RPF

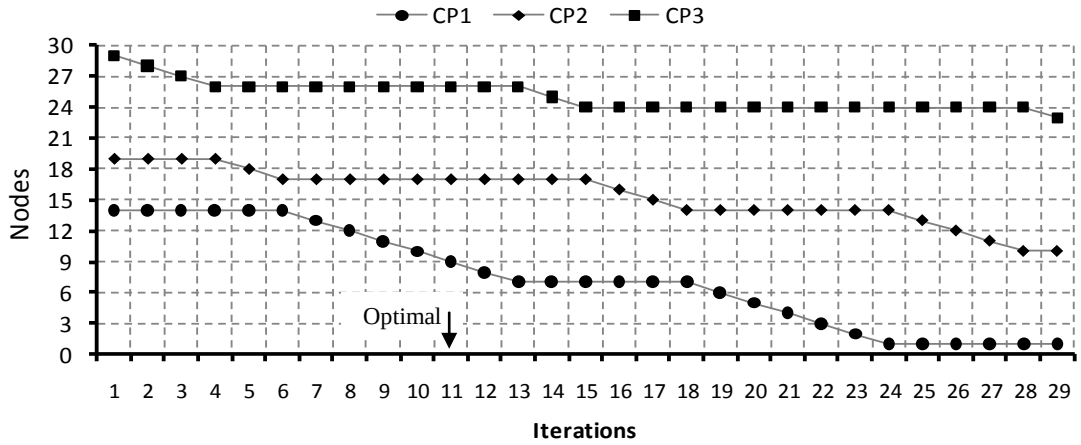

Figure 5.22 CP nodes vs. iterations of three PVDG units on feeder F2, avoiding RPF

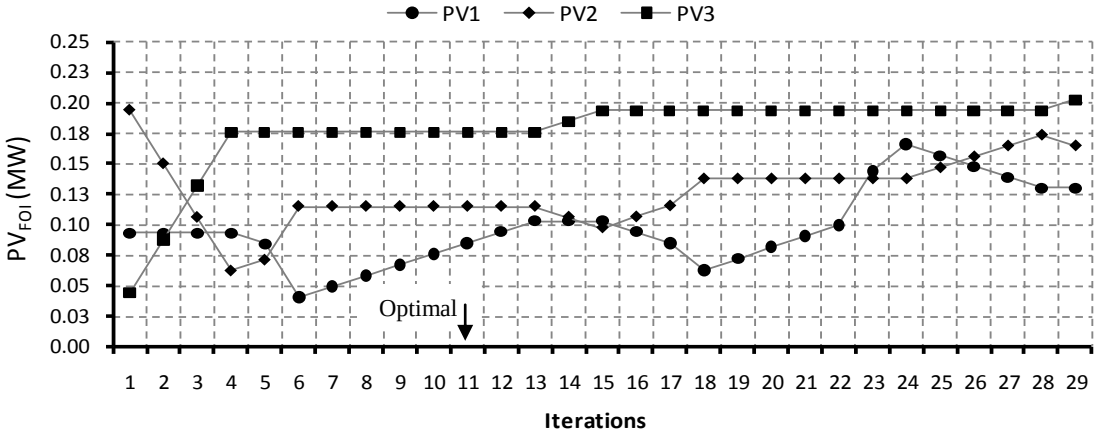

Figure 5.23 PV_{FOI} vs. iterations of three PVDG units on feeder F2, avoiding RPF

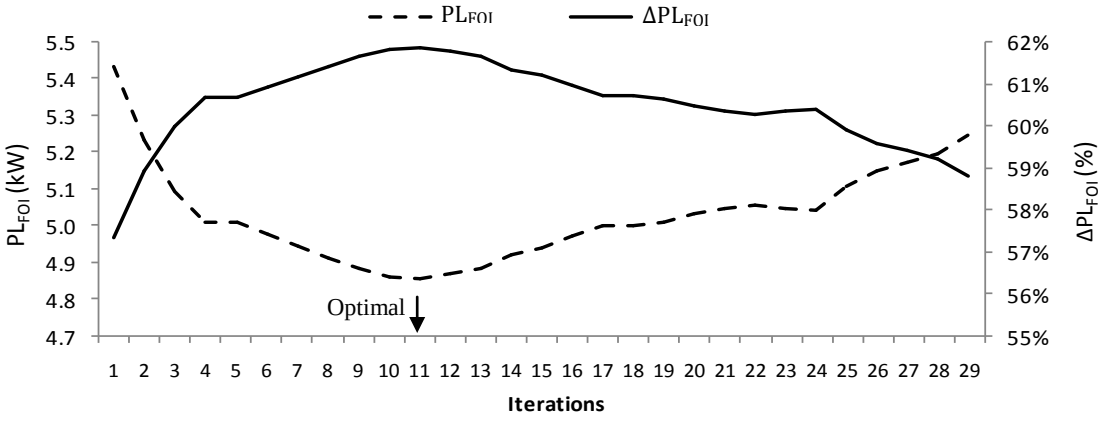

Figure 5.24 PL_{FOI} & ΔPL_{FOI} with three PVDG units on feeder F2, avoiding RPF

The optimal solutions that result in maximum line power loss reduction according to Figs.5.19 to 5.24 at the FOI (ΔPL_{FOI}) are presented in Table 5.12.

Table 5.12 Optimal solution considering two and three PVDG units on feeder F2

	Two PVDG units (x = 2)		Three PVDG units (x = 3)		
	PVDG 1	PVDG 2	PVDG 1	PVDG 2	PVDG 3
Optimal CP node	14	26	9	17	26
Optimal PV_{FOI} (MW)	0.1552	0.176	0.0852	0.115	0.176
Optimal Tot_PV_{FOI} (MW)	0.3312		0.3762		
Resulting PL_{FOI} (kW)	5.1903		4.8581		
Resulting ΔPL_{FOI}	59.262%		61.87%		

Figure 5.25 illustrates the current flow profile by phase at the FOI with two PVDG units at the optimal solution. The same illustration, with three PVDG units, is given in Fig.5.26.

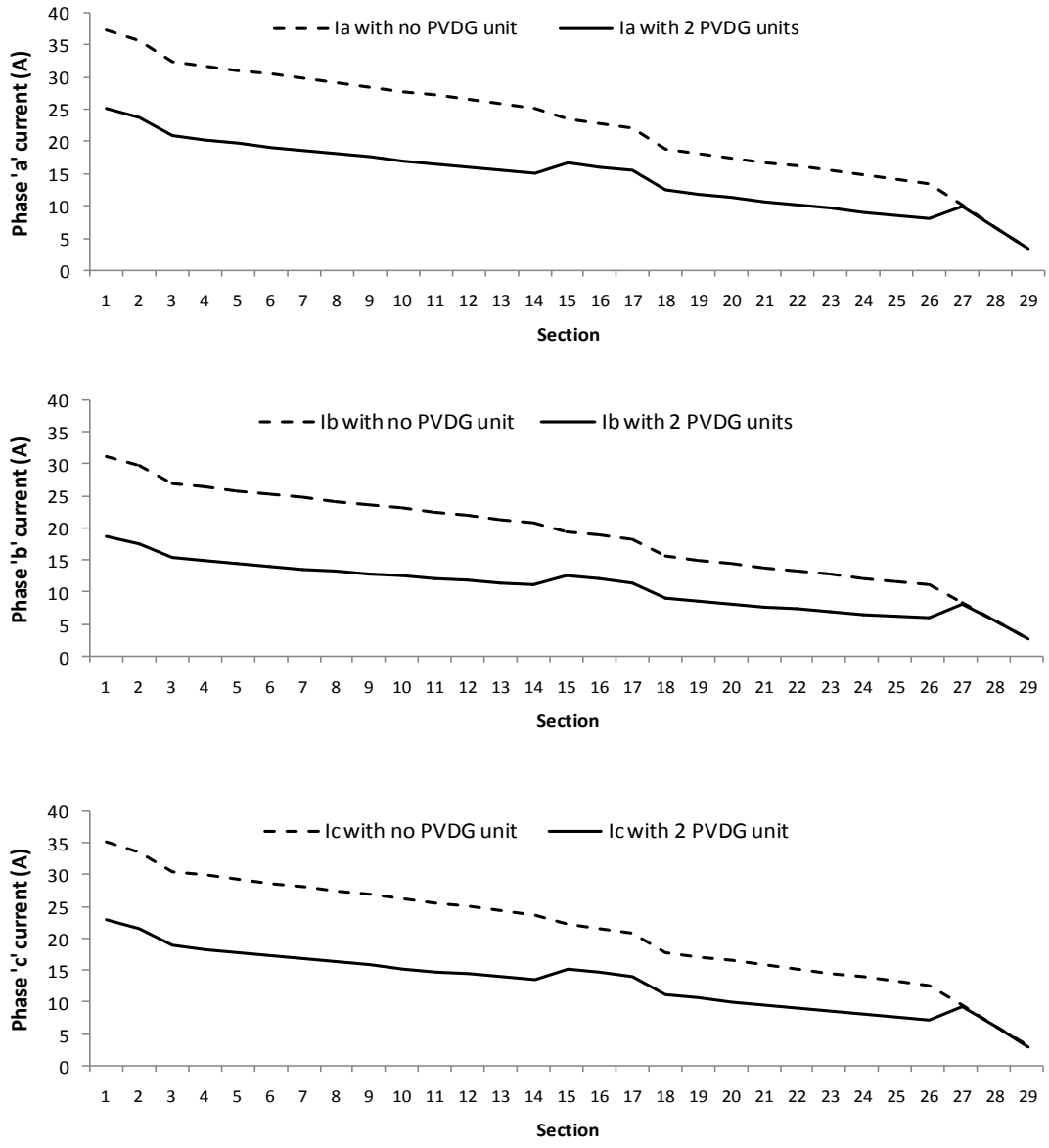

Figure 5.25 Feeder F2 current at the FOI with optimal two PVDG units, avoiding RPF

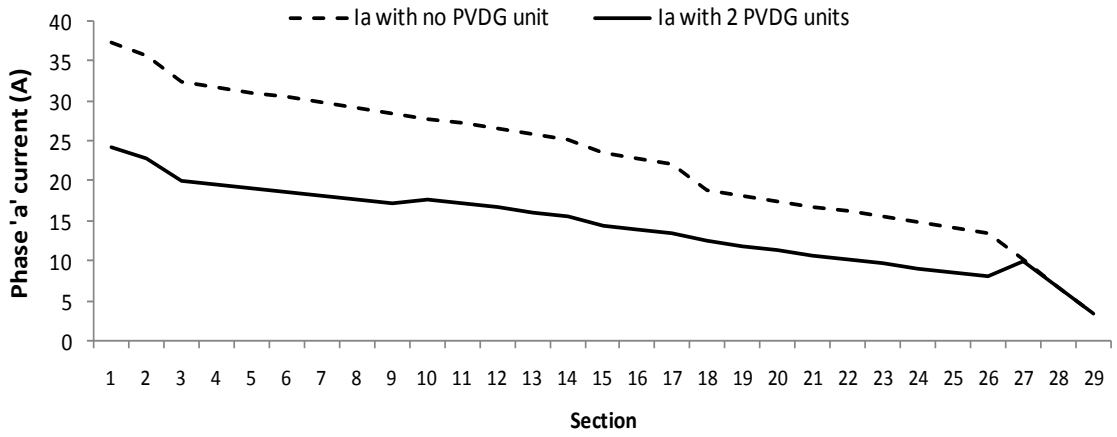

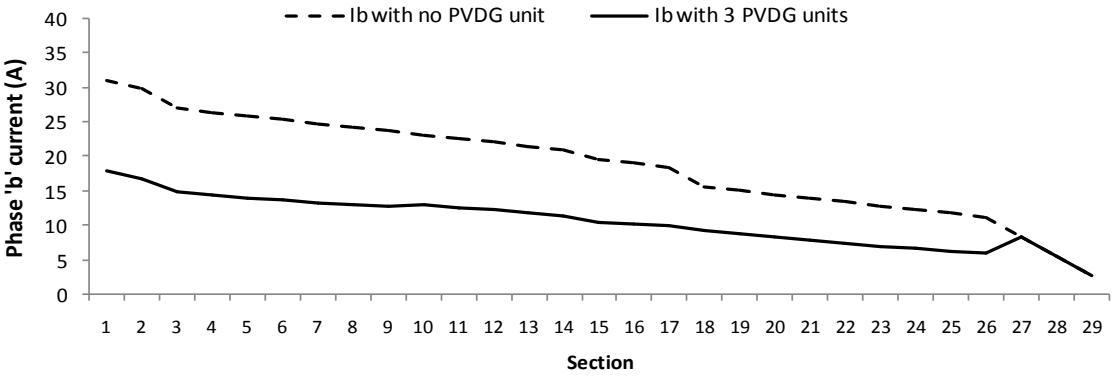

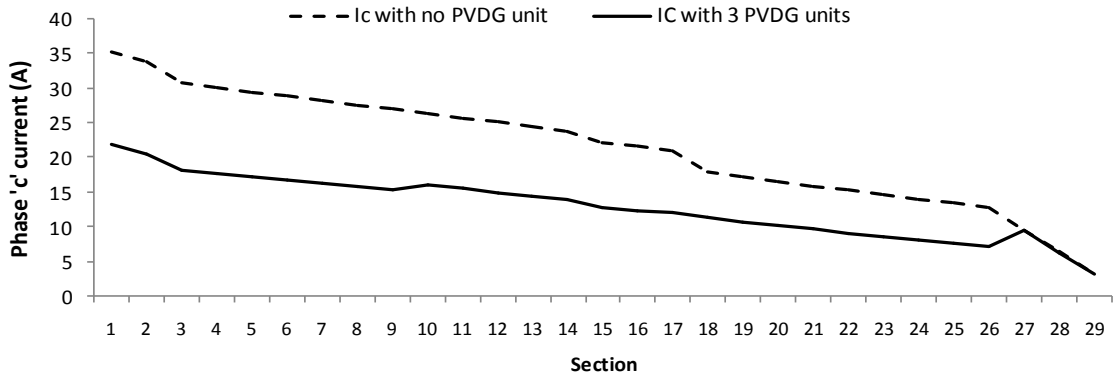

Figure 5.26 Feeder F2 current at the FOI with optimal three PVDG units, avoiding RPF

Validation of the optimal solution

The credibility of the optimization procedure has been checked by modifying the MATLAB program to consider every possible solution on feeder F2. In other word, it has been modified to iterate the calculations without applying the feasible iterative steps formula. Consequently, the top four solutions ranking the lowest PL_{FOI} (or highest ΔPL_{FOI}) are compared with the optimal solution from the developed optimization procedure. The results, related to feeder F2 considering two and three PVDG units, are given in Tables 5.13 and 5.14 respectively.

It is important to mention that the number of iterations in the procedure is limited by the number of nodes along the feeder. This means that the maximum number of iterations in feeder F2 is 29. However, Figs.5.21 and 5.24 shows that the line power loss benefits over iterations track concave and convex trends for the PL_{FOI} and ΔPL_{FOI} respectively. Hence the iterations of the developed procedure are not necessarily continued after the bottom of the PL_{FOI} profile (or peak of the ΔPL_{FOI} one). On this basis, the procedure is set to stop the iteration process if it tracks two successive iterations with results divergent from the best result most recently realized. The two successive iterations in this work are called 'affirming iterations'.

Table 5.13 Optimal solution validation of two PVDG units on feeder F2, avoiding RPF

No. of the iterations in the optimization procedure = 7 (+2 affirming iterations)						
	CP1 node	CP2 node	$PV1_{FOI}$ (MW)	$PV2_{FOI}$ (MW)	Tot_PV_{FOI} (MW)	PL_{FOI} (kW)
Optimal	14	26	0.1552	0.176	0.3313	5.1903
Iterations without initial locations and feasible iterative steps = 406						
Top 1	14	26	0.1552	0.1760	0.3312	5.1903
Top 2	14	24	0.1376	0.1937	0.3313	5.1964
Top 3	14	25	0.1464	0.1848	0.3312	5.2025
Top 4	13	24	0.1467	0.1937	0.3404	5.2507

Table 5.14 Optimal solution validation of three PVDG units on feeder F2, avoiding RPF

No. of the iterations in the optimization procedure = 11 (+2 affirming iterations)								
	CP1 node	CP2 node	CP3 node	$PV1_{FOI}$ (MW)	$PV2_{FOI}$ (MW)	$PV3_{FOI}$ (MW)	Tot_PV_{FOI} (MW)	PL_{FOI} (MW)
Optimal	9	17	26	0.0852	0.115	0.176	0.3762	4.8581
Iterations without initial locations and feasible iterative steps = 3654								
Top 1	09	17	26	0.0852	0.1150	0.1760	0.3762	4.8581
Top 2	10	17	26	0.0762	0.1150	0.1760	0.3762	4.8622
Top 3	08	17	26	0.0943	0.1150	0.1760	0.3853	4.8705
Top 4	07	17	26	0.1033	0.1150	0.1760	0.3943	4.8852

The tables above show that the optimal solution resulting from the developed procedure exactly matches the 'Top 1' solution in both cases. The tables show also that the 'Top 1' solution is the best among 406 and 3654 possible solutions considering two and three PVDG units respectively.

The whole optimization procedure with two and three PVDG units has been repeated on feeder F1 specified earlier in Table A2.1. The same practice of checking every possible solution, without applying the feasible steps formula, has been applied. The validation results are stated below in Tables 5.15 and 5.16.

Table 5.15 Optimal solution validation of two PVDG units on feeder F1, avoiding RPF

No. of the iterations in the optimization procedure = 10 (+2 affirming iterations)						
	CP1 node	CP2 node	$PV1_{FOI}$ (MW)	$PV2_{FOI}$ (MW)	Tot_PV_{FOI} (MW)	PL_{FOI} (kW)
Optimal	5	10	0.4301	0.3439	0.774	5.3201
Iterations without initial locations and feasible iterative steps = 91						
Top 1	05	10	0.4301	0.3439	0.7740	5.3201
Top 2	05	11	0.5161	0.2579	0.7740	5.3643
Top 3	05	09	0.3441	0.4299	0.7740	5.3721
Top 4	06	10	0.3441	0.3439	0.6880	5.4184

Table 5.16 Optimal solution validation of three PVDG units on feeder F1, avoiding RPF

No. of the iterations in the optimization procedure = 8 (+2 affirming iterations)								
	CP1 node	CP2 node	CP3 node	$PV1_{FOI}$ (MW)	$PV2_{FOI}$ (MW)	$PV3_{FOI}$ (MW)	PVT_{FOI} (MW)	PL_{FOI} (kW)
Optimal	5	8	12	0.2581	0.3153	0.2006	0.774	5.0568
Iterations without initial locations and feasible iterative steps = 364								
Top 1	02	07	11	0.3733	0.3440	0.2579	0.9752	5.0345
Top 2	02	06	10	0.2873	0.3441	0.3439	0.9753	5.0517
Top 3	02	06	11	0.2873	0.4301	0.2579	0.9753	5.0542
Top 4	05	08	12	0.2581	0.3153	0.2006	0.7740	5.0568

Table 5.15 shows that the optimal solution, with two PVDG units, perfectly matches the 'Top 1' solution of the validation procedure. Also the PL_{FOI} of the optimal solution, with three PVDG units, matches the 'Top 4' solution (out of 364) of the validation procedure. It misses the 'Top 1' solution by 0.0223 kW, which corresponds to only 0.443%.

Comparing the benefits of single, couple and three PVDG units with RPF avoidance

The improvement in voltage profile due to the connection of single, couple and three PVDG units are compared by phase in Fig.5.27. On the other hand, Fig.5.28 depicts the line power loss (ΔPL_{FOl}) vs. the total size of the PVDG units (PV_{FOl}) for the same applications.

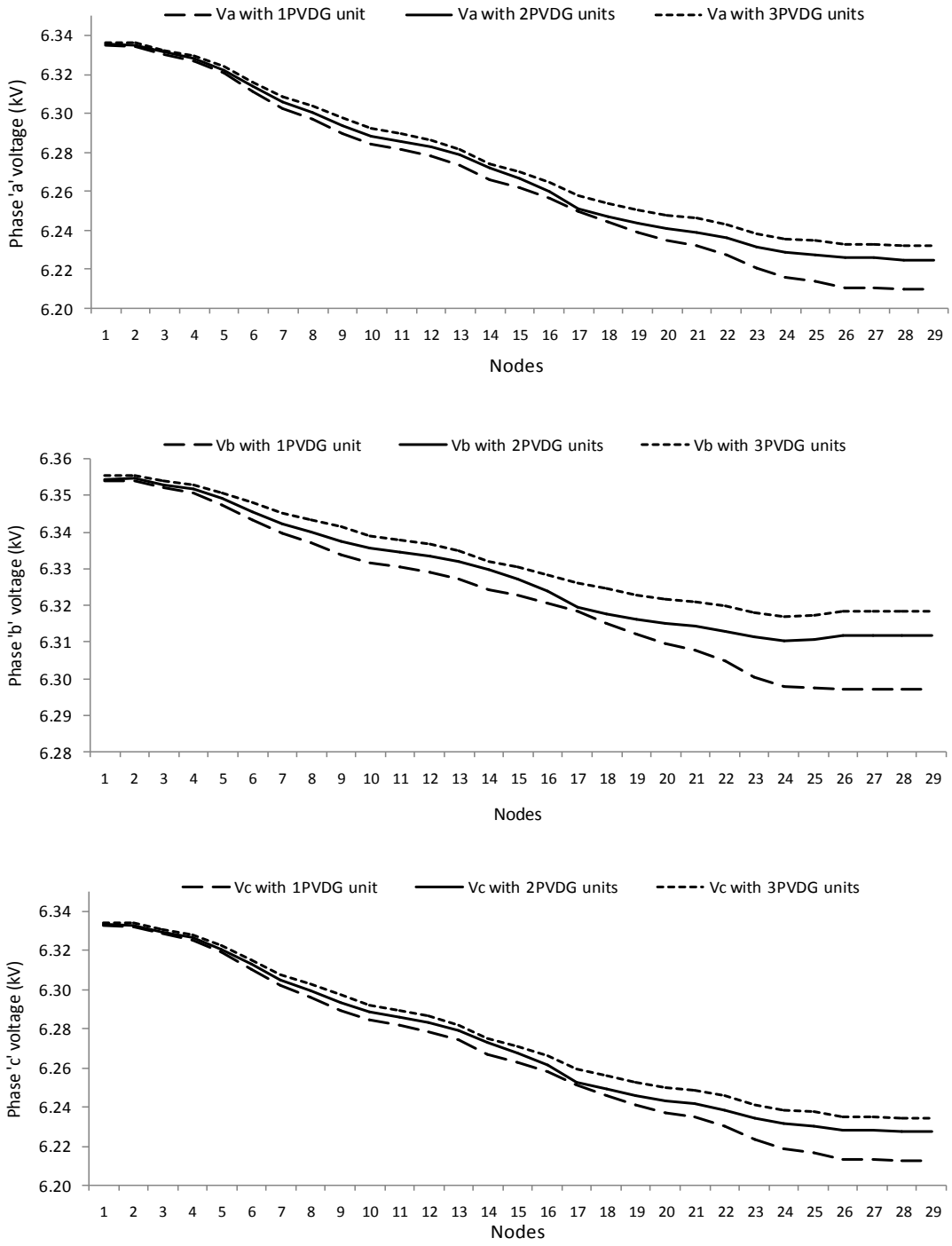

Figure 5.27 Comparing the voltage profile with single & multiple PVDG units, avoiding RPF

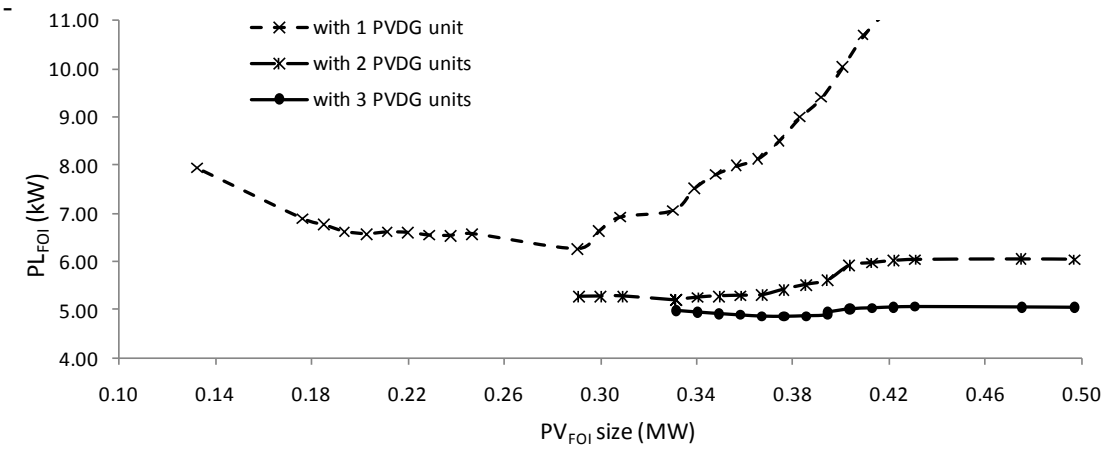

Figure 5.28 Comparing the PL_{FOI} with single and multiple PVDG units, avoiding RPF

Figures 5.27 & 5.28 show a preference for the scenario of three units over that of couple and single units. This is in terms of voltage profile improvement and line power loss reduction.

5.2 Optimization Procedure Allowing Reverse Power Flow

Some distribution networks are equipped with advanced protection and control systems that could be able to deal with reverse power flow (RPF) conditions. In such a case, setting the RPF as a constraint in the optimization process is no longer valid. The optimization procedure has been developed further to solve for the optimal sizing and location of PVDG unit(s) allowing RPF. However, the RPF is allowed to the extent that it does not reach the substation. This way, the voltage profile is deemed not to exceed the voltage level at the substation. Additionally, the current flow will thus comply with the ampacity of the feeder. Beside it avoids the crossing the substation transformer back to higher voltage level that may disturb the voltage regulation and protection devices.

5.2.1 Single PVDG unit on unbalanced 3-phase feeder allowing RPF

In order to continue the trend of previous sections, two optimization procedures are developed to deal with single and multiple PVDG units allowing RPF. This section is dedicated to the application of a single PVDG unit.

The optimization procedure

As in the previous sections of this work, the optimization procedure is solved for maximum line energy loss reduction (ΔEL). Hence, based on the derivations of Section 4.3.3, the optimization problem is solved for maximum line power loss reduction at the FOI (ΔPL_{FOI}).

On the other hand the optimization concept of this section is somehow different from those of previous sections. In the previous ones the PVDG unit was sized up to the amount of power flow, at the FOI, in the line section it is located at. Because of that, there was one specific size associated to each location. In the current case, however, the size is allowed to exceed the power flow at the location of the PVDG unit. This means that at certain location there will be several sizing possibilities; the matter that widens the domain of feasible solutions. The only limitation here is to avoid the substation from seeing the RPF, which still leaves the process with a lot of sizing possibilities. Figure 5.29 is drawn for better explanation.

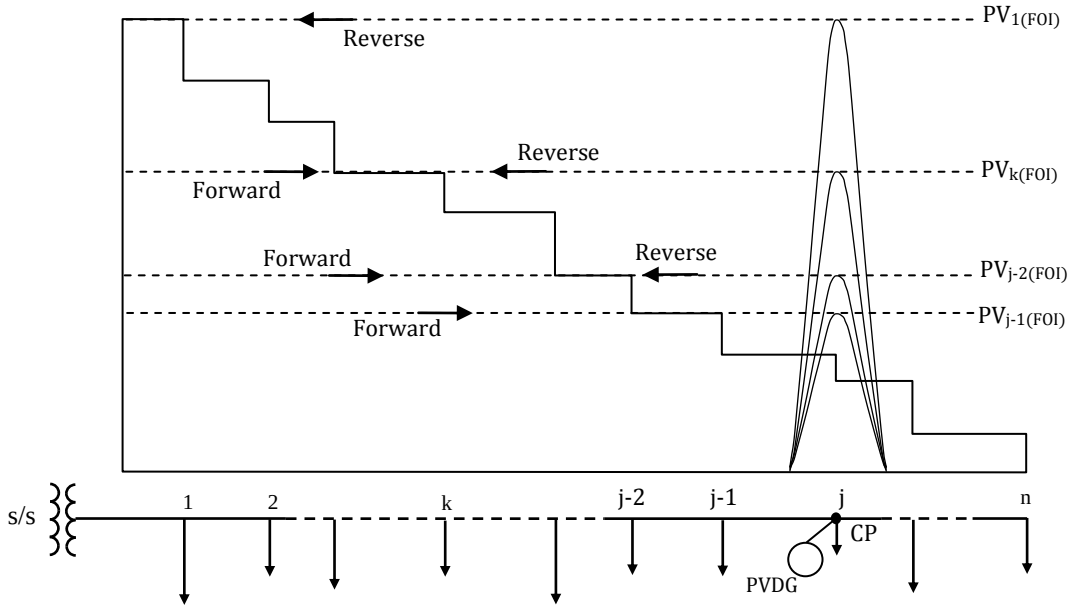

Figure 5.29 Alternatives of single PVDG unit sizing at CP node j with RPF allowance

Figure 5.29 illustrates that the PVDG unit at the CP node j has divided the power flow along the feeder to forward and reverse zones. The two zones meet together in points at which the RPF clears away.

Determining local optimal size for the PVDG unit

Running the optimization procedure with different sizes at each location will end up with a lengthy iteration process. Hence, a suitable method has been developed to determine the local optimal size at each PVDG location. To explain the method, assume that the PVDG unit in Fig.5.29 is set to $PV_{j\text{-}2(FOI)}$, which is equal to the power flow in line section j-2. Based on that, the PVDG production will be enough to serve the downstream nodes j to n in the forward direction. At the same time, there will be plenty of surplus production to send power in the reverse direction up to node j-2. In other words, the load demand of node j-2 is now flowing from node j back to node j-2 rather than from the substation to j-2. At this point, if the distance from j back to j-2 is shorter than from the substation up to j-2 then it is more feasible to serve node j-2 from

the PVDG unit. Otherwise, it is more feasible to reduce the size of the PVDG unit so that node j-2 is served by the substation.

In light of the above, assume node k is located at the midpoint between the substation and the CP node j. Hence, node k will be the last upstream node that is feasibly served from the PVDG unit rather than from the substation. This means that sizing the PVDG unit at node j equals to $PV_{k(FOI)}$ will give the preference to the PVDG unit over the substation to serve all the nodes from k to n. As a conclusion, the local optimal size of the PVDG unit at node j is $PV_{k\,(FOI)}$.
However, in practical cases the midpoint is likely to fall in-between two successive nodes. Consequently, the solution could be enhanced further by rounding the midpoint to the node that brings more benefits over the other.

The aforementioned concept of determining the actual midpoint and local PVDG size for certain location is expressed below in mathematical form based on Fig.5.30.

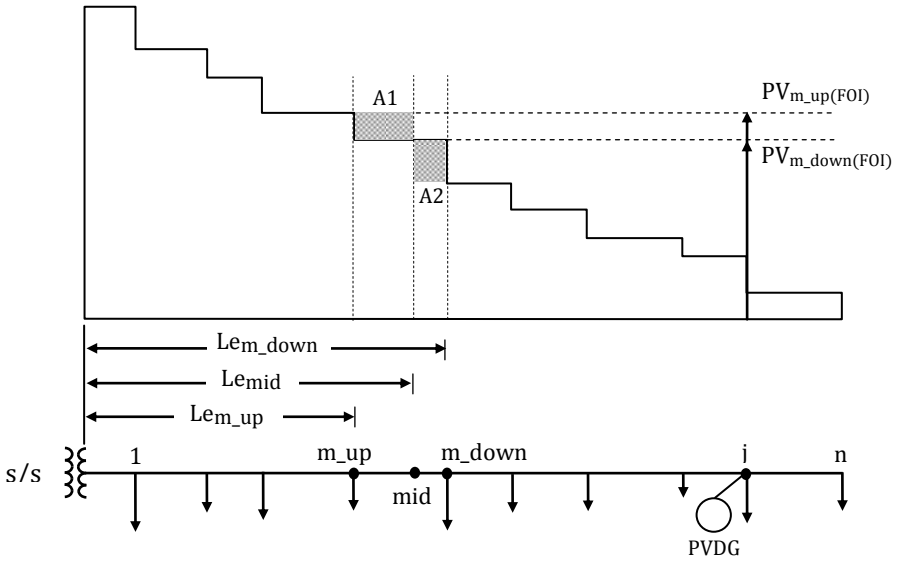

Figure 5.30 Local optimal size of single PVDG unit with RPF allowance

The midpoint 'mid' divides equally the length from the substation up to node j. As the line sections could be constructed from different wire sizes, the lengths are determined in terms of normalized lengths. Thus, the length form the s/s to 'mid' (Le_{mid}) is determined as follows:

$$Le_{mid} = 0.5 \times \sum_{k=1}^{j} Le_{k\_norm} \tag{5.32}$$

The nodes m_up and m_down are the nearest nodes on both sides of 'mid'. Hence, the lengths from the s/s to each of m_up (Le_{m_up}) and m_down (Le_{m_down}) are,

$$Le_{m\_up} = \sum_{k=1}^{m\_up} Le_{k\_norm} \quad \text{and} \quad Le_{m\_down} = \sum_{k=1}^{m\_down} Le_{k\_norm} \tag{5.33}$$

On one hand, if the PVDG unit is sized to $PV_{m\_down(FOI)}$ then the reverse power will reduce to zero at node m_down. Thus, the solution will miss the saving of power flow area A2 that to be served by the PVDG unit. On the other hand, if the PVDG unit is sized to $PV_{m\_up(FOI)}$ then the reverse power will continue to node m_up. In this case the power flow area A1 will be served by the PVDG unit, which is a loss that it would be more feasible to serve it from the substation.

Based on the above the actual midpoint node (mid_j), at which the PVDG unit connected to CP node j is cleared away, is determined as follows:

$$mid_j = \begin{Bmatrix} m\_up\,, \text{ if } A1 < A2 \\ \\ m\_down\,, \text{ if } A1 > A2 \end{Bmatrix} \tag{5.34}$$

To this end, the local optimal sizing of the PVDG unit connected at the CP node j is:

$$\left[PV_{j(FOI)}\right]_{abc} = \sum_{k=midj}^{n} \begin{bmatrix} LD^{b}_{k(FOI)} \\ LD^{b}_{k(FOI)} \\ LD^{b}_{k(FOI)} \end{bmatrix}^{P} \tag{5.35}$$

Where, midj - Actual midpoint of the CP node j,
$LD_{k(FOI)}$ - Load demand of node k at the FOI,
P - Real component of $LD_{k(FOI)}$,
b - Phase carrying the lowest power flow among the three phases,

In the same connection, the load demand at the CP node after the connection of the PVDG unit is then updated by applying Eq.5.20.

Application considering single PVDG unit

The developed procedure is applied on feeder F2 under unbalanced load conditions and considering winter load demand. The line impedance of the feeder is taken from the phase impedance matrix stated in Table 5.5. Also the load demand of nodes, phase voltage and current along the feeder are substituted from Tables 5.8, 5.9 and 5.10 respectively.

The steps of the optimization procedure are illustrated in the flowchart of Fig.5.31. The first four blocks in the flow chart are similar to the flowchart in Sections 5.1.2 and 5.1.3. Starting from there, the normalized length of line sections along the feeder are generated by applying Eq.5.22. The wire conductor resistance of line section 1, equals to 0.098 (Ω/km), is taken as the reference of the normalized lengths.

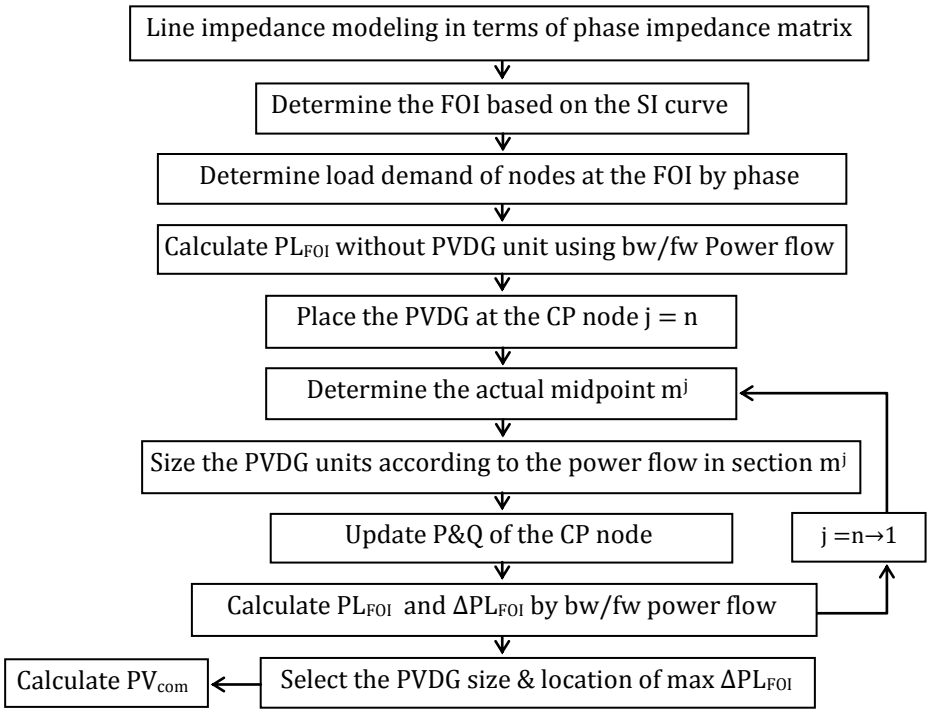

Figure 5.31 Optimization of single PVDG unit allowing RPF

The optimization procedure is then iterated, with the method of the first two iterations as follows:

Iteration1:

The process is commenced by locating the PVDG unit at the CP node n. The actual midpoint is then determined by applying Eq.5.34 and the PVDG unit is sized by using Eq.5.35.

The load demand of the CP node is updated by applying Eq.5.20. The resulting line power loss at the FOI (PL_{FOI}) is calculated by the means of backward/forward power flow then applying Eqs.5.17 and 5.18. It is worth mentioning that Eq.5.17 is arranged as follows to count the accumulated line losses along the feeder even with sections witnessing reverse current. Note to mention that the $|\bullet|$ is added to take positive voltage difference all the time.

$$\left[PL_{k(FOI)}\right]_{abc} = \left\{\left|\left[VP_{k-1(FOI)}\right]_{abc} - \left[VP_{k(FOI)}\right]_{abc}\right|\right\} \times [I_k]_{abc} \quad (5.36)$$

The results of the first iteration is stated in the table below

$CP^{(1)}$ node	mid_{29}	$PV_{FOI}^{(1)}$ size (MW)	$PL_{FOI}^{(1)}$(kW)	$\Delta PL_{FOI}^{(1)}$
29	13	0.3404	5.1462	59.60%

Iteration2:

The second iteration is commenced by moving the CP node back to node 28.

$CP^{(2)}$ node	mid_{28}	$PV_{FOI}^{(2)}$ size (MW)	$PL_{FOI}^{(2)}$(kW)	$\Delta PL_{FOI}^{(2)}$
28	13	0.3404	5.1447	59.62%

The CP and associated midpoint nodes over iterations are depicted in Fig.5.32, with the corresponding sizes of the PVDG unit is illustrated in Fig.5.33. Figure 5.34 shows the line power loss and line power loss reduction at the FOI (PL_{FOI} and ΔPL_{FOI}) at each iteration.

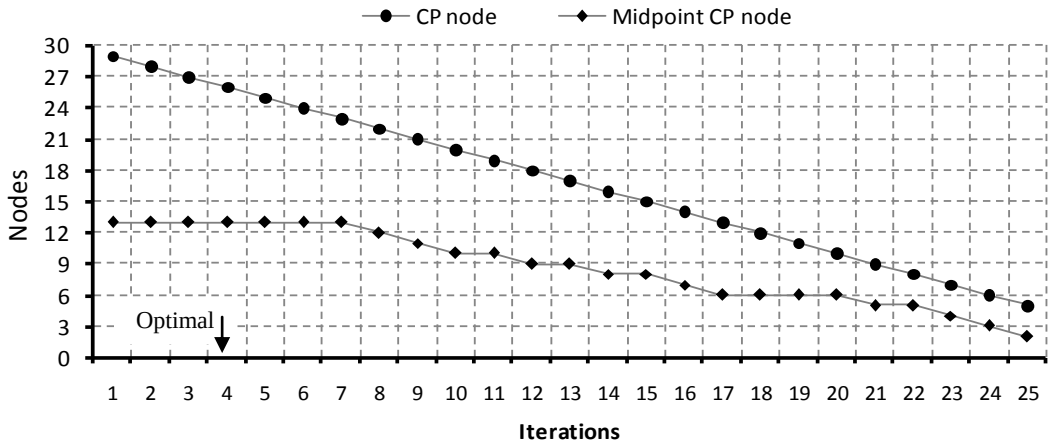

Figure 5.32 CP & mid nodes vs. iteration of single PVDG unit on feeder F2, allowing RPF

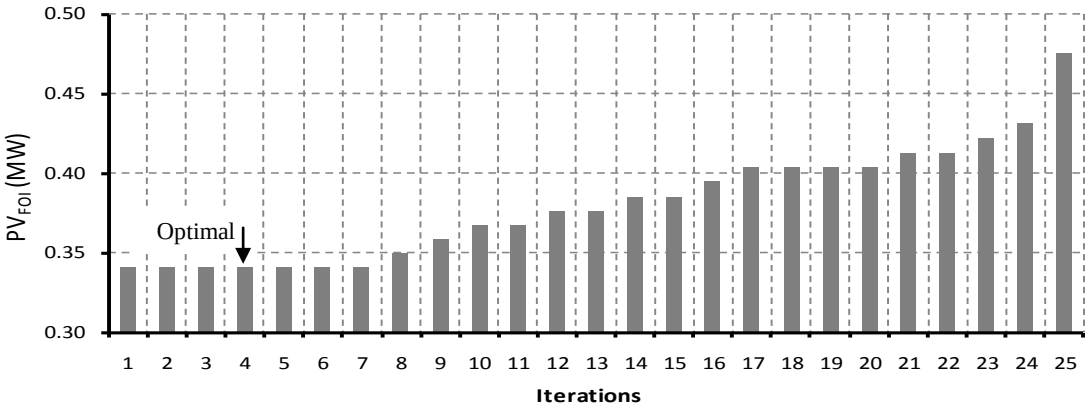

Figure 5.33 PV_{FOI} vs. iterations of single PVDG unit on feeder F2, allowing RPF

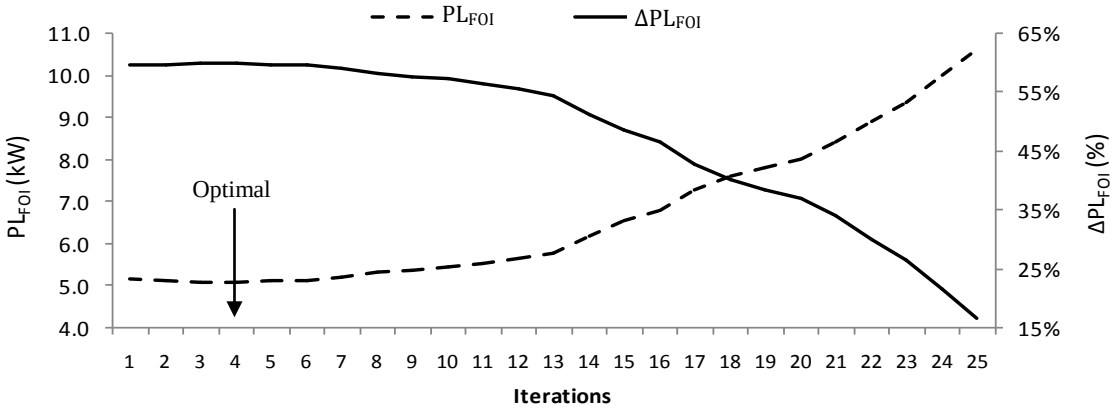

Figure 5.34 PL_{FOI} & ΔPL_{FOI} with single PVDG unit on feeder F2, allowing RPF

According to the Figs.5.32 to 5.34, the optimal solution is the one related to iteration 4. This has resulted in the maximum line power loss benefits at the FOI stated Table 5.17.

Table 5.17 Optimal solution with single PVDG unit on feeder F2 allowing RPF

Optimal CP node	Optimal midpoint node	Optimal PV_{FOI} (MW)	PL_{FOI} (kW)	ΔPL_{FOI}
26	13	0.3404	5.1009	59.964%

The resulting current flow profile by phase along feeder F2 at the optimal solution is represented below in Fig.5.35.

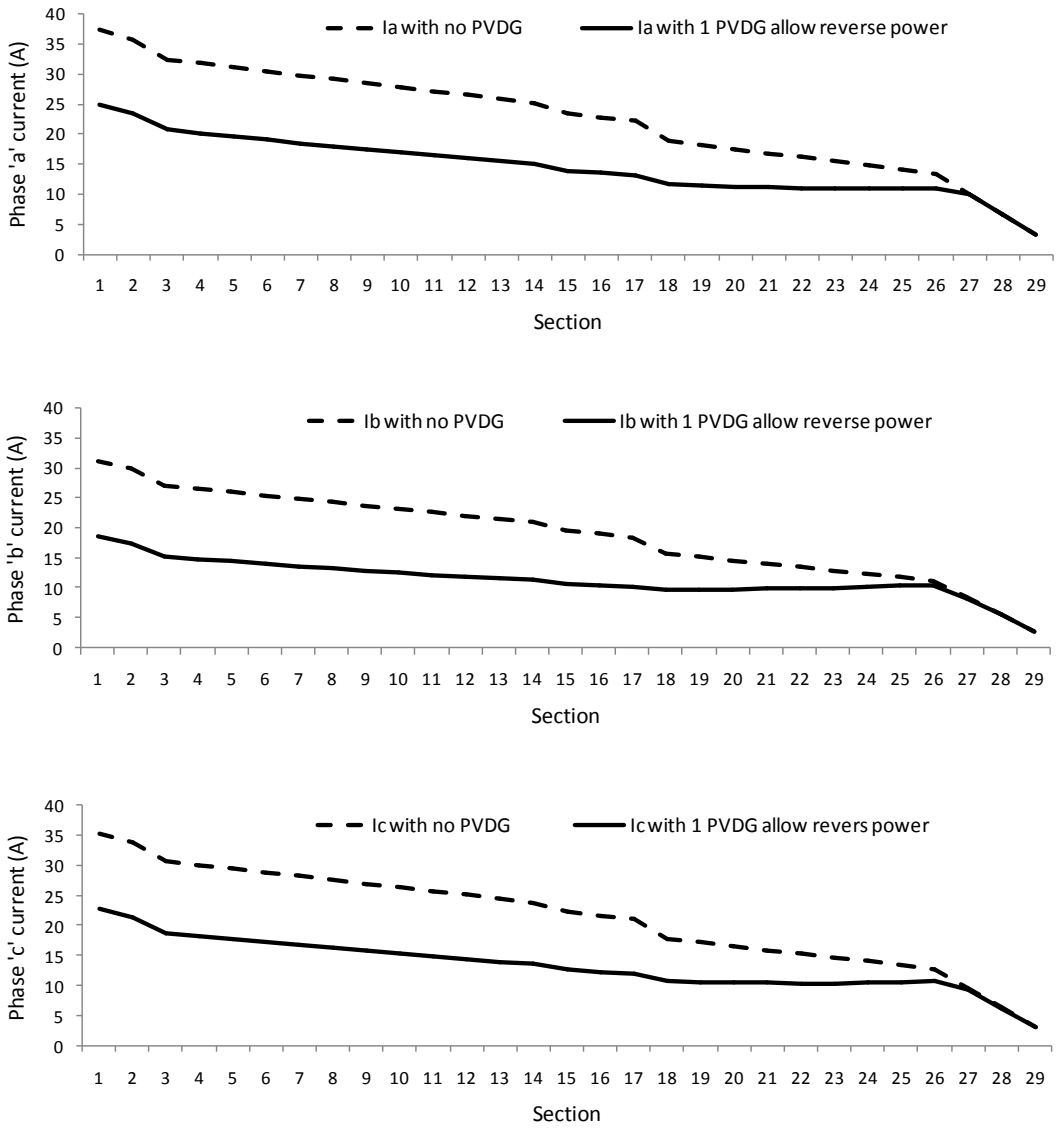

Figure 5.35 Feeder F2 current at the FOI with optimal single PVDG units, allowing RPF

Fig.5.35 shows that the PVDG unit reduces the current flow in the line sections between the substation and the CP node 26. However, it has insignificant effect on the current flow in the downstream sections after the CP node.

Additionally, the figure shows that the current of phase ‘b’ is affected by the PVDG unit to a greater level than the currents of phases ‘a’ and ‘c’. This is due to the fact that the original current flow of phase ‘b’ is the lowest in this case study, as was shown earlier in Table.5.10. The figure illustrates also that the current profile of phase ‘b’ increases in the downstream direction in line sections 19 to 26 due to the impact of RPF by the PVDG unit.

It is worth mentioning that the PVDG unit is set to work at unity power factor; so it mainly affects the real component of feeder current. However, the current flow in Fig.5.35 represents the apparent current including the real and reactive components. For this reason the figure does not show clearly the impact of the RPF.

The impact of the reverse current flow is illustrated clearly in Fig.5.36, which represents the real current profile of phase b along the feeder. The figure shows insignificant impact of the PVDG unit on the line sections after the CP node 26. However, the surplus production of the PVDG unit at the CP node has resulted in RPF from node 26 back to the midpoint node 13. At node 13 the reverse current falls to zero so the current in the line sections between the substation and node 13 flows in the forward direction.

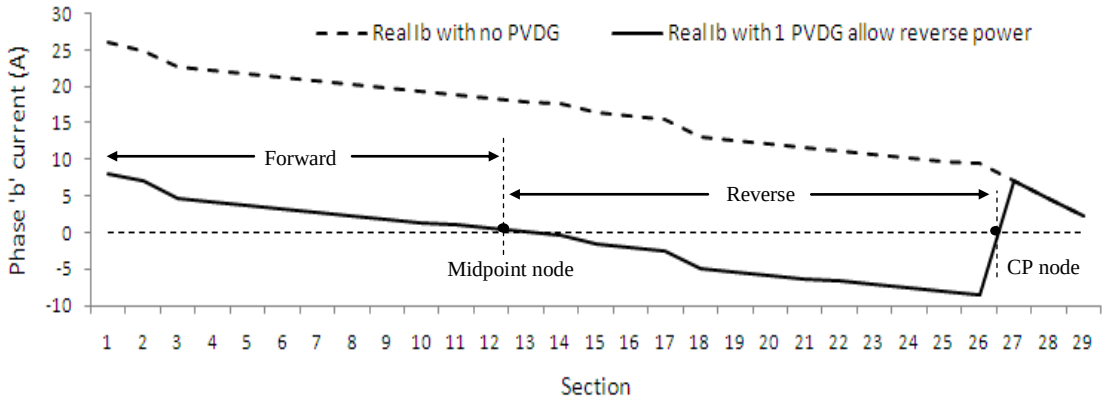

Figure 5.36 Feeder F2 real current at the FOI with optimal single PVDG unit allowing RPF

For the voltage profile, some line sections on the upstream side of the CP node show a slight decrease in voltage level due to the impact of RPF. The impact is shown more clearly on phase b that it carries lower current than the other phases in the case study. Nevertheless, the voltage level along the feeder is not anticipated to exceed the upper limit because the RPF is not allowed to reach the s/s. Figure 5.37 depicts the improvement in voltage profile along feeder F2 at the optimal solution.

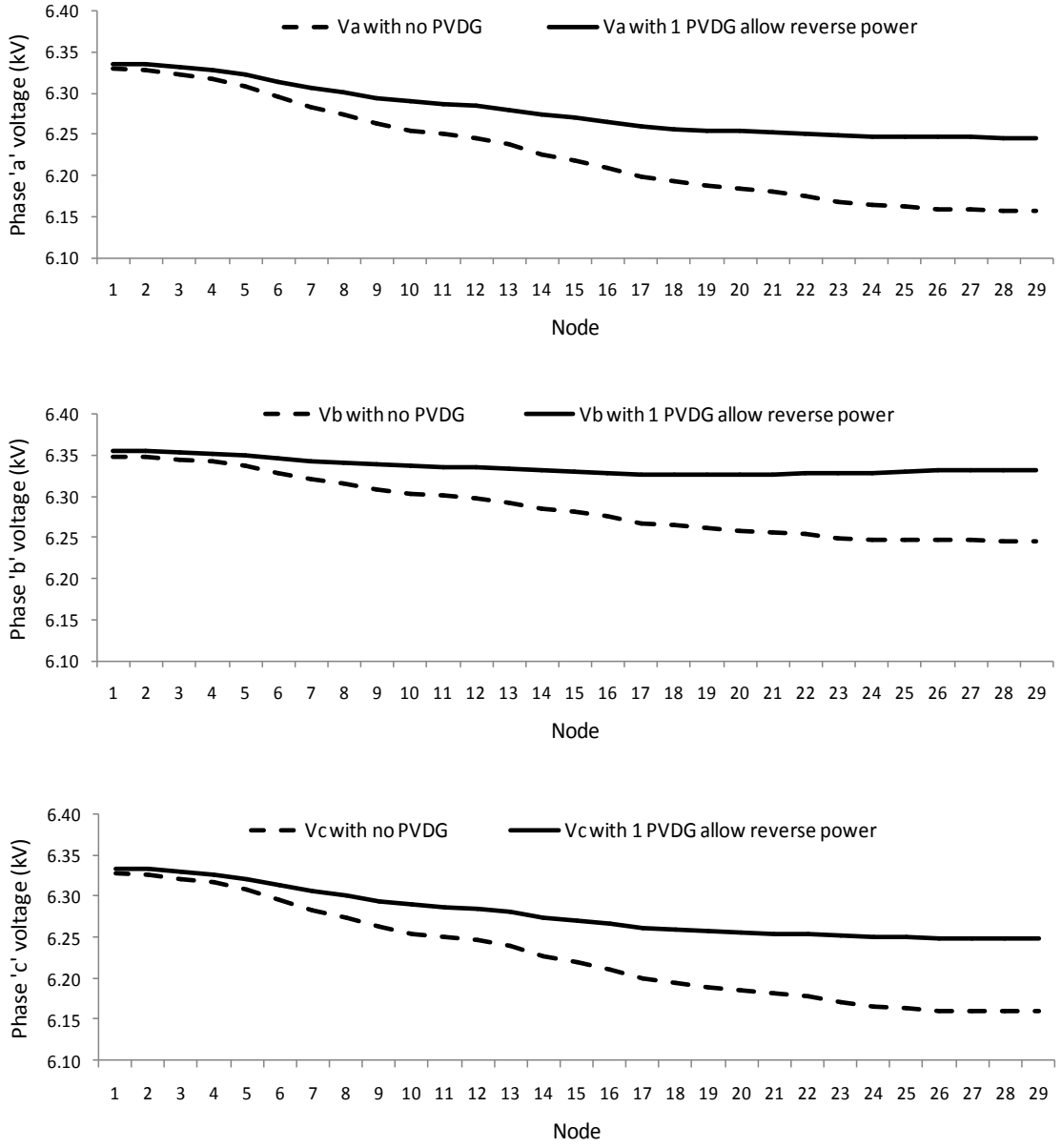

Figure 5.37 Feeder F2 phase voltage at the FOI with optimal single PVDG unit, allowing RPF

Validation of optimal solution

The credibility of the optimization procedure has been checked by modifying the MATLAB program to consider every possible solution on feeder F2. The program has been modified to iterate the calculations along the nodes of the feeder without applying the method of local optimal size. This means that the solution at CP node j is checked with j-1 possible sizes.

For more clarification assume that the optimization procedure is checking the solution at the CP node 29. Based on Fig.5.29, there will be 28 possible sizes related to the power flow in each line

section between the substation and the CP node. Moving to CP node 28 will end up with 27 possible sizes, and so on.

The program has been run on the above concept, and the top four solutions rank the lowest PL_{FOI} (or highest ΔPL_{FOI}) are recorded. The top four solutions are compared with the optimal solution from the optimization procedure, with the results are as stated below in Table 5.18.

Table 5.18 Optimal solution validation of single PVDG unit on feeder F2, allowing RPF

No. of the iterations in the optimization procedure = 4 (+2 affirming iterations)				
	CP node	Midpoint node	PV_{FOI} (MW)	PL_{FOI} (kW)
Optimal	26	13	0.3404	5.1009
Iterations without optimal local size method = 756				
Top 1	26	12	0.3439	5.1004
Top 2	27	12	0.3439	5.1008
Top 3	26	13	0.3404	5.1009
Top 4	27	13	0.3404	5.1012

The whole optimization procedure has been repeated on feeder F1 specified in Table A2.1. The same practice of checking every possible solution, without applying the local optimal size method, has been applied. The validation results are stated in Tables 5.19.

Table 5.19 Optimal solution validation of single PVDG unit on feeder F1, allowing RPF

No. of the iterations in the optimization procedure = 6 (+2 affirming iterations)				
	CP node	Midpoint node	PV_{FOI} (MW)	PL_{FOI} (kW)
Optimal	9	4	0.8031	5.3285
Iterations with optimal local size method = 156				
Top 1	9	4	0.8031	5.3285
Top 2	9	3	0.8893	5.3401
Top 3	9	5	0.7740	5.3492
Top 4	8	3	0.8893	5.3643

The validation results show the potential of the optimization procedure. Regarding feeder F2, the procedure matched the 'Top 3' solution in 6 iterations out of 756 possible iterations. As for feeder F1, the developed procedure matched the 'Top 1' solution in 8 iterations out of 156 possible ones.

5.2.2 Multiple PVDG unit on unbalanced 3-phase feeder allowing RPF

Consideration of multiple PVDG units complicates the optimization procedure in that it significantly increases the number of location possibilities. Thus, incorporation of suitable

methods determining initial CP nodes (ini_CP) along with feasible iterative steps over iterations is essentially required.

The optimization procedure

Installation of multiple PVDG units on the same feeder will result in hundreds and even thousands of possible PVDG locations. Thus, it is deemed infeasible to iterate the optimization procedure in the same way as for a single PVDG unit. In this course, a suitable method to determine an initial feasible location for the PVDG units has been developed. The optimization procedure commences at these locations, and then is iterated consecutively at new locations in the upstream direction until the optimal solution is realized. Hence, one more method has been developed in this section determining feasible new locations over the iteration process.

Determination of initial feasible locations

The method of Section 5.1.3 associated with multiple PVDG units avoiding RPF can be modified and applied in this section. The actual feeder is normalized to one wire size by applying Eq.5.22. An equivalent uniformly distributed feeder of length Leq is then modeled by applying Eqs.5.23 & 5.24 resulting in the same power flow profile of Fig.5.15. Assuming two PVDG units providing power in both directions, Fig.5.38 is drawn to illustrate the resulting power flow profile.

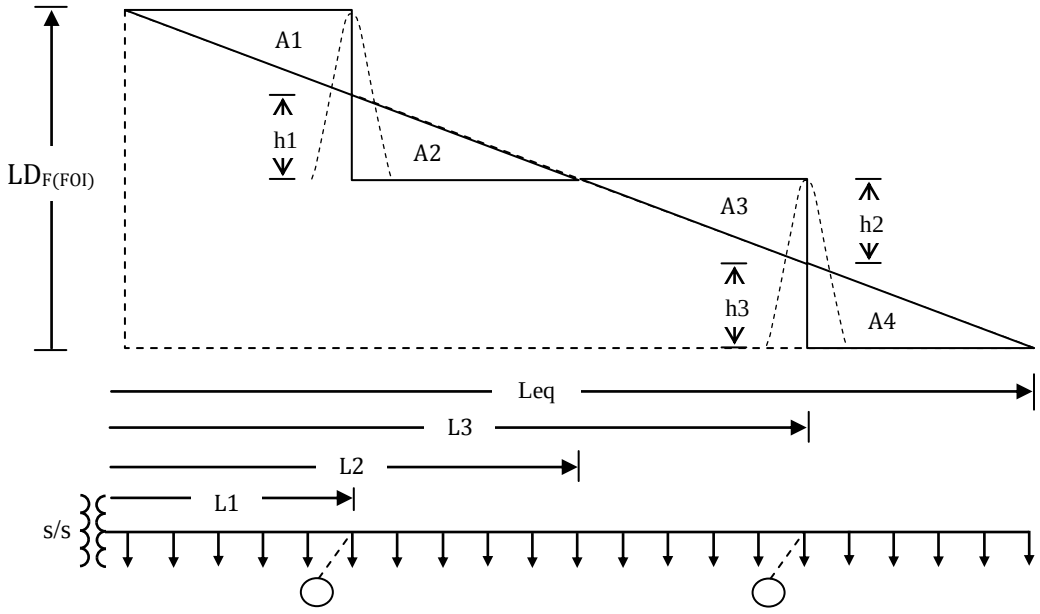

Figure 5.38 Power flow profile of uniform feeder with two PVDG units allowing RPF

The minimum total power flow along the feeder is realized when the total power flow area (A) is minimum. Hence,

$$A = A1 + A2 + A3 + A4 \tag{5.37}$$

Where,

$$A1 = 0.5 \times \left(LD_{F(FOI)} - h1 - h2 - h3\right) \times L1 \tag{5.38.a}$$

$$A2 = 0.5 \cdot h1 \cdot (L2 - L1) \tag{5.38.b}$$

$$A3 = 0.5 \cdot h2 \cdot (L3 - L2) \tag{5.38.c}$$

$$A4 = 0.5 \cdot h3 \cdot (Leq - L3) \tag{5.38.d}$$

Minimum 'A' can be realized by taking its first derivative with respect to each of h1, h2 and h3 equals to zero as follows:

$$\frac{dA}{dh1} = 0 \rightarrow 0.5 \times (-L1 + L2 - L1) = 0$$

$$\therefore L2 = 2\,L1 \tag{5.39.a}$$

$$\frac{dA}{dh2} = 0 \rightarrow 0.5 \times (-L1 + L3 - L2) = 0$$

$$\therefore L3 = L1 + L2 = 3L1 \tag{5.39.b}$$

$$\frac{dA}{dh3} = 0 \rightarrow 0.5 \times (-L1 + Leq - L3) = 0$$

$$\therefore Leq = L1 + L3 = 4L1 \tag{5.39.c}$$

Equation 5.39 shows that the two PVDG units divide the 'Leq' into four equal parts that each one them equals the length span L1. In general form, the length span (Leq_{span}) on the equivalent uniform feeder with 'x' PVDG units is expressed as follows:

$$Leq_{span} = \frac{Leq}{2x} \tag{5.40}$$

Consequently, the initial feasible locations (ini_CP) and midpoints on the equivalent uniform feeder are determined by certain multiples of Leq_{span}. For example, the ini_CP1 and ini_CP2 in Fig.5.38 are located at $1\times Leq_{span}$ and $3\times Leq_{span}$ respectively.

The initial locations are then returned to their counterpart ini_CP nodes on the normalized feeder by applying certain formula. However, it is known that the equivalent uniform feeder is modeled by approximation, so the ini_CP locations could return inaccurate ini_CP nodes on the normalized feeder. To this end, if the ini_CP node is located on the downstream side of the

actual optimal locations then there will be no problem. The reason is that the optimization process is set to move in the upstream direction so the optimal location will be found. On the contrary, if it happened that the ini_CP node is located on the upstream side of the actual optimal location, even by one node, the optimization procedure will miss it.

Based on the above, the optimization results can be enhanced further by shifting the initial locations, to some extent, in the downstream direction. In this work, the ini_CP locations on the uniform feeder are shifted by one $\mathrm{Leq_{span}}$ as follows:

$$\mathrm{Leq\_CPj} = 2\mathrm{j} \times \mathrm{Leq_{span}} \qquad (5.41.\mathrm{a})$$

Where Leq_CPj is the length on the equivalent uniform feeder at which the $\mathrm{j^{th}}$ PVDG unit is located.

The Leq_CPj is returned to its equivalent node on the normalized feeder by solving the following formula for the node Nj,

$$\sum_{\mathrm{k=1}}^{\mathrm{N_{CPj}}} \mathrm{Le_{k\_norm}} \cong \mathrm{Leq\_CPj} \times \frac{\mathrm{L_{norm}}}{\mathrm{Leq}} \qquad (5.42.\mathrm{a})$$

Then,

$$\mathrm{ini\_CPj} = \mathrm{N_{CPj}}\Big|_{\mathrm{j=1:x}} \qquad (5.42.\mathrm{b})$$

Where,

L_{norm} - Length of the normalized feeder,

N_{CPj} - Best node realizing Eq.5.42.a, at which the CPj is located,

x - Number of installed PVDG units,

Feasible PVDG sizing at the initial locations

In Section 5.2.1 a suitable method has been developed to determine the initial optimal size at each PVDG location. The method has ended up sizing the PVDG unit to the amount of power flow associated with optimal midpoint between the substation and the CP node.

The same concept can be applied in determining the size of the multiple PVDG units at their initial locations. Assume two PVDG units result in two midpoints as shown in Fig.5.39. The same concept can be applied on any number of PVDG units. The downstream midpoint (mid2) mediates the length between the nodes CP1 and CP2. Similarly, the upstream midpoint (mid1)

mediates the length between the substation and CP1. If any of the two midpoints falls between two nodes then it will be rounded to the one that brings more line power loss saving.

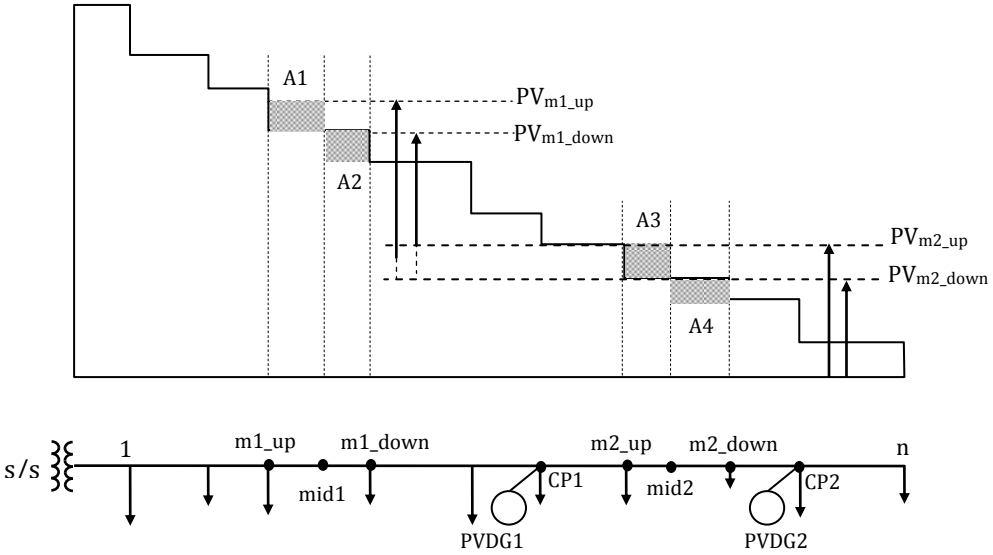

Figure 5.39 Mid nodes associated with the ini_CP nodes of two PVDG units, allowing RPF

Based on the above, the length from the s/s to mid1 (Le_{mid1}) on the normalized feeder is determined as follows:

$$Le_{mid1} = 0.5 \times \sum_{k=1}^{CP1} Le_{k\_norm} \tag{5.43}$$

Then, the length from the s/s to mid2 (Le_{mid2}) is

$$Le_{mid2} = Le_{CP1} + 0.5 \times \sum_{k=CP1+1}^{CP2} Le_{k\_norm} \tag{5.44}$$

The nodes m1_up & m1_down and m2_up & m2_down are the nearest nodes on both sides of mid1 and mid2 respectively. Then,

$$Le_{m1\_up} = \sum_{k=1}^{m1\_up} Le_{k\_norm} \quad \text{and} \quad Le_{m1\_down} = \sum_{k=1}^{m1\_down} Le_{k\_norm} \tag{5.45}$$

And,

$$Le_{m2\_up} = \sum_{k=1}^{m2\_up} Le_{k\_norm} \quad \text{and} \quad Le_{m2\_down} = \sum_{k=1}^{m2\_down} Le_{k\_norm} \tag{5.46}$$

Consequently, each midpoint is rounded to the nearest upstream or downstream node based on the fact that each one of them brings a greater power flow reduction. Hence, the midpoints associated with the CP nodes (ini_mid1 & ini_mid2) are rounded as follows:

$$\text{ini\_mid1} = \left\{ \begin{array}{l} \text{m1}_{\text{up}},\ \text{if A1} < \text{A2} \\ \\ \text{m1}_{\text{down}},\ \text{if A1} > \text{A2} \end{array} \right\} \tag{5.47.a}$$

$$\text{ini\_mid2} = \left\{ \begin{array}{l} \text{m2\_up},\ \text{if A3} < \text{A4} \\ \\ \text{m2\_down},\ \text{if A3} > \text{A4} \end{array} \right\} \tag{5.47.b}$$

Where A1- A4 represents the loss area in power flow reduction associated with the relevant alternatives of midpoint rounding.

In general form, the size of the PVDG unit is determined based on the power flow at the midpoint node associated to its location. Hence, the size of j^{th} PVDG unit out of '×' units on the feeder is expressed as follows:

$$\left[\text{PV}_{\text{CPj(FOI)}}\right]_{\text{abc}} = \sum_{\text{k=midj}}^{\text{n}} \begin{bmatrix} \text{LD}^{\text{b}}_{\text{k(FOI)}} \\ \text{LD}^{\text{b}}_{\text{k(FOI)}} \\ \text{LD}^{\text{b}}_{\text{k(FOI)}} \end{bmatrix}^{\text{P}} - \sum_{\text{u=CP(j+1)}}^{\times} \left[\text{PV}_{\text{u(FOI)}}\right]_{\text{abc}} \tag{5.48}$$

Where

CPj	- Coupling point node at which the j^{th} PVDG unit is located,
$\text{PV}_{\text{CPj(FOI)}}$	- Peak of the ac PVDG production curve of j^{th} PVDG unit,
midj	- midpoint of the j^{th} PVDG units,
b	- Phase carrying the lowest power flow among the three phases,
$\text{LD}^{\text{b}}_{\text{k(FOI)}}$	- Phase b load demand of node k at the FOI,
P	- Real power component,
x	- Number of multiple PVDG units,
u	- Index of the PVDG units on the downstream side of CPj,

Determining feasible iterative steps over iterations:

Running the iteration process with multiple PVDG units the same way as with single PVDG units will require thousands of iterations. Hence, a suitable formula that can reduce the number of iterative steps considerably has been developed. The formula checks the possible moving steps of the multiple units in the upstream direction and then selects the more appropriate one.

Assuming two PVDG units; the stepping possibilities (Poss) over iterations are taken below starting from the initial CP nodes and their associated midpoint nodes. Note to mention that the superscripts at the symbols define the iteration number.

Table 5.20 Determining feasible iterative steps with two PVDG units allowing RPF

		Iteration 1		
Poss.1	$CP1^{(1)} = ini\_CP1$	$mid1^{(1)} = ini\_mid1$	$CP2^{(1)} = ini\_CP2$	$mid2^{(1)} = ini\_mid2$
		Iteration 2		
Poss.1	$CP1^{(2)} = CP1^{(1)}$	$mid1^{(2)} = mid1^{(1)}$	$CP2^{(2)} = CP2^{(1)} - 1$	$mid2^{(1)} = mid2^{(1)}$
Poss.2	$CP1^{(2)} = CP1^{(1)}$	$mid1^{(2)} = mid1^{(1)}$	$CP2^{(2)} = CP2^{(1)}$	$mid2^{(1)} = mid2^{(1)} - 1$
Poss.3	$CP1^{(2)} = CP1^{(1)} - 1$	$mid1^{(2)} = mid1^{(1)}$	$CP2^{(2)} = CP2^{(1)}$	$mid2^{(1)} = mid2^{(1)}$
Poss.4	$CP1^{(2)} = CP1^{(1)}$	$mid1^{(2)} = mid1^{(1)} - 1$	$CP2^{(2)} = CP2^{(1)}$	$mid2^{(1)} = mid2^{(1)}$
		Iteration 3		
Poss.1	$CP1^{(3)} = CP1^{(2)}$	$mid1^{(3)} = mid1^{(2)}$	$CP2^{(3)} = CP2^{(2)} - 1$	$mid2^{(3)} = mid2^{(2)}$
Poss.2	$CP1^{(3)} = CP1^{(2)}$	$mid1^{(3)} = mid1^{(2)}$	$CP2^{(3)} = CP2^{(2)}$	$mid2^{(3)} = mid2^{(2)} - 1$
Poss.3	$CP1^{(3)} = CP1^{(2)} - 1$	$mid1^{(3)} = mid1^{(2)}$	$CP2^{(3)} = CP2^{(2)}$	$mid2^{(3)} = mid2^{(2)}$
Poss.4	$CP1^{(3)} = CP1^{(2)}$	$mid1^{(3)} = mid1^{(2)} - 1$	$CP2^{(3)} = CP2^{(2)}$	$mid2^{(3)} = mid2^{(2)}$
	⋮	⋮	⋮	⋮
	⋮	⋮	⋮	⋮
		Iteration t		
Poss.1	$CP1^{(t)} = CP1^{(t-1)}$	$mid1^{(t)} = mid1^{(t-1)}$	$CP2^{(t)} = CP2^{(t-1)} - 1$	$mid2^{(t)} = mid2^{(t-1)}$
Poss.2	$CP1^{(t)} = CP1^{(t-1)}$	$mid1^{(t)} = mid1^{(t-1)}$	$CP2^{(t)} = CP2^{(t-1)}$	$mid2^{(t)} = mid2^{(t-1)} - 1$
Poss.3	$CP1^{(t)} = CP1^{(t-1)} - 1$	$mid1^{(t)} = mid1^{(t-1)}$	$CP2^{(t)} = CP2^{(t-1)}$	$mid2^{(t)} = mid2^{(t-1)}$
Poss.4	$CP1^{(t)} = CP1^{(t-1)}$	$mid1^{(t)} = mid1^{(t-1)} - 1$	$CP2^{(t)} = CP2^{(t-1)}$	$mid2^{(t)} = mid2^{(t-1)}$

Considering that the iteration process is set to move in the upstream direction, there is a possibility of moving each of the two CP nodes individually by one node in the upstream direction. For better results, however, two similar possibilities have been added for the locations of the associated midpoint nodes. Thus, the process has ended up at four possibilities per iteration.

To illustrate the above concept, the possibilities at iteration ‘t’ are illustrated in Fig.5.40. The first and second possibilities are represented in the figure, whereas the third and fourth show a similar pattern to the previous ones respectively. Each of the possibilities realizes a saving by compensating part of the original power flow area but also introduces loss by adding certain amount of RPF. The striped areas represent the saving (S) while the shaded areas represent the loss (L) in power flow area. Thus, net compensated power flow area is determined by subtracting loss area from the saving area.

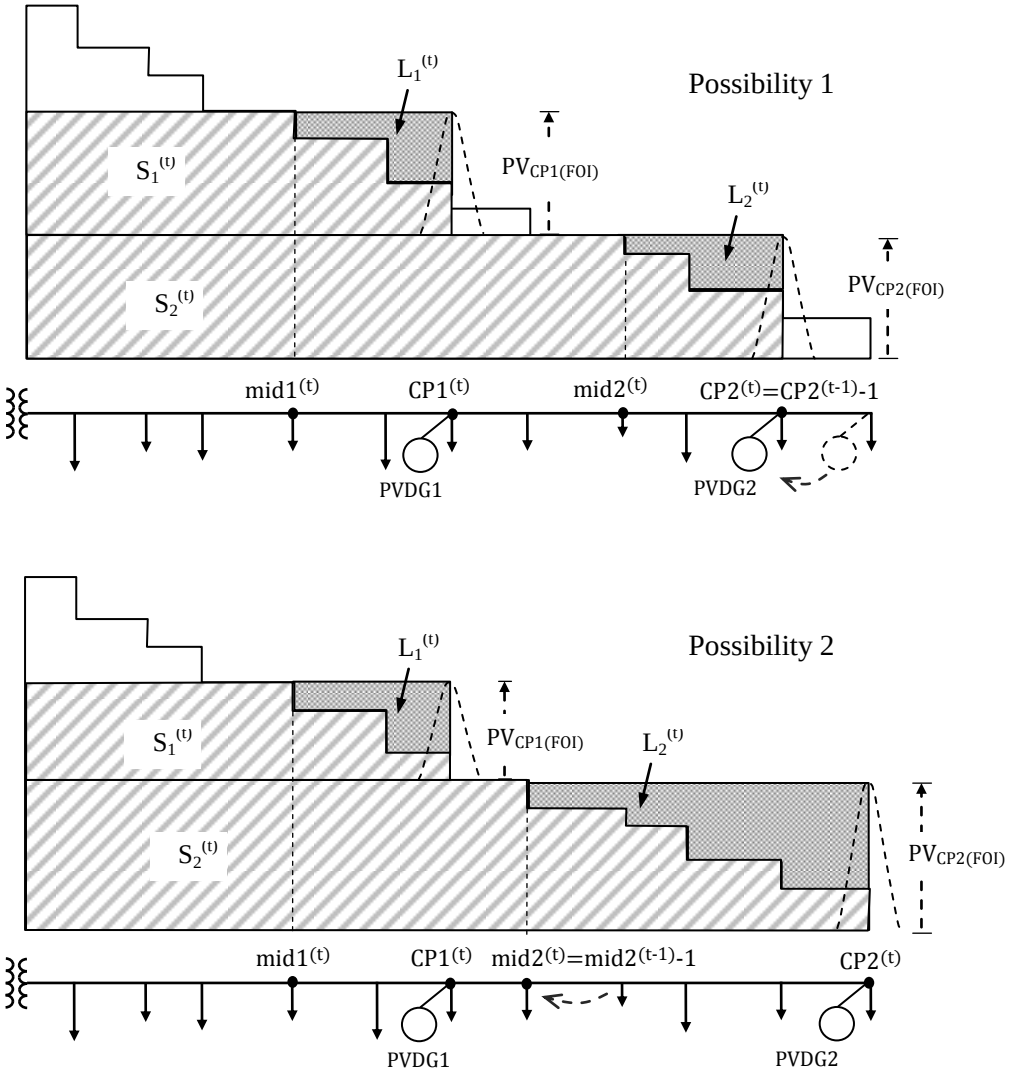

Figure 5.40 Possible steps of two PVDG units at iteration t with RPF allowance

According to Fig.5.40, the PVDG units are sized according to the amount of power flow, at the FOI, in the line sections of their associated midpoints. Hence, Eq.5.49 is applied to calculate the net compensated power flow area related to any of the relevant possibilities.

$$A_{Poss}^{(t)} = \left(S_1^{(t)} + S_2^{(t)}\right) - \left(L_1^{(t)} + L_2^{(t)}\right) \tag{5.49}$$

Where; $A_{Poss}^{(t)}$ - Net compensated power flow area with any of the relevant possibilities.

The amount of power flow is directly proportional to the amount of line power loss reduction. Therefore, the higher the compensated power flow area the lower is the resulting power flow and the higher is the ΔPL_{FOI}. To this end, the feasible CP and midpoint nodes for iteration t are taken from the possibility resulting in maximum net compensated power flow area.

Determination of initial locations and midpoints along with the application of the feasible iterative steps method will reduce significantly the number of iterations. The following case study conducted on feeder F2 shows an actual indication on that.

Application considering two PVDG units

The developed procedure is applied on feeder F2 under unbalanced load conditions and considering winter load demand. The line impedance of the feeder is taken from the phase impedance matrix stated in Table 5.5. Also the load demand of nodes, phase voltage and current along the feeder are substituted from Tables 5.8, 5.9 and 5.10 respectively. The steps of the optimization procedure are illustrated in the flowchart of Fig.5.41.

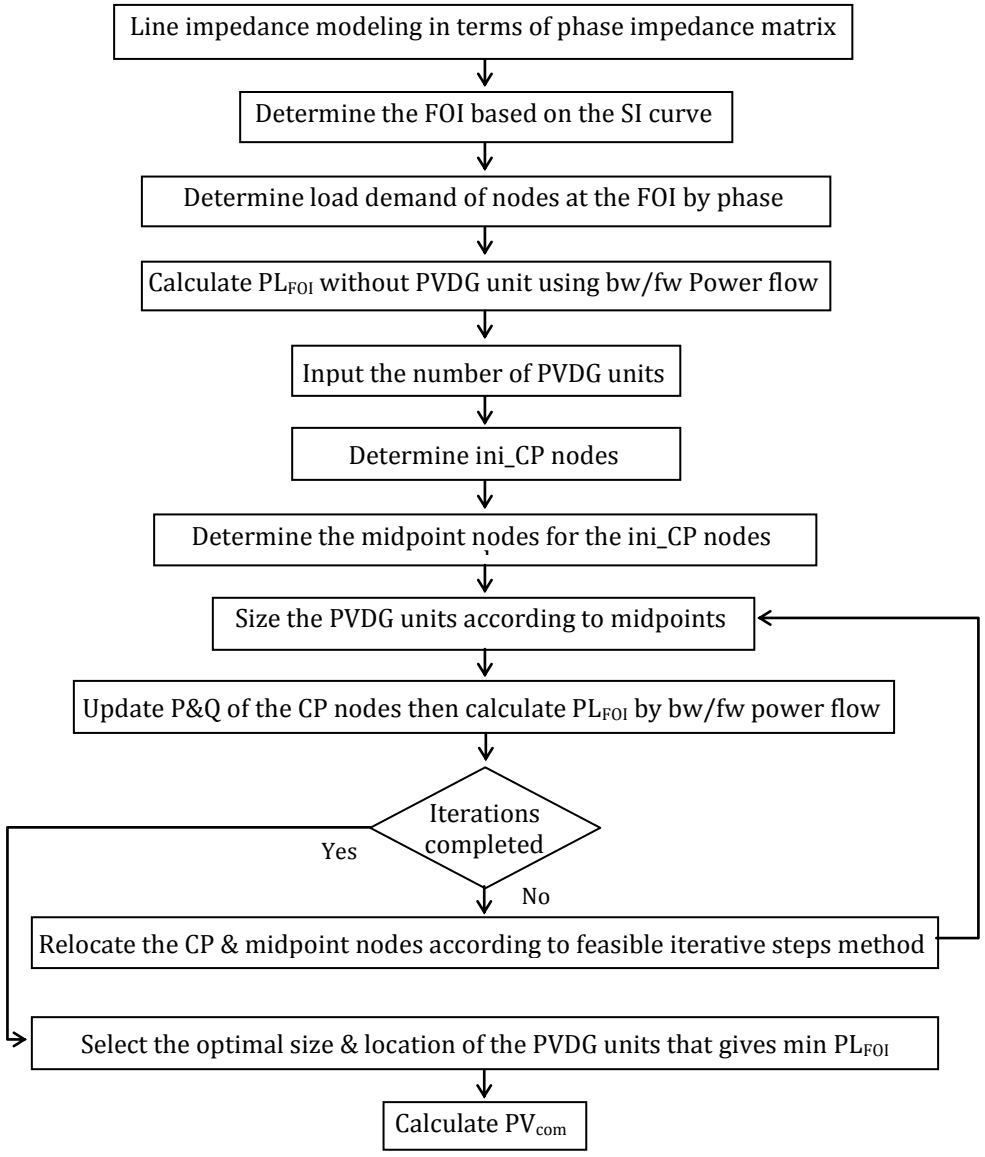

Figure 5.41 Optimization of multiple PVDG units with RPF allowance

The calculations of the first four blocks are conducted the same way as in the previous procedures. The ini_CP nodes and associated midpoint nodes are then determined by applying Eqs.5.42 to 5.47, which yields:

ini_CP1	ini_mid1	ini_CP2	ini_mid2
14	7	29	19

The optimization procedure is then iterated with the results of the first two iterations as follows:

Iteration1:

The initial locations for the CP nodes and their associated midpoints are applied and then sized according to their locations by applying Eq.5.48. The load demands of the CP nodes are then updated by applying Eq.5.20. The resulting line power loss at the FOI (PL_{FOI}) is calculated by the means of backward/forward power flow then applying Eqs.5.36 and 5.18. The results of iteration 1 are as tabulated below.

$CP1^{(1)}$	$mid1^{(1)}$	$PV1_{FOI}^{(1)}$	$CP2^{(1)}$	$mid2^{(1)}$	$PV2_{FOI}^{(1)}$	$PL_{FOI}^{(1)}$	$\Delta PL_{FOI}^{(1)}$
14	7	0.1563MW	29	19	0.2380MW	4.7554kW	62.67%

Iteration2:

The locations of the CP and midpoint nodes are updated according to the feasible iterative steps method. The resulting line power loss at the FOI (PL_{FOI}) is the then calculated. Below are the results by the end of iteration 2.

$CP1^{(2)}$	$mid1^{(2)}$	$PV1_{FOI}^{(2)}$	$CP2^{(2)}$	$mid2^{(2)}$	$PV2_{FOI}^{(2)}$	$PL_{FOI}^{(2)}$	$\Delta PL_{FOI}^{(2)}$
14	6	0.1655MW	29	19	0.2380MW	4.7417kW	62.78%

The CP and associated midpoint nodes over the whole iteration process are depicted in Fig.5.42. The corresponding sizes of the PVDG unit are illustrated in Fig.5.43, while the resulting PL_{FOI} and ΔPL_{FOI} are represented in Figure 5.44.

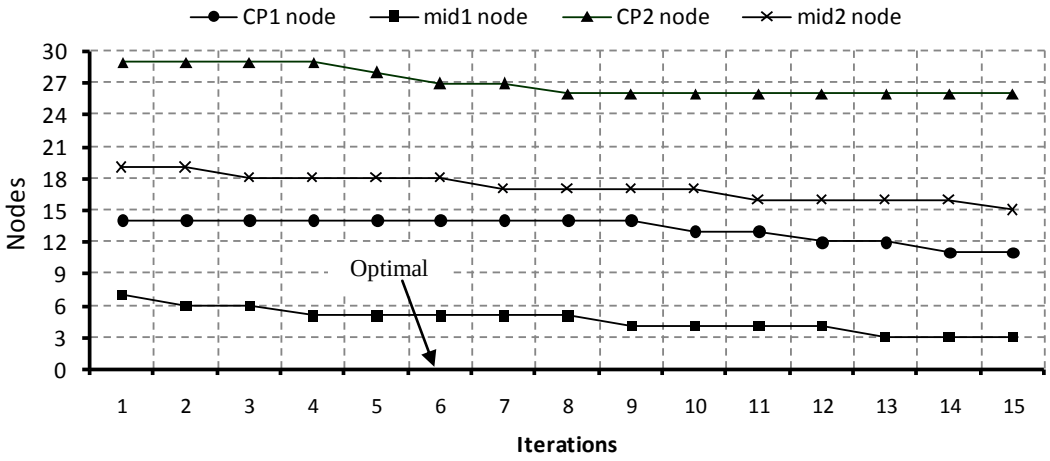

Figure 5.42 CP & mid nodes vs. iteration of two PVDG nits on feeder F2 over iterations

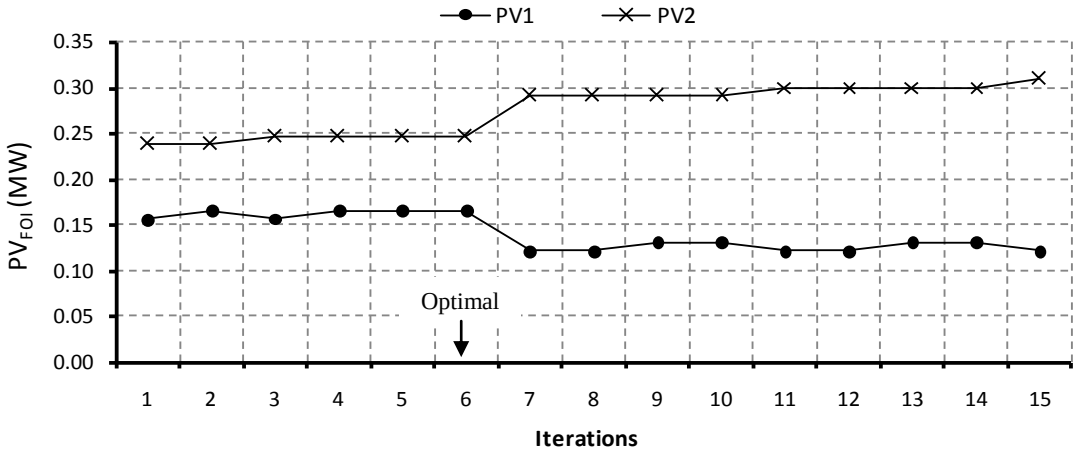

Figure 5.43 PV_{FOI} vs. iterations of two PVDG unit on feeder F2, allowing RPF

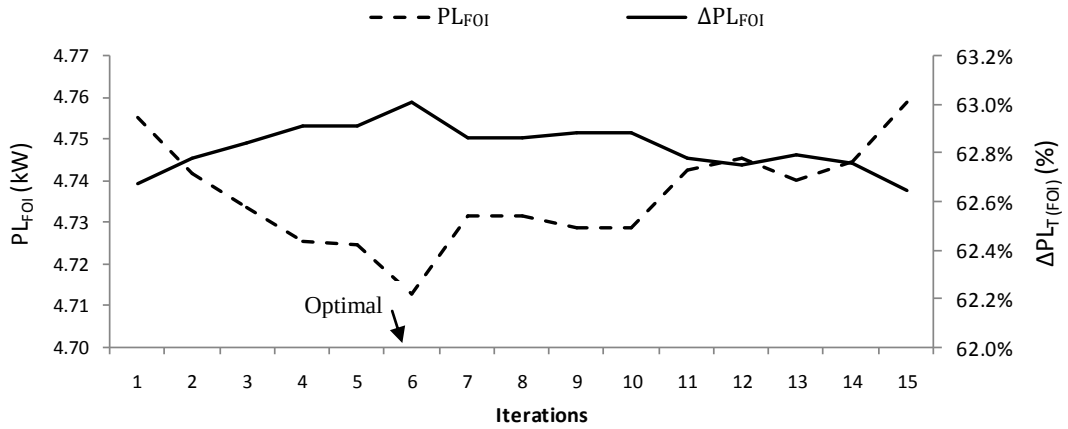

Figure 5.44 PL_{FOI} & ΔPL_{FOI} with two PVDG units on feeder F2, allowing RPF

According to Figs.5.42 to 5.44, the optimal solution is the one related to iteration 6. This has resulted in the maximum line power loss benefits at the FOI as stated Table 5.21.

Table 5.21 Optimal solution of two PVDG units on feeder F2 allowing RPF

PVDG1			PVDG2		
Opt_CP1	Opt_mid1	Opt_ $PV1_{FOI}$	Opt_CP1	Opt_mid1	Opt_ $PV2_{FOI}$
14	5	0.1658MW	27	18	0.2469MW
$PL_{FOI} = 4.7130kW$ $\Delta PL_{FOI} = 63\%$					

The resulting current flow profile by phase along feeder F2 at the optimal solution is represented below in Fig.5.45.

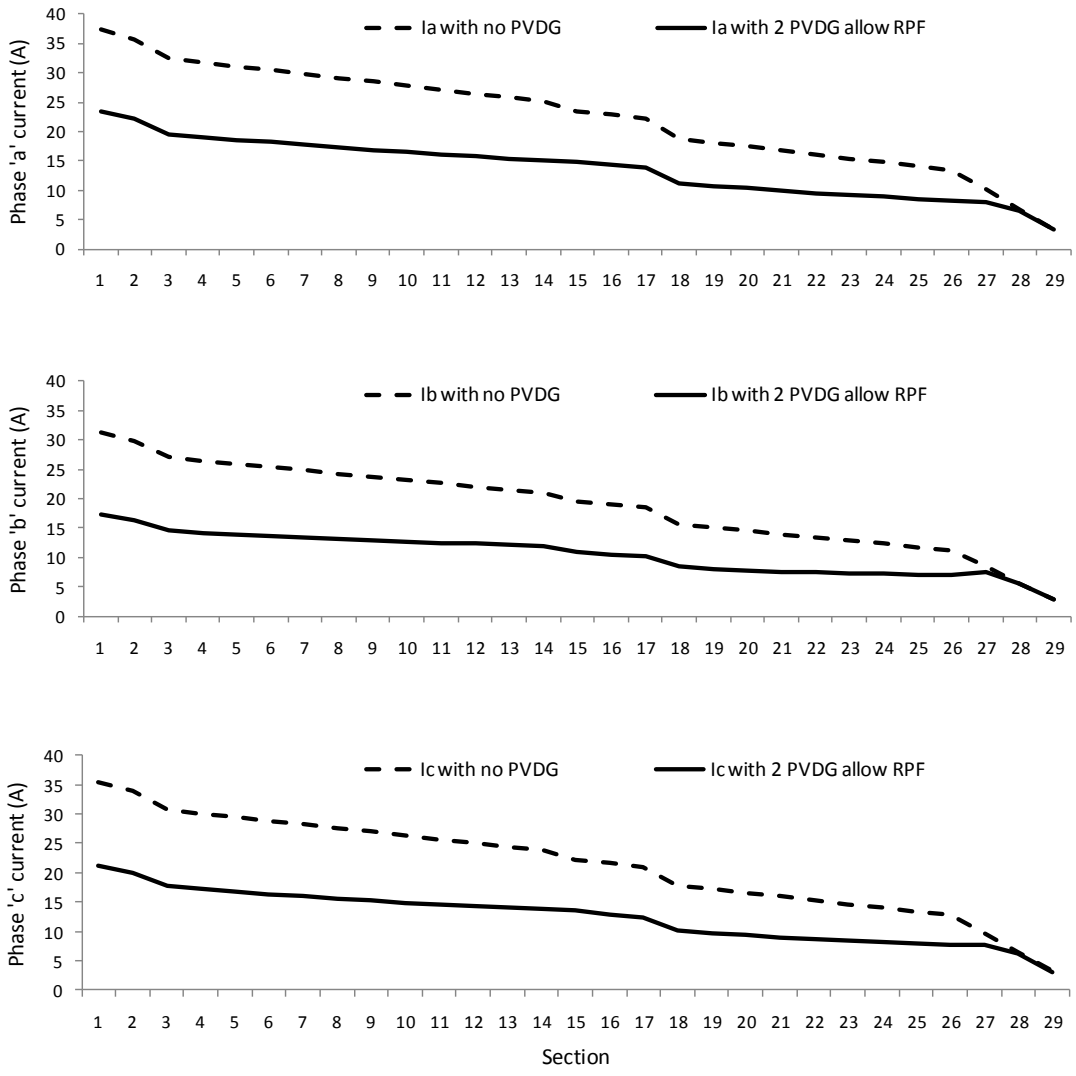

Figure 5.45 Feeder F2 current at the FOI with optimal two PVDG units, allowing RPF

Similar to the previous applications, the voltage profile along the feeder shows considerable improvement without exceeding the level of the substation. The reason is that the RPF is cleared away before reaching the substation. Figure 5.46 depicts the improvement in voltage profile along feeder F2 at the optimal solution.

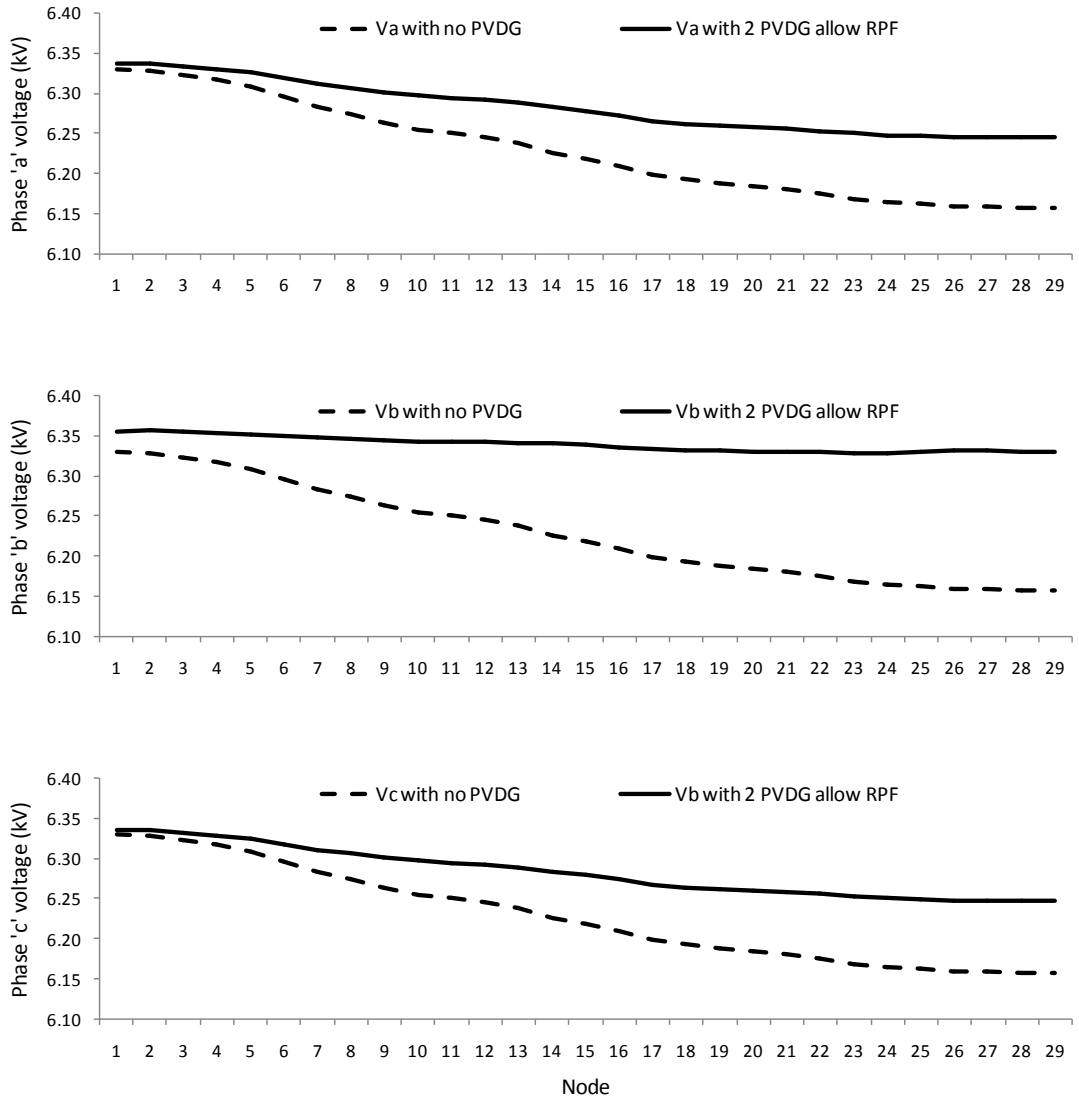

Figure 5.46 Feeder F2 phase voltage at the FOI with optimal two PVDG units, allowing RPF

Validation of optimal solution

The credibility of the optimization procedure has been checked by modifying the MATLAB program to check every possible solution on feeder F2. The program has been modified to iterate the calculations along the feeder without determining initial locations and feasible iterative steps. At the beginning, the CP2 is placed at node 29 with its reverse power falling to

zero at node 28. Accordingly, CP1 can be placed at node 27 the matter that ends up with 26 sizing possibilities according to the 26 nodes between it and the substation.

The next set of solutions is checked by keeping CP2 and its associated size as is but moving CP1 to node 26 that ends up with 25 sizing possibilities. The process is continued until CP2 reaches node 4 and sized according to line section 3, with CP1 located at node 2 and sized according to line section 1. At the end, the process has resulted in 23751 solutions. Table 5.22 validates the optimal solution of the developed optimization procedure by comparing it with the top 10-ranked solution out of the 23751 ones. Note that the variation margin of the resulting line power loss (PL_{FOI}) at the top ranked solutions has been found to be narrow. Table 5.22 shows the margin up to the 100th top-ranked solution. Nevertheless, the optimal solution has matched the 9th top ranked solution with a PL_{FOI} exceeds that of the 1st top-ranked by only 0.0615%.

Table 5.22 Optimal solution validation of two PVDG unit on feeder F2, allowing RPF

No. of the iterations in the optimization procedure = 6 (+2 affirming iterations)

	CP1	mid1	$PV1_{FOI}$	CP2	mid2	$PV2_{FOI}$	PL_{FOI}
Optimal	14	5	0.1658MW	27	18	0.2469MW	4.7130kW
Iterations without initial locations and feasible iterative steps = 23751							
Top 1	14	4	0.1749MW	27	18	0.2469MW	4.7101kW
Top 2	14	4	0.1749MW	26	18	0.2469MW	4.7103kW
Top 3	15	5	0.1658MW	27	18	0.2469MW	4.7106kW
Top 4	15	5	0.1658MW	26	18	0.2469MW	4.7108kW
Top 5	15	4	0.1749MW	27	18	0.2469MW	4.7116kW
Top 6	15	4	0.1749MW	26	18	0.2469MW	4.7118kW
Top 7	14	3	0.1839MW	27	18	0.2469MW	4.7125kW
Top 8	14	3	0.1839MW	26	18	0.2469MW	4.7126kW
Top 9	14	5	0.1658MW	27	18	0.2469MW	4.7130kW
Top 10	14	5	0.1658MW	26	18	0.2469MW	4.7131kW
⋮	⋮	⋮	⋮	⋮	⋮	⋮	⋮
Top 100	15	3	0.1839MW	28	18	0.2469MW	4.7301kW
⋮	⋮	⋮	⋮	⋮	⋮	⋮	⋮
⋮	⋮	⋮	⋮	⋮	⋮	⋮	⋮
23751	2	1	0.0664	4	3	0.4308	11.1265

Comparing the benefits of single and couple PVDG units with RPF allowance

The improvement in voltage profile due to the connection of single and couple PVDG units are compared by phase in Fig.5.47. On the other hand, Fig.5.48 depicts the line power loss (PL_{FOI}) vs. the total size of the PVDG units (PV_{FOI}) for the same applications.

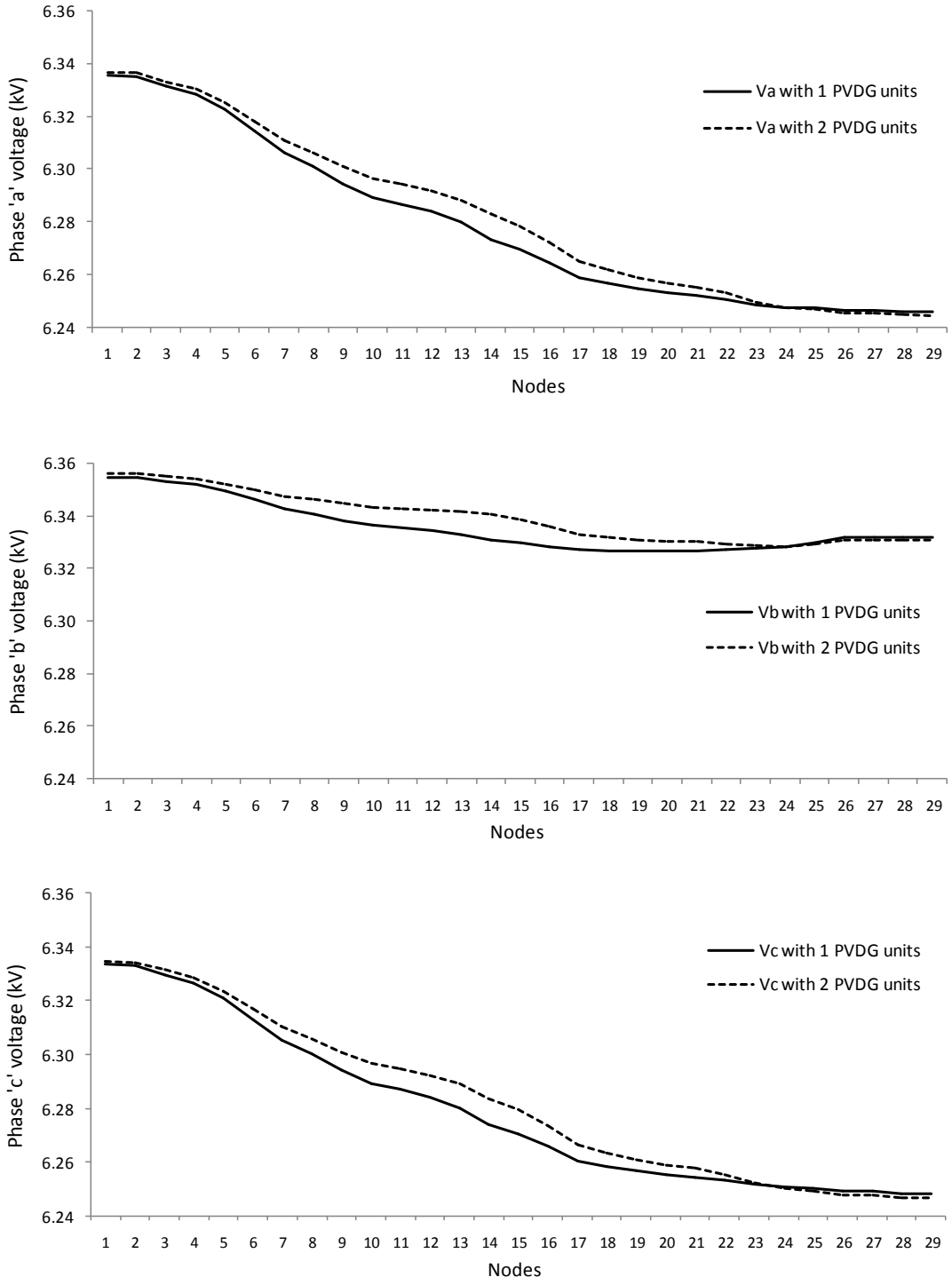

Figure 5.47 Comparing of voltage profile with single & multiple PVDG units, allowing RPF

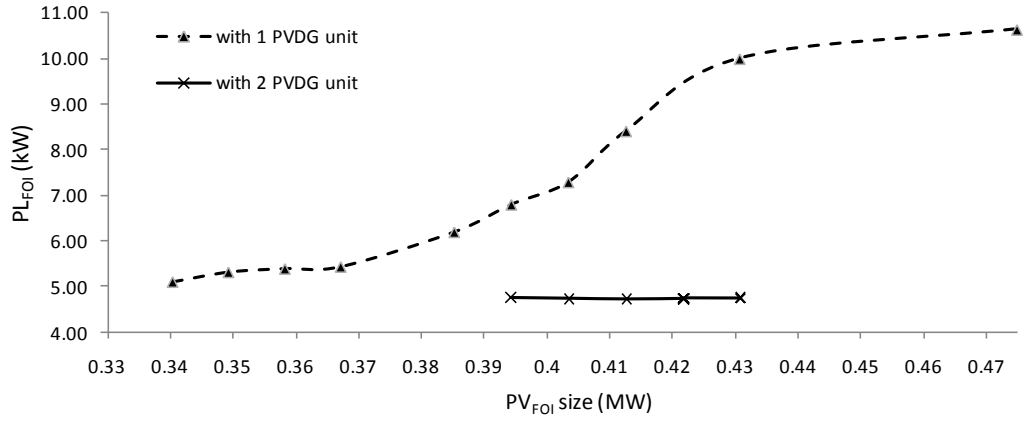

Figure 5.48 Comparing of PL_{FOI} with single and multiple PVDG units, allowing RPF

Figures 5.47 & 5.48 show a preference for the scenario of two PVDG units over that of a single PVDG unit. This is in terms of voltage profile improvement and line power loss reduction. However, the single PVDG is more flexible in terms of PVDG sizes. Also Fig.5.48 shows the narrow margin of PL_{FOI} saving near the top-ranked solution.

Comparing the benefits of the avoidance and allowance of RPF scenarios

At this point there is a reasonable level of data that can compare the benefits of avoidance and allowance RPF scenarios. The comparison is conducted in terms of line power loss and voltage profile benefits considering single and couple PVDG units.

Hence, Figs.5.49 and 5.50 illustrate the line power loss (PL_{FOI}) along feeder F2 with single and two PVDG units for the two scenarios.

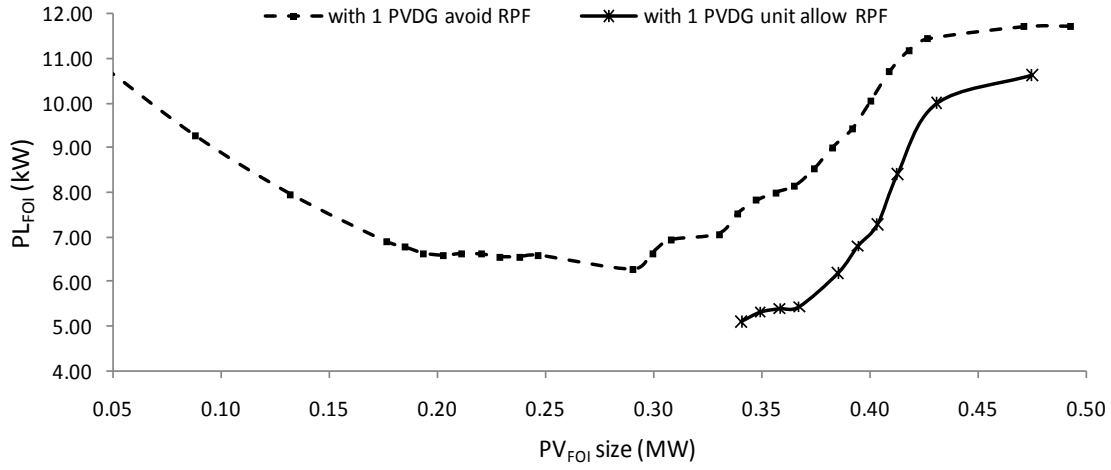

Figure 5.49 PL_{FOI} vs. PV_{FOI} with single PVDG for avoidance and allowance RPF scenario

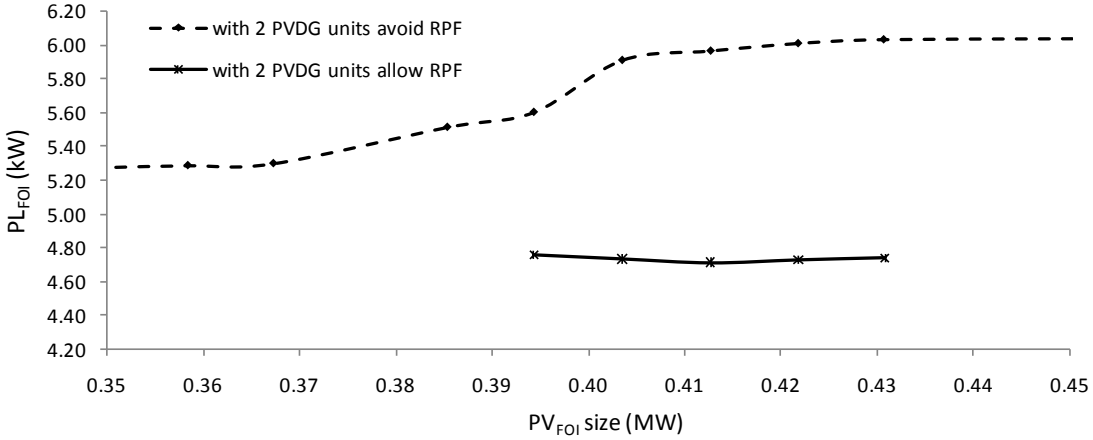

Figure 5.50 PL_{FOI} vs. PV_{FOI} with two PVDG considering avoidance and allowance RPF

The figures show the preference for the scenario of RPF allowance in that it yields lower line power flow for the same PVDG size. However, the scenario of RPF avoidance shows more flexibility in the range of PVDG sizing.

In the same connection, Fig.5.51 and 5.52 represent the phase voltage profile along feeder F2 for the same. Again, the two figures give the preference to the RPF allowance scenario that it more improves the voltage profile without exceeding the voltage level at the s/s.

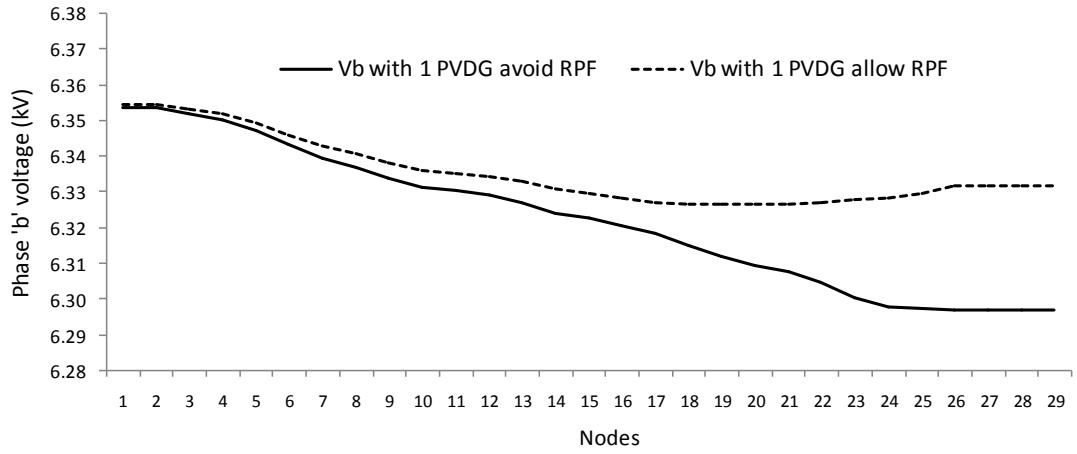

Figure 5.51 Voltage profile with single PVDG considering avoidance & allowance of RPF

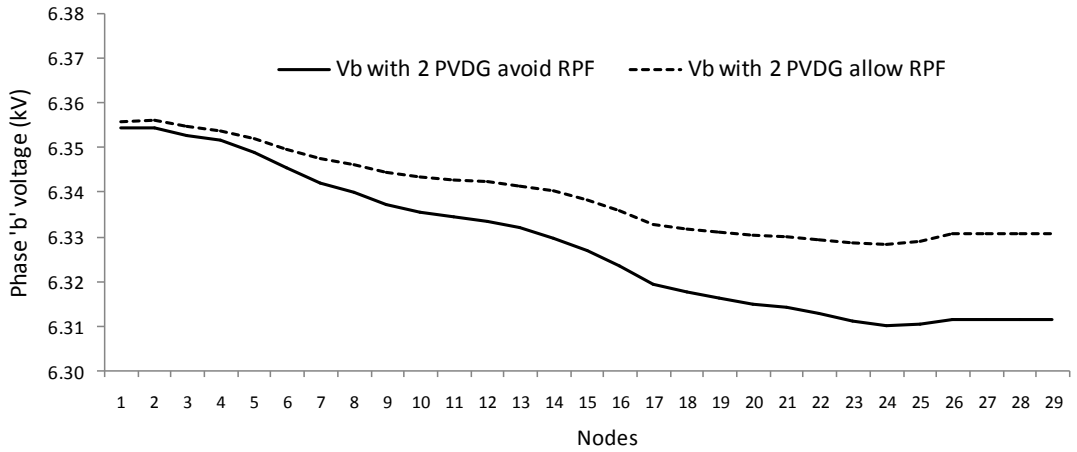

Figure 5.52 Voltage profile with two PVDG considering avoidance & allowance of RPF

5.3 Summary

Four procedures for optimal sizing and location of PVDG units on a radial distribution feeder have been developed. The procedures solve for the maximum benefits of accumulated line power loss reduction over the day, namely line energy loss reduction (ΔEL). The concept of rating the ΔEL by the line power loss reduction at the FOI (ΔPL_{FOI}), derived in Chapter 4, has been applied successfully.

The work has been carried out considering two scenarios of avoiding and allowing RPF. Two procedures have been developed per scenario considering single and multiple PVDG units on 3-phase unbalanced load feeder.

The procedures have been applied on two case study feeders existing in Abu Dhabi distribution network at the 11kV level. The resulting benefits, in terms of line power loss reduction (ΔPL_{FOI}) vs. the size of PVDG unit (PV_{FOI}), gave preference to the application of multiple PVDG units over single PVDG unit. This is true for both scenarios of avoidance and allowance of RPF. Similarly, the application of multiple PVDG units of both scenarios results in a greater improvement of the voltage profile along the feeder. It is worth mentioning that even with the RPF allowance scenario, the RPF falls to zero before reaching the s/s. To this end, the voltage profile values along the feeder shall remain below the voltage level of the s/s, which is one of the benefits of the developed procedures.

In the same connection, the scenario of RPF allowance showed more benefits of ΔPL_{FOI} and voltage profile improvement. However, the avoidance scenario showed more flexibility in the range of PVDG sizing.

References

[1] W. H. Kersting, "Distribution System Modeling and Analysis," *Electric Power Engineering Series, CRC Press LLC*, USA, 2002, ch.1.

[2] J. J. Grainger and W. D. Stevenson, "Power System Analysis," *McGRAW-Hill*, International Edition, USA, 1994, ch4.

[3] W. H. Kersting, "Distribution System Modeling and Analysis," *Electric Power Engineering Series, CRC Press LLC*, USA, 2002, ch.10.

[4] M. AlHajri and M. El-Hawary, "Optimal Distribution Generation Sizing via Fast Sequential Quadratic Programming", *in Proc. Oct. 2007 IEEE Power Engineering Conf.*, pp. 63–66.

[5] A. Al-Sabounchi, E. Al-Hammadi, S. Yalyali, and H. Al-Thani, "Photovoltaic-Grid Connection in the UAE: Technical Perspectives", *in Proc. Sep. 2010 World Renewable Energy Congress-XI, Abu Dhabi*, pp.1207-1213.

[6] W. H. Kersting, "Distribution System Modeling and Analysis," *Electric Power Engineering Series, CRC Press LLC*, USA, 2002, ch.4.

[7] T. Hoff and D.S. Shugar, "The Value of Grid-Support Photovoltaics in Reducing Distribution System Losses," *IEEE Transactions on Energy Conversion*, vol.10, No.3, pp 569-576, Sep. 1995.

[8] M.E. Baran and F.F. Wu, "Optimal Capacitor Placement On Radial Distribution Systems," IEEE Transactions on Power Delivery, vol. 4, no. 1, pages 725 – 734, Jan.1989.

[9] D.I.H. Sun, S. Abe, R.R. Shoults, M.S. Chen, P. Eichenberger, and D. Farris, "Calculation of Energy Losses in a Distribution System," *IEEE Transactions on Power Apparatus and Systems*," vol. PAS-99, No. 4, pp 1347-1356, July/Aug 1980.

[10] L. Ochoa, R. Ciric, A. Padiha-Feltrin, and G. Harrison, "Evaluation of Distribution System Losses due to Load Unbalance", *in Proc. August 2005 15th Power Systems Computation Conf., (PSCC'05)*, session 10, paper 6, page 4.

[11] J. J. Grainger and S. H. Lee, "Optimum Size and Location of Shunt Capacitors for Reduction of Losses on Distribution Feeders," *IEEE Trans. on Power Apparatus and Systems*, vol. PAS-100, no.3, pp.1105-1118, Mar.1981.

[12] R. F. Cook, "Optimizing the Application of Shunt Capacitors for Reactive-Volt-Ampere Control and Loss Reduction," *AIEE Transaction*, part III, vol. 80, pp. 430-444, Aug.1961.

[13] H.L. Willis, "Analytical methods and rules of thumb for modeling DG-distribution interaction," *in Proc. Jul.2000 IEEE Power Engineering Society Summer Meeting*, vol.3, pp.1643 - 1644.

6 DISCUSSION AND CONCLUSIONS

The optimal sizing and location of PVDG units on a distribution feeder is an important field that seems not to be considered potentially in the related reviewed literature. That was one of the main reasons behind this work, which tackled several interesting concepts in this area. Among those considered are the modeling of the PVDG unit as an uncontrollable DG system, the correlation of the load and PVDG production curves, the peak mismatch of the these curves and the impact of that on the objective function, the rating of energy-based benefits at one time interval over the day, the avoidance and allowance of reverse power flow (RPF) and the feasible iterative steps method. However, it is not claimed that this work has covered and solved all of the related concerns in the field. As a matter fact, this work is deemed to have the potential of contributing to further complementary development and promising avenues for future research.
In light of the above, this chapter is dedicated to discuss the potential of the developed optimization procedures and the findings resulting from them. Additionally, it summarizes the acquired conclusions and sheds the light on promising future avenues of research that could extend this work.

6.1 Discussion

The threat of global warming and the negative impact of conventional energy generation on the environment have become a driving force for wider deployment of PV systems. One of the main methods to achieve greater deployment of these systems is by connecting them at the distribution level of the utility grid, in so called Photovoltaic Distributed Generation (PVDG). In many practical systems considered, most of the distribution networks use radial feeders to distribute the electricity to the consumers. Hence, connection of PVDG units at optimal sizes and locations along the radial distribution feeder has ended up as a matter of significant importance.

6.1.1 Work achieved and objectives

A reasonable number of credible works has been reviewed in the field of optimal sizing and location of distributed generation (DG) units. The majority of them were found to deal with

conventional DG units –such as diesel generators- of controllable power generation. Because of that, the objective function is most likely to solve for maximum line peak power loss reduction (ΔPPL). The reason is that the conventional DG units can be easily controlled to yield its contribution at the peak load interval, resulting in certain amounts of peak shaving benefit.
In the event of PVDG units, however, the concept is different in that the production of the PV arrays is mainly driven by the rates of solar irradiance (and to a lesser degree, changes in panel temperature). Hence, the PVDG production is no longer controllable so that it can yield its best at the peak load demand interval. As a result, the optimization procedure will end up dealing with two performance curves varying independently over the period during the day when sunlight is available. These curves are the feeder load curve, driven by consumers, and the PVDG production curve, driven by the solar irradiance. Having this in mind, one should be aware that the peaks of the load and the PVDG production curves are likely to occur at different intervals. With such peak mismatch, the PVDG unit can produce only part of its capacity at the time the feeder meets its peak load demand. Figure 4.3 given earlier in Section 4.1 shows this mismatch clearly. To this end, the concept of the previous work in solving the optimization problem for maximum ΔPPL is no longer effective with PVDG units.

In view of these limitations, this work has developed a solution for the optimization problem for accumulated line power loss reduction over the day, namely line energy loss reduction (ΔEL). This is deemed to make more sense in that it takes into account the accumulated benefits of the PVDG production over the whole day.

However, dealing with energy-based quantities may need to repeat the calculations on an hourly basis, then to take the summation of the whole duration. This is the trend that has been applied in the related reviewed work. Hence, determination of a certain time interval at which the whole ΔEL can be rated will be significantly helpful. This objective has been realized in Chapter 4. As a result, it was sufficient to run the optimization procedure only at this 'feasible optimization interval (FOI)', with no need to go through the lengthy energy-based calculations. It is worth mentioning that the FOI is determined in Section 4.2 as the point where the time interval concurs with the peak (amplitude) of the PVDG production curve. At this interval, the PVDG unit yields its highest possible contribution to the load with respect to the original power flow coming from the substation. This can be incorporated in the developed procedures by calculating the line power loss reduction at the FOI (ΔPL_{FOI}) due to the connection of the PVDG units. Consequently, the optimal PVDG sizing and location that result in maximum ΔPL_{FOI} also results in maximum ΔEL. The concept has been proven mathematically in Section 4.3 considering single and multiple PVDG units on a radial distribution feeder.

On the other hand, the connection of PVDG plant (and any DG plant) at some coupling point along a radial distribution feeder will inject a certain amount of power. At any interval if this power exceeds the demand, the surplus amount will flow in the reverse direction towards the substation. As been mentioned earlier in Section 1.3; RPF may result in undesirable effects that disturb traditional automatic voltage regulators and directional protection equipment, in addition to the possibility of overvoltage occurrence and incompliance with the ampacity of the feeder and potential increase in line losses in the upstream direction. Among the reviewed work, none was found considering the impact of RPF in solving the relevant optimization problem. To this end, the impact of RPF along the feeder has been considered in this work. New optimization procedures determining the optimal sizing and location of single and multiple PVDG units on radial distribution feeder have been developed. The optimal solution is realized subject to no surplus PVDG power production along the feeder over the day. For wider consideration, two procedures have been developed considering single and multiple PVDG units.

Nevertheless, some power companies upgrade their networks with smart control and protection devices that might be able to deal with RPF. Apart from discussing the feasibility of such devices, this work has been extended to develop an additional optimization procedure allowing RPF. In this approach, RPF is allowed to the extent that it does not reach the substation. This way, the voltage profile is deemed not to exceed the voltage level at the substation. Additionally, the current flow will thus comply with the ampacity of the feeder. The procedure has been applied successfully to feeders containing both single and multiple PVDG units.

The other issue to be mentioned in this section is the status of the 3-phase load condition of the distribution feeder. Primary distribution feeders are usually installed as a 3-phase system. However, lateral feeders of 1-phase, 2-phase, and 3-phase systems maybe branched out from them. As a result, loads with different characteristics and demands are served by different phases of the feeders and laterals. In this essence, the distribution feeders are most likely to be operated with an unbalanced load. In spite of that, previous work reviewed in the field generally considers the 3-phase feeder in a balanced load condition, which is deemed an obvious shortcoming. Hence, the optimization procedures of this work have been developed to deal effectively with the feeder under 3-phase unbalanced load condition. To achieve this, the line impedances along the feeder are modeled using a phase impedance matrix. At the same time, modeling of feeder load curves along with the power flow calculations and the resulting losses in the lines are applied per-phase.

As for solving the optimization problem, suitable methods of determining initial locations and feasible iterative steps over iterations have been developed as part of this work. The methods

are implemented successfully in Chapter 5 then validated by a process that showed credible accuracy. Figures 6.2-6.4 of this chapter are some good examples on that.

6.1.2 Review of the results

The developed procedure has been applied on feeders F1 and F2. The mathematical derivations of Section 4.3, for matching the optimal solution of maximum ΔEL with that of maximum ΔPL_{FOI}, have been proven numerically. The optimization procedure has been applied twice in Section 5.1.1 for the optimal size and location of a single PVDG unit resulting in maximum ΔPL_{FOI} and maximum ΔEL separately. The optimization results are represented in Figs.5.4&5.5 and Fig.5.7&5.8 and demonstrated matching in the optimal solutions.

On a different note, solving the optimization procedure considering summer load demands has resulted in considerable amounts of surplus power during the other seasons. Figure 5.9 of Chapter 5 depicts the daily load curves over seasons of line section 7 on feeder F1, at which the optimal location of the PVDG unit was determined. The curves are correlated, with the corresponding PVDG production curves resulting from the PVDG unit sized based on summer data. The figure showed a considerable drop in the winter load curve with an almost insignificant drop in the amplitude of the winter PVDG production curve. Hence, if the RPF is to be avoided over the year, then it is recommended, in hot summer regions, to solve the optimization procedure based on winter data.

As a matter of fact, the consideration of the winter load demand is not only suitable for the reason above, but also for the applicability of the optimal solution. Sizing the PVDG unit according to summer load demand (which for example in Abu Dhabi is almost 4 times that of winter) will end up over-sizing the PV array. In this course, Section 5.1.1 showed that the optimal size of the PVDG unit on feeder F1 according to summer is 2.3384 MW. Considering the space area and capital cost of the current PV modules in the markets, the cost and site area required to install the PV array is deemed to be too great. On the other hand, modifying the size according to winter has reduced the size significantly to 0.662 MW, which is much more practical and cost-effective. It is worth mentioning that the approximate area of multi-crystalline silicon PV modules that can produce 1kW at standard conditions is around 7.5-8.0m^2 [1].

The optimization procedures of Chapter 5 have thus been solved at the FOI, rather than repeated over the whole daily duration. Also for rational comparison between the benefits of the proposed scenarios, the winter load demand has been considered in all of the applications, and the actual condition of 3-phase unbalanced load feeder has been applied. Below is a brief overview of the results of the conducted applications.

Single PVDG unit avoiding reverse power flow

This scenario is presented in Section 5.1.2. The line impedance of the case study feeders is modeled using a phase impedance matrix due to the unbalanced load condition. For the same reason, the load curves along the feeder and the size of the PVDG unit are modeled per-phase. The PVDG unit is modeled as a PQ bus delivering negative power at unity power factor. Hence, the sizing of the PVDG unit is set according to the real load demand of the line section it is connected at. However, the power flow analysis and the line power loss calculations are carried out using complex number quantities so that the impact of reactive power flow is included.

The calculations are made at the FOI rather than considering the whole duration of the day, the matter that significantly reduces the process. Regarding the PVDG unit size, there will be one local optimal size per location that is equal to the real power flow of the line section ending by the CP node. This size shall provide maximum contribution of the original power flow coming from the substation subject to no surplus PVDG power production at the CP node. The next step is to check the solutions at each node along the feeder, then to select the one resulting in maximum ΔPL_{FOI} and consequently maximum ΔEL. This procedure has been applied on feeder F2 with the results are as shown in Fig.5.10 of Chapter 5. According to the figure, the optimal solution is to install a PVDG unit at node 17 with a total size equals to 0.2905MW. Note to mention that this size is determined in terms of the amplitude of the ac PVDG production curve. The solution reduces the total line power loss of the feeder at the FOI (PL_{FOI}) from 12.7408 kW to 6.2593kW. This corresponds to total ΔEL, rated by ΔPL_{FOI}, equal to 50.872%.

For presentation, Fig.5.10 of Chapter 5 is drawn for 29 iterations, which is the number of nodes along the feeder. However, the curvy trend of the PL_{FOI} and ΔPL_{FOI} shown with increasing number of iterations makes it possible to stop the iteration process soon it passes the climax point. In this work, the iteration process is set to stop in two iterations after the climax, (referred to as 'affirming iterations'). To this end, the optimal solution of this case study is obtained in 15 iterations, considering the fact that the process is commenced from the far end of the feeder.

Considering the resulting voltage and current flow profile along the feeder at the optimal solution, Figs.5.11 and 5.12 of Chapter 5 are drawn respectively. Figure 5.11 shows obvious improvement in the voltage profile for the three phases due to the reduction in current flow. It is worth mentioning that the avoidance of RPF shall remove the concern of over voltage along the feeder as long as the current is flow in the downstream direction all the time.

The current flow profile is depicted in Fig.5.12, which shows considerable reduction in current flow in the line sections on the upstream side of the CP node 17. However, the rest of line sections after node 17 are not affected by the PVDG unit. It is worth mentioning that the current

flow in Fig.5.12 represents the apparent current values including real and reactive components. This explains the non-zero current in the line section 17 in which the PVDG unit completely compensates its real power flow.

A final note regarding the optimal locations of the PVDG unit: the optimal location of the PVDG unit determined on feeders F1 and F2 are found to be at the CP nodes 7 and 17 respectively. This may leave a loose impression that the optimal location is always at a CP node around the mid of the feeder.

Multiple PVDG units avoiding reverse power flow

The optimization procedure has been developed further in Section 5.1.3 to deal with multiple PVDG units on the same feeder. This created two new concerns related to the sizing of the PVDG units and the iteration process of the optimization procedure.

The sizing concern is that the size of the PVDG unit at a certain CP node should be considered when sizing any unit on its upstream side. Hence, each PVDG unit is sized to the power flows in the line section of its location, minus the sizes of all the PVDG units on its downstream side.

Regarding the iteration process, it has been determined that with multiple PVDG units it becomes infeasible to run the iteration process in a similar way to that used for a single PVDG unit. Doing so will result in hundreds or even thousands of possible PVDG locations over iterations. To avoid this effect a two-stage sub-procedure determining feasible iterative steps over iterations has been developed. In the first stage, a suitable method is evolved to determine initial feasible locations (ini_CP) for any number of PVDG units on radial distribution feeder. The second stage consists of a feasible iterative step method to check the possible moving steps of the units per iteration and select the one brings more benefits.

In light of the developments above, the optimization procedure has been applied on feeder F2, considering case studies with two and three PVDG units. The two-stage sub-procedure of the feasible iterative steps has shown excellent results. It realized the optimal solution of the two PVDG units in 7 iterations out of 406 possible solutions. Also it arrived at the optimal solution in 11 iterations out of 3654 possible solutions for three PVDG units. The optimal solutions of both applications are shown in Table 5.12 of Chapter 5.

One more interesting issue has been observed regarding the optimal location of the PVDG units. To start with, the optimal locations of two and three PVDG units on feeders F1 and F2 are summarized in Fig.6.1. The figure loosely shows a rule-of thumb that the optimal location of the j^{th} PVDG unit is most likely at a CP node within the j^{th} zone of the feeder. Another interesting observation is that the CP node gets closer to the zone end as the zone is closer to the substation.

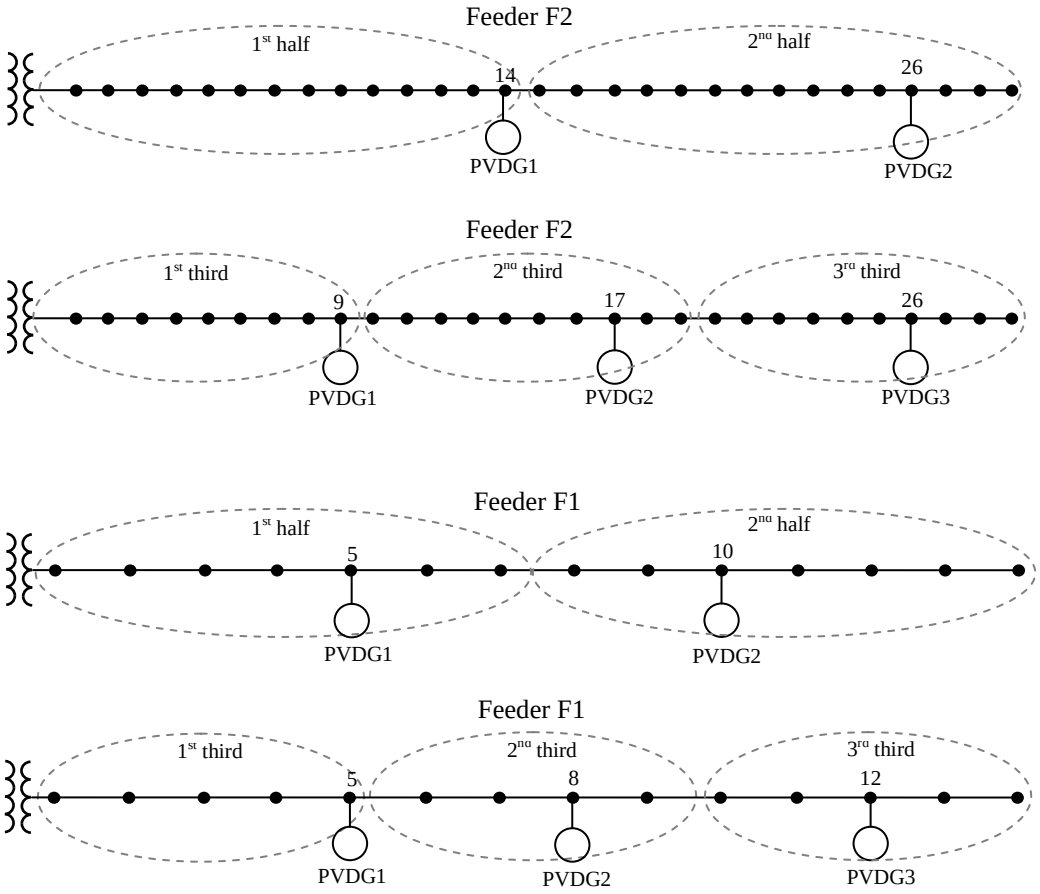

Figure 6.1 Optimal locations of multi PVDG units on feeders F1 and F2

Validation:

In order to validate the results, the calculation program has been modified to iterate the process without applying the sub-procedure of feasible iterative steps. Thus, it checked all of the possible solutions associated with every possible alternative of PVDG locations along the feeder. The resulting number of possible solutions relating to the connection of two and three PVDG units on feeder F2 was 406 and 3654 respectively. The top four solutions of both cases, ranking the highest line power loss benefits, are stated in Tables 5.13 and 5.14 of Chapter 5. For greater validation, the same application has been done on feeder F1. The resulting number of possible solutions relating to the case of two and three PVDG units was 91 and 364 respectively. Similarly, the top four solutions of feeder F1 are stated in Tables 5.15 & 5.16.

Figure 6.2 below summarizes the validation results by matching the optimal solution from the developed procedure with the top four of the validation procedure. The figure shows validity of the developed procedure.

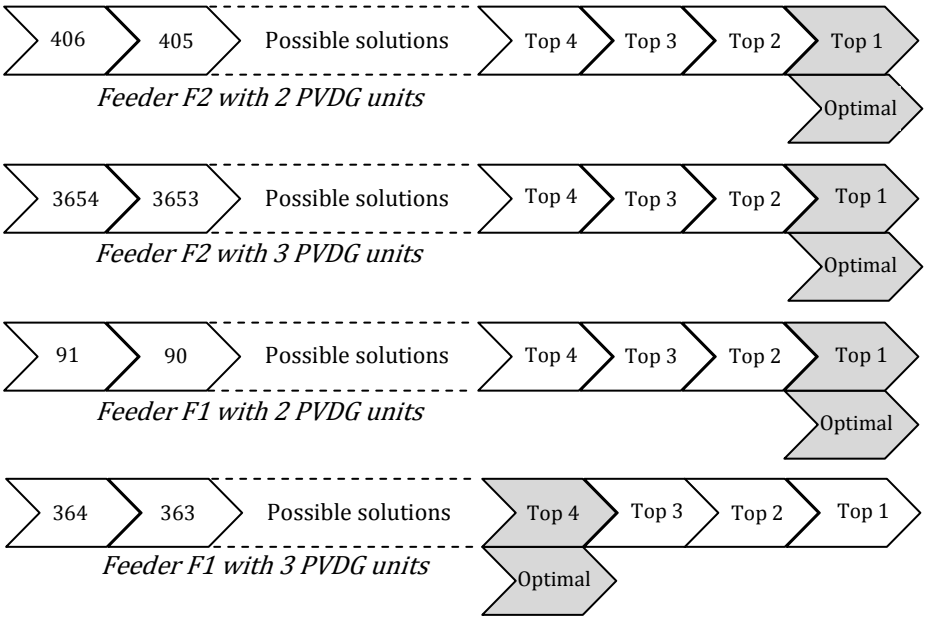

Figure 6.2 Validation of optimal solutions for multi PVDG units avoiding RPF

According to the figure, the optimal solutions of feeder F2 perfectly matched the Top 1 solution for both two and three PVDG units. The same matching is realized with the optimal solution of two PVDG units on feeder F1. At the same time, the optimal solution of three PVDG units on feeder F1 matches the Top 4 solution with very slight difference from the Top 1 solution.

Single PVDG unit allowing reverse power flow

In the previous procedures avoiding RPF, the size of the PVDG unit is arranged to be equal to the power flow at the FOI in the line section ending at the CP node. Owing to this arrangement one specific size is associated with each location. For the scenario allowing RPF, however, the size is allowed to exceed the power flow at the CP location. This means that at each location there will be several sizing possibilities; widening the domain of feasible solutions. The only sizing constraint is that the RPF should fall to zero before reaching the substation. This will keep the voltage profile along the feeder from rising above the substation voltage while keeping the current flow within feeder ampacity. However, this still leaves the process with a lot of sizing possibilities. Figure 5.29 of Chapter 5 is drawn to illustrate the case.

A suitable method has been developed to determine local optimal size for the PVDG unit at each location. The method is based on the idea of serving the nodes on the upstream side of the CP node from whatever comes closer; the substation or the PVDG unit. Consequently, a midpoint that halves the distance between the substation and the CP node is determined and rounded to the nearest node according to a certain formula. The size of the PVDG unit is then

arranged to be equal to the power flow in the line section ending at the midpoint node. The method and the rounding formula are explained in Fig.5.30 of Chapter 5.

The developed procedure starts with locating single PVDG unit at the far end node of the feeder then sizing it according to the associated midpoint node. The line power loss reduction at the FOI (ΔPL_{FOI}) is then calculated, as in the previous applications, using the backward/forward power flow. The same steps are iterated for the next upstream nodes one after one until the optimal solution is realized.

The procedure has been applied to a single PVDG unit on feeder F2 specified in Appendix 2 under unbalanced load conditions and by considering winter load demand. The optimal solution was to connect a PVDG unit at the CP node 26 with PV_{FOI} size equals to 0.3404 MW, according to the midpoint node 13. It is worth mentioning that the optimal solution has been realized in 6 iterations out of 756 possible solutions.

Validation:

The optimal solution has been validated by running the calculations without applying the local optimal size method. Thus, it checked all of the possible sizes at each location along the feeder that ended up with 756 possible solutions. For greater validation, the same application has been done on feeder F1 resulting in 156 possible solutions. The top four solutions of both applications, ranking the highest ΔPL_{FOI} benefits, are stated in Tables 5.18 and 5.19 of Chapter 5. Figure 6.3 summarizes the validation results by matching the optimal solution from the developed procedure with the top four of the validation procedure. Again, the figure shows credible accuracy of the developed procedure.

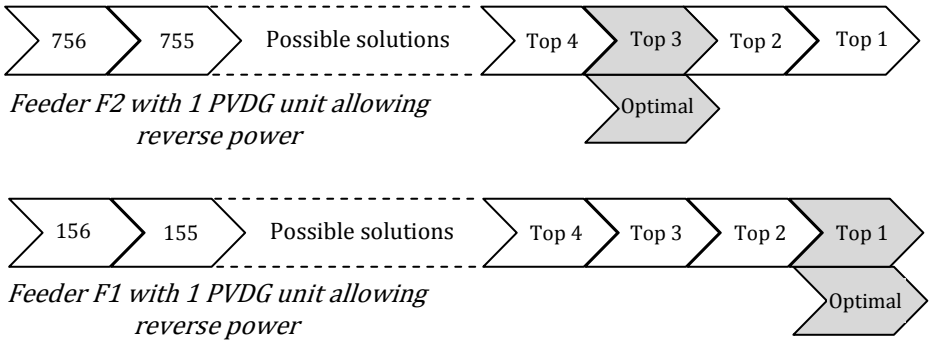

Figure 6.3Validation of optimal solutions for 1 PVDG unit allowing RPF

According to the figure, the optimal solution of feeder F2 matched the Top 3 solution of the validation procedure. The difference is only in the midpoint node that missed the Top 1 solution, insignificantly, by one step. As for feeder F1, the optimal solution has perfectly matched the Top 1 solution of the validation procedure.

Multiple PVDG units allowing reverse power flow

Dealing with RPF allowance scenario considering multiple PVDG units brings greater complication in solving the optimization problem. A suitable optimization procedure has been developed combining the features of multiple PVDG units while avoiding RPF, along with the application of single PVDG unit allowing RPF. At the beginning, the actual feeder is modeled by an equivalent uniform feeder as in Section 5.1.3. After that, initial CP and midpoint locations that result in minimum power flow area along the equivalent uniform feeder are determined based on Fig.5.38. The initial CP and midpoint locations are then returned to the equivalent nodes on the actual feeder based on Eq.5.42. At the initial locations, the PVDG units are sized based on the midpoint concept illustrated in Fig.5.39. The iteration processes is then started with the initial sizes and locations and moved on according to a certain iterative formula that moves the CP nodes and associated midpoints on a feasible path.

The procedure has been applied with two PVDG units on feeder F2 under unbalanced load conditions and by considering winter load demand. The optimal solution was to connect the PVDG units at CP nodes 14 and 27 with size of 0.1658MW and 0.2469MW respectively. It is worth mentioning that the optimal solution has been realized in 8 iterations, out of 23471 possible solutions.

Validation:

The optimal solution has been validated by running the calculations with two PVDG units on feeder F2 without applying the iterative step method. All of the possible combinations of CP locations and sizes have been checked through the following loops that ended up with 23741 possible solutions.

$$\sum_{CP2=29}^{4}\left[\sum_{mid2=28}^{3}\left\{\sum_{CP1=27}^{2}\left(\sum_{mid1=26}^{1}\text{calculate } PL_{FOI}\right)\right\}\right]$$

The solutions are ranked according to the minimum PL_{FOI} with the results of the top 10 along with the100th and 23751st solution are stated in Table 5.22. Figure 6.4 summarizes the validation results by matching the optimal solution from the developed procedure with the top 10 of the validation procedure. The figure shows that the optimal solution matches the 9th top-ranked solution, which results in higher PL_{FOI} by only 0.0615% from that of 1st top-ranked solution.

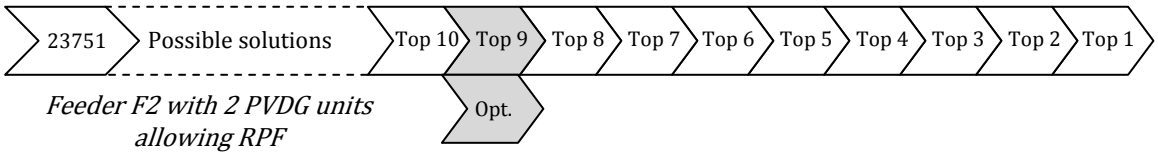

Figure 6.4 Validation of optimal solutions for 2 PVDG unit allowing RPF

Compare the benefits of proposed scenarios

The resulting benefits from the proposed applications are compared to each other in terms of PL_{FOI} along with voltage and current flow profile.

Comparison of PL_{FOI} benefits:

Regarding the PL_{FOI} benefits, Fig.5.28 of Chapter 5 depicts the rates associated with single and multiple PVDG units, considering RPF avoidance scenario. Based on the overlapping zone of the total PVDG size, the preference goes for distributing the total size on multiple units along the feeder. On the other hand, the same figure shows that the PVDG size extends over a wider range with single than with multiple PVDG units. It is worth mentioning that the wider range may bring more flexibility in the sizing of installed PVDG unit.

Figure 5.48 shows a similar comparison to the applications of single and multiple (represented by two) PVDG units, considering RPF allowance scenario. Again, the comparison comes in the interest of multiple over single PVDG units. Similarly, the size with single PVDG unit extends over a wider range than with multiple PVDG units.

In the same course, Figs.5.49 and 5.50 compare the PL_{FOI} benefits realized from each of the avoidance and allowance scenarios of RPF. Both of the figures give preference to the allowance of RPF over the avoidance scenario. However, the size of the PVDG units extends over a wider range with the avoidance of RPF than with the allowance of RPF.

Comparison of voltage and current flow profile:

The voltage profile at the optimal solution, considering the avoidance of RPF, is evaluated for single and multiple PVDG units with Fig.5.27 of Chapter 5. According to the figure, the preference has gone again for distributing the total size on multiple PVDG units rather than single unit. Actually this result should be expected in light that the application with three PVDG units has already realized higher PL_{FOI} benefits than with two and single units.

For current flow, Fig.6.5 depicts the relevant profile at the optimal solution of the RPF avoidance scenario. Note that the phase current is the current of phase b, but any of the other two phases can be used and show similar trend. As expected, the current flow with multiple PVDG units shows a lower profile than with a single PVDG unit.

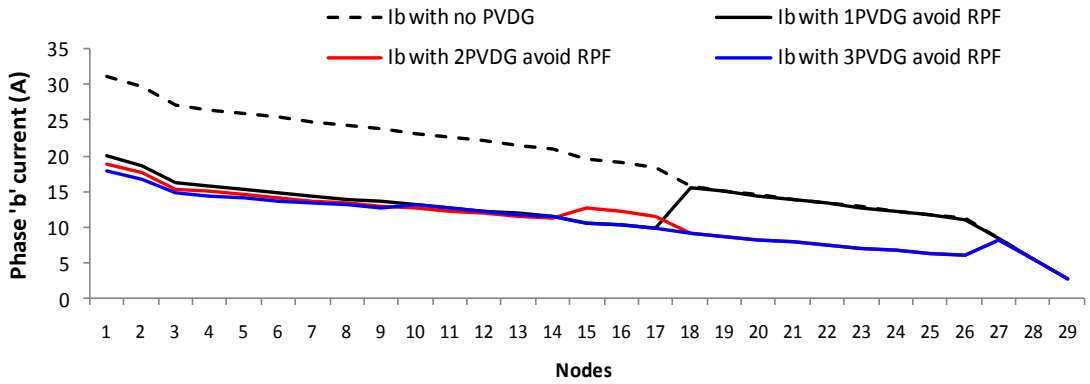

Figure 6.5 Optimal current flow with the avoidance of RPF

Coming to the RPF allowance scenario, Fig.5.47 shows a better voltage profile with two PVDG units than with a single PVDG unit. The same is said for the current flow profile, where Fig.6.6 manifests a slightly lower current profile with two than with one PVDG units.

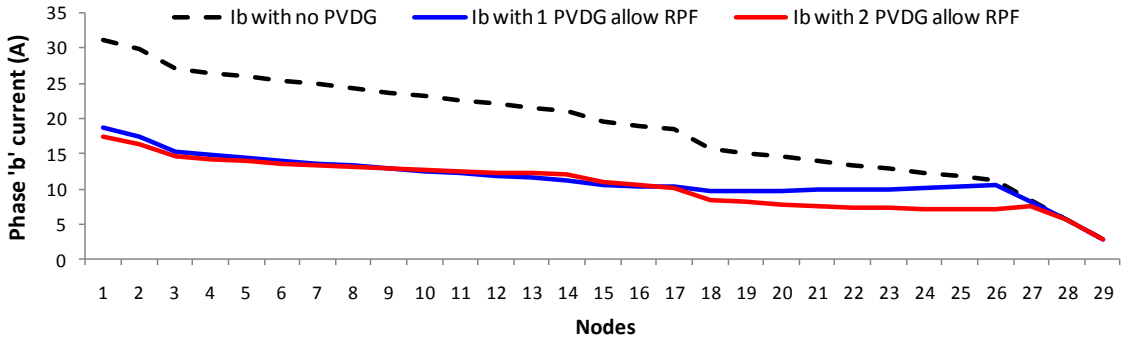

Figure 6.6 Optimal current flow with the allowance of RPF

In the same course, Figs.6.7 and 6.8 compare the voltage profile resulting from each of the avoidance and allowance scenarios of RPF. Both of the figures show a preference for allowance of RPF over the avoidance of RPF.

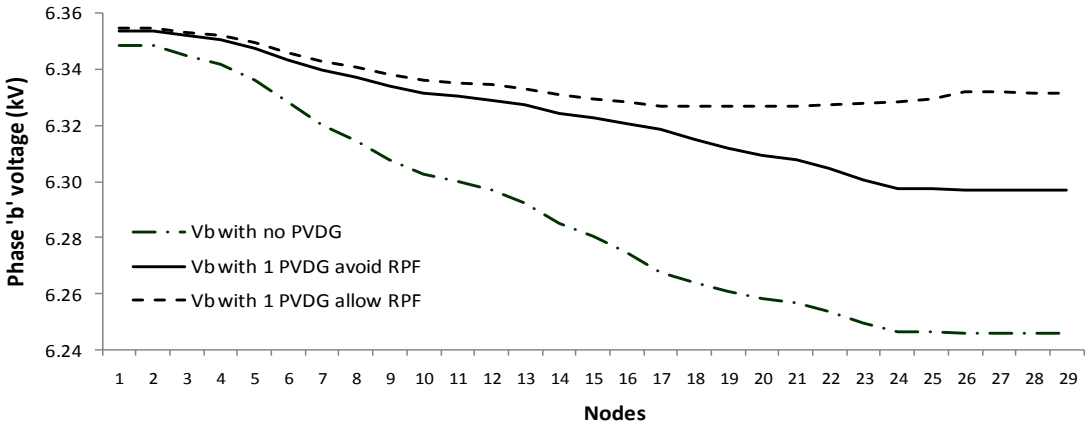

Figure 6.7 Voltage profile of single PVDG unit with avoidance and allowance scenario

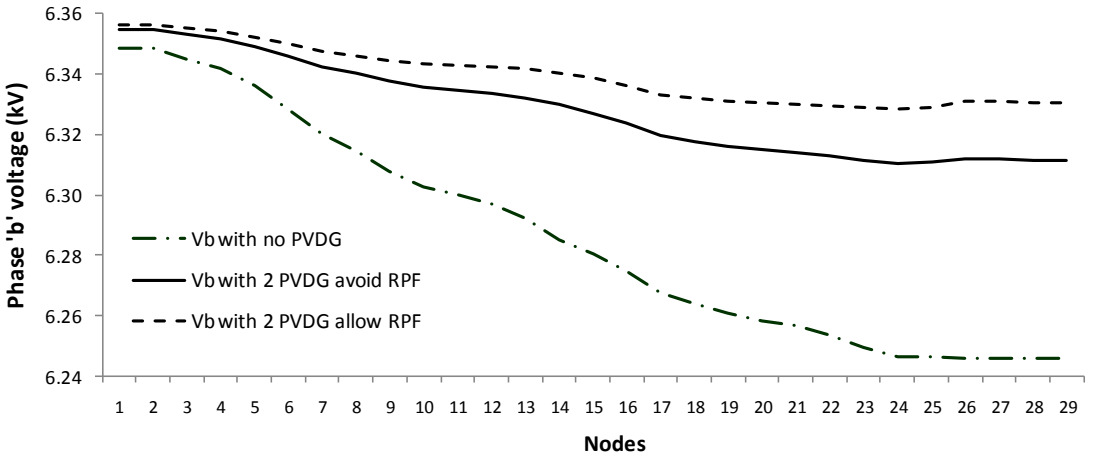

Figure 6.8 Voltage profile of two PVDG units with avoidance and allowance scenarios

Similarly, the current flow at the optimal solution considering allowance and avoidance of RPF is compared with single PVDG unit with Fig.6.9. As expected, the scenario that allows RPF gives better results.

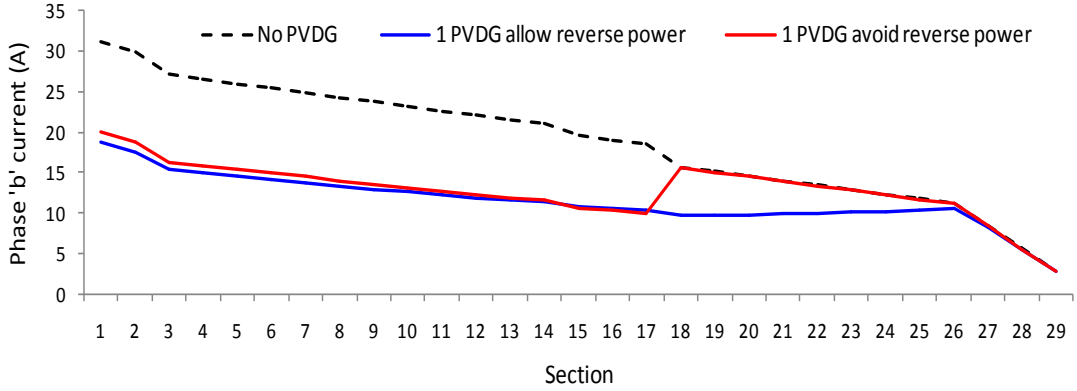

Figure 6.9 Current profile of avoidance and allowance scenarios with single PVDG unit

6.1.3 Further developments and opportunities of future work

Possible applications with conventional DG units:

As has been presented in the previous sections, the developed procedures have been applied considering the daily load demand in winter. However, the optimization procedures were rerun considering the daily demands of other seasons. Table 6.1 states the results of optimal locations and total size of the PVDG units on feeder F2 considering RPF avoidance. Also Table 6.2 states the same considering RPF allowance.

Table 6.1 Optimal CP nodes and total PV_{FOI} over seasons, avoiding RPF

Feeder F2 optimal	CP1 node	CP2 node	CP3 node	Total PV_{FOI}
Single PVDG unit avoiding RPF				
Winter load demand	17	N/A	N/A	0.2905 MW
Summer load demand	17	N/A	N/A	1.0906 MW
Spring & Autumn load demand	17	N/A	N/A	0.5316 MW
Two PVDG units avoiding RPF				
Winter load demand	14	26	N/A	0.3313 MW
Summer load demand	14	26	N/A	1.2574 MW
Spring & Autumn load demand	14	26	N/A	0.6082 MW
Three PVDG units avoiding RPF				
Winter load demand	9	17	26	0.3762 MW
Summer load demand	9	17	26	1.4369 MW
Spring & Autumn load demand	9	17	26	0.6919 MW

Table 6.2 Optimal CP & midpoint nodes and total PV_{FOI} over seasons, allowing RFP

Feeder F2 optimal	CP1 node	mid1 node	CP2 node	Mid2 node	Total PV_{FOI}
Single PVDG unit allowing RPF					
Winter load demand	26	13	N/A	N/A	0.3404 MW
Summer load demand	26	13	N/A	N/A	1.2949 MW
Spring & Autumn load demand	26	13	N/A	N/A	0.6253 MW
Two PVDG units allowing RPF					
Winter load demand	14	5	27	18	0.4126 MW
Summer load demand	14	5	27	18	1.5885 MW
Spring & Autumn load demand	14	5	27	18	0.7608 MW

The interesting observation from Tables 6.1 and 6.2 is that the optimal locations remain the same over seasons. However, optimal PVDG sizes change with the changes in load curve levels. Practically speaking it is deemed inappropriate to set the PVDG unit according to the highest demand of summer, and then inactivating certain parts of the PV array to meet the lower demand in the other seasons. Considering the relatively high capital cost of PV system components (*~14 times that of diesel generator**), the practical application must be designed to exploit the maximum capacity of the PVDG unit at all times. It is worth mentioning that the optimization procedures in this work have been applied considering winter load demand. Thus, the production of the PVDG units is completely exploited over the year with no need to inactivate any part of the PV array.

However, the observation of Tables 6.1 and 6.2 could be useful with conventional distributed generation (DG) units. The reason is that the capital cost of conventional DG units and the required installation area are relatively small comparing to that of PVDG units. It is thus feasible to install two or three conventional DG units at the CP node and to manage them in a

suitable mode of operation over changing seasons. To discuss the concept in further detail, the results of a single PVDG unit in Table 6.1 are taken as an example. According to the table, the connection of two DG units rated at 0.25 MW each and third one rated at 0.5 MW could be a good combination. The three units are connected to node 17, but managed to operate one by one to meet the optimal size requirements over seasons to the best possible. Figure 6.10 may illustrate the idea where only DG1 is put in service during winter, then joined by DG2 in spring and autumn, and finally joined by DG3 in summer.

**(http://en.wikiversity.org/wiki/DFE2008_Off-Grid_Electricity_for_Cottages)*

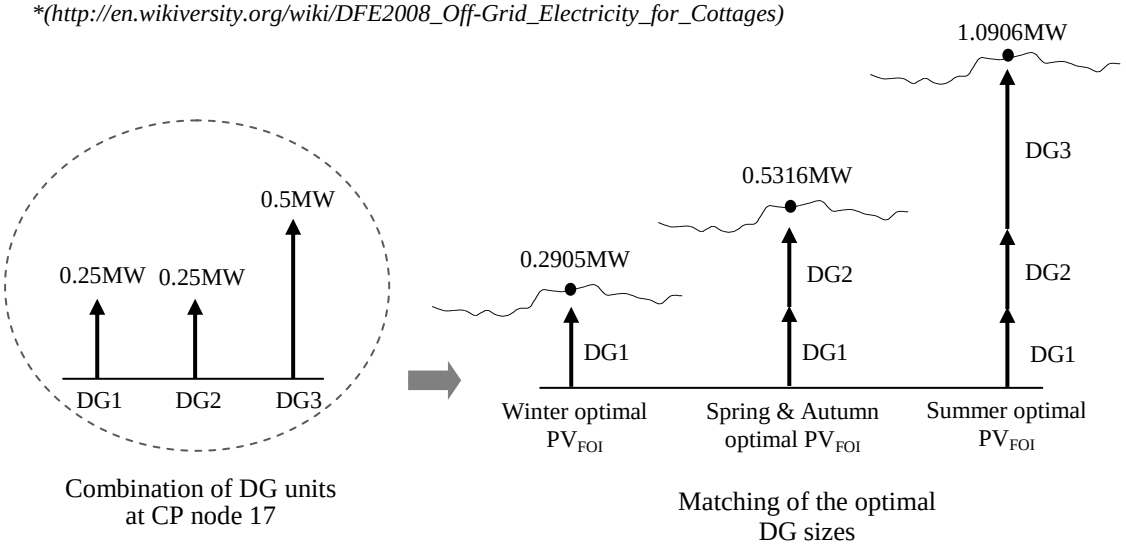

Figure 6.10 Conventional DG units compensating the power flow at the CP node

Back to the PVDG unit applications; it has been mentioned earlier in this work that there will be a sort of peak mismatch of the load and PVDG production curves. With such mismatch, the PVDG unit can produce only part of its capacity at the time the feeder meets its peak load demand. In that event, the optimization procedures were solved for maximum line energy loss reduction (ΔEL) rather than line peak power loss reduction (ΔPPL). Because of that, the optimization problem was solved at the FOI, at which the ΔEL can be rated.

The above concern is no longer valid with conventional DG unit for it can be managed to meet the peak load interval (PLI) of the feeder. Thus, the optimization procedure can be solved at the PLI, rather than the FOI, so that the optimal solution exhibits ΔPPL and ΔEL benefits at the same time. Thus, the same optimization procedures developed in this work can be applied with conventional DG units for maximum ΔPPL benefits. Not only this; the procedures can be solved at each season to determine the sizes of the required DG units.

However, in addition to the ΔPPL benefits, the three DG units of Fig.6.10 can be shown to have ΔEL benefits. The amounts of these benefits are dependent on the operating durations of the DG units. Based on the same derivations of Section 4.3, the ΔEL benefit is rated by the line power loss reduction, this time at the PLI (ΔPL_{PLI}). Figure 6.11 may illustrate the idea.

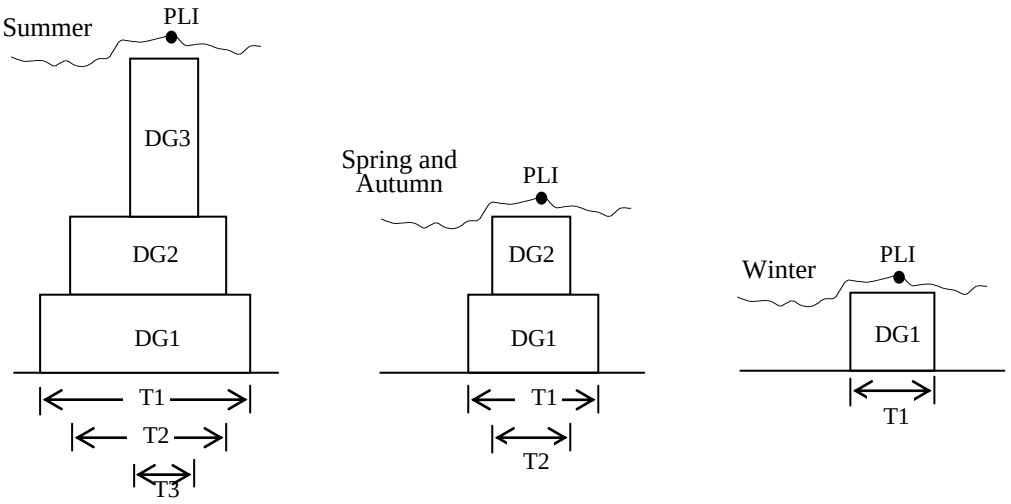

Figure 6.11 Development opportunity with conventional DG units

According to Fig.6.11, the amount of ΔEL is dependent on the size and operating time (T) of the DG units. From this point, further development could be conducted to determine optimal T values that can realize maximum ΔEL, subject to certain constraints.

Additional increase in PVDG size considering RPF allowance

The optimization procedures developed in this work have been solved considering winter load demand. As a matter of fact, solving the optimization problem based on winter load demand is shown to minimize the possibility of RPF over the year. This goes along with the scenario that avoids RPF, but it is not necessarily a problem with the RPF allowance scenario as long as the reverse power does not reach the substation. Hence, there is space for further increase in the size of the PVDG unit in a manner that keeps the RPF from reaching the substation over the year. Figure 6.12 may help in describing this issue. According to the figure, there is space for additional increase in size as far as the new PV_{FOI} does not exceed the power flow of line section 1 in winter. Hence, additional work is proposed to realize the optimal size of the PVDG unit within this condition.

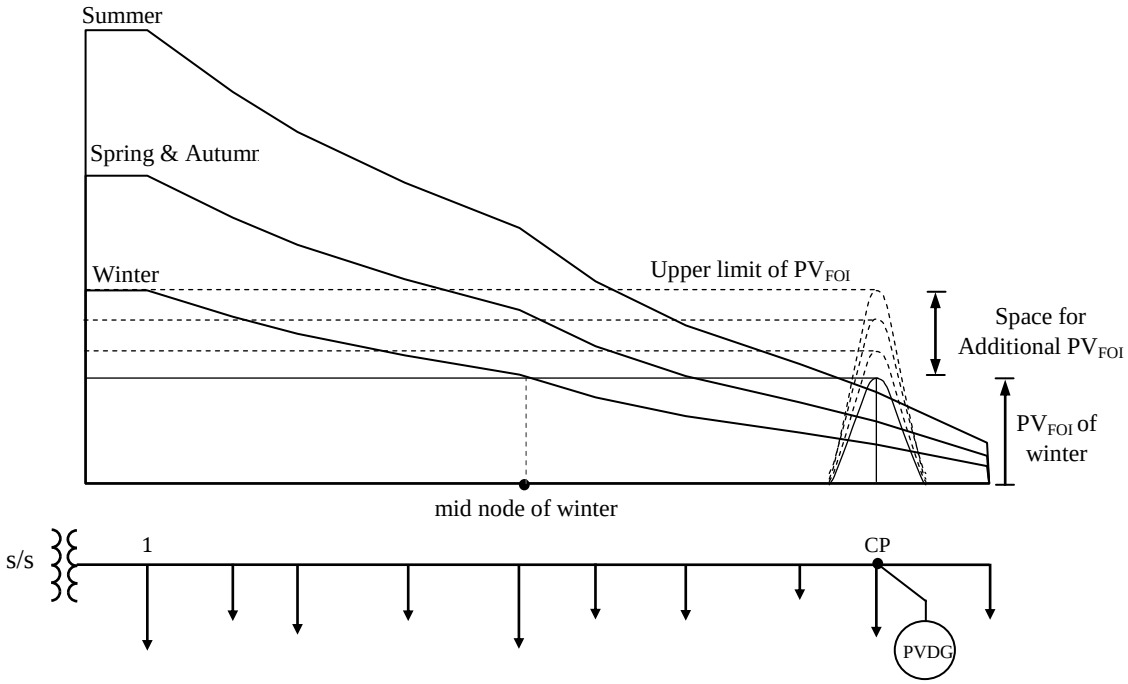

Figure 6.12 Opportunity for additional PV_{FOI} with allowance of RPF

Other possible cases of PVDG sizing and location

There could be a case for dealing with the optimal sizing and location of PVDG units on a radial feeder that already had a unit on it. Another case could be to determine the optimal location of a PVDG unit where the plant is of a fixed predefined size. Thus, the developed procedures are proposed to be modified in a way that can deal with these cases.

Incorporation of non-linear programming techniques

The concept of this work in rating the ΔEL by the ΔPL_{FOI} has removed the need for repeating the energy-based calculations over the day. Further reduction in the calculation process has been realized by developing a suitable method for determining feasible iterative steps over iterations. The idea is to select the size and location of the PVDG units that result in minimum power flow area per iteration. The method has succeeded in reducing the number of overall iterations significantly. To this end, a greater reduction in the number of iterations could be realized by incorporating one of the non-linear programming techniques in the optimization procedure. This could serve in determining the minimum power flow area over the iteration process much more quickly.

6.2 Conclusions

New procedures for optimal sizing and location of PVDG units on radial distribution feeders have been developed. In this course, it is known that the production of the PVDG unit is largely driven by the rates of solar irradiance fall on its PV array. Hence, the PVDG production varies independently from the variation in feeder load demand. This will result in two performance curves, which are the feeder daily load curve driven by the consumers, and the PVDG daily production curve driven by the solar irradiance. Most likely the peaks of the curves will occur at different intervals. Due to this peak mismatch the PVDG unit might well end up with producing only part of its capacity at the time the feeder meets its peak load demand. Consequently, solving the optimization problem for maximum line power loss reduction (ΔPPL) is inappropriate when considering the connection of PVDG units.

Based on the above, this work has arrived at a conclusion of solving the optimization problem for maximum line energy loss reduction (ΔEL), rather than ΔPPL. This counts the accumulated benefits of the PVDG production over the whole day. The line peak power loss reduction (ΔPPL) is still considered as a sub-benefit in case it occurs during daylight hours.

However, dealing with energy-based quantities may require the repetition of the calculations on hourly basis, or even shorter, and to take the summation of the whole duration. Hence, a suitable concept has been developed to rate the ΔEL benefits at certain interval, namely the feasible optimization interval (FOI). At this interval, the PVDG unit yields its highest possible compensation of the original power flow coming from the substation. Consequently, the optimal PVDG sizing and location that results in maximum line power loss reduction at the FOI (ΔPL_{FOI}) also results in maximum ΔEL.

On the other hand, the connection of PVDG unit (and any DG unit) along a radial distribution feeder will inject certain amount of power. If this power exceeds the demand, the surplus amount will flow in the reverse direction towards the substation. Reverse power flow (RPF) may disturb the traditional automatic voltage regulators (AVR) and unidirectional protection devices. Also it may undesirably raise the voltage level at some nodes along the feeder. This is apart from the possibility of incompliance with the ampacity of some line sections. In light of that, suitable optimization procedures determining the optimal sizing and location of single and multiple PVDG units have been developed. The optimal solution is realized subject to no surplus PVDG power production along the feeder over the day.

Nevertheless, upgrading the distribution network with advanced AVR and bidirectional protection devices could deal with the inconvenience of RPF. Therefore, additional optimization

procedures allowing reverse power flow have been developed for optimal sizing and location of single and multiple PVDG units. In order to keep the voltage levels along the feeder within the upper limit, the RPF is allowed to the extent that no reverse power flow reaches the substation. This will also secure the compliance of current flow with the ampacity of the feeder.

Another conclusion related to the modeling of the distribution feeder has been realized. Three-phase distribution feeders often operate under unbalanced load condition. In spite of that, the previous work reviewed has been found considering the feeder in balanced load condition, which is a shortcoming. Hence, the optimization procedures of this work have been developed to deal effectively with a 3-phase feeder supplying an unbalanced load. Based on that, the line impedances along the feeder have been modeled in terms of a phase impedance matrix. At the same time, the modeling of feeder load curves along with the power flow calculations and the resulting losses in the lines have been applied on a per-phase basis.

As related to the iteration process, it is important to incorporate the optimization procedure with suitable iterative steps in a formula that can reduce the number of iterations. Hence, an effective iterative step method has been developed in this work and showed a great deal of success.

Solving the optimization procedure considering summer load demand has ended up with considerable amounts of surplus power during other seasons. Hence, if the RPF is to be avoided over the year, then it is recommended to solve the optimization procedure in hot summer regions based on winter data. As a matter of fact, consideration of winter load demand is not only suitable for the reason above, but also for the applicability of the optimal solution. An analysis of the load curves of many distribution feeders in Abu Dhabi over changing seasons showed that the summer load demand is around 4 times that of winter. Hence, considering the capital cost and space area of the current PV modules in the markets, optimal sizing the PVDG unit based on winter load demand seems more applicable.

The developed optimization procedures have been applied to actual feeders at the 11kV level of the Abu Dhabi distribution network. Two main scenarios have been considered in the applications are related to the avoidance and allowance of RPF. In this course, several case studies with single and multiple PVDG units have been solved and validated successfully. The benefits resulting from each application have been evaluated and compared in terms of line power loss reduction at the FOI (ΔPL_{FOI}) along with voltage and current flow profile.

Regarding the RPF avoidance scenario, the resulting ΔEL benefit rated by the ΔPL_{FOI} has exceeded 50% of the original line losses with no PVDG units. In this course, the highest benefit has been realized with the application of three PVDG units, followed by two then one unit

respectively. Based on that, it is better to distribute the total installed PVDG capacity between multiple PVDG units along the feeder rather than putting it all in a single unit.

As related to the voltage profile, the applications showed considerable improvement, but with the same decreasing trend in the downstream direction. The order of ranking of applications has taken the same ranking of three PVDG units, followed by two then one unit respectively. As a matter of fact, the reduction in voltage drop at the end of the feeder has exceeded 25% in each of the three applications.

The same ranking has been also realized when evaluating the current flow profile, where the application of three PVDG units showed the lowest over the others. The reduction in current flow has exceeded 35% in the line sections affected by the PVDG units for the three applications.

Hence, in terms of voltage and current flow profile, the preference is to distribute the total installed PVDG capacity between multiple PVDG units along the feeder rather than putting it all in a single unit.

Coming to the RPF allowance scenario this work considered single and multiple PVDG units applications. The application of multiple PVDG units -represented by two units- showed more benefits in terms of line loss reduction along with voltage and current flow profiles.

In order to compare the benefits of the RPF avoidance and allowance scenarios, the application of a single PVDG unit in both scenarios is considered. In terms of ΔEL, rated by the ΔPL_{FOI}, the allowance scenario has resulted in a rate exceeds that of avoidance scenario by around 9%. Also the RPF allowance scenario has shown higher voltage profile and lower current profile than the avoidance scenario.

Another interesting observation has been realized regarding the optimal locations of the PVDG units, considering the avoidance of RPF. For a single PVDG unit, the optimal location is likely to be at a CP node around the midpoint of the feeder. In the same course, a rule-of thumb could be concluded in the event of multiple PVDG units. The rule is that the optimal location of the j^{th} PVDG unit is most likely at a CP node within the j^{th} zone on the feeder. Other interesting observation is that the CP node gets closer to the zone end as the zone is closer to the substation.

For the RPF allowance scenario considering single PVDG unit, the optimal CP node is found to be at a node in the downstream half of the feeder. At the same time, the associated mid node is located in the upstream half. The same concept is applied with two PVDG units, where CP2, mid2, CP1 and mid1 are located in the relevant quarters starting for last downstream quarter upwards respectively.

Apart from the aforementioned conclusion, the work has left some promising proposals for further applications and/or avenues of research. Among the proposed applications is to use the developed procedures in solving for optimal sizing and location of conventional DG units for peak shaving benefits. Additional research topic has been proposed to size the PVDG unit considering the load demand over seasons. The incorporation of non-linear programming technique to reduce number of iterations was also among the proposed topics.

References

[1] A. Al-Sabounchi, E. Al-Hammadi, S. Yalyali, and H. Al-Thani, "Photovoltaic-Grid Connection in the UAE: Technical Perspectives", *in Proc. Sep. 2010 World Renewable Energy Congress-XI, Abu Dhabi*, pp.1207-1213.

APPENDIX 1 – *Chapter 3*

Concentric Neutral Cable

Each phase conductor in concentric neutral type is provided with its own neutral strands distributed on the outer circle as shown in Fig.A1.1. Much published work could be found dealing with this topic; for this thesis, the literature in [1] is used as a starting point.

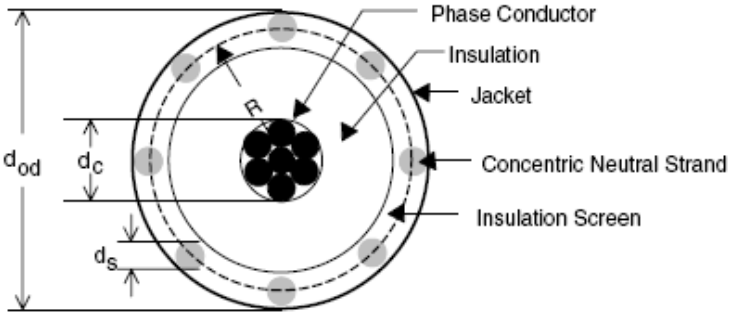

Figure A1.1 Cross sectional of concentric neutral cable for single conductor

In order to apply the modified Cason's equations on such cables, an equivalent values for the GMR, resistance, and spacing of the multi neutral strands are required. Hence, the equivalent GMR of the whole neutral strands ($GMR_{n\text{-}eq}$) is:

$$GMR_{eq-n} = \sqrt[k]{GMR_{ns} \,.\, k.\, R^{k-1}} \ \text{(ft)} \qquad \text{(A1.1)}$$

$$R = \frac{d_{od} - d_S}{24} \qquad \text{(ft)} \qquad \text{(A1.2)}$$

Where,

GMR_{ns} - Geometric mean radius of a neutral strand (ft)
k - Number of concentric neutral strands (ft)
R - Distance from any of the neutral strands to the center of its phase conductor
d_{od} - Nominal diameter over the concentric neutrals (inches)
d_S - Diameter of a concentric neutral strand (inches)

As for the equivalent resistance of the concentric neutral strands ($r_{eq\text{-}n}$), the following equation is applied; where r_S is the resistance of a solid neutral strand (Ω/mile):

$$r = r_S / k \quad (\Omega/\text{mile}) \qquad \text{(A1.3)}$$

Coming to neutral strands spacing, Fig.A1.2 is drawn. The equivalent spacing between the concentric neutral strands to an adjacent phase conductor (D_{nc}) is realized as follows:

$$D_{nc} = \sqrt[k]{D_{nm}^{k} - R^{k}} \ \text{(ft)} \qquad \text{(A1.4)}$$

Where, D_{nm} is the distance from concentric neutral to an adjacent concentric neutral. According to Fig.A1.2, D_{nm} is also the distance between two phase conductors.

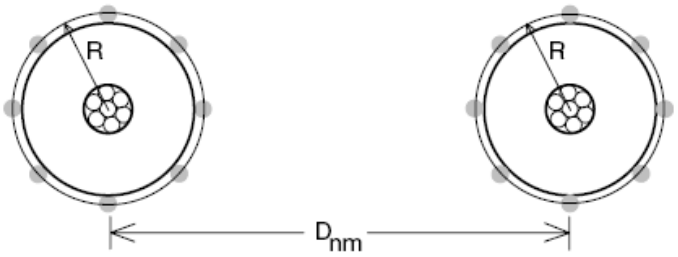

Figure A1.2 Two adjacent concentric neutral cables

Tape-Shielded Cable:

The neutral of the tape-shielded cable is a bare copper tape surrounding the insulation screen in a helical shape. The parameters of the tape-shielded cable are shown in the Fig.A1.3.

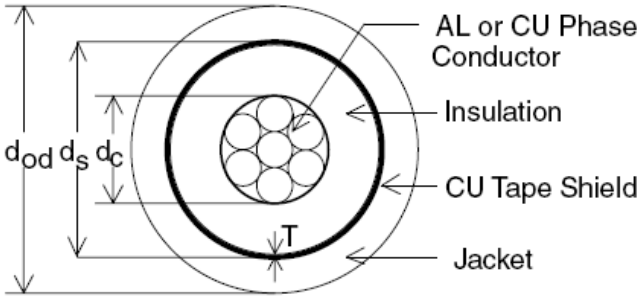

Figure A1.3 Cross sectional tape-shielded cable for single conductor

The resistance of the tape shield (r_{sh}) is calculated as follows, bearing in mind that the resistivity (ρ) must be expressed in Ω.meter at 50°C:

$$r_{sh} = 7.9385 \times 10^{8}.\frac{\rho}{d_S.T} \qquad (\Omega/\text{mile}) \qquad \text{(A1.5)}$$

Where:

d_c - Phase conductor diameter (inches)
d_S - Outside diameter of the tape shield (inches)
d_{od} - Outside diameter over tape shield (inches)
T - Thickness of copper tape shield (mils)

The equivalent GMR of the whole tape shield is the radius of a circle passing through the middle of the shield and is given by:

$$\mathrm{GMR}_{\mathrm{eq-sh}} = \frac{\mathrm{d_S} - (\mathrm{T}/1000)}{24} \quad \text{(ft)} \qquad \text{(A1.6)}$$

The spacing between the tape shield neutral and the adjacent conductors are as follows:

To its own phase conductor = Radius to midpoint of the shield (ft.)

To an adjacent phase or neutral conductor = Center-to-Center distance between phase conductors (ft.).

References

[1] W. H. Kersting, "Distribution System Modeling and Analysis," *Electric Power Engineering Series, CRC Press LLC*, USA, 2002, ch.4.

APPENDIX 2 – *Chapter 5*

Specifications of Case Study

The procedures developed in this work have been applied on two 11kV distribution feeders existing in the distribution network of Abu Dhabi. The first feeder (F1) consists of fourteen 11/0.4kV distribution transformers served by XLPE-insulated 3-core underground cable. The second feeder (F2) consists of twenty nine 11/0.4kV distribution transformers served mostly by overhead lines, with few sections served by XLPE (Cross Linked Polyethylene) cable. The daily average load curves of the feeders over seasons are illustrated in Fig.A2.1 to Fig.A2.6. In the same course, Table A2.1 and Table A2.2 state the electrical configuration of the two feeders.

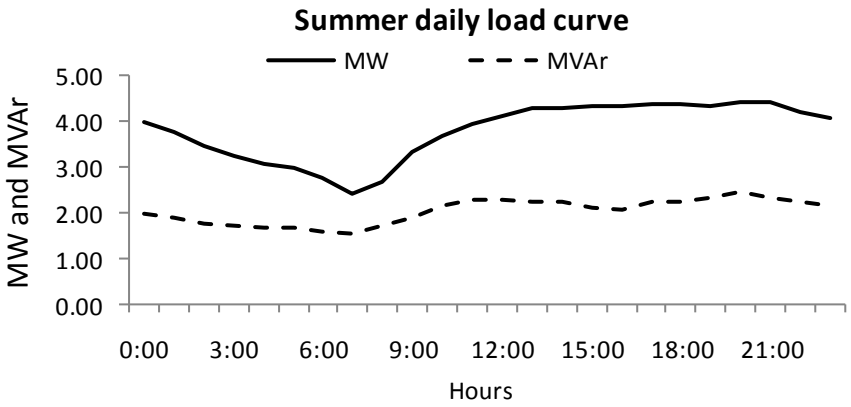

Figure A2.1 Summer daily average load curve of feeder F1

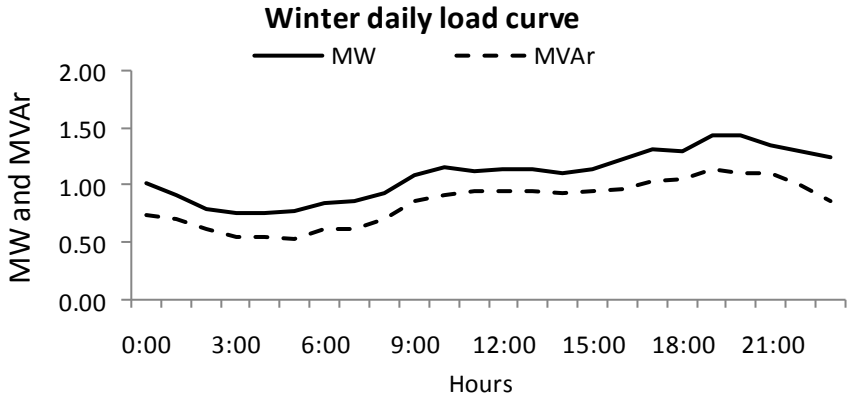

Figure A2.2 Winter daily average load curve of feeder F1

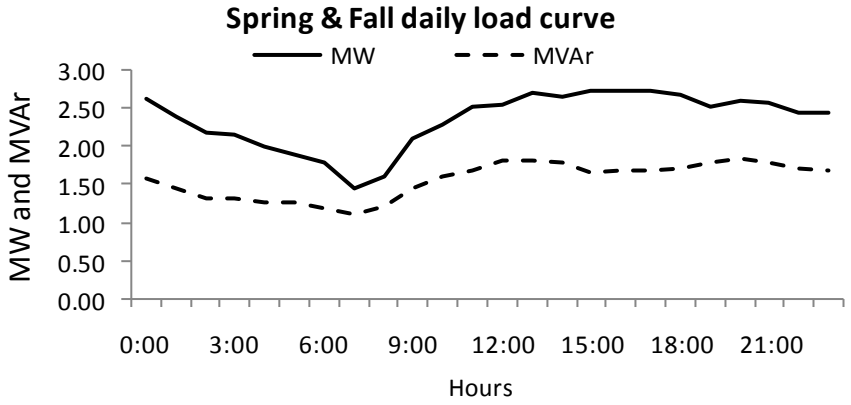

Figure A2.3 Spring and fall daily average load curve of feeder F1

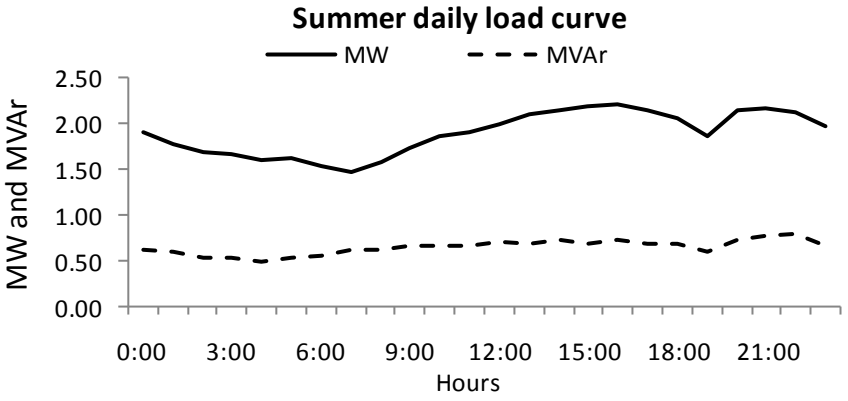

Figure A2.4 Summer daily average load curve of feeder F2

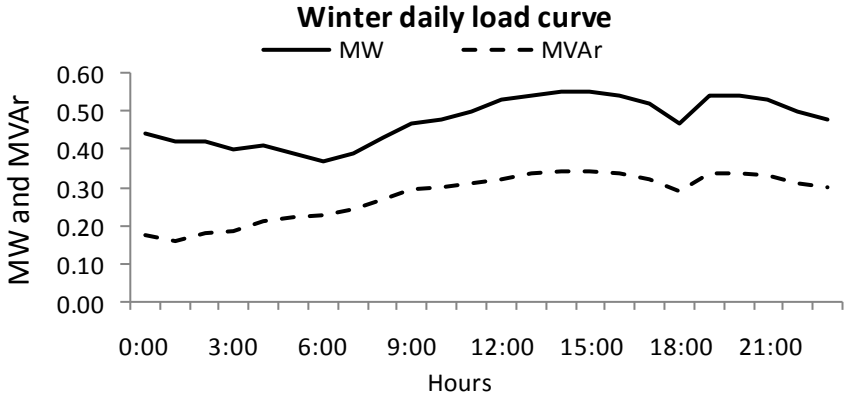

Figure A2.5 Winter daily average load curve of feeder F2

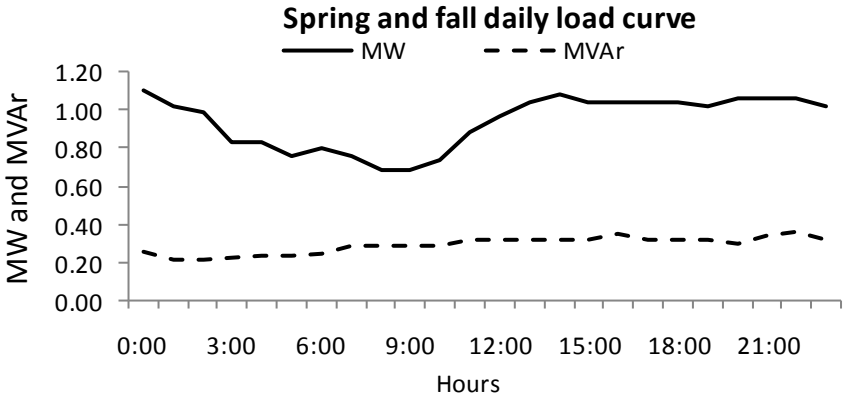

Figure A2.6 Spring and fall daily average load curve of feeder F2

Table A2.1 Configuration of feeder F1

Section	Send node	Receive node	Receive node cap. (MVA)	Length (km)	System	Wire size (mm^2)	Conductor spacing (ft)	Wire resistance (Ω/km)	Type
1	S.S	1	1.5	1.200	Δ – 3wire	240	0.0938	0.098	XLPE cable
2	1	2	1.5	0.620	Δ - 3wire	185	0.0866	0.128	XLPE cable
3	2	3	1.5	0.053	Δ - 3wire	240	0.0938	0.098	XLPE cable
4	3	4	0.5	0.410	Δ - 3wire	185	0.0866	0.128	XLPE cable
5	4	5	1.5	1.500	Δ - 3wire	185	0.0866	0.128	XLPE cable
6	5	6	1.5	0.630	Δ - 3wire	240	0.0938	0.098	XLPE cable
7	6	7	1.5	0.800	Δ - 3wire	240	0.0938	0.098	XLPE cable
8	7	8	1.5	1.068	Δ - 3wire	240	0.0938	0.098	XLPE cable
9	8	9	1.5	0.488	Δ - 3wire	185	0.0866	0.128	XLPE cable
10	9	10	1.5	0.975	Δ - 3wire	185	0.0866	0.128	XLPE cable
11	10	11	1.0	1.535	Δ - 3wire	240	0.0938	0.098	XLPE cable
12	11	12	1.5	0.850	Δ - 3wire	185	0.0866	0.128	XLPE cable
13	12	13	1.0	0.290	Δ - 3wire	240	0.0938	0.098	XLPE cable
14	13	14	1.0	0.290	Δ - 3wire	240	0.0938	0.098	XLPE cable

Table A2.2 Configuration of feeder F2

Section	Send node	Receive node	Receive node cap. (MVA)	Length (km)	System	Wire size (mm^2)	Conductor spacing (ft)	Wire resistance (Ω/km)	Type
1	S.S	1	0.5	3.576	Y -3wire	240	0.0938	0.098	XLPE cable
2	1	2	1.0	0.1	Y -3wire	240	0.0938	0.098	XLPE cable
3	2	3	0.2	0.411	Y -3wire	95	4.46	0.253	Overhead
4	3	4	0.2	0.365	Y -3wire	95	4.46	0.253	Overhead
5	4	5	0.2	0.719	Y -3wire	95	4.46	0.253	Overhead
6	5	6	0.2	1.026	Y -3wire	95	4.46	0.253	Overhead
7	6	7	0.2	1.045	Y -3wire	95	4.46	0.253	Overhead
8	7	8	0.2	0.724	Y -3wire	95	4.46	0.253	Overhead
9	8	9	0.2	0.900	Y -3wire	95	4.46	0.253	Overhead
10	9	10	0.2	0.735	Y -3wire	95	4.46	0.253	Overhead
11	10	11	0.2	0.367	Y -3wire	95	4.46	0.253	Overhead
12	11	12	0.2	0.438	Y -3wire	95	4.46	0.253	Overhead
13	12	13	0.2	0.700	Y -3wire	95	4.46	0.253	Overhead
14	13	14	0.5	1.152	Y -3wire	95	4.46	0.253	Overhead
15	14	15	0.2	0.736	Y -3wire	95	4.46	0.253	Overhead
16	15	16	0.2	0.969	Y -3wire	95	4.46	0.253	Overhead
17	16	17	1.0	1.300	Y -3wire	95	4.46	0.253	Overhead
18	17	18	0.2	0.700	Y - 3wire	95	4.46	0.253	Overhead
19	18	19	0.2	0.661	Y -3wire	95	4.46	0.253	Overhead
20	19	20	0.2	0.567	Y -3wire	95	4.46	0.253	Overhead
21	20	21	0.2	0.391	Y -3wire	95	4.46	0.253	Overhead
22	21	22	0.2	0.721	Y -3wire	95	4.46	0.253	Overhead
23	22	23	0.2	1.108	Y -3wire	95	4.46	0.253	Overhead
24	23	24	0.2	0.739	Y -3wire	95	4.46	0.253	Overhead
25	24	25	0.2	0.791	Y -3wire	240	0.0938	0.098	XLPE cable
26	25	26	1.0	1.500	Y -3wire	240	0.0938	0.098	XLPE cable
27	26	27	1.0	0.015	Y -3wire	240	0.0938	0.098	XLPE cable
28	27	28	1.0	0.750	Y -3wire	240	0.0938	0.098	XLPE cable
29	28	29	1.0	0.015	Y -3wire	240	0.0938	0.098	XLPE cable

As for the solar irradiance data, Fig.A2.7 illustrates the daily average solar radiation over seasons in the city of Abu Dhabi.

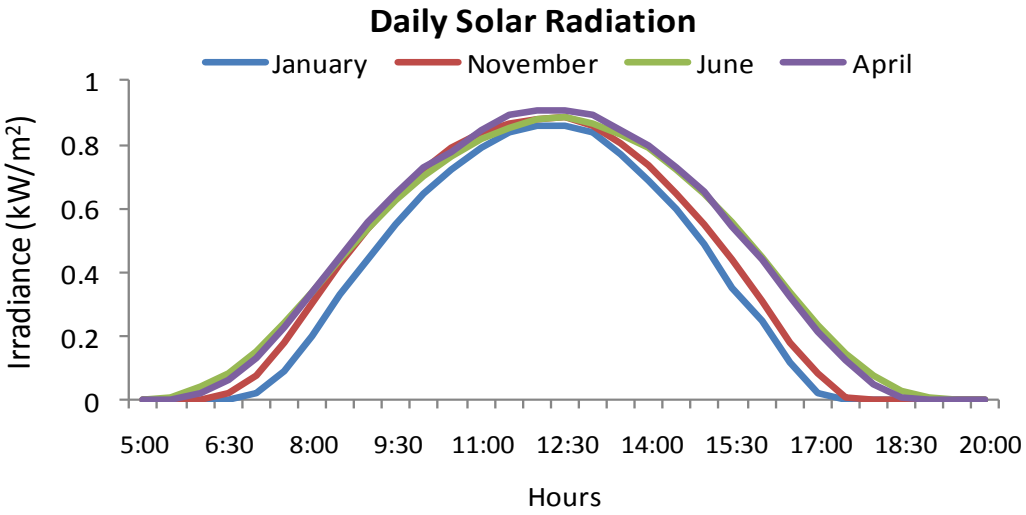

Figure A2.7 Daily average trends of solar radiation in Abu Dhabi